POLITECNICO DI MILANO

Department of Energy

Doctoral Program in

Energy and Nuclear Science and Technology

EXPERIMENTAL INVESTIGATION ON DMFC DEGRADATION

Doctoral Dissertation of:
Fausto Bresciani

Supervisor:
Prof. Renzo MARCHESI
Co-supervisor:
Dr. Andrea CASALEGNO
Tutor:
Prof. Fabio INZOLI
The Chair of the Doctoral Program:
Prof. Carlo E. BOTTANI

Year 2014 - XXVI Cycle

This work is dedicated to Federica and to my family.

Acknowledgements

My first thought is addressed to Federica, for everything we have done together and what I hope we will do. My gratitude also goes to my parents Francesco and AnnaMaria, my brothers Ettore and Daniela and my nephews Aimone, Giulia and, finally, Gaia, whose birth has filled me of joy; a major acknowledgement goes to my advisor prof. Renzo Marchesi, my tutor Prof. Fabio Inzoli and, particularly, to my supervisor Dr. Andrea Casalegno that taught me anything in the academic world.
A special thank goes to the M.R.T. Fuel Cell Lab staff: to Matteo Zago and Andrea Baricci that shared and sustained all my PhD path, to Claudio Rabissi, our new entry, to Behzad Najafi and Dr. Fabio Rinaldi; my grateful goes also to Samuele Galbiati and Carlo Santoro, which have contributed to the M.R.T. Fuel Cell Lab growth and to my PhD success. I received a great support in the experimental activities from Geo DeSuza, Giacomo Varisco, Marzio Olivati, Matteo Confalonieri, Giuseppe Fares and Matteo Sanarico: I thank them very much. I would like to thank the Premium ACT project partners, particularly Sylvie Escribano and Laure Guetaz of CEA, Pawel Gazdzicki and Thomas Jahnke of DLR, Carlo Tregambe of ICI Caldaie and, finally, Jacob L. Bonde and Madeleine Odgaard of IRD Fuel Cells A/S where I spent a few months during my PhD.
My final gratitude is for my longtime friends for their continuous support in all my life.

"How often have I said to you that
when you have eliminated the impossible,
whatever remains, however improbable,
must be the truth ?"
A. Conan Doyle

Abstract

A severe performance degradation is one of the main issues for Direct Methanol Fuel Cells (DMFC) commercialization; the experimental investigations founded in the literature show that degradation has both permament and temporary contributions. The latter can be recovered after an operation interruption, but its origin is not fully understood.
This work aims to propose a systematic experimental investigation on both DMFC temporary and permanent degradation mechanisms. A combined approach based on electrolytic and galvanic operation is used to separate the effects of the degradation at the anode, highlighting the existence of an anode temporary degradation, which is attributed to the accumulation of CO_2 in the anode Gas Diffusion Layer (GDL) and electrode. The comparison between different DMFC operating strategies permits to evaluate temporary degradation mechanisms such as platinum oxides formation and reduction or hydrogen evolution at the anode when the cathode oxygen content is low.
The influence of the Gas Diffusion Layers characteristics is investigated ex-situ and in-situ; the experimental tests reveal that the MicroPorous Layer presence on the anode GDL, which corresponds to an increase in GDL mass transport resistance and breakthrough threshold, determines a worsening of the DMFC anode operation but an improvement of the DMFC operation involving both performance and degradation.
A long-term test of 1100 hours has been performed and analysed both in-operando, with electrochemical and mass transport measurements, and post-mortem in order to quantify the permanent degradation and to identify the main permanent degradation mechanimsms.
Finally a preliminary Accelerated Stress Test for DMFC degradation, based on Open Circuit Voltage cycles, has been designed and tested.

Keywords: Direct Methanol Fuel Cell; Degradation; Operating Strategy; Gas Diffusion Layer; Mass transport; Accelerated Stress Test.

Sommario

L'eccessiva degradazione delle prestazioni è una delle problematiche principali per la commercializzazione delle celle a combustibile a metanolo diretto (DMFC); le indagini sperimentali disponibili in letteratura mostrano che la degradazione ha due contributi, uno permanente ed uno temporaneo. Quest'ultimo può essere recuperato a seguito di un'interruzione del funzionamento, ma la sua origine non è del tutto compresa.
Questo lavoro di dottorato propone un'indagine sperimentale sistematica sui meccanismi di degradazione temporanea e permanente delle DMFC. Basandosi su un approccio combinato di funzionamento elettrolitico e galvanico, si sono separati gli effetti della degradazione anodica evidenziando l'esistenza di una degradazione temporanea all'anodo che è stata attribuita all'accumulo di CO_2 nel Gas Diffusion Layer (GDL) e nell'elettrodo anodico. Dal confronto tra differenti strategie di funzionamento per le DMFC, è possibile valutare altri meccanismi di degradazione temporanea, tra cui la formazione e riduzione di ossidi di platino al catodo e la formazione di idrogeno all'anodo quando il catodo è in carenza di ossigeno.
L'influenza del tipo di GDL è indagata sia ex-situ che in-situ evidenziando come la presenza dello strato microporoso (MPL) sul GDL anodico, che determina un aumento della resistenza al trasporto di massa e alla permeazione, causi uno scadimento delle prestazioni anodiche ma un miglioramento di quelle di cella e una degradazione inferiore.
Un test di più di 1100 ore è stato condotto e analizzato sia in-operando, grazie a misure elettrochimiche e di trasporto di materia, che post-mortem per quantificare la degradazione permanente e individuare i suoi principali meccanismi.
Infine, una procedura preliminare di degradazione accelerata per le DMFC, basata su cicli in circuito aperto (OCV), è stata progettata e testata.

Parole Chiave: Cella a combustibile a metanolo diretto; Degradazione; Strategie di funzionamento; Gas Diffusion Layer; Trasporto di materia; Procedure di degradazione accelerata.

Contents

Introduction

Polymer Electrolyte Membrane Fuel Cells (PEMFCs) received important attention as energy conversion systems, especially for stationary and automotive applications, due to their advantageous features: high efficiency and power density, low emissions and modularity. However, there are issues such as cost, degradation and, mainly, the limited availability of the anode feeding fuel, hydrogen, which play a crucial role for the large market diffusion of PEMFCs.

Among the PEMFCs, Direct Methanol Fuel Cells has attracted interest as portable and uninterruptible power source due to the liquid fuel, good power density and fast start-up because of the low operation temperature (lower than 90^oC). In the last decades, the main research activities on DMFC have been mainly focused on the development of innovative materials in order to improve performance, as, for example, reducing methanol crossover from anode to cathode resulting in a fuel waste, and increasing the effectiveness of the catalysts. However, further critical issues still must be overcome to reach market competitiveness, among which severe performance degradation is one of the most relevant.

The high interest of automotive industries for PEMFCs has led to significant efforts for the investigations on PEMFC degradation mechanisms involving catalysts, carbon support, diffusion layers and electrolytic membrane; the similarities between the two technologies (PEMFC and DMFC) allow the DMFC degradation understanding to benefit of the studies performed on the PEMFC, identifying degradation mechanisms such as platinum dissolution, carbon corrosion, membrane thinning and others.

The experimental investigations on DMFC degradation mainly focus only on

catalysts characterization before and after the degradation test, highlighting mechanisms analogous to PEMFCs or typical of DMFCs such as ruthenium dissolution or crossover. DMFC performance loss can be partially recovered interrupting the operation for diagnostic or appositely developed procedures: for this reason, it is possible to define a permanent degradation and a temporary degradation. Temporary degradation is seldom investigated in the literature even though some temporary degradation mechanisms are proposed; the operation interruptions for diagnostic determine a strong increase of the DMFC performances but the effectiveness of performance recovery is very variable. The literature reports also that cathode air feeding interruption permits an effective recovery of performance; this leads to the adoption of suitable operating strategies such as load cycles or periodic operation. However, there is a lack of systematic analysis on both DMFC temporary and permanent degradation phenomena because temporary degradation is rarely separated by means of procedures for its minimization.
Mass Transport phenomena play a key role for a correct DMFC operation ensuring high performances and low degradation, avoiding, for example, fuel starvation, a inadequate membrane hydration or very high methanol crossover. The DMFC component, regulating the mass balances, is the Gas Diffusion Layer (GDL), a porous media with hydrophobic properties that ensures the reactants and product diffusion; on the GDL, a MicroPorous Layer (MPL) is usually deposited to guarantee a better water management. However, the relationship between degradation mechanisms and mass transport phenomena occurring in a DMFC has yet to be investigated.
DMFC permanent degradation, which corresponds to the effective performance loss, is usually investigated through laboratories long-term tests simulating the real DMFC lifetime; the degradation mechanisms are highlighted by powerful post-mortem analysis as, for example, Transmission Electron Microscopy. However, the continuous improvements in both lifetime market targets and degradation minimization hinders the performance of laboratories long-term test due to the high cost and time consumption. For this reason Accelerated Stress Tests (AST) have to be developed to representatively accelerated the DMFC degradation in order to simulate long-term tests degradation mechanisms.
Considering the presented framework of research activities, this work aims to propose a systematic experimental analysis on DMFC degradation in order to increase the understanding of both the temporary and permanent degradation mechanisms and the relationship between degradation and mass transport phenomena that occur in a DMFC. This work is organized as follows:

- chapter 1: the fundamental aspects and the research activities regarding DMFC degradation are described together with the European research project to which this PhD thesis belongs;
- chapter 2: the experimental methodology to perform and analyse DMFC degradation tests is developed; some preliminary tests on DMFC operating strategies are presented in order to identify the key-points for temporary and permanent degradation investigation;
- chapter 3: the common technique of electrolytic operation is used, for the first time in the literature, to investigate DMFC anode degradation and a mechanism for the anode temporary degradation is proposed;
- chapter 4: the previously proposed interpretation is validated by means of gas composition measurements and other DMFC temporary degradation mechanisms are investigated highlighting the influence of mass transport (regulated by Gas Diffusion Layer properties) on DMFC degradation;
- chapter 5: the GDL properties effects on mass transport are investigated thanks to an ex-situ developed experimental setup, clarifying the effect of MicroPorous Layer on GDL mass transport properties. Moreover a preliminary AST of GDL is developed in order to elucidate the effect of a possible degradation of GDL during a DMFC degradation test;
- chapter 6: DMFC permanent degradation is investigated through a 1100 hours long-term test in reference conditions. Diagnostic tools are introduced and tuned to characterize degradation, permitting to quantify the contributions of the single DMFC components (electrodes, membrane, GDLs). Post-Mortem analysis, provided by research project partners, here summarized for completeness, gives an insight into DMFC permanent degradation mechanisms;
- chapter 7: the effect of a different GDL configuration on DMFC performances and degradation is investigated through mass transport analysis and Electrochemical Impedance Spectroscopy (EIS);
- chapter 8: preliminary batches of Accelerated Stress Tests are designed and tested in order to representatively accelerate DMFC degradation and reduce lifetime tests duration.

Chapter 1

State of the Art on Direct Methanol Fuel Cell degradation

In the following chapter the state of the art on the research about Direct Methanol Fuel Cell is presented, mainly focusing on the characterization of performance degradation; temporary and permanent degradation mechanisms identified in the literature are critically described. Finally the european project Premium ACT is presented and the aims of this PhD thesis work are itemised.

1.1 Fundamental aspects

A fuel cell is an electrochemical device that converts the chemical energy available in a fuel directly into CC electrical energy. Fuel cells are usually classified for operating temperature and electrolyte materials. Among the low temperature polymer electrolyte membrane fuel cells (LT-PEMFC), the direct methanol fuel cell (DMFC) is very promising because of the direct use of a liquid fuel and the low operation temperature (lower than 90^oC) that allows fast starting and lack of cooling issues. The basic operating principle of the DMFC is shown in Fig. 1.1.
On the anode, the fed methanol and water solution is transported from the channel to the catalyst layer, where part of methanol is electrochemically

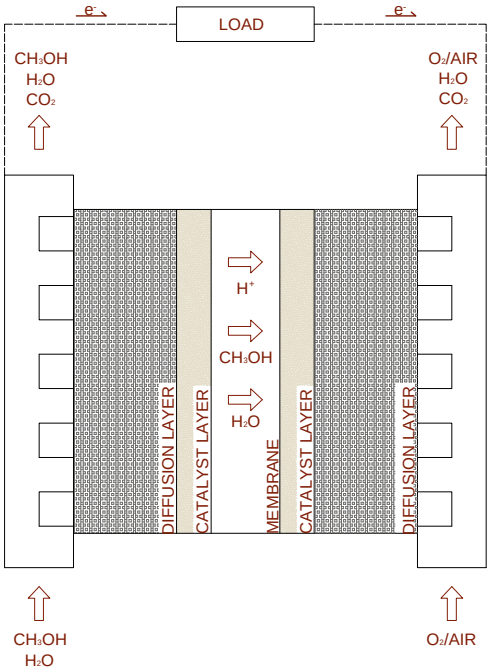

Figure 1.1: DMFC operating principle.

oxidized to form protons, electrons, and CO_2, the remainder is not used for the reactions and a significant quantity is transported to the cathode through the membrane resulting in fuel waste named "methanol crossover". The electrochemical reaction on the anode catalyst layer is:

$$CH_3OH + H_2O \longrightarrow CO_2 + 6H^+ + 6e^- \qquad (E_{0,anode} = 0.046\,V) \qquad (1.1)$$

The produced carbon dioxide is transported through the gas diffusion layer (GDL) to the flow channel, determining a liquid and gas two-phase flow, and it is then vented out of the cell. This results in a rather complicated mass transport process that can influence DMFC performances.
Instead the protons are transported through the proton-conducting membrane to the cathode, where they react with oxygen and electrons, transported through the external circuit, to form water. The electrochemical reaction on the cathode catalyst layer is:

$$6H^+ + 6e^- + \frac{3}{2}O_2 \longrightarrow 3H_2O \qquad (E_{0,cathode} = 1.23\,V) \qquad (1.2)$$

It follows that the overall reaction in the DMFC is:

$$CH_3OH + H_2O + \frac{3}{2}O_2 \longrightarrow CO_2 + 3H_2O \qquad (E_{0,cell} = 1.18\,V) \qquad (1.3)$$

Calculating the thermodynamic open circuit cell voltage (OCV, i.e. without current flow), the Nernst equation predicts a potential value around 1.2 V, depending on methanol feed concentration [1]. Considering an ideal behaviour, the theoretical fuel cell voltage of 1.2 V would be realized at all operating currents. Instead, during the real operation, DMFC achieves its highest output voltage at OCV and then the voltage drops off with increasing current. This behaviour is known as polarization losses or overpotentials and it is represented by the polarization curve, which characterizes the output voltage as a function of the current density. An example of a typical DMFC polarization curve is reported in Fig. 1.2.

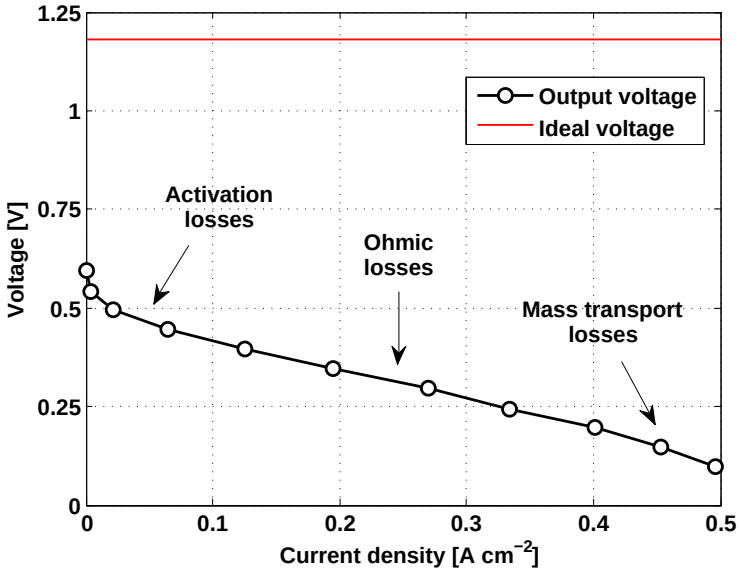

Figure 1.2: DMFC polarization curve.

It is evident that the output voltage is significantly lower than the ideal value. The curve reflects the different limiting mechanisms occurring during DMFC operation: at low current densities the voltage is mainly influenced by the kinetic limitations (activation losses), while at high current densities mass transport limitations are predominant (concentration losses). In between, where the curve shows a nearly linear trend, the voltage is mainly affected by membrane overpotential, that is due to its proton conductivity (ohmic losses).
DMFC presents cathode and membrane overpotentials very similar to hydrogen PEMFC, instead the anode overpotential is much more important, because the methanol oxidation reaction rate is at least three to four orders of magnitude slower than hydrogen electro-oxidation [2], whose overpotential is

generally negligible. Moreover the membrane is permeable to methanol and water that are transported to the cathode with negative effects on DMFC performance and operation. In particular when methanol reaches the cathode (methanol crossover), it is oxidized, leading to a mixed potential [3] and an inevitable decrease of cathode performance. Furthermore the oxidized methanol is effectively wasted fuel with clear negative impact in the overall efficiency of the cell.
In conclusion, in spite of a similar ideal voltage of about 1.2 V, DMFC exhibits lower voltage than PEMFC at similar current density. Therefore DMFC presents lower efficiency (30%[1]) and power density (0.1-0.2 $W \cdot cm^{-2}$) compared to PEMFC, characterized by an efficiency of nearly 50% and a power density up to 1.5 $W \cdot cm^{-2}$.

1.2 DMFC components

Fig. 1.3 illustrates the components of a typical DMFC that consists of a membrane electrode assembly (MEA), which is the electrochemical heart of the fuel cell, sandwiched by anode and cathode distributors. The MEA is a multilayered structure that is composed of an anode gas diffusion layer (GDL), an anode catalyst layer (CL), a polymer electrolyte membrane (PEM), a cathode catalyst layer (CL) and a cathode gas diffusion layer (GDL). A brief description of these components is reported in the following paragraphs.

1.2.1 Proton exchange membrane

The main function of the membrane is to conduct protons from the anode to the cathode and to provide electronic insulation between the two catalyst layers. Due to the strong similarity between common low temperature hydrogen fuel cells and DMFC, the most commonly used membrane is the perfluorinated sulfonic acid (PFSA) polymer membrane, developed by DuPont and named Nafion as in PEMFC. PFSA polymers exhibit high proton conductivity only when fully hydrated due to their typical water assisted proton transport mechanism. In fact in such systems the proton transfer is mainly due to the physical movement of hydronium ions (H_3O^+) that cross the polymer membrane. Water is thus involved with proton transport: at least 3 molecules of water can move together with a proton, generating what is named water electro-osmotic drag [4, 5]. The liquid nature of DMFC anode

[1]The efficiencies reported in this work are calculated on the base of low heating value (LHV), under the hypothesis of fuel recirculation, to permit a direct comparison with traditional technologies.

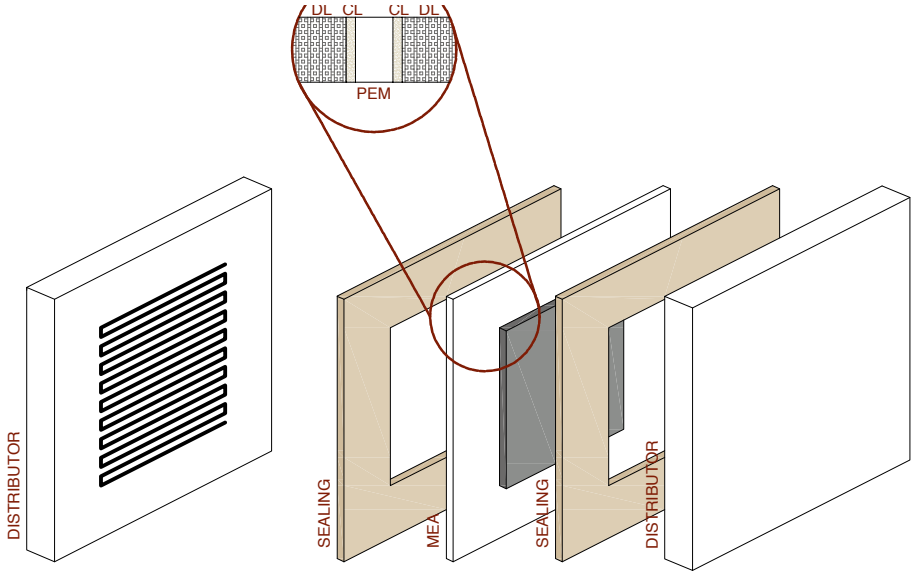

Figure 1.3: DMFC components.

feeding favours membrane hydration but, at high temperatures and cathode airflow, dehydration could occur.
Typical thickness of PFSA membranes for DMFC applications is included between 100-200 μm; it is higher than PEMFC one (50-60 μm) in order to partially reduce methanol crossover that is typically related to both electro-osmotic drag and methanol concentration gradient across the membrane.

1.2.2 Catalyst layers

The fundamental function of the anode and cathode catalyst layers (CLs) is to promote methanol oxidation and oxygen reduction, respectively. The CLs are also characterized by good proton and electron conductivity. In fact both anode and cathode CLs are made of carbon supported catalysts mixed with ionomer in order to provide the so called "triple-phase boundaries", where the simultaneous transport of protons, electrons and reactants/products takes place [6]. The necessity of this triple-phase boundary results in a lower real electrochemical active surface respect to the theoretical one calculated from the catalyst loading; indeed, not all the deposited catalyst is simultaneously linked to both ionomer (for proton conduction) and carbon support (for electrode conduction).
Methanol oxidation is a slow reaction that requires multiple active sites for the adsorption of methanol and for the formation of OH_{ads} species, which completely oxidize to CO_2 the adsorbed methanol residues. Until now the

best effective catalyst is the bimetallic platinum-ruthenium, in ratio from 1:1 to 2:1.
Instead the most utilized catalyst for oxygen reduction at DMFC cathode is platinum, the same catalyst of PEMFC technology. However in DMFC electrodes a higher catalyst loading is necessary, 1-2 $mg \cdot cm^{-2}$, in order to enhance the slow methanol electro-oxidation at the anode and to improve oxygen reduction at the cathode, limited by methanol crossover from anode to cathode. Usually catalyst layers have a reduced thickness, included between 10 and 25 μm.

1.2.3 Gas Diffusion layers

The function of the gas diffusion layers (GDL) is to ensure a uniform distribution of reactants over the catalyst layers and to provide the removal of reaction products from the electrodes to the channels. In addition the gas diffusion layers are the support to the corresponding catalyst layer and the electrical conductor, which transports electrons to the current collector [7]. Typically, gas diffusion layers are constructed from porous carbon paper, carbon felt or carbon cloth, with a thickness in the range of 100-300 μm.
The diffusion layers also assist in water management during DMFC operation. Diffusion layers are normally wet-proofed with a PTFE (Teflon) coating, so that the surface and pores in the diffusion layer are not fully obstructed by liquid water resulting in the flooding of the electrode that determines a strong reduction of fuel cell performances. Moreover to the gas diffusion layer is often added an additional micro porous layer (MPL), characterized by a reduced porosity and high hydrophobicity. The presence of MPL plays a significant role in regulating methanol crossover and water management [8, 9] and [10] during DMFC operation.

1.2.4 Distributors

Distributors are designed to permit reactants and products transport to and from the corresponding diffusion layers. Moreover distributors have to ensure electron conduction to the current collector and to minimize pressure losses, in order to reduce the power demand of auxiliary components, as pumps and compressors. Distributors are composed by a system of channels, with a typical cross-section of about 1 mm x 1 mm, which are machined in a metallic or graphite plate. The most common distributors have serpentine or parallel channels. The MRT Fuel Cell Laboratory has available single and triple serpentines graphite distributors ad-hoc for single cell lab testing.

1.3 Research activities

Despite the strong effort of industries and research centers in the last decade, the Direct Methanol Fuel Cells commercialization is still hindered by four main technological issues:

- high anode overpotential that determines low performances;
- complex mass transport phenomena due to water management issues and two-phase flows;
- methanol crossover from anode to cathode resulting in a waste of fuel and in cathode difficult operation;
- severe performance degradation;

These aspects are exposed in this paragraph taking into account the state of art of the literature but, due to the main focus of this PhD thesis, the performance degradation literature analysis is carried out in paragraph 1.3.1 in order to act as a starting point for this work.
The electrochemical oxidation of methanol is complex; in the overall reaction six electrons are transferred and, consequently, many reaction intermediates can be expected. A relatively large number of publications propose different reaction mechanisms [11, 12, 13, 14]. The conclusion of all these works is the presence of some very stable reaction intermediates and a widely accepted opinion is that carbon monoxide is the long-living intermediate [1], which is the responsible of the slow overall reaction kinetics. However the reaction mechanism is still not fully understood and the optimization of the catalysts is thus more complicated. Up to now the most common catalyst for methanol oxidation is the carbon supported platinum-ruthenium. Researchers are aiming to optimize the nature of the support, the catalyst particle size and the atomic ratio between platinum and ruthenium. A thinner support layers can improve the performance [15] and a reduced particles size is beneficial for methanol oxidation [16].
Another critical issue related to the anode feeding is the methanol crossover. When methanol comes into contact with the membrane it is transported to the cathode by three transport mechanisms: electro-osmotic drag by proton transport, diffusion by methanol concentration gradient and convection by the hydraulic pressure gradient [17]. During typical DMFC operation diffusion is the predominant transport mechanism. In the literature methanol crossover has been extensively studied both experimentally and theoretically

[18, 19, 20, 21, 22]. It has been widely demonstrated that it is closely related to membrane structure, morphology and thickness, and DMFC operating conditions such as temperature, pressure, and methanol concentration. The understanding of the physical phenomena governing methanol crossover is already consolidated in the literature and the researches are focusing on the modifications of electrolytic membranes to reduce crossover. The most promising solutions include the deposition of palladium films on the surface [23, 24] and the creation of composite membranes. In [17, 25] a detailed review on DMFC membranes is reported. Furthermore, recent works performed in MRT Fuel Cell Laboratory [8, 9, 26, 27] showed that the anode Gas Diffusion Layer type has a strong influence on methanol crossover due to the relation between anode electrode methanol concentration (governed by anode GDL) and the methanol crossover.
Furthermore the simultaneous presence of gas-phase CO_2 and liquid-phase methanol and water determining a two-phase interaction both in the anode GDL and distributor; some works in the literature investigated the bubble formation and crowding in the channels [28] at different orientation of inlet/outlet. Also cathode can be subjected to water management issues due to dehydration or cathode electrode flooding phenomena dependent on the operating conditions that could results in performance loss and unsteady operation [9].

1.3.1 DMFC degradation

Among the technical issues of Direct Methanol Fuel Cells, a limited lifetime is the focus of this PhD thesis and it is actually lower than the requirements for both mobile applications (5000 hours) and stationary applications ($>$ 10000 hours). The lifetime optimization can be obtained by means of two main pathways:

- an improvement of DMFC materials;
- a better understanding of the effect of the operation on degradation in order to minimize performance decay;

However, the first way is not feasible because both the laboratory theoretical background and the experimental equipment are not suitable for this purpose. For this reason, this work is oriented on the understanding of degradation mechanisms in order to provide the tools for the optimization of DMFC lifetime.

The number of experimental and modelling investigations on Direct Methanol Fuel Cells, available in the literature, is continuously increasing and many works follow the same logical pattern [29, 30, 31, 32]:

- ex-situ characterization of the pristine MEA;
- a non-systematic degradation test performed at constant current or at constant voltage with some interruption (usually not periodic) with diagnostic to partially recover temporary degradation;
- ex-situ characterization of the degraded MEA

This kind of approach is typical for hydrogen-fed Polymer Electrolyte Membrane Fuel Cells (PEMFC) that are simpler than DMFC and they do not present singular characteristics. Unfortunately, DMFC degradation understanding is even more complex due to a temporary contribution that results in a recoverable performance loss [33, 34]. Cha [35] defined the existence of a permanent degradation and a temporary degradation that can be recovered by means of operation interruption or ad-hoc developed procedures. However the separation of the two components is usually not performed and temporary degradation is rarely characterized and this results in a lack of systematicity in the DMFC degradation analysis.

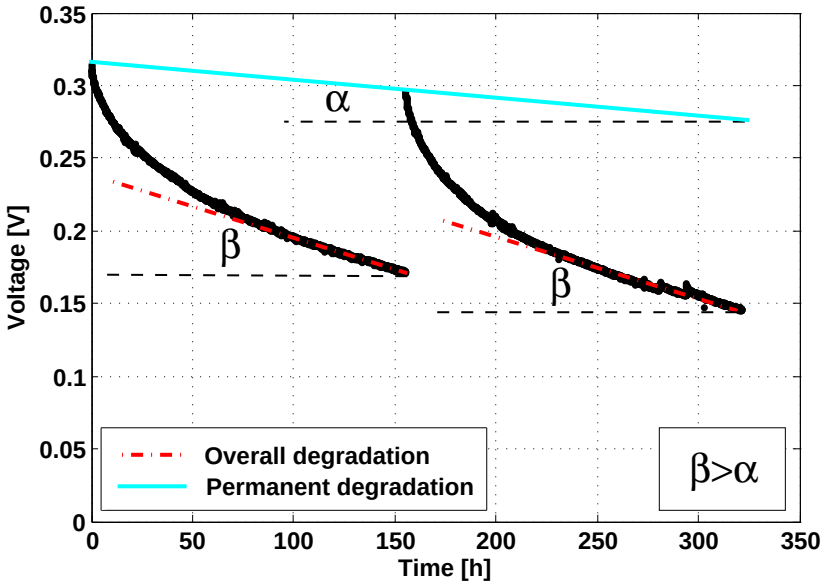

Figure 1.4: Permanent and temporary degradation in DMFC.

Figure 1.4 reports the voltage decay of two steady state operation degradation tests of about 150 hours each; they are interspersed by means of an

operation interruption for diagnostic that determines an increase of performance. The performance loss that occurs during each steady state operation period has a "exponential shape" that can be approximated, after some hours, to a line in order to get the slope and, hence, the degradation rate. The β angle represents the DMFC apparent degradation rate and it is significantly higher than α angle, which represents the permanent degradation that cannot be recovered during the interruption.
Figure 1.4 permits to state that it is not possible to continuously operate Direct Methanol Fuel Cells, in an industrial framework, because of the excessive performance decay related to temporary degradation accumulation. Therefore DMFC usually works by means of operating strategies, some of which have been tested and compared in paragraph 2.4.
A literature review has been performed and it is reported in the next paragraphs where temporary and permanent degradation mechanisms are identified and described. This division is one of the main innovative key-points of this work.

1.3.2 Temporary degradation mechanisms

The DMFC temporary degradation is the part of the performance loss that is recoverable and it is due to the accumulation of phenomena effects related to the operation that could have origin due to chemical or mass transport phenomena. Temporary degradation is attributed to flooding of cathode electrode [33] that could determine a reduction of oxygen diffusion coefficient and, hence, of the performances. Furthermore the two-phase regime could result in a complex management of CO_2 and liquid solution in the anode channel [36].
Other works propose the oxides formation on catalysts as temporary degradation mechanisms; Eickes et al. [37] reported that during the operation the potential continuously degrade while a positive effect on performances is obtained during an interruption of cathode air feeding resulting in a lowering of cathode potential: they attribute this behaviour to the formation (at high potential typical of DMFC cathode operation) and reduction (at low potentials) of platinum oxides on the cathode catalyst. They conclude that the oxides layer determines a decrease of cathode surface area that results in a recoverable performance loss. An analogous phenomenon is suggested in [38] where temporary degradation is partially attributed to Ruthenium oxides formation on anode catalyst.
Another interesting mechanism, which is deepened in paragraph 4.7.2, regards the local spontaneous generation of hydrogen at the anode electrode, in particular operating conditions, when the oxygen content in the cathode

is very low. The consequent hydrogen presence could act as a promoter for anode reaction.
Despite certain dispersion in the literature about the DMFC temporary degradation mechanisms, it is known that each operation interruption determines a performance recovery; particularly, it is well known that the interruption of cathode air feeding determines a strong removal of temporary degradation [39]. Thus, thanks to the analysis of the literature, it is possible to summarize that temporary degradation is a combination of different mechanisms, whose relative weight is unknown; furthermore a characterization of temporary degradation minimization (hence the maximization of performance recovery) has never been carried out in the literature.

1.3.3 Permanent degradation mechanisms

According to figure 1.4, not all the performance loss is reversible; the fraction of performance that is not recoverable is called "permanent degradation" [35] and it is due to chemical/physical/mechanical permanent alteration of the MEA components. Thanks to the strong similarity between DMFC and PEMFC, some degradation mechanisms deeply studied for PEMFC could be proposed also for DMFC and they are listed in the following starting from electrodes degradation mechanisms to electrolyte membrane and GDL. However the permanent degradation of DMFC (10-50 $\mu V \cdot h^{-1}$ is significantly higher than PEMFC degradation.

Modified Ostwald Ripening

For Low Temperature Fuel Cells that uses platinum carbon supported as catalyst, the electrochemical surface area loss can be, in principle, related to two mechanisms:

- Platinum Migration and Coalescence, where catalyst particles migrate on the catalyst support surface and coalesce as in figure 1.5 drawn from [40]. This phenomenon could to be negligible at DMFC operation tem-

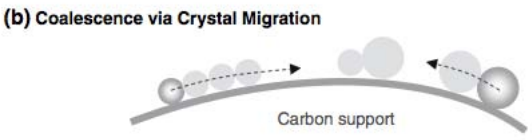

Figure 1.5: Coalescence mechanism for platinum particles.

peratures but it is difficult to easy distinguish the several phenomena involving particles size increase;

- Platinum dissolution and redeposition, where platinum small particles are dissolved, they diffuse through the ionomer and redeposit in larger particles as in figure 1.6 drawn from [40]. This mechanisms, also called

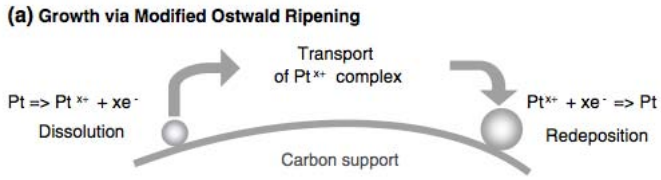

Figure 1.6: Pt dissolution and redeposition mechanism for platinum particles.

"modified Ostwald Ripening" is next explained;

According to [41], the chemical potential of a metallic platinum particle of radius r is 1.4:

$$\mu_{Pt}(r) = \mu^0_{Pt}(\infty) + \frac{2\gamma V_m^{Pt}}{r} \tag{1.4}$$

thus $\mu_{Pt}(r_0) > \mu_{Pt}(r_1)$ if $r_0 < r_1$. In eq. 1.4, $\mu^0_{Pt}(\infty)$ is the chemical potential of Platinum in a very large particle (bulk that, for radius approximation, is infinity), V_m^{Pt} is the molar volume of Platinum and γ is the interfacial energy.

Because the solubility of Pt^0 (zero valence state) in liquids or in the ionomer is considered as negligible, the transport of Pt^0 from a smaller particle to a larger particle is kinetically hindered. In principle Platinum can move into an acqueous liquid or the ionomer as a charged species (ion) (Pt^{2+}). However, as electrons are confined to the metallic particles because of negligible electron concentration in aqueous media, the smaller particles will become negatively charged and the larger particles will become positively charged, which will shut down further Pt ion transport, as the electrochemical potential of Pt ions in the charged particles equilibrates. That is, once the electrochemical potential of Pt^{2+} has equilibrated, no further transport of Pt^{2+} can occur, shutting down dissolution, precipitation, and growth. Under the assumption of existence of Platinum Pt^{2+} ion, its electrochemical potential in a catalyst particle of r radius is 1.5:

$$\mu_{Pt^{2+}}(r) = \mu^0_{Pt^{2+}}(\infty) + \frac{2\gamma V_m^{Pt}}{r} + 2F\phi(r) \tag{1.5}$$

where $\mu^0_{Pt^{2+}}(\infty)$ is the standard state chemical potential of Pt^{2+} ions in platinum corresponding to a flat surface, $\phi(r)$ is the electrostatic potential at the surface of a radius r particle and F is the Faraday constant.
Platinum transport from smaller to larger particles is hindered as long as the electrochemical potentials are equilibrated as in 1.6:

$$\mu_{Pt^{2+}}(r_0) = \mu_{Pt^{2+}}(r_1) \tag{1.6}$$

that can be rewritten as in 1.7:

$$\mu^0_{Pt^{2+}}(\infty) + \frac{2\gamma V^{Pt}_m}{r_0} + 2F\phi(r_0) = \mu^0_{Pt^{2+}}(\infty) + \frac{2\gamma V^{Pt}_m}{r_1} + 2F\phi(r_1) \tag{1.7}$$

From the equilibrium definition it is possible to state that 1.8:

$$\phi(r_0) < \phi(r_0) \tag{1.8}$$

Under the equilibrium assumption that $Pt \rightleftharpoons Pt^{2+} + 2e^-$ and from the definition of the electrochemical potential of electrons in a platinum particle of size r reported in eq. 1.9:

$$\tilde{\mu_e}(r) = \mu_e - F\phi(r) \tag{1.9}$$

where μ_e is the chemical potential of electrons in platinum (Fermi Level), it is possible to conclude that 1.10:

$$\tilde{\mu_e}(r_0) > \tilde{\mu_e}(r_1) \tag{1.10}$$

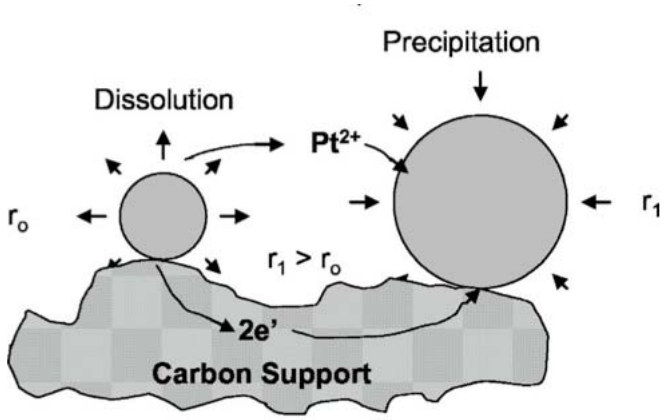

Figure 1.7: Pt dissolution and redeposition mechanism on the carbon support.

Hence, there is a thermodynamic potential for electrons transport from smaller to larger particles; however, into a DMFC, an alternative pathway is the carbon support. Thus it is possible to assume a dissolution and redeposition mechanism as in figure 1.7 drawn from [41].

$$Pt_0(\text{small particles}) \rightleftharpoons Pt^{2+} + 2e^- \text{dissolution} \tag{1.11}$$

$$Pt^{2+} + 2e^- \rightleftharpoons Pt_0(\text{large particles}) \text{redeposition} \tag{1.12}$$

The limiting factor is platinum dissolution while electron transport and ionic species diffusion are faster than the reaction; since the electrical conduction of the support is a key-point of the DMFC, platinum dissolution and agglomeration will be always present. In the literature, platinum has been found on GDL surface in contact with electrode and this is coherent with dissolution and redeposition mechanism [30], which is related to the electrode potential.

Carbon corrosion

Catalyst particles may also detach due to the corrosion of the carbon support and it can agglomerate. This mechanism is clearly related to the electrode potential and it has been found in literature as very important for potentials higher than 0.85 V [42, 43]. The reaction mechanism can be characterized by means of the following reactions [44]:

$$C + H_2O \rightleftharpoons (C - O) + 2H^+ + 2e^- \tag{1.13}$$

$$(C - O) + H_2O \rightleftharpoons CO_2 + 2H^+ + 2e^- \tag{1.14}$$

This mechanism may result in a further platinum agglomeration, in a reduction of electrode thickness and in a strong increase of contact resistance between electrode and membrane.

Other DMFC catalyst degradation mechanisms

The previously explained degradation mechanisms are typical of PEMFC operation and they are probably as much important for DMFC. However, also the anode has been found to be subjected to catalyst degradation mechanisms involving Ruthenium dissolution and crossover [31, 29, 33].

Some works propose that ruthenium dissolution is faster than platinum dissolution during the operation. Its dissolution implies that the specific

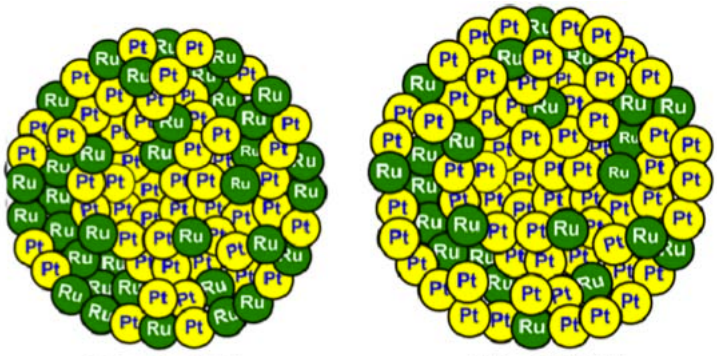

Figure 1.8: Ruthenium dissolution effect on anode electrode catalyst composition of a DMFC before and after the operation.

ratio between platinum and ruthenium changes during the operation as in fig 1.8 drawn from [31] and this determines a reduction of anode effectiveness. Furthermore, they propose that part of the dissolved ruthenium is carried away by means of the reactants while the other part can cross the membrane and it has been found both in the cathode electrode and in the membrane. It is also showed that ruthenium in the cathode electrode hinders the cathode performances.

Membrane and GDL degradation

Despite the main focus of researcher regards catalyst degradation mechanisms, permanent degradation can occur also due to membrane failures or Gas Diffusion Layer properties alteration.
Membrane degradation is deeply investigated for PEMFC where the water management is a key-point to get high performances and researchers highlight four main degradation effects [45, 46, 47]:

- Membrane thinning that results in a decrease of mechanical resistance;
- Membrane delamination that determines a decrease of the contact between membrane and electrode;
- Catalyst particle deposition into the membrane that can alter the membrane properties;
- Pinholes formation that results in an increase of reactants crossover (this phenomenon is a key-point for PEMFC degradation).

On the other hand, Gas Diffusion Layer properties are rarely investigated [31] but some works observe that a reduction of cathode GDL hydrophobicity occurs during the operation while anode GDL is less investigated.

1.4 Premium ACT European Project

In the last five years, European Community research projects has been strongly addressed to the study of fuel cell degradation and, among these projects [48], Premium ACT involves the "Politecnico di Milano" and, particularly, the MRT Fuel Cell Laboratory [49].
Premium ACT is the acronym for "*Predictive Modelling for Innovative Unit Management and Accelerated Testing Procedures of PEMFC*"; this project aims to develop a prediction tool for PEMFC lifetime combining modelling and experimental approach; this prediction tool should be validated by means of reference degradation tests and Accelerated Stress Tests.
Partners of this research project are *CEA - LITEN, IRD FUEL CELL A/S, DLR, POLITECNICO DI MILANO, ICI CALDAIE, JRC, SOPRANO* and, in the frame of this project, the activities carried out at MRT Fuel Cell Laboratory mainly regarded Direct Methanol Fuel Cells modelling and experimental characterizations. In the frame of Premium ACT project, two PhD thesis has been carried out in "Nuclear and Energy Science and Technology" (STEN) PhD school of Politecnico di Milano: the first one regarded DMFC modelling of performances, mass transport phenomena and Impedance spectra [50] while the second one, whose aims are described in 1.5, regards DMFC degradation characterization.

1.5 Aims of the work

This work aims to provide a systematic experimental analysis of Direct Methanol Fuel Cell degradation, including the study of both temporary and permanent degradation mechanisms; the improvement of the understanding of the degradation mechanisms is going to permit the development of Accelerated Stress Tests (AST) for DMFC and the optimization of the operating strategies with the goal of the lifetime increase.
The combined approach of galvanic and electrolytic operation is very innovative in the literature: it permits to specifically analyse the anode electrode in order to improve the comprehension of the mechanisms and to apply the principle of effects superposition.
The most important goals of this PhD thesis work include:

- the development of an experimental methodology to perform and analyse DMFC degradation tests;
- the quantitative evaluation of the different operating strategies for the DMFC operation;
- the investigation of the DMFC temporary degradation mechanisms in order to minimize it and improve DMFC lifetime;
- the analysis of the mass transport phenomena that occurs through a Gas Diffusion Layer and the effect of this component on performances and degradation of a DMFC;
- the investigation on DMFC permanent degradation mechanisms thanks to the development and tuning of own diagnostic tools and to the ex-situ analysis provided by EU project partners;
- the development of preliminary Accelerated Stress Tests to representatively increase the permanent degradation in order to reduce the cost of the degradation tests;

Notes for the reader

The presentation of the several topics of this PhD thesis not always can follow a logical or chronological approach because there are some interconnections between the different chapters; for example, it is not possible to talk about the operating strategies without explaining some temporary degradation mechanisms; in the same time, it is not possible to talk about the temporary degradation mechanisms without developing an experimental methodology including the operating strategies.
Furthermore Gas Diffusion Layer properties have a strong influence on DMFC performances and degradation regulating mass balances through the fuel cell but, on the other hand, it is necessary to present DMFC temporary degradation in order to understand the motivation for working on the GDL.
The order in which the chapters are presented in this PhD thesis tries to reproduce the most effective way for the exposition of all the arguments and, despite some inevitable repetition, permits to follow the continuous improvement in both experimental activities and degradation mechanisms understanding.

Chapter 2

Experimental methodology for DMFC degradation tests

In the following chapter the experimental methodology to perform and analyse DMFC degradation tests is presented. The experimental setup, the consolidated diagnostic tools and the methods to quantify the degradation rate during steady state operation and operating strategies are reported. Furthermore a batch of different operating strategies is compared in order to define the one that will be used during the following chapters.

2.1 Introduction

It is really hard to define a starting point for the development of an experimental methodology for DMFC degradation tests analysis and the experimental investigation presented in the literature are not always significant for an engineer, because they are mainly focused on the catalysts characterization after and before the degradation test. This kind of approach, typical in the literature, can be classified as *"What is happened during the degradation test I performed?"*; our approach, foundation of this PhD thesis, can be classified as *"What is happening during the test I am performing?"*. Indeed, the quantification of the degradation rate is necessary to get a comparison between several tests or different DMFCs and operating strategies, and no

work in the literature provides a reliable quantification of DMFC degradation.
It is well known, both from the literature and the industry, that it is not feasible to continuously operate a DMFC due to an excessive degradation rate; the operation interruption determines a strong recovery of performances as explained before in 1.3.2; nevertheless, a comparison of the different operating strategies effectiveness on the reduction of temporary degradation has never been performed.
Luckily, the M.R.T. Fuel Cell Laboratory has, since 2007, a strong background in the experimental characterization of Direct Methanol Fuel Cells performances and mass transport phenomena such as methanol crossover and water transport; the previously existing experimental setups have been adapted for the 7/24 operation and the quality of the measurements and, hence, of the interpretation has been amended also thanks to a better comprehension of the Electrochemical Impedance Spectra performed in [50]. However, the systematicity in the experiment performance and in the data analysis (also evaluating measurement reliability thanks to measurement uncertainty) is the other foundation of the experimental methodology for the analysis of the DMFC degradation tests.
This chapter aims to present the experimental setups and the main measurements for performances, degradation and mass transport investigation; furthermore a preliminary experimental campaign on DMFC is described that aims to:

- present a method to quantify permanent degradation in steady state operation tests;
- present a comparison among different operating strategies for the minimization of the degradation rate;
- present a method to quantify the degradation rate during each type of operating strategies (providing degradation rate measurement uncertainty);
- identify the key-issues concerning the DMFC temporary degradation that act as a starting point for the following chapters 3 and 4.

2.2 Experimental methodology for DMFC characterization

In this PhD thesis both the experimental setup and the diagnostic tools for the DMFC characterization has been extended thanks to literature analysis and experimental efforts. The resolution of mass balances, by means of the experimental measurements, permits to characterize the behaviours of performances, methanol crossover and water content in cathode outlet during degradation tests. The investigation of mass transport phenomena evolution during mass transport analysis is very innovative. Furthermore the combined approach of anode and galvanic operation for the degradation investigation is not yet present in the literature and it will be one of the most innovative contents of this work.

2.2.1 Mass Balances

Methanol Crossover Quantification

In the following section a carbon conservation analysis is reported in order to describe the methodology applied to estimate methanol crossover from measurement data. Methanol flow rate at anode outlet depends on the flux converted by the electrochemical reaction and crossover, as expressed in the following equations 2.1 2.2:

$$N_{CH_3OH}^{a,out} = N_{CH_3OH}^{a,in} - N_{CH_3OH}^{a,reaction} - N_{CH_3OH}^{crossover} \tag{2.1}$$

$$N_{CH_3OH}^{a,reaction} = \frac{I}{6F} \tag{2.2}$$

Gas phase flow rate at anode outlet is composed of the contributes of carbon dioxide, methanol and water[1] 2.3:

$$N_{tot,(g)}^{a,out} = N_{CO_2}^{a,out} + N_{H_2O,(g)}^{a,out} + N_{CH_3OH,(g)}^{a,out} \tag{2.3}$$

Carbon dioxide flow rate at anode outlet depends on the electrochemical reaction rate and CO_2 flow through the membrane 2.4:

$$N_{CO_2}^{a,out} = \frac{I}{6F} - N_{CO_2}^{mem} \tag{2.4}$$

[1]Water and methanol flows in gas phase can be minimized cooling down the gas mixture near to ambient temperature, then water and methanol fractions can be estimated in condensing conditions. Methanol flow rate in gas phase near ambient temperature is negligible in comparison to the other terms

Consequently CO_2 flow through the membrane can be estimated measuring properly gas phase flow rate at anode outlet.
Assuming complete methanol oxidation at cathode side [51], methanol crossover is equal to CO_2 flow rate at cathode outlet subtracted by CO_2 flow through the membrane and CO_2 flow rate at cathode inlet, due to ambient concentration:

$$N_{CH_3OH}^{crossover} = N_{CO_2}^{crossover} - N_{CO_2}^{mem} - N_{CO_2}^{c,in} \tag{2.5}$$

CO_2 flow rate at cathode outlet can be estimated measuring CO_2 fraction at cathode outlet, where total flow rate depends on: air inlet, O_2 consumption (due to electrochemical reaction and crossover methanol oxidation), water flow, methanol crossover, CO_2 flow through the membrane, as expressed in 2.6, 2.7 and 2.8:

$$N_{CO_2}^{c,out} = x_{CO_2}^{c,out} \cdot N_{tot}^{c,out} \tag{2.6}$$

$$N_{tot}^{c,out} = N_{air}^{c,in} - N_{O_2}^{c,reaction} + N_{H_2O}^{c,out} + N_{CO_2}^{crossover} + N_{CO_2}^{mem} \tag{2.7}$$

$$N_{O_2}^{c,reaction} = \frac{I}{4F} + \frac{3}{2} N_{CO_2}^{crossover} \tag{2.8}$$

The contributions of water production, oxygen consumption and CO_2 flow through the membrane can affect methanol crossover estimation, thus they have to be carefully considered. However, from measurements reported in [8] and confirmed in this work, it is possible to conclude that CO_2 flow through the membrane can be assumed as negligible.

Cathode Water Content Quantification

The thermo-hygrometer for humidity and temperature measurements permits to measure the water content in the cathode exhaust $x_{H_2O}^c$ as will be described in 2.2.2; considering the mass balance equations reported in 2.2.1, the water flow at the cathode outlet is given by following equation 2.9.

$$N_{H_2O}^{c,out} = x_{H_2O}^c \cdot N_{tot}^{c,out} \tag{2.9}$$

2.2.2 Experimental equipment

DMFC characterization setup

The here-described experimental setup was already developed in the MRT Fuel Cell Lab. In the experimental investigations a DMFC unit that has

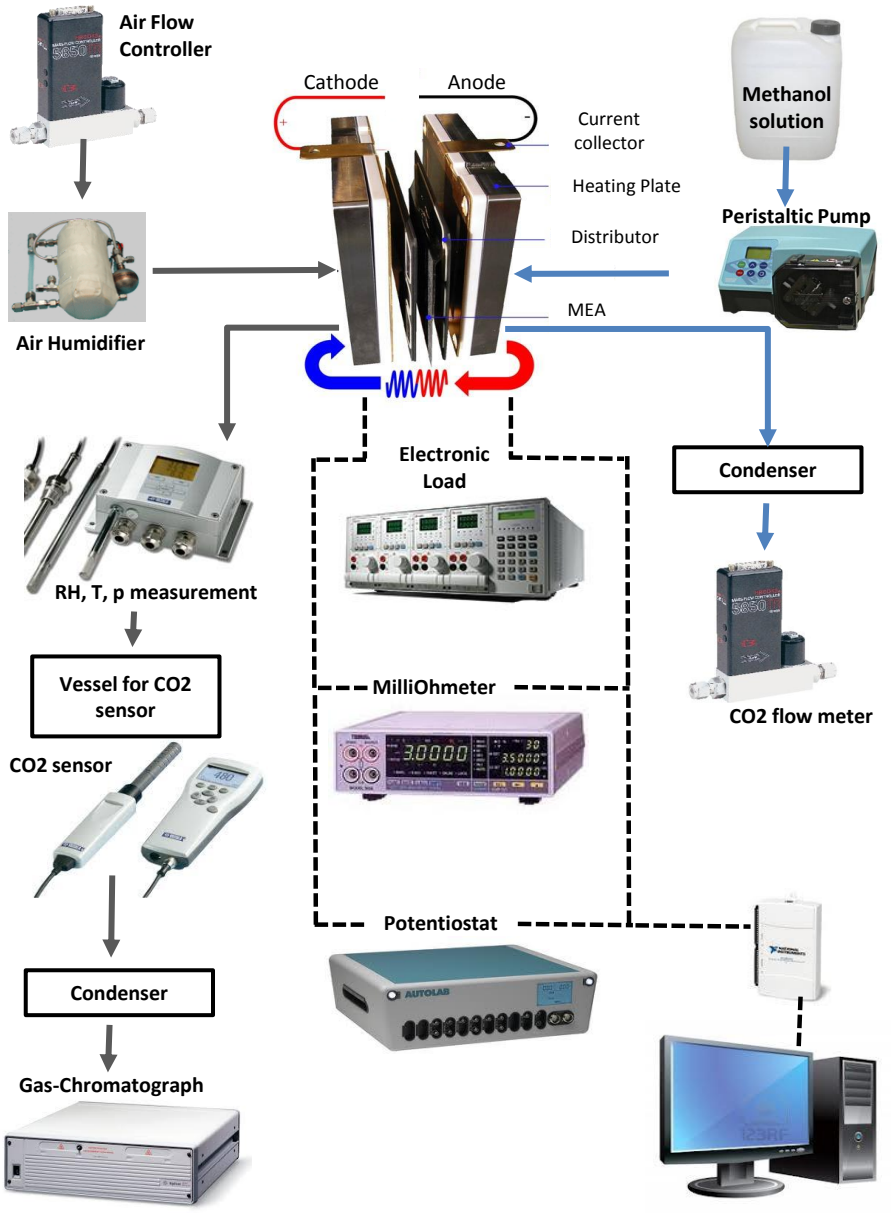

Figure 2.1: Experimental setup for DMFC characterization: solid lines are flows, dotted lines are signals

a maximum cross-sectional area of 25 cm^2 is used. The MEA is contained between two graphite blocks where fluid distributors are cut out, (triple serpentine channel, square section: depth 0.8 mm, width 0.8 mm). The cell is held together with two stainless steel plates using 8 retaining bolts, which were closed applying a torque of 12 $\pm$ 0.5 Nm with a calibrated instrument. A slot is present in the cathode steel plate to accommodate a calibrated thermocouple (uncertainty 0.05 K), connected both with a temperature controller and an acquisition system. Two electrical heaters, connected to a PID temperature controller, are placed within the steel plates, one for each electrode, to control the cell temperature. The graphite blocks have electrical contacts with gold plates, connected to a high accuracy electronic load (current uncertainty 0.25% + 0.001 A; voltage uncertainty 0.5% + 0.01 V). The anode solution if fed by a peristaltic pump with a resolution of 1 rpm and a speed uncertainty of 0.5%; anode mass flow rate is measured with an uncertainty of 1%, thanks to a calibration that permits one to relate it to pump speed. The methanol solutions were produced mixing bidistilled water and methanol (grade 99.9%w) and measuring the solution mass fractions with a calibrated balance (uncertainty 0.1 g). The airflow rate, supplied by a departimental compressor, is controlled and measured by a calibrated flowmeter (uncertainty 0.02 $Ndm^3 \cdot min^{-1}$).
Cathode carbon dioxide measurements are performed with a Vaisala sensor GMP70 (uncertainty 50 + 2% ppm) in a vessel of 0.5 dm^3 volume provided with a liquid separator and a thermocouple in the vessel (in order to evaluate the vessel saturation temperature). The obtained data are corrected by subtracting the measured ambient carbon dioxide concentration, thus the uncertainty of the final measurements is evaluated to be 70 + 2.8%ppm [52, 53]. Anode side is provided of a condenser and a liquid separator with a thermocouple and a CO_2 calibrated flowmeter (uncertainty 0.7% + 0.4 $Ncm^3 \cdot min^{-1}$) but, as explained in 2.2.1 the CO_2 permeation through the membrane is negligible and this measurement has been soon removed in order to increase system reliability for the 7/24 operation. A heat exchanger to warm up the cathode exhaust to evaporate eventual liquid water and a thermo-hygrometer for humidity (uncertainty 2%) and temperature (uncertainty 0.2 ^oC) measurements, located in a thermo-stated housing to avoid water condensation permits to measure the water flow in the cathode outlet as explained in 2.2.1. All the data are acquired by means of a NI-USB 6218 acquisition board if excluded for the thermocouple measurements acquired by means of a NI-USB 9162 compensated acquisition board.

In this PhD thesis work some measurements have been added to the experimental setup above presented, in order to improve the characterization

of performance and degradation. The voltage of the fuel cell is simultaneously measured by the electronic load and by a high precision acquisition board (NI 6218, estimated uncertainty: 1 mV) directly connected to the fuel cell, in order to have multiple readings. The voltage values reported in this work are the ones measured with the acquisition board in order to reduce measurement uncertainty.
An A/C milliohmeter (TSURUGA 3566, estimated uncertainty: 1 $m\Omega \cdot cm^2$) continuously measures the impedance of the fuel cell at 1 kHz single frequency, which represents a good approximation of the membrane Ohmic resistance.
Some other electrochemical measurements are progressively added during the thesis such as EIS and CV and they are performed using a potentiostat (Autolab PGSTAT 30) provided with a frequency response analysis (FRA) module and a Scan250 Module for the CV performance.
Furthermore, in some DMFC tests, a micro Gas Chromatograph (SRA R-3000) provided with certified gas samples cylinders, has been added to the experimental setup as explained in 3 and 4. The carrier gases are provided to the GC from two cylinders, after two pressure reducers, at the pressure of 5.6 bar. All the cylinders are contained in a safety cabinet. The full scheme of the DMFC characterization experimental setup is reported in figure 2.1 and further details on the components are available in the appendix.

Anode polarization setup

The here-described experimental setup was already developed in the MRT Fuel Cell Lab. In the experimental investigations a DMFC unit that has a maximum cross-sectional area of 25 cm^2 is used. The MEA is contained between two graphite blocks where fluid distributors are cut out, (triple serpentine channel, square section: depth 0.8 mm, width 0.8 mm). The cell is held together with two stainless steel plates using 8 retaining bolts, which were closed applying a torque of 12 ± 0.5 Nm with a calibrated instrument. A slot is present in the cathode steel plate to accommodate a calibrated thermocouple (uncertainty 0.05 K), connected both with a temperature controller and an acquisition system. Two electrical heaters, connected to a PID temperature controller, are placed within the steel plates, one for each electrode, to control the cell temperature. The graphite blocks have electrical contacts with gold plates, connected to a high accuracy power supply (current uncertainty 0.1% of the effective value + 0.012 A; voltage uncertainty 0.5% + 0.008 V).
The anode solution if fed by a peristaltic pump with a resolution of 1 rpm and a speed uncertainty of 0.5%; anode mass flow rate is measured with

an uncertainty of 1%, thanks to a calibration that permits one to relate it to pump speed. The methanol solutions were produced mixing bidistilled water and methanol (grade 99.9%w) and measuring the solution mass fractions with a calibrated balance (uncertainty 0.1 g). Hydrogen, produced by a water electrolyser (grade 99.999%$mole$), is supplied to cathode side, as a reference electrode.
The described equipment permits thus to determine anode polarization, because cathode is considered a reference electrode, in particular a pseudo-DHE (dynamic hydrogen electrode) [74], whose potential is nearly constant and negligible in comparison to anode, when determining anode polarization curves. Therefore, measured voltage variations are mainly attributable to anode and membrane overpotentials, as described in [51], and all the anode measurements are reported versus reversible hydrogen electrode. All the data are acquired by means of a NI-USB 6210 acquisition board if excluded for the thermocouple measurements acquired by means of a NI-USB 9211 compensated acquisition board.

In this PhD thesis work some measurements have been added to the experimental setup above presented, in order to improve the characterization of performance and degradation. The voltage of the fuel cell is simultaneously measured by the electronic load and by a high precision acquisition board (NI 6210, estimated uncertainty: 1 mV) directly connected to the fuel cell, in order to have multiple readings. The voltage values reported in this work are the ones measured with the acquisition board in order to reduce measurement uncertainty.
An A/C milliohmeter (TSURUGA 3566, estimated uncertainty: 1 $m\Omega \cdot cm^2$) continuously measures the impedance of the fuel cell at 1 kHz single frequency, which represents a good approximation of the membrane Ohmic resistance.
Some other electrochemical measurements are progressively added during the thesis such as EIS and CV and they are performed using a potentiostat (Autolab PGSTAT 30) provided with a frequency response analysis (FRA) module and a Scan250 Module for the CV performance.
The full scheme of the anode characterization experimental setup is reported in figure 2.2 and further details on the components are available in the appendix.

2.2.3 Data acquisition and processing

The experimental stations are controlled by MRT Fuel Cell laboratory staff and managed by means of a Labview ad-hoc developed software, which per-

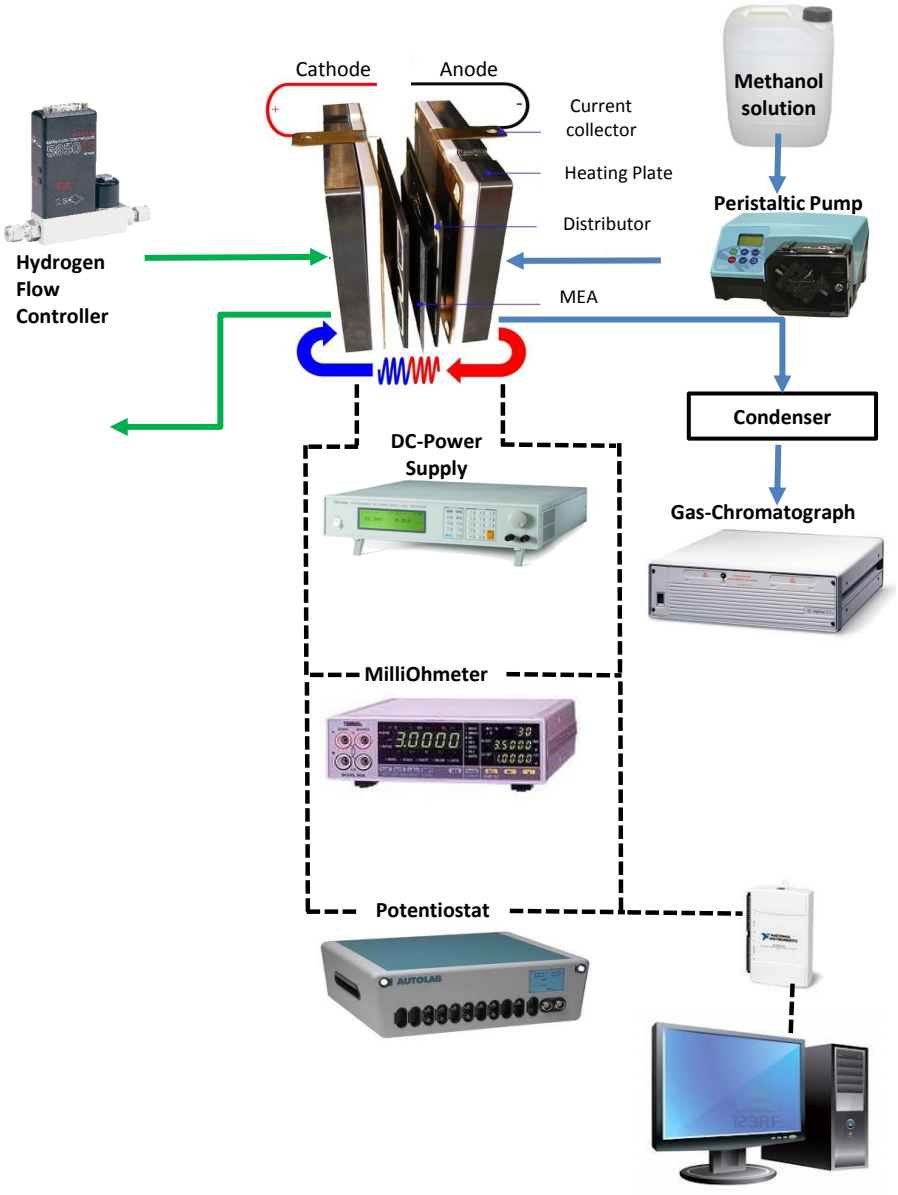

Figure 2.2: Experimental setup for DMFC anode characterization: solid lines are flows, dotted lines are signals.

mits to control all the instruments, to change operation parameters and to display on screen the acquired ones. Both the two experimental setups are provided with safety systems that allow to continuously work in 7/24 configuration; all the experimental data are acquired at 0.5 Hz frequency and recorded, in $1-hour$ data files, on a workstation expressly dedicated to each experimental setup. Data are processed by means of a ad-hoc developed Matlab software that permits to analyse both mass balances and degradation calculation.
The potentiostat (Autolab PGSTAT 30) is managed from the household software NOVA while the micro Gas Chromatograph is controlled from the household software Soprane on a dedicated workstation.

2.2.4 Consolidated Diagnostic Tools

This PhD thesis has some very innovative aspects regarding diagnostic tools for DMFC characterization; however, since this is not the first work carried out in MRT Fuel Cell Lab, it should be considered that some diagnostic tools were still available and consolidated due to some previous PhD works [50, 54] such as Polarization Curves with Mass Transport measurements and Electrochemical Impedance Spectroscopy. For this reason these tools are here reported, while the innovative ones will be described in the following chapters just before they are used.

Polarization Curves

Polarization curve is a typical tool for the fuel cell performance evaluation and it allows to identify the three main loss of a fuel cell: activation, ohmic and concentration losses. Since this argument is widely investigated in the literature [62], the theoretical explanation will not be provided in this work. In this thesis both the anode and the galvanic DMFC polarizations are performed at constant massflows in order to ensure fast achievement of steady state operation that can permit reliable EIS performance. The experimental procedure to perform polarization curves is reported in details in chapters 3 and 4 but, briefly, it consists in a starting transitory and a series of acquisition points at constant current interspersed by EIS performance.

Electrochemical Impedance Spectroscopy

The Electrochemical Impedance Spectroscopy is a powerful *in-situ* measurement technique that permits to evaluate the kinetic and transport phenomena

of an electrochemical system. It consists in perturbing the fuel cell operation with a small AC current signal over a wide range of frequencies and in measuring the voltage response. The module and the phase shift between voltage response and current perturbation are due to the electrical impedance of the fuel cell. According to the frequency of the AC current signal, different physical phenomena are excited depending on their typical time scale: the membrane responds at very high frequencies, while electrochemical reactions and mass transport phenomena are excited at medium-high and low frequencies, respectively. This will originate changes in the impedance module and phase giving useful information on the entity of internal fuel cell losses [56, 57, 58].
Despite the potentialities of this measurement technique the interpretation of experimental observations is very complex. In the literature it has mostly been carried out on the base of equivalent circuit method [59, 60, 61]: even though simple and fast, this method is not reliable, since the equivalent circuit is not unique. Moreover the DMFC anode sluggish kinetic makes the interpretation of impedance spectra more difficult. In fact in hydrogen-air fuel cells, contributions of the anode are usually negligible due to fast kinetics of hydrogen oxidation reaction and a standard practice consists in neglecting anode impedance. In DMFC the slow methanol electro-oxidation does not permit to clearly distinguish anode and cathode contributions by measuring the full fuel cell impedances.

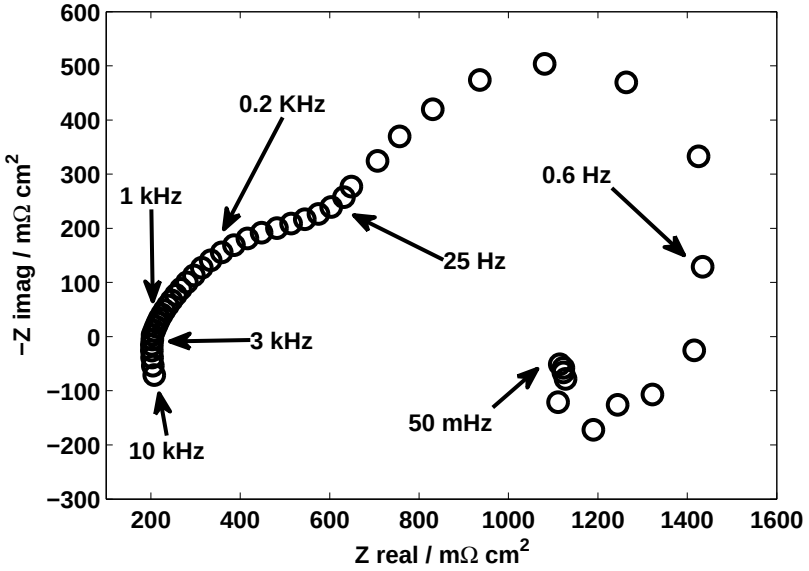

Figure 2.3: Example of DMFC EIS @ 0.1 $A \cdot cm^{-2}$.

An example is reported in Fig. 2.3: the contributions of anode and cathode are superimposed and the resulting shape of impedance spectrum is almost one ideal semicircle. It is possible to state that, at high frequencies, membrane and electrode response at high frequencies, the charge transfer kinetics response at medium frequencies while at low frequencies mass transport phenomena are excited.

2.2.5 Standard activation procedure description

After the DMFC has been assembled and linked to the experimental plant, an activation procedure is needed in order to reach the begin-of-life performances. The DMFC producer provided a detailed procedure for the activation, which consists in a step-by-step increase of the current density interspersed with refresh cycles, which are described in paragraph 2.4, until the reference current has been reached. Prior to the current ramp, the cell is hydrated with water to cathode and anode until it reaches the nominal temperature of 75 ^oC. At the end of the step-by-step procedure, in the first day the DMFC is shut down, while in the second and third day it operates at constant current of 0.25 $A \cdot cm^{-2}$ in 20 minutes cycles interspersed by the refresh. At the end of the third day, the begin-of-life performances are reached. The procedure suggests to shut down the DMFC each day of the activation and flushing with water at the anode and cathode for 5 minutes after the load has been open.

2.3 Steady state operation

2.3.1 Experimental Setup

The experimental setup for single cell DMFC characterization is described in 2.2.2. For the long term tests commercial 22 cm^2 MEAs are used in this work: membrane is Nafion117, anode catalyst loading is 3 $mg{\cdot}cm^{-2}$ (Pt/Ru), cathode catalyst loading is 1.2-1.4 $mg \cdot cm^{-2}$ (Pt). Anode diffusion layer is SGL10CA, while cathode diffusion layer is SGL10CC. Data acquisition system acquires at a 0.5 Hz frequency. During testing anode and cathode are fed respectively with 1M methanol solution with stoichiometric factor equal to 3 and dry air with stoichiometric factor equal to 4. Nominal current density is 0.15 $A \cdot cm^{-2}$. The fuel cell temperature is kept at 60^oC by means of a PID temperature controller.
On the other hand, for the comparison of the different operating strategies 180 cm^2 commercial MEAs provided by IRD Fuel Cell A/S are used and

the tests was conducted at IRD facilities: membrane is Nafion115, anode catalyst loading is 1.8 $mg \cdot cm^{-2}$ (Pt/Ru), cathode catalyst loading is 1.2-1.4 $mg \cdot cm^{-2}$ (Pt). Both anode diffusion layer and cathode diffusion layer are SGL35DC. Data acquisition system acquires at a 1 Hz frequency. During testing anode and cathode are fed respectively with preheated 1 M methanol solution with stoichiometric factor equal to 6 and humidified air (saturation temperature 70^oC) with stoichiometric factor equal to 3. Nominal current density is 0.25 $A \cdot cm^{-2}$. The fuel cell temperature is kept at 75^oC.
Two different temperatures, for the two different MEAs, have been used according to reference operating conditions provided by the MEAs manufacturers.

2.3.2 Permanent degradation quantification

The steady state operation test, performed on the first MEA, is composed of two periods of continuous operation at constant current density (0.25 $A \cdot cm^{-2}$ for 150 hours) interspersed with an interruption when diagnostics is performed. Diagnostics tools used in this work are polarization curves; furthermore the following refresh procedure is performed before and after performing polarization curve: OCV for five seconds, then the air supply is cut off, while the methanol solution circulation is kept for two hours. This procedure, which will be depth and optimized in chapter 6 allows recovering the temporary degradation but the reasons are still not fully clear [63].
Steady state operation of a DMFC is investigated in [64] and in [65] where a biexponential model is proposed in order to predict lifetime during these tests according to second order kinetic phenomena. In this work, the biexponential model is applied to calculate permanent degradation in order to minimize the uncertainties related to performance fluctuations present in the experimental data.
The method is composed of the following steps:

1. the average voltage value is calculated every minute after outliers elimination;

2. each one of the continuous tests is modelled as in the following relation 2.10:

$$V(t) = \phi_1 \cdot e^{-\gamma_1 \cdot t} + \phi_2 \cdot e^{-\gamma_2 \cdot t} \tag{2.10}$$

   where V is the voltage prediction and t is the time value from the beginning of the continuous test.

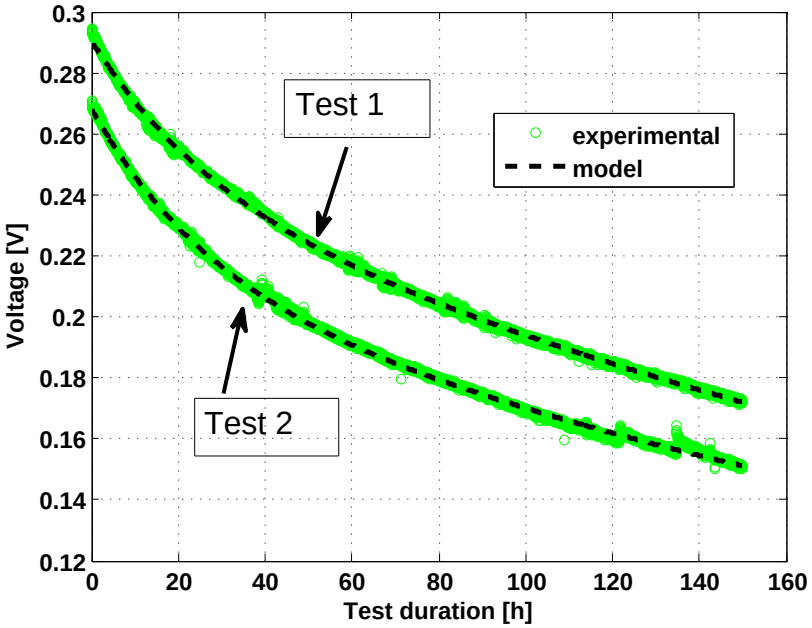

Figure 2.4: Permanent degradation as comparison between two equal and consecutive superimposed continuous tests performed on the first MEA (0.15 $A \cdot cm^{-2}$, 60^oC). The lines represent the biexponential curves fitting the experimental data.

Figure 2.4 shows two consecutive continuous degradation tests, superimposed, and the biexponential curves approximating the experimental data[2]. The good agreement between the model and the experimental data is confirmed by the high values of the coefficients of determination R^2, respectively 0.96 and 0.98, and normal distributed residuals as obtained from goodness of fit functions of Matlab (gof2.rsquare function);

3. The permanent degradation a is calculated as the ratio of ΔV, the averaged point-by-point voltage difference between the two biexponential curves, and the duration of the first test expressed in hours Δt as in the following 2.11:

$$a = \frac{\Delta V}{\Delta t} \tag{2.11}$$

The uncertainty associated to permanent degradation is evaluated from the standard deviation of ΔV.

The proposed method permits to quantify a permanent degradation of 148 $\mu V \cdot h^{-1}$ with a low uncertainty (10%) performing 2 tests of approximately 150 h. The begin-end degradation is calculated as the ratio between overall voltage loss (from the beginning to the end of the test) and test time and it has a value of around 800 $\mu V \cdot h^{-1}$; its uncertainty cannot be quantified because the first acquired voltage values are in highly unsteady state.
It is evident that permanent degradation is only a small part of the begin-end degradation while the main part is recoverable; the literature attributes temporary degradation to mass transport issues in cathode GDL and oxide formation on the electrodes [34].

Figure 2.5 shows polarization curves performed at beginning and end of the first continuous degradation test: the difference of polarization curves confirms the value of permanent degradation: 167 $\mu V \cdot h^{-1} \pm$ 20%. However, such estimation is affected by high uncertainty and by an unknown contribution of temporary degradation while performing the polarization curve.

2.4 Operating strategies comparison

The steady state operation, as above explained, determines a strong performance loss that, despite is largely recoverable, results in low DMFC efficiency

[2]The obtained fitting values are respectevely for test 1 and for test 2: TEST 1: $\phi_1 = 0.048$, $\phi_2 = 0.242$, $\gamma_1 = 9.82e^{-6}$, $\gamma_2 = 6.37e^{-7}$; TEST 2: $\phi_1 = 0.058$, $\phi_2 = 0.21$, $\gamma_1 = 9.85e^{-6}$, $\gamma_2 = 6.13e^{-7}$.

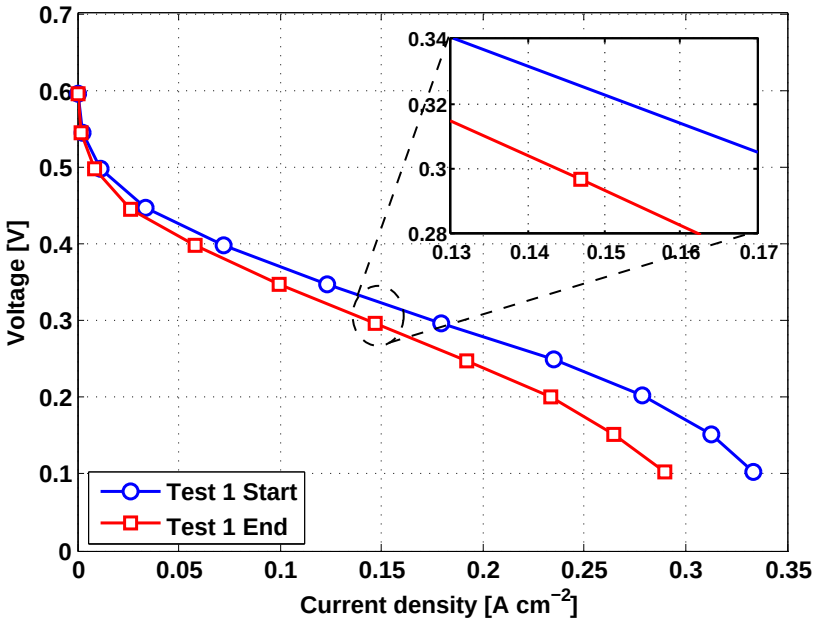

Figure 2.5: Polarization curves at beginning and end of continuous test 1 performed on the first MEA (60^oC); 1 $g \cdot min^{-1}$ mixture at 3.25% MeOH, 0.62 $g \cdot min^{-1}$ air.

and power density. For this reason DMFCs are usually coupled with batteries in order to ensure power continuity when the cell is switched off to recover performances; these not-continuous operation ways are also known as operating strategies or cycling operations and they consist in repeated sequences of steady state operation and operation interruptions with OCV and/or air interruption as for example in [39].

Different operating strategies are tested on the second MEA in a short duration tests in order to highlight the better strategy among them; a description of each strategy is reported in table 2.1. The time of steady state operation at constant current between two operation interruptions has been kept constant in order to remove the influence of this parameter on the analysis; the instantaneous values of the voltage in comparison with the maximum voltage of each test are reported in figures 4.7 and 2.7.

Figure 4.7 shows the comparison between the continuous operation and the OCV operating strategy where the normalized voltage is defined for each test as the ratio between the actual voltage and the initial one; the last one consists in 20 minutes of steady state operation and 1 minute of Open

Name	Operation	Interruption
Continuous	Continuously at constant current	No operation interruption
OCV	Cycles of 20 minutes at constant current	1 minute of OCV every 20 minutes
Refresh	Cycles of 20 minutes at constant current	1 minute of Refresh (OCV+Air Break) every 20 minutes
Air Break	Cycles of 20 minutes at constant current	1 second of Air Break at constant current every 20 minutes

Table 2.1: Operating strategies description

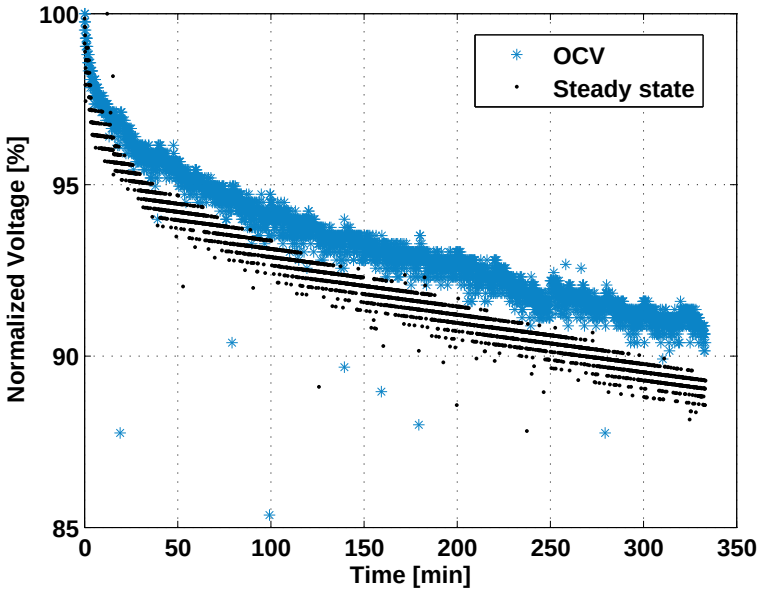

Figure 2.6: Comparison between continuous operation and cycling operation with 1 minute OCV every 20 minutes of operation at 0.25 $A \cdot cm^{-2}$ and 75^oC performed on the second MEA.

Circuit Voltage with both continuous anode and cathode feedings. Since DMFC OCV is lower than the accepted strong carbon corrosion threshold, 0.8 V, it is known that a short period in OCV can have a positive effect on DMFC performances [66]; it is probably due to cathode electrode water removal due to the lack of water production in the OCV period while the membrane hydration is maintained as adequate by means of water and methanol diffusion into the membrane or to the washing of the anode electrode and GDL with fresh mixture leading to the gas-phase CO_2 or intermediates removal. However, in spite of an improvement of cell performances after 5 hours operation, the OCV operating strategy seems to be not suitably effective because after a few hours of operation in OCV operating strategy the DMFC efficiency would be too low. The performance fluctuations that are present also in steady state operation can be due to the complex two phase anodic fluid-dynamic that could result in instantaneous drops of voltage [67]. IRD Fuel Cell A/S has suggested another operation strategy and it consists of 20 minutes of operation interspersed by 1-minute refresh procedure. The latter consists in a sequence of OCV and air feeding interruption, similar to that reported in [33], and allows recovering the temporary degradation.

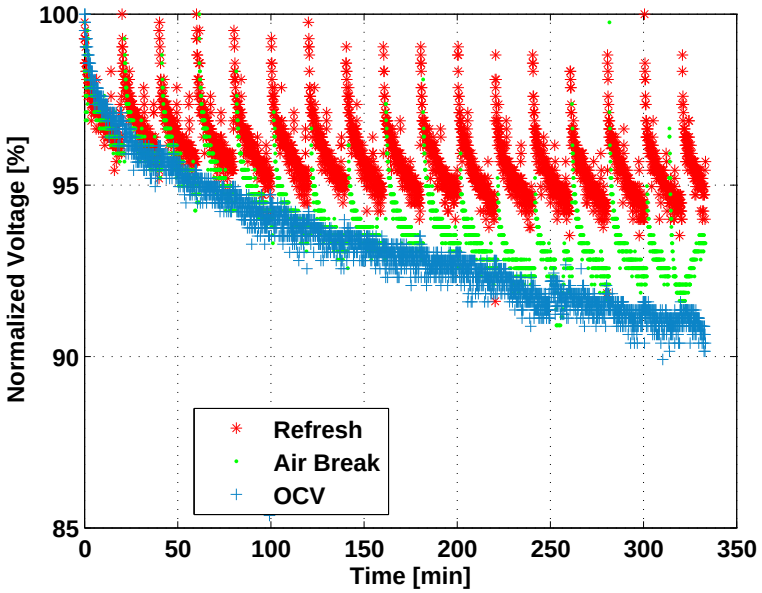

Figure 2.7: Comparison between different operating strategies at 0.25 $A{\cdot}cm^{-2}$ and 75^oC performed on the second MEA.

During the OCV period when the cathode air feeding is stopped, the cathode potential drops at less than 0.3 V and, when the air restarts and the load

is closed, an important positive effect on performances is obtained, Figure 2.7. The following interpretation is proposed as a possible explanation of the positive refresh effect on temporary degradation: the OCV period reduces the cathode flooding because of the temporary absence of electro-osmosis and water production, as also reported in [35]. Furthermore, when the air feeding is interrupted, oxygen is depleted by methanol crossover leading to a strong reduction of the cathode potential. As a consequence, platinum oxides are reduced [37] and cathode catalyst active surface increases leading to performance recovery. Furthermore, as above explained, it is possible to hypothesize about a positive effect on mass transport and kinetic at the anode [68] where, during the refresh cycle, the intermediates and the gas-phase CO_2 could be removed.
For this reason, another operation strategy has been implemented and tested and the experimental results are reported in Figure 2.7 as air break operating strategy. It consists in 20 minutes of continuous operation and 1 second of cathode air interruption without opening the circuit; during this short interruption, the cell potential decrease under 0.1 V. Since the anode overpotential at 0.15 $A \cdot cm^{-2}$ measured during the anode polarization, with cathode set as a hydrogen reference electrode as in [69], is about 0.4 V, it is possible to hypothesize that the variation of anode overpotential in 5 hours of test will be slight. As a consequence the cathode potential during the short interruption will be lower than 0.5 V, where it is possible to start the reduction of platinum oxides. However, this operation strategy does not permit to remove water at the cathode and to remove CO_2 in gas-phase from the anode, probably leading to an increase of mass transport issues. Hence, despite this operating strategy permits a quasi-continuous operation of the DMFC, it seems less effective than the refresh operating strategy; however, lowering the cathode potential to reduce platinum oxides seems to be a keypoint in order to recover DMFC performances and its effect is very important compared with mass transport issues such as flooding.

As a summary it is possible to assert that temporary degradation in DMFC is a combination of different and complex phenomena; the most important ones are reported in Table 2.2 together with the recovery factor that could occur during the refresh cycle.

2.5 Degradation tests in cycling operation

The refresh operating strategy, suggested by IRD Fuel Cell, Figure 2.7, is the most effective among the tested strategies and it permits to recover most of

During the Operation	During the Interruption
$PtO, PtOH$ formation at the cathode	$PtO, PtOH$ reduction at the cathode when cathode potential is lowered
Intermediates reaction at the anode due to reaction mechanisms	Intermediates removal due to anode washing with fresh mixture
CO_2 formation at the anode	CO_2 removal
Flooding of cathode electrode and GDL due to water production	Water removal due to reaction absence and air feeding at the cathode

Table 2.2: Preliminary temporary degradation mechanisms summary

temporary degradation. Then a 150 hours test with such strategy (i.e. the cycling operation with refresh cycles as showed in figure 2.7) has been performed on the first MEA to analyse its influence on permanent degradation.

2.5.1 Method

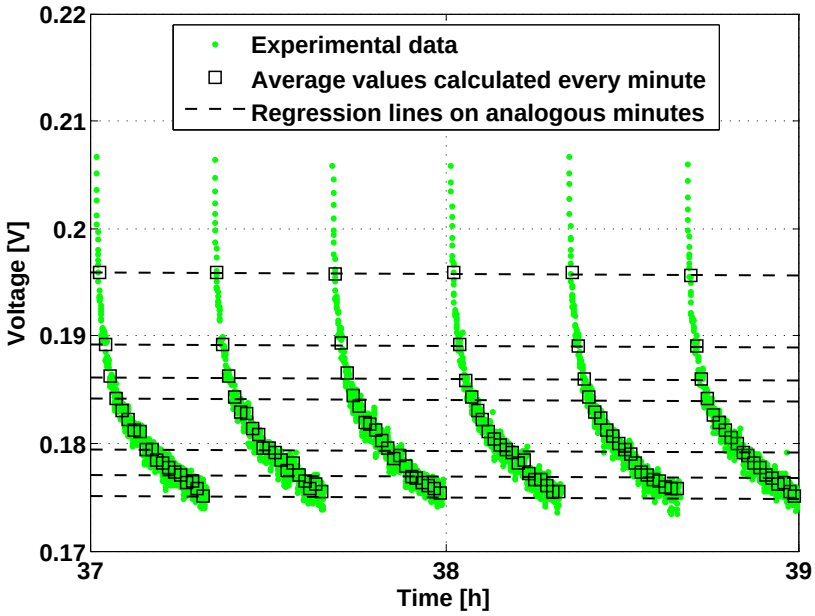

Figure 2.8: Cycling operation; regression lines are plotted for minutes i = 1,2,3,4,10,15,20 performed on the first MEA.

Figure 2.8 shows a sample of the time-voltage curve in cycling operation: the refresh cycles allow recovering temporary degradation, eliminating

the necessity of a second consecutive test and reducing testing time. With this operating strategy the method previously proposed is not compatible. A statistical method is then designed. The proposed approach consists in comparing several consecutive cycles in order to evaluate if the typical exponential behaviour is kept constant in time and the cycles are just translated to lower values. This analysis is carried out comparing analogous points in several cycles and evaluating if constant degradation can be assumed, examples are shown in Figure 2.8. The method is composed of the following steps a description of the adopted statistical tools can be founded in [70]:

1. the average voltage value is calculated every minute after outliers elimination. For each cycle the 20 consecutive voltage values are indexed from 1 to 20 considering the acquiring minute;

2. the acquired data set is divided into 10 hours packages, each containing 30 voltage cycles of 20 minutes; each package is split in 20 vectors grouping 30 voltage values related to the analogous minute;

3. for each vector linear regression and residuals normality analysis are performed to select the vectors that can be approximated by a straight line. With this procedure till 20 straight lines with their own slope and confidence interval for each package can be obtained;

4. the slopes of the lines related to a single package are compared with ANOVA (i.e. the Analysis Of Variance) [70]. If the slopes of at least 10 lines are statistically equal, then that slope represents the permanent degradation rate of the package. This analysis is applied to all the packages;

5. when at least 5 packages, also not strictly consecutive, have the same slope, the degradation is confirmed to be constant for a period of at least 50 hours. Degradation a and its uncertainty[3] u_a are evaluated as follows:

$$V(t) = a \cdot t + b \tag{2.12}$$

[3]These uncertainties are evaluated neglecting instrument uncertainty; this approximation is valid till the analysed quantities are calculated as the difference of 2 close measures (for example $V(t_1) - V(t_2)$) or as a derivative (for example a); in such cases instrument uncertainty can be considered constant and therefore is simplified, calculating the difference or the derivative.

$$u_a = 2 \cdot \sigma_a = 2 \cdot \tau_{\alpha,\nu} \cdot \sqrt{\frac{\hat{\sigma}^2}{S_{xx}}} \tag{2.13}$$

where τ is the percentage point of a t distribution with $1-\alpha$ confidence interval and ν degrees of freedom;

6. the test is concluded at the time tend, when both the following requirements are satisfied:
   - at least 5 packages have the same degradation rate;
   - uncertainty on degradation estimation is less than 10%

This method is valid in principle for all types of load cycles as long as they are periodic and present a reasonably constant behaviour and it could be very important in order to have a comparison between different operating conditions effect on degradation rate.
Degradation during this cycling operation appears statistically constant for a long time period; this does not imply that the degradation mechanisms are effectively a linear function of time nor that this behaviour is still observable on much longer test duration especially. It should be noted that for very long test the degradation rate could change due to the complex phenomena involved in DMFC degradation but a long-term test is needed to investigate this evolution.
Adopting cycling operation and the proposed method allows to compare accurately the effect of different cycling strategies on DMFC degradation.

2.6 Application of the biexponential interpolation to the operating strategy tests

Another tool available for the comparison of experimental tests performed in different operating strategies consists in the bi-exponential interpolation already described in paragraph 2.3.2. This tool has been far used only for the interpolation of voltage-time curve for the DMFC continuous operation; however the bi-exponential interpolation can be applied also to cycling operation basing on the methodology described in the following key-points:

- the voltage values of each 20 minutes period of operation included between two operation interruptions is identified and separated;

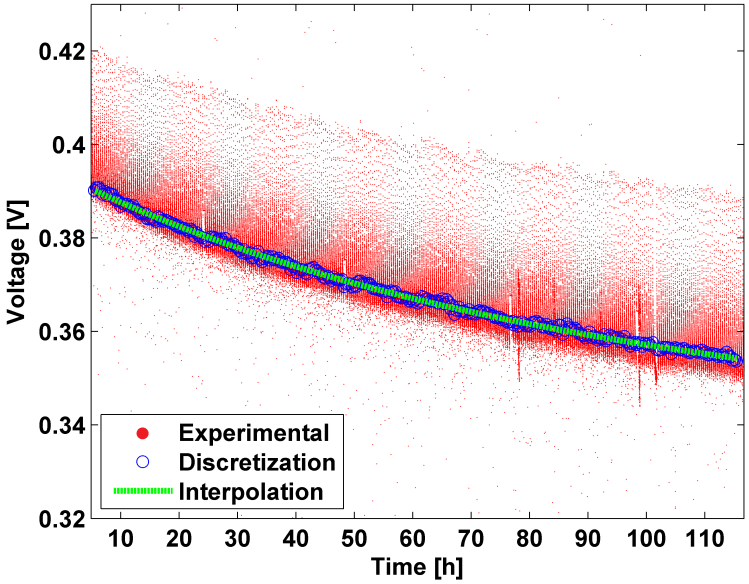

Figure 2.9: Application of the biexponential interpolation to the tests based on the operating strategies.

- the average voltage value is calculated every minute after outliers elimination. For each cycle the 20 consecutive voltage values are indexed from 1 to 20 considering the acquiring minute;
- the average value between the 5^{th} and the 18^{th} minute of each cycle is calculated (in order to avoid the penalizing effect of performances fluctuations on the average calculation) and it is used as the voltage value that is representative of the cycle; the voltage-time curve is hence discretized in one voltage value for each 20 minutes operation cycle;
- the bi-exponential interpolation based on the equation 2.10 is applied to the array of the cycles discretized voltage values above calculated as explained in figure 2.9 where the discretization and the interpolation are superimposed with the real experimental data.

2.7 Conclusions and Open issues

The experimental approach presented in this chapter is the foundation stone for all the continuation of this work because it provides the instruments for the further investigations but, on the other hand, it highlights the lack of the

experimental investigations reported in the literature.
The main important achievements described in this chapter are: the upgrade of the experimental setup for the degradation tests performance, the development of different methods for the degradation rate calculation in different tests and, finally, the comparison of different operating strategies to minimize the degradation rate [24]. However, at the end of this preliminary investigation, there are some open issues, mainly on temporary degradation, that are itemized in the following list:

- there is a strong lack of knowledge regarding DMFC temporary degradation; some mechanisms are described in few works in the literature but, generally, there is no systematicity in the temporary degradation analysis;
- the anode of the DMFC is seldom investigated and its possible temporary degradation mechanisms, introduced in this chapter, have never been described;
- among the operating strategies, the refresh cycle seems to be the most effective one but it is not well known if this procedure determines a complete removal of temporary degradation or it can be optimized or improved. Moreover the comprehension of the refresh effectiveness motivation is very limited;
- mass transport measurements, available in the experimental setups, can provide important additional information on temporary and permanent degradation mechanisms but in the literature no work provides this kind of investigation.

Chapter 3

A parametric analysis on DMFC anode degradation

In the following chapter the existence of an anode temporary degradation is demonstrated for the first time in the literature by means of the anode degradation tests. The qualitative interpretation of the impedance spectra and the preliminary modelling interpretation permits to propose a degradation mechanisms; as a last part the effect of hydrogen crossover is investigated.

3.1 Introduction

The high anode overpotential is one of the main issues of the Direct Methanol Fuel Cells because it strongly limits the overall efficiency of this technology. Among the several issues that determines a high overpotential, two are the main causes:

- a complex reaction mechanism for the methanol oxidation including, coherently with the most common reaction mechanisms, the CO absorption on platinum sites and its oxidation by means of hydroxide absorbed on the Ruthenium [12];
- the two-phase flow both in the distributor and in the Gas Diffusion Layer that determines significant variation on GDL saturation and on

void fraction into the distributor channels.

For this reasons, literature presents several investigations on the anode overpotential thanks to the anode polarization technique: it consists in setting the cathode as a dynamic hydrogen reference electrode (DHE), applying a current by means of a power supply and measuring the anode overpotential respect to DHE. It allows to simulate the anode operation in quasi-representative conditions of the typical operating conditions of a DMFC anode. The anode polarization, corrected with the Membrane Internal Resistance, is generally subtracted to the DMFC polarization to get the cathode overpotential. This technique has been used to validate catalysts improvements, to evaluate the effect of CO_2 bubbles and it is a consolidated tool in the DMFC research field.
However no work proposes an experimental investigation on the DMFC anode overpotential evolution in time and no work proposes an analysis on the influence of the operating strategies on the anode overpotential. In this chapter, the anode polarization technique is adopted to investigate the evolution of anode overpotential and the effect of operating strategies during different degradation tests in order to achieve a higher comprehension of DMFC anode degradation through the following steps:

- experimental comparison of different operating strategies to mitigate anode degradation;
- qualitative interpretation of impedance spectra performed during degradation tests in order to propose possible origins of anode degradation;
- interpretation of impedance spectra through an existing physical model of anode impedance [72], in order to further confirm the proposed origins of anode degradation.

3.2 Experimental methodology

3.2.1 Experimental Setup

The experimental setup for the single cell DMFC anode polarization has been previously described in 2.2.2. The single cell DMFC of 25 cm^2 active area was manufactured by IRD Fuel Cells A/S. Anode catalyst loading is 1.8 $mg \cdot cm^{-2}$ (Pt/Ru) and cathode catalyst loading (Pt) is 1.2 $mg \cdot cm^{-2}$. Both anode and cathode diffusion layers are SGL35DC. The methanol mixture at the anode and the hydrogen flow at the cathode, constant and equal to

0.0035 $Nl \cdot min^{-1}$, are fed through a triple serpentine graphite flow field. Electrochemical Impedance Spectroscopy (EIS) is periodically performed using a Galvanostat (Autolab PGSTAT 30) provided with a frequency response analysis module. The amplitude of the sinusoidal signal increases by increasing current density in order to provide a trade-off between the linear response in voltage and an adequate measurement quality. However the amplitude of the sinusoidal current signal is adjusted so that the potential amplitude does not exceed 10 mV. The impedance is measured at frequencies included between 10 kHz and 50 mHz with a logarithmic distribution. Measures consistency is verified by a retrospective use of Kramers-Kronig transforms [73, 56]: the impedance values that do not satisfy such relations are not considered meaningful.
Moreover anode exhaust composition has been measured by means of a SRA R-3000 μGC analyser equipped with three columns and preceded by a liquid-gas gravity separator. The first column is nitrogen fed Molsieve for the hydrogen identification, the second one is helium fed Molsieve for the nitrogen, oxygen, CO and methane identification while the third one is helium fed PlotU for the CO_2 and light hydrocarbons identification such as methanol.

3.2.2 Performance Characterization

	Unit	Reference Conditions	Other tested condition
T	^oC	75	65
CH_3OH conc.	M	1	2
Anode Mass flow	$g{\cdot}min^{-1}$	3.86 ($\lambda = 6$ @ $0.25\, A \cdot cm^{-2}, 1M$)	1.93 ($\lambda = 6$ @ $0.25\, A \cdot cm^{-2}, 1M$)
Current density	$A \cdot cm^{-2}$	0.25	0.01/0.05/0.1/0.15/ 0.2/0.3/0.35/0.4

Table 3.1: Investigated operating conditions

According to the manufacturer, the reference conditions for the single cell DMFC are used as reference conditions also for the anode polarization, Tab. 3.1. EIS is the most common *in situ* measurement technique that could be performed as a diagnostic tool to quantify fuel cell internal losses during a degradation tests; for this reason it is adopted also in the present work. Since the interpretation of DMFC anode impedance is not consolidated in the literature, a systematic experimental analysis has been performed in order to

carefully analyse the influence of operating conditions on impedance spectra, prior to proceeding with degradation tests.
The experimental setup permits to determine anode polarization, because cathode is considered a dynamic hydrogen electrode (DHE), [74], whose potential is nearly constant and negligible in comparison to anode. Therefore, measured voltage is mainly attributable to anode and membrane overpotentials, as described in [51]. Moreover an acquisition procedure has been developed to determine anode polarization characteristics for defined operating conditions and to evaluate measurement reproducibility. It includes two steps: initial transitory and characteristic acquisition. The initial transitory consists in an acquisition period, performed in the investigated operating conditions at a current density of 0.1 $A \cdot cm^{-2}$, measuring voltage and current at 0.5 Hz for 30 min. The characteristic acquisition is composed of 9 single measurement points referred to different current densities (see Tab. 3.1), collected following one-way curves increasing current. Each single acquisition point is performed at constant current, measuring voltage and current at 0.5 Hz frequency for 600 s. After this time period, anode EIS is performed.
The data obtained from each single acquisition point are elaborated eliminating the initial transitory and outliers. The first 60 values are discarded, because resulting from the transitory caused by current variation. Instead a robust method is used to individuate outliers. It eliminates values not included in the interval median $\pm$ 2.5 times standard deviation, estimated through median absolute deviation. Finally, the last 240 points are selected as significant and mean values of voltage and current are calculated [8, 69].
The reference and the other tested operating conditions for the performance characterization are reported in Tab. 3.1; measurement repeatability has been verified by performing the test three times in three different days. Each anode polarization curve is performed with reactants constant flow rates in order to ensure the steady state operation and hence a good reproducibility of the anode spectra.

3.2.3 Anode degradation test

The manufacturer suggests to operate its DMFC with a specific operating strategy, based on cycles, to mitigate degradation [71]. Therefore also anode degradation tests have been conducted adopting a suitable cycling operation, that consists in series of 20 minutes of continuous operation and a variable number of minutes in OCV[1] .

[1] In anode polarization the OCV corresponds to about 0 V.

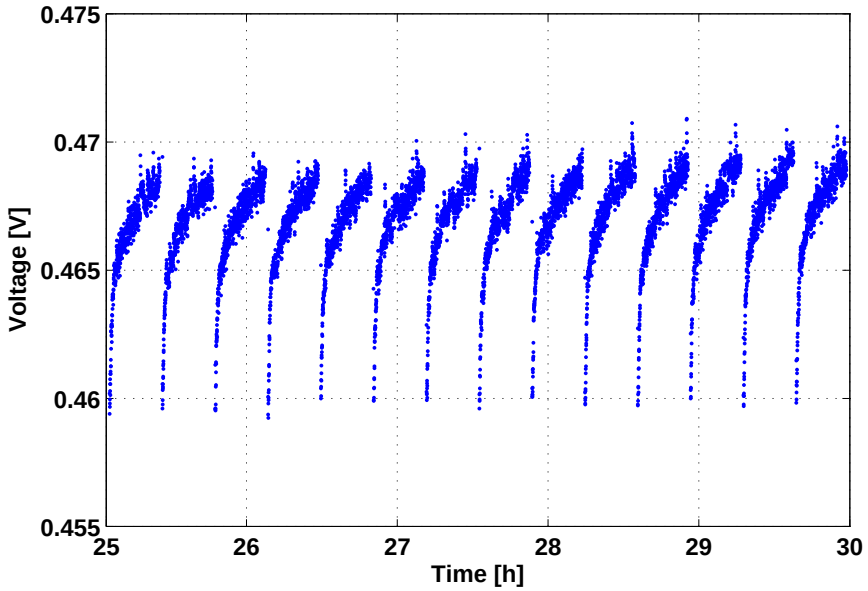

Figure 3.1: Anode performance recovery during cycling operation.

Fig. 3.1[2] reports 14 consecutive cycles performed in the reference condition, Tab.3.1. Fig. 3.1 shows that the anode overpotential continuously increases with operation and that the OCV period determines a performance recovery. The reasons of such behaviour are not yet explained in the literature.
The duration of the OCV period is one of the parameters investigated to evaluate the effectiveness of different operating strategies on anode degradation. At the beginning of each degradation test, anode polarization curve is performed and the DMFC remains shut off with methanol mixture flowing in the anode side for more than 12 hours at a very low mass flow (0.6 $g \cdot min^{-1}$); such long refresh procedure is necessary to equilibrate water and methanol concentrations within the whole MEA. EIS is performed during both degradation and anode polarization tests.
The degradation rate is calculated by linear regression on a revised set of the experimental data as explained in the paragraph 2.5.1. It is possible to estimate the uncertainty of the degradation rate as the confidence interval (95%) on the slope of the packages that satisfy the requirements. For this reason the degradation uncertainty changes test by test: for the cycling operation it is always lower than 10%, while for the continuous test, from hour 320 to 410

[2]In anode polarization a decrease of performance determines an increase of anode overpotential.

in Fig. 3.5, it is very high due to the strong non-linearity of the overpotential behaviour. The estimation of degradation rate during the continuous test is valid only for the comparison with the other cycling tests. This method is valid also for anode DMFC degradation. Despite the DMFC degradation presents a bi-exponential behaviour [65], this method, involving data linear regression, is useful in order to provide a reliable evaluation of anode degradation to get a comparison between the different operating conditions. Instead the permanent component of degradation is calculated through the comparison between anode polarizations performed at the beginning and end of each degradation test.

3.3 Performance Characterization

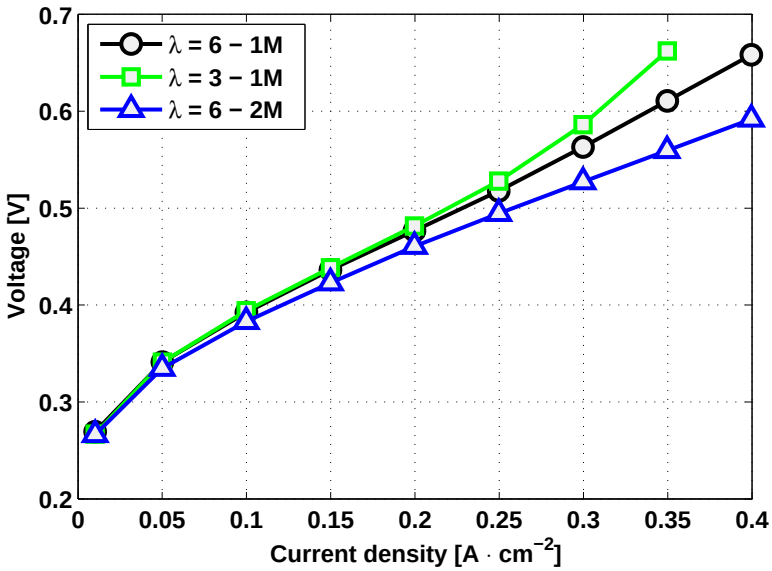

Figure 3.2: Anode polarizations at 75^oC where λ is fuel stoichiometry.

Fig. 3.2 shows the anode polarizations for different methanol feeding concentration and mass flow rate. Anode polarization is slightly affected by anode mass flow rate, excluding conditions where mass transport limitation is clearly evident. Since the mass flow remains constant during each anode polarization, the mass transport limitation occurs mainly at high current density and low methanol concentration. EIS has been systematically performed at each point of anode polarization curves (see tab.3.1). The interpretation of anode EIS is not fully consolidated in the literature [75], due to the complex anode reaction and the two-phase mass transport through

porous components. However it is possible to qualitatively individuate the main phenomena involved. In this paragraph only the most interesting results are discussed.

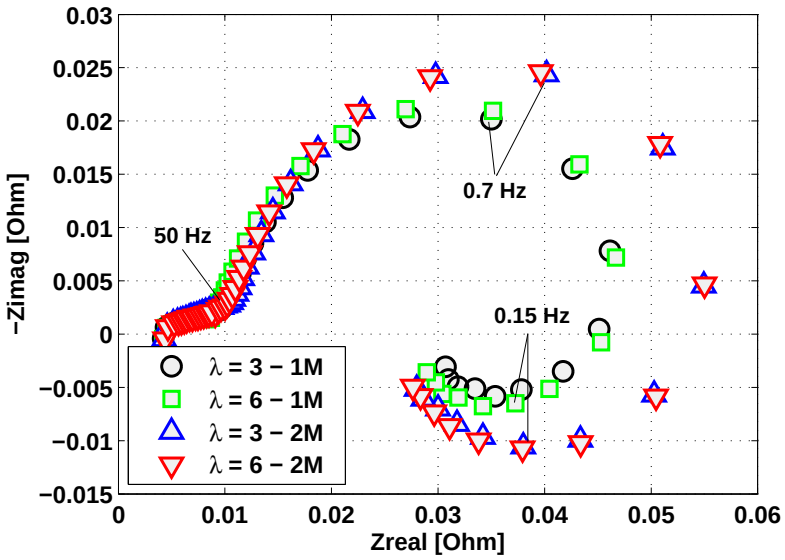

Figure 3.3: Anode EIS at 0.1 $A \cdot cm^{-2}$ at 75^oC.

Fig. 3.3 illustrates different anode spectra at 0.1 $A \cdot cm^{-2}$ varying methanol inlet concentration and flow rate. The impact of doubling methanol stoichiometry is not significant on the whole spectrum whereas doubling the methanol concentration determines a strong modification on it. The anode impedance is an elongated semicircle: this is partially due to proton transport losses in the electrode, that manifest themselves as a linear branch at frequencies lower than 50 Hz (high frequencies region). At nearly 1 Hz (high-medium frequencies region), the effect of the current induced by the charging-discharging of the electrical double layer that is formed at the anode-membrane interface during voltage perturbations is evident. At 0.15 Hz (low frequencies region) an inductive behaviour is evident: this could be due to the catalyst surface coverage by adsorbed reaction intermediates. Doubling the methanol concentration it is possible to notice a small extension of the linear branch: this could be due to a slight catalyst layer dehydration that increases proton transport resistance. Moreover an increase of methanol concentration implies a larger loop, while the mass flow rate has no relevant influence on inductive behaviour.

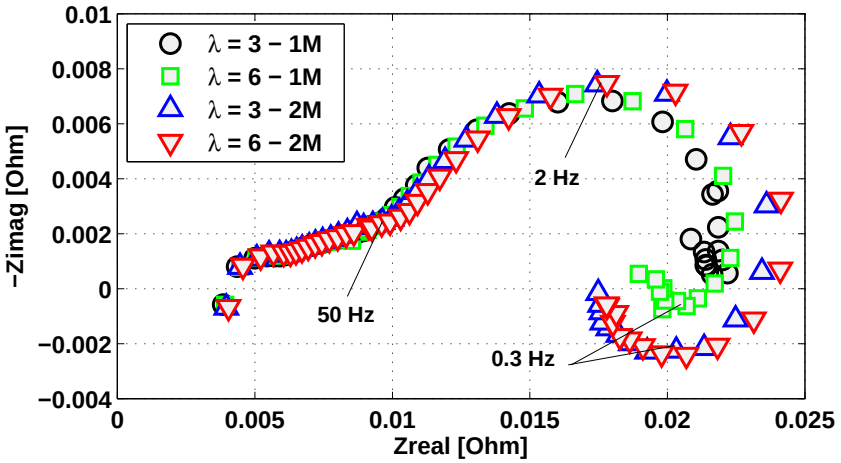

Figure 3.4: Anode EIS at 0.25 $A \cdot cm^{-2}$ at 75^oC.

Increasing cell current density, Fig. 3.4[3] , the total resistance decreases, coherently with the results reported in the literature [61]. But at high current density, the lower concentration combined to the lower flow rate enhances mass transport limitations, reducing the inductive loop. However, keeping constant the solution flow rate and doubling the methanol concentration the enlargement of inductive loop is again evident.
Therefore from this systematic analysis it is possible to figure out that mass transport phenomena have a relevant influence on the magnitude and the shape of the anode impedance. In particular methanol concentration turns out to strongly affect the low frequency region: low methanol concentration enhances mass transport effects, while high methanol concentration enlarges the inductive loop.

3.4 Anode degradation test

A sensitivity analysis of degradation in DMFC has been carried out varying the anodic stoichiometry as well as the OCV duration of the operating strategy on a pristine DMFC, that showed slightly better performance than the DMFC previously characterized. However, some anode polarization tests have been performed on the second cell in order to evaluate the reliability of the obtained performance results and a good accordance between the two

[3]Note that the evident discontinuity in the spectra at high frequency is due to the DC power supply limitation, that reduces the reliability of the measures over 3 kHz, as evidenced by Kramers-Kroning analysis.

DMFCs behaviour has been found.

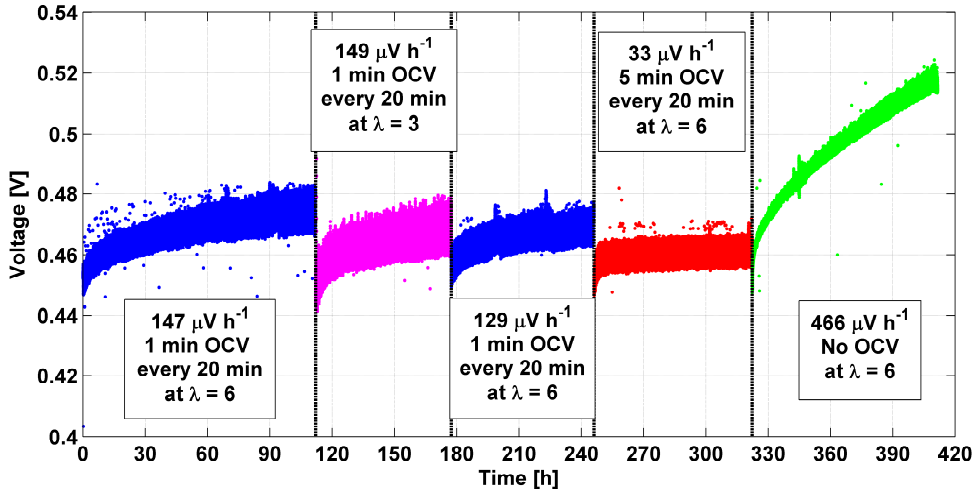

Figure 3.5: Sensitivity analysis on the effect of OCV duration and anodic λ on degradation at 0.25 $A \cdot cm^{-2}$.

In Fig. 3.5 a summary of the most interesting results is reported. In reference condition, acquisition from hour 0 to 110 in Fig. 3.5, operating with a 1 *min* interruption at OCV every 20 *min*, the anode degradation is considerably high, 147 $\mu V \cdot h^{-1}$, but the most of it is temporary. In fact after a diagnostic interruption (including anode polarization curve, EIS), the voltage is restored to lower values demonstrating the existence of anodic temporary degradation, not reported yet in the literature.
During the second period, from hour 110 to 175, even though anode feeding stoichiometry is reduced from 6 to 3, the degradation rate does not vary significantly. However, the behaviour of the overpotential becomes less stable and performance fluctuations appear, as confirmed by the higher width of the acquisition points.
In the third period, from hour 175 to 250, operating again with a 1 min interruption at OCV every 20 min in reference condition, no coupling effects are evident and the most of degradation is still recoverable. The slight difference in the anode degradation between the first and the third period is included in the confidence intervals of the calculated degradation rates and for this reason it is negligible.
Instead increasing the OCV duration from 1 to 5 *min*, period from hour 250 to 320, anode degradation dramatically reduces till 33 $\mu V \cdot h^{-1}$, confirming that permanent contribution is much lower than the temporary one. A fur-

ther small recover is still evident after the diagnostic tests. During the last acquisition period, from hour 320 to 410, the DMFC is operated without OCV interruption and degradation rate increases till 466 $\mu V \cdot h^{-1}$.

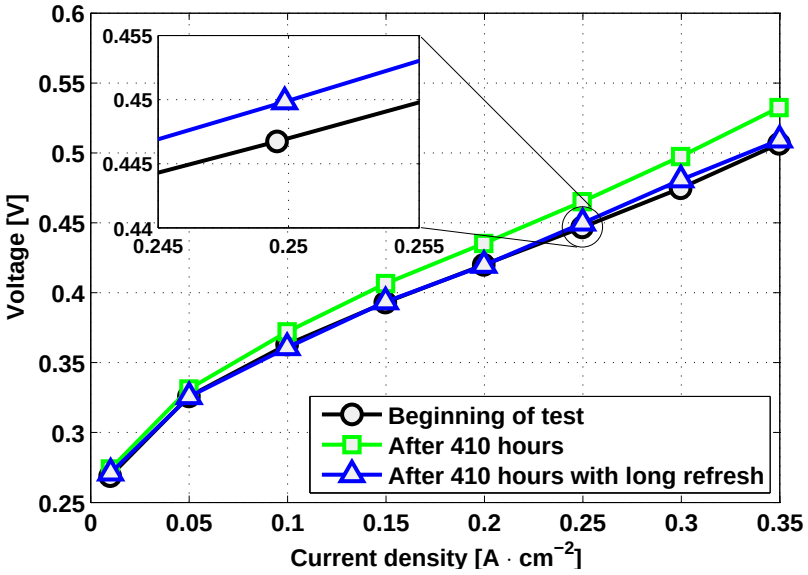

Figure 3.6: Anode polarizations performed at the beginning and end of the degradation test.

The permanent degradation during the overall degradation test reported in Fig. 3.5, from hour 0 to 410, is less than 10 $\mu V \cdot h^{-1}$, as confirmed by the anode polarization reported in Fig. 3.6. It has been calculated as the ratio between the overpotential increase (at 0.25 $A \cdot cm^{-2}$) in the anode polarizations of Fig. 3.6 and the overall test duration.
Anode polarizations reported in Fig. 3.6 confirm the presence of a strong temporary degradation; indeed the anode polarization curve performed at the 410^{th} hour shows a strong overpotential increase if compared with the one performed at the beginning of the test. However, after a long refresh procedure, the anode overpotential dropped to lower values, comparable with the ones acquired at the beginning of test.
From the data reported in Fig. 3.5 it is evident that the duration of OCV period strongly affects the DMFC anode temporary degradation.

Fig. 3.7 shows the results of three EIS performed during the first test, cycling operation with 1 minute of OCV in reference condition. The recorded spectra show in the first 70 hours an extension of the linear branch, a reduction of the inductive loop and an increase of the total resistance; while in the next 30 hours the spectra are almost superimposed.

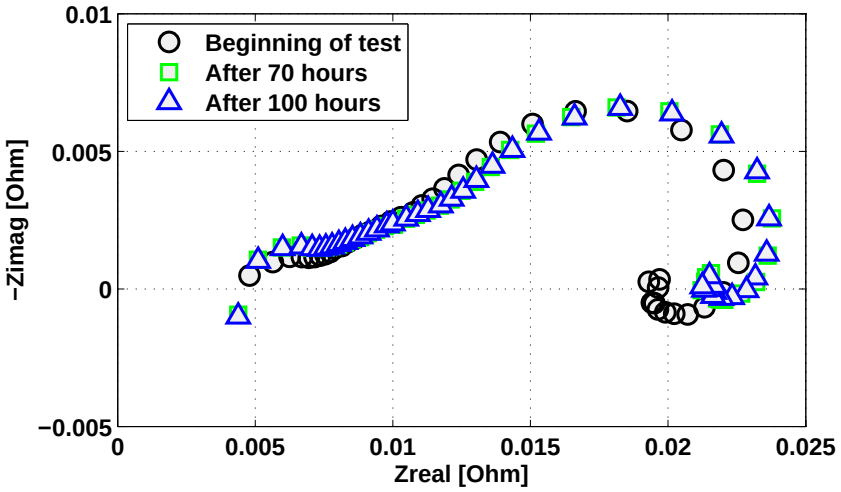

Figure 3.7: Anode EIS in time at 0.25 $A \cdot cm^{-2}$.

These preliminary results suggest that one mechanism responsible for the anode temporary degradation could be the dehydration of electrode ionomer, caused by the reduction of saturation in gas diffusion layer (GDL) and electrode, promoted by CO_2 production at the anode electrode. Indeed hydrophobic porous media transport properties are strongly dependent on the saturation and, according to [76, 77] and chapter 5, a wetted GDL permits a higher water transport than a dry GDL, hence, it has a lower mass transport resistance; thus the OCV period tends to increase the GDL saturation due to absence of electrochemical reactions while the operation tends to decrease GDL saturation due to CO_2 accumulation in the electrode, reducing the effective electrode water concentration. The dehydration of the electrode ionomer appears as an extension of the linear branch at high frequency that determines a translation of the whole spectrum.
The performance characterization, reported in Fig. 3.3 and 3.4, revealed that the reduction of the loop magnitude and the increase of total resistance could be related to a reduction of methanol concentration at the anode electrode, in agreement with water concentration reduction.

The spectra variation during the period with 5 minutes of OCV interruption, Fig. 3.8 at hours 250 and 320, is similar to the previous one but less intense.
Indeed the inductive loop magnitude seems to have no significant changes. Instead after the operation without any OCV interruption a considerable mass transport effect appears at low frequency in the spectrum, Fig. 3.8 at hour 410. In agreement with the previous interpretation, this behaviour

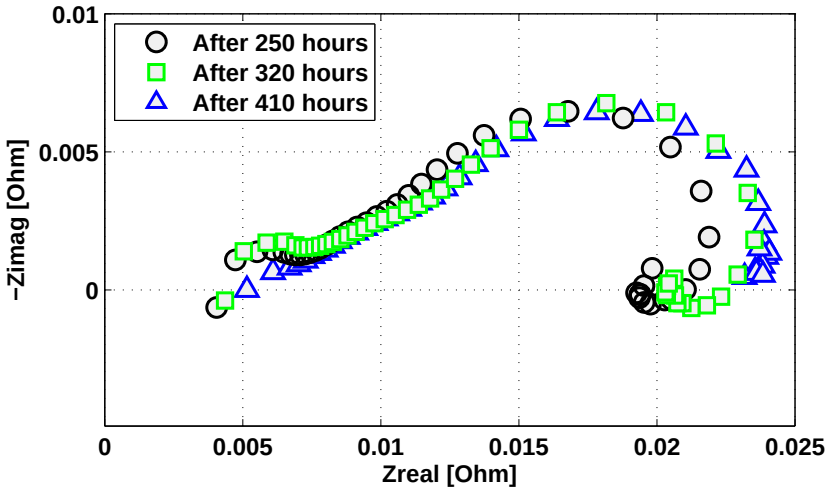

Figure 3.8: Anode EIS in time at 0.25 $A \cdot cm^{-2}$.

could be probably due to the continuous accumulation of gas-phase CO_2 in both electrode and GDL, implying a lower average methanol concentration at the anode electrode. Instead, during the 5 minutes OCV periods, the methanol solution continues to feed the anode side increasing GDL and electrode saturation and removing gas-phase CO_2, as confirmed by the bubble presence in the anode exhaust also during the OCV. An increased saturation determines both an increase of the effective methanol and water concentrations in the electrode and a reduction of GDL and electrode mass transport resistance. Therefore, the longer the OCV period, the higher the average water and methanol concentrations in the electrode because of the improved CO_2 removal from the electrode. According to this interpretation, the continuous operation promotes a strong CO_2 accumulation, decreasing the GDL saturation and causing a significant reduction of the methanol concentration in the electrode, as confirmed by the mass transport limitations in the EIS performed at the end of the continuous degradation test, Fig. 3.8 at hour 410.

To further confirm this interpretation, the methanol concentration in the anode feeding has been changed from 1M to 2M and a 150 hours test has been performed, operating with a 1 *min* interruption at OCV every 20 *min*. The anode degradation is calculated equal to 47 $\mu V \cdot h^{-1}$, significantly lower than the reference conditions test showed in Fig. 3.5 in which anode degradation is calculated equal to 147 $\mu V \cdot h^{-1}$.

3.5 Analysis of Hydrogen Content at Anode Outlet

In principle, the anode temporary degradation could be also caused by the presence of hydrogen at the anode, as demonstrated in the literature, or by the possible accumulation and removal of reaction intermediates such as methyl-formate. However, hydrogen evolution occurs at DMFC anode only at very low cathode oxygen concentration [78, 79]. During anode polarization there is no oxygen at the cathode, however it is possible to suppose hydrogen crossover from cathode to anode due to concentration gradients, positively affecting anode performances.
Thus additional specific measurements have been performed in order to evaluate the presence and the effects of hydrogen at anode side. Since the hydrogen crossover is mainly related to hydrogen partial pressure in the cathode side, two different cathode feeding have been tested: 0.0035 $Nl \cdot min^{-1}$ of nitrogen and hydrogen, respectively. The change of cathode feeding results in a negligible variation of the anode overpotential.

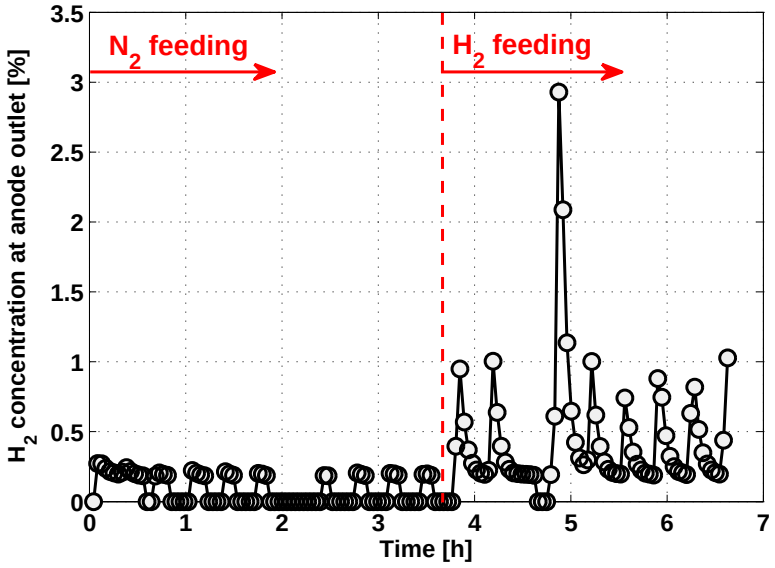

Figure 3.9: Hydrogen concentration measurements at anode outlet.

Fig. 9 shows the hydrogen content in the anode exhaust during cycling operation at 0.25 $A \cdot cm^{-2}$, firstly performed with nitrogen and afterwards with hydrogen at the cathode side. The measurement reported in Fig. 9 evidences the presence of hydrogen at the anode outlet during the nitrogen

feeding. An increase of hydrogen concentration is evident during hydrogen feeding, coherently with increased hydrogen cross-over from cathode to anode, as expected. During the nitrogen feeding no high hydrogen peaks are visible. Because of the absence of cathode hydrogen production during the OCV, cathode hydrogen concentration decreases due to the continuous nitrogen feeding. Moreover during OCV at the anode there is no CO_2 production, that allows measuring the gas composition acting as a carrier. For these reasons a negligible hydrogen content is reported each 20 minutes; as a confirmation a long OCV of 20 minutes has been performed and it results in a longer hydrogen absence. Instead, during the hydrogen feeding, concentration peaks are visible each 20 minutes due to the continuous hydrogen flow at OCV. These peaks are caused by the hydrogen accumulation at the anode that is promoted by crossover also during the OCV and that cannot be detected since the CO_2 flow, which acts as a carrier gas, is not present. As a confirmation a long OCV of 20 minutes has been performed and it confirms two key points. Firstly, it is not possible to measure anode exhaust composition during the OCV periods due to the absence of CO_2 production, resulting in the measured negligible hydrogen content before the concentration peaks. Secondly, the highest peak confirms that the detected hydrogen is due to crossover from cathode to anode: in fact the longer the OCV duration, the higher the hydrogen peak.

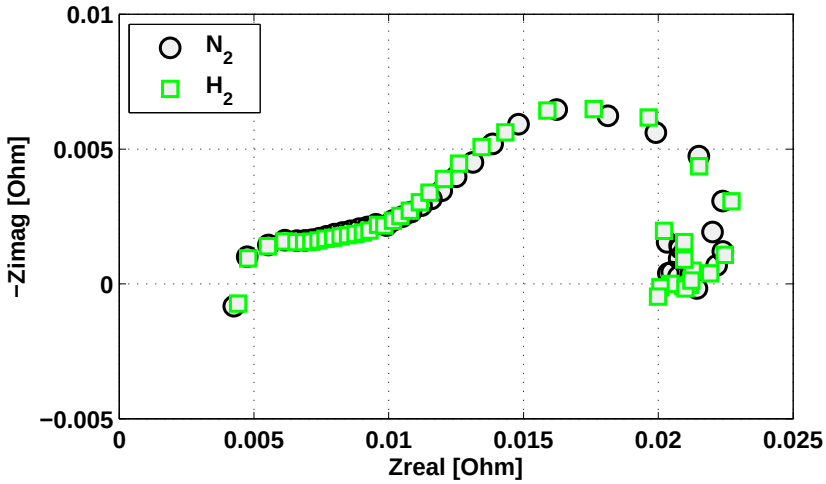

Figure 3.10: Anode EIS with different cathode feeding at 0.25 $A \cdot cm^{-2}$.

However the different hydrogen concentration at anode side affects negligibly the impedance spectra, as reported in Fig. 3.10, where the results

of EIS acquired with nitrogen and hydrogen cathode feeding are compared. Furthermore, the positive effect of the OCV interruption on anode degradation is confirmed with both the cathode feedings: for this reason the effect of hydrogen crossover on the anode temporary degradation is considered as negligible.
Instead, by measuring the gas composition it is very hard to detect the presence of reaction intermediates, such as methyl-formate, because they could be measured only by composition analysis of liquid phase. However, some works show the presence of intermediates at anode outlet, but these compounds have a negative effect on the DMFC performances only at high concentration [80] and with fuel recirculation [81]. For this reason in this work the reaction intermediates have been assumed to have negligible effects on anode temporary degradation.

3.6 Preliminary Modelling Interpretation

An existing physically based model of anode impedance [72] has been finally used as a diagnostic tool to analyse the origins of anode temporary degradation. The model [72] includes the two-phase (gas and liquid phases) mass transport of both methanol and water, through diffusion and catalyst layers, and the methanol oxidation reaction involving CO adsorbed intermediate.
The model reproduces the experimental observations with sufficient accuracy despite it underestimates the magnitude of the inductive behaviour[4]. However there is full agreement between the simulated and measured relaxation frequencies: therefore all the main involved physical phenomena are correctly described. The poor agreement between experimental and modelling in the high frequency region is due to instrument limitations in the experimental setup as explained in paragraph 3.3. Afterwards the proposed origins of anode temporary degradation, reported in paragraph 3.4, have been introduced in the model as a reduction of both the proton conductivity in the catalyst layer and the liquid saturation in the diffusion layer.

Model simulations, Fig. 3.11, qualitatively reproduce experimental observations, confirming the proposed origin of anode temporary degradation. In particular lower values of saturation within the GDL mainly imply a decrease of methanol concentration in the catalyst layer that strongly affects the magnitude of the inductive behaviour. These considerations are also coherent with the performance characterization of paragraph 3.3, in which low

[4]Model calibration is a time consuming activity; it would be possible to obtain a better fit of the experimental data, but this is not the aim of the present work.

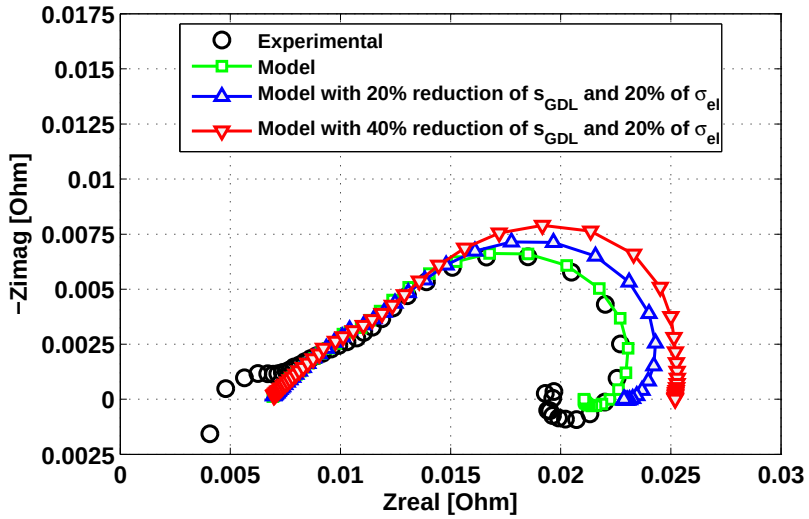

Figure 3.11: Simulated anode EIS with temporary degradation effects at 0.25 $A \cdot cm^{-2}$.

methanol concentration enhances mass transport effects, while high methanol concentration enlarges the inductive loop.

3.7 Preliminary Investigation at very low methanol concentration

The experimental investigation on the anode operation permits to identify that the complex two-phase and two-components mass transport phenomena that occur in the anode Gas Diffusion Layer and Electrode are one of the key issues for the anode degradation; a test with very low methanol concentration is reported as a confirmation of the complexity of the anode operation, especially when it can be periodically in fuel starvation.

Figure 3.12 reports the anode overpotential acquired during a anode degradation test conducted at 0.1 $A \cdot cm^{-2}$, 75^oC and 3.9 $g \cdot min^{-1}$ of low concentration (1%) methanol solution that guarantee a adequate electrode hydration and a anode stoichiometry equal to 5.4 (the reference one is equal to 6). This test has been performed with 1 min of OCV every 20 min of operation as in the tests reported in figure 3.5. This test shows a very high degradation rate with large magnitude periodic overpotential peaks that were never highlighted at reference methanol concentrations. This unusual behaviour, which does not permit reliable EIS measurements, is related to the

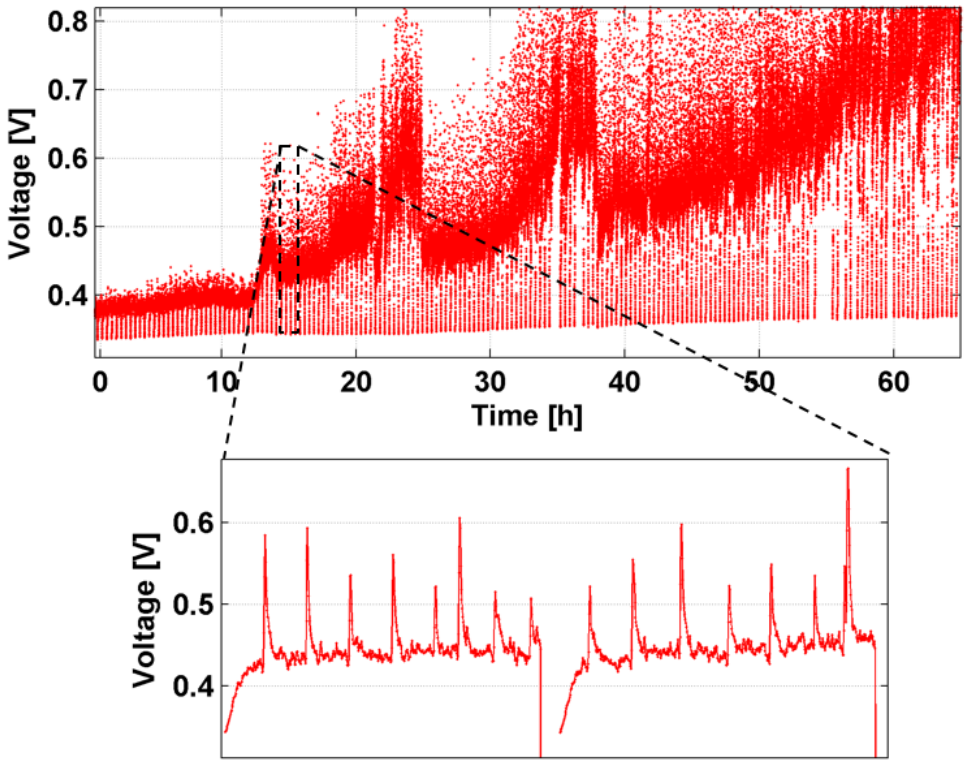

Figure 3.12: Anode degradation test performed at 1% methanol concentration at 0.1 $A \cdot cm^{-2}$.

mass transport phenomena that occurs at the anode during the DMFC operation; the very low methanol concentration is probably determining local fuel starvation resulting in strong and periodic increase of the anode overpotential that can be observed in the zoom of figure 3.12. Coherently with the previously presented interpretation on the anode degradation mechanism, the dynamic of the overpotential peaks confirms the interpretation thanks to the following considerations:

- in this operating conditions the anode has a lower CO_2 production in comparison with the reference current, a lower methanol concentration but a significantly higher water concentration in the anode electrode and diffusion layer;
- a higher water concentration can result in anode GDL pore obstruction and in a very high liquid partial pressure; according to the results presented in chapter 5, the CO_2 transport from the electrode to the channel is more difficult;
- a low methanol concentration and the accumulation of CO_2 in the anode electrode could determine local fuel starvation;
- the distributor channel configuration (supply from above, removal from the bottom) can hinder the bubble removal from the channel resulting in a additional resistance to the mass transport; indeed, according to [36], bubbles tends to crowd and to form plugs that thanks to the buoyancy forces, cannot easily be removed from the distributor.

To confirm the last point, the distributor inlet and outlet were inverted and the overpotential peaks presented a more muffled behaviour. Another interesting consideration on the low methanol concentration test regards the strong inertia in the overpotential during the first 10 hours of the test that was performed after a diagnostic interruption at 1M methanol concentration. In these conditions the re-equilibrium of mass transport phenomena through the membrane and the electrode takes a long period to reach the steady state operation that, in this case, results in a very unsteady anode operation.
The greatest part of the degradation obtained during the low methanol concentration test has been recovered just after a long refresh and 5 *hours* of reference test at 1M methanol concentration confirming that the mass transport phenomena through the anode electrode and GDL are responsible for the DMFC anode temporary degradation.

3.8 Conclusions

This chapter presents an experimental study on DMFC anode degradation during cycling operation, varying the anode feeding stoichiometry and the duration of OCV period, integrated with a preliminary modelling interpretation and a systematic analysis of operating conditions influence on anode performance and impedance spectra. The main conclusions are the following:

- anode degradation is characterized by a relevant temporary contribution, never highlighted in the literature [82];
- cycling operation (by means of operating strategies), adopting OCV interruption, permits to drastically decrease temporary degradation compared to continuous operation;
- the duration of the OCV period strongly affects temporary contribution: the longer the OCV period, the lower the temporary degradation;
- the effects of anode temporary degradation manifest themselves on a Nyquist plot as an extension of the linear branch and a reduction of the inductive loop;
- the origin of such temporary effects could be related to a reduction of water and methanol concentrations in both the GDL and the electrode, promoted by the accumulation of gas-phase CO_2 during continuous operation that determines variation in GDL mass transport properties;
- the physically based model interpretation further supports the proposed origin of anode temporary degradation;
- the effect of hydrogen crossover on the anode temporary degradation is negligible.

Chapter 4

DMFC temporary degradation and role of methanol crossover

In the following chapter the experimental characterization of methanol crossover evolution during DMFC degradation tests is presented and it confirms the proposed mechanism for anode temporary degradation described in chapter 3. Furthermore some other temporary degradation mechanisms are identified and evaluated such as platinum oxides formation, water management and electrolytic hydrogen evolution.

4.1 Introduction

As already explained in chapter 1, methanol crossover and performances degradation are two of the main issues concerning DMFC technology; particularly, methanol crossover is a technical issue of fundamental significance, because it determines a strong reduction of cathode potential, lowering DMFC performance, and a waste of fuel, decreasing system efficiency [3, 8]. The analysis of methanol crossover behaviour during degradation tests is crucial, because the variation of both performance and efficiency is closely related to such phenomenon. In the literature there is a lack of in situ mass transport measurements during DMFC durability tests. Both methanol crossover and water transport in DMFC strongly depend on membrane and gas diffusion

layer (GDL) properties [9, 83] that may fade during operation. In Ref. [84] the analysis of water transport during durability test is presented, but up to our knowledge no work proposes an investigation of methanol crossover evolution during degradation tests.
Furthermore, in the literature, temporary degradation is usually poorly investigated due to the only apparent performance loss; however, it is a fundamental issue because it directly affects power generation and DMFC efficiency. There are several mechanisms highlighted in the literature for DMFC temporary degradation as explained in paragraph 1.3.2 and in the chapter 3 a mechanism for anode temporary degradation is proposed and should be confirmed in galvanic operation.
This chapter aims to investigate the evolution of methanol crossover during degradation tests, performed on two different Membrane Electrode Assemblies (MEAs), evaluating the influence of two operating strategies and anode methanol concentration. Moreover the effect of such methanol crossover variation on DMFC efficiency is investigated. As a last part of the chapter, several temporary degradation mechanisms such as hydrogen evolution, platinum oxides and water management are identified and evaluated with proper experimental tests in order to provide a complete overview on the different issues that occurs during the DMFC operation and determine recoverable performance losses.

4.2 Experimental methodology

The experimental setup used for the following tests has been previously described in 2.2.2; the most important modification of the experimental setup from the preliminary tests reported in chapter 2 is the introduction of the μGC setup for the anode and cathode DMFC effluents composition. The exhausts composition is measured by an SRA R-3000 μGC analyser equipped by three columns and preceded by a liquid-gas gravity separator at room temperature that has been developed ad-hoc for this purpose. The first column is nitrogen fed Molsieve for the hydrogen identification, the second one is helium fed Molsieve for nitrogen, oxygen and CO identification while the third one is helium fed PlotU for the CO_2 and light hydrocarbons identification such as methanol.

4.2.1 MEAs description

The first MEA used in this work is a commercial 22 cm^2 MEA: membrane is Nafion117, anode catalyst loading is 3 $mg \cdot cm^{-2}$ (Pt/Ru), cathode catalyst

loading is 1.2-1.4 $mg \cdot cm^{-2}$ (Pt). Anode diffusion layer is Sigracet SGL10CA (thickness 400 μm, 10% PTFE content, without microporous layer), while cathode diffusion layer is Sigracet SGL10CC (thickness 415 μm, 10% PTFE content, with microporous layer). During testing anode and cathode are fed respectively with 1.0 M methanol solution with stoichiometry equal to 3 and dry air with stoichiometry equal to 4. Nominal current density is 0.15 $A \cdot cm^{-2}$. The fuel cell temperature is kept at 60^oC by mean of a proportional, integral and derivative (PID) temperature controller.
Instead the second MEA used in this work is a commercial 25 cm^2 manufactured by IRD Fuel Cell A/S: membrane is Nafion115, anode catalyst loading is 1.8 $mg \cdot cm^{-2}$ (Pt/Ru), cathode catalyst loading is 1.2 - 1.4 $mg \cdot cm^{-2}$ (Pt). Both anode and cathode diffusion layer are Sigracet SGL35DC (thickness 325 μm, 20% PTFE content, with microporous layer). During testing, unless differently indicated, anode and cathode are fed respectively with 1.0 M methanol solution with stoichiometry equal to 6 and air, saturated by water at ambient temperature, with stoichiometry equal to 3. Nominal current density is 0.25 $A \cdot cm^{-2}$ and the fuel cell temperature is kept at 75^oC.

4.2.2 Performance characterizaton

	Unit	Reference Conditions	Other tested condition
T	^oC	75	65
CH_3OH conc.	M	1	2
Anode Mass flow	$g \cdot min^{-1}$	3.86 ($\lambda = 6$ @ $0.25\, A \cdot cm^{-2}, 1M$)	1.93 ($\lambda = 6$ @ $0.25\, A \cdot cm^{-2}, 1M$)
Cathode Mass flow	$Nl \cdot min^{-1}$	0.336 ($\lambda = 3$ @ $0.25\, A \cdot cm^{-2}$)	0.672 ($\lambda = 6$ @ $0.25\, A \cdot cm^{-2}$)
Current density	$A \cdot cm^{-2}$	0.25	0.01/0.05/0.1/0.15/ 0.2/0.3/0.35/0.4

Table 4.1: Investigated operating conditions

Prior to the investigation of DMFC degradation, a sensitivity analysis on the effect of operation parameters on the performances, mass transport phenomena and Electrochemical Impedance Spectra has been carried out.
An acquisition procedure has been developed to determine DMFC polarization characteristics for defined operating conditions and to evaluate mea-

surement reproducibility. It includes two steps: initial transitory and characteristic acquisition. The initial transitory consists in an acquisition period, performed in the investigated operating conditions at a current density of 0.1 $A \cdot cm^{-2}$, measuring voltage and current at 0.5 Hz for 30 min. The characteristic acquisition is composed of 9 single measurement points referred to different current densities (see Tab. 4.1), collected following one-way curves increasing current. Each single acquisition point is performed at constant current, measuring voltage and current at 0.5 Hz frequency for 600 s. After this time period, EIS is performed.
The data obtained from each single acquisition point are elaborated eliminating the initial transitory and outliers. The first 60 values are discarded, because resulting from the transitory caused by current variation. Instead a robust method is used to individuate outliers. It eliminates values not included in the interval median $\pm$ 2.5 times standard deviation, estimated through median absolute deviation. Finally, the last 240 points are selected as significant and mean values of voltage and current are calculated [67, 69]. The reference and the other tested operating conditions for the performance characterization are reported in Tab. 4.1; measurement repeatability has been verified by performing the test three times in three different days. Each polarization curve is performed with reactants constant flow rates in order to ensure the steady state operation and hence a good reproducibility of the impedance spectra.

4.3 Performance and mass transport characterization

Fig. 4.1 shows the polarization curves performed at the same temperature (75^oC) and cathode feeding (0.336 $Nl \cdot min^{-1}$) by changing the anode feeding (massflow and methanol concentration); the polarization curves performed at low methanol flow and concentration is the highest performances at low current densities and the lowest and high current densities. The former is due to the low methanol crossover from anode to cathode while the latter is due to mass transport limitations at the anode as confirmed by figure 3.2 in paragraph 3.3.

Fig. 4.2 reports the methanol crossover measurements acquired in different polarization curves during the sensitivity analysis; the higher the methanol concentration and the higher the methanol crossover confirming that it

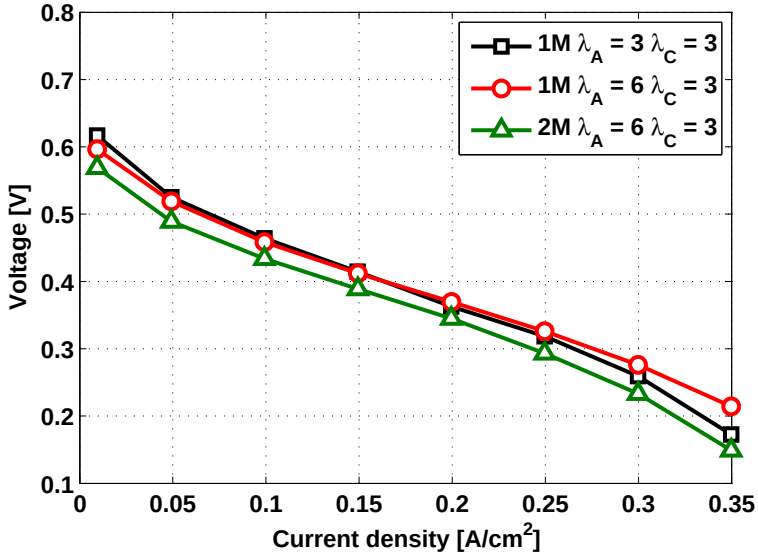

Figure 4.1: DMFC polarizations at 75^oC where λ is equivalent anode stoichiometry and cathode stoichiometry is constant and equal to 3.

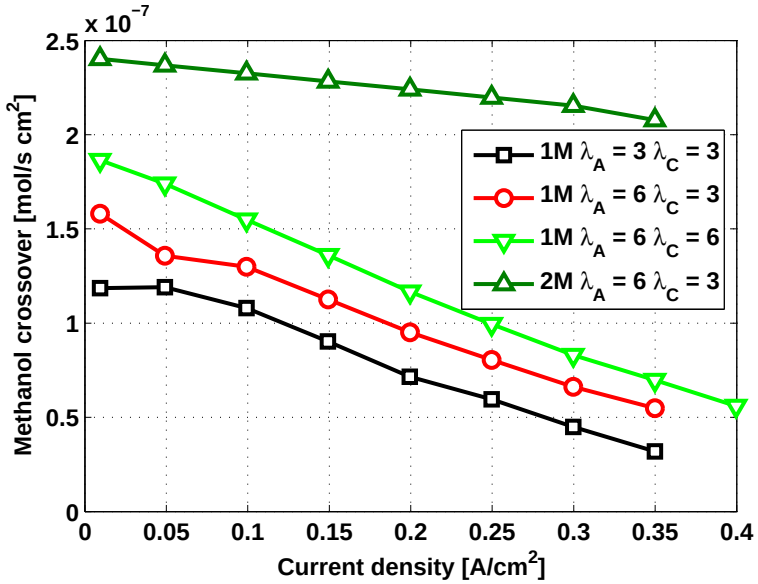

Figure 4.2: Methanol crossover during DMFC polarizations at 75^oC where λ_A is equivalent anode stoichiometry and λ_C is equivalent cathode stoichiometry.

is mainly due to diffusion and, hence, dependent on concentration gradient across the electrolytic membrane. Also the anode flow and the cathode flow have a slight effect on methanol crossover acquisition:

- a higher methanol massflow results in a higher methanol crossover due to a higher flow through the gas diffusion layer; it is probably due to a reduced effect of both two phase flow in the GDL and in the distributor channel;
- a higher cathode airflow results in a higher methanol crossover due to a reduction of the average methanol concentration at the cathode side as reported in [8].

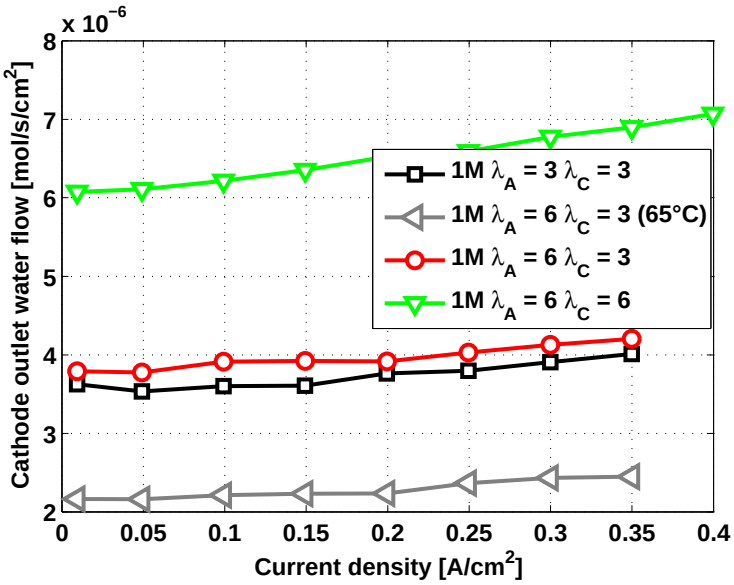

Figure 4.3: Water Content in cathode outlet during DMFC polarizations at 75^oC and 65^oC where λ_A is equivalent anode stoichiometry and λ_C is equivalent cathode stoichiometry.

In figure 4.3 the water content in cathode outlet is reported as a function of different operating parameters;

- the higher the air flow rate and the higher the water content due to the lower average water concentration in the cathode electrode;
- the lower the temperature, the higher the water content in cathode outlet strongly decreases;

- the water content in cathode outlet does not significantly change by increasing the current density (that is the water production);

These results confirm that the water transport through the cathode GDL occurs by water diffusion; indeed the GDL diffusion coefficient is dependent on temperature as in [83] and the water transport depends also on the concentration gradient across the GDL (regulated by the saturation concentration that depends on DMFC temperature).
The third key-point of the previous list reveals that the cathode electrode water concentration is probably equal to the saturation value and the increase in current density determines a increase in liquid water pressure; in these conditions, since the GDL with MPL is strongly hydrophobic (chapter 5), the increase in water pressure is not enough to make the GDL breakthrough occurring and the mass transport occurs by diffusion regulated by the saturation concentration at the electrode-GDL interface.

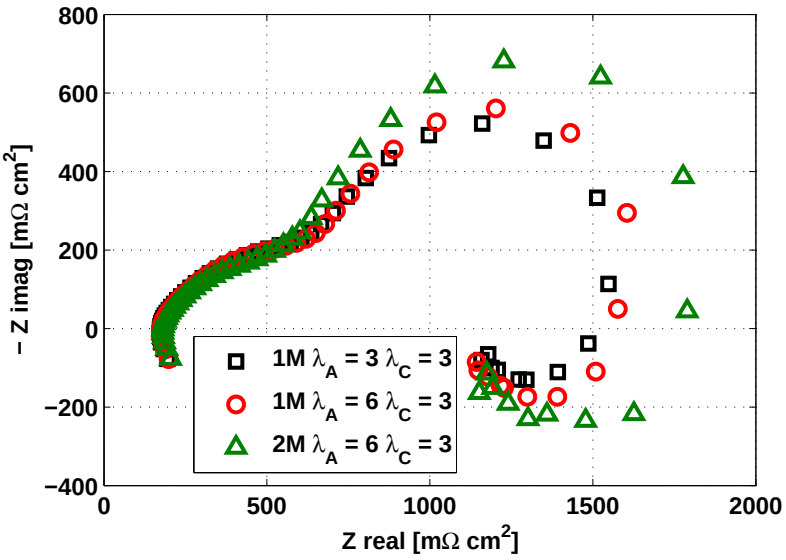

Figure 4.4: DMFC EIS at 0.1 $A \cdot cm^{-2}$ at $75^{o}C$.

Fig. 4.4 illustrates different DMFC spectra at a low current density equal to 0.1 $A \cdot cm^{-2}$ varying methanol inlet concentration and flow rate at constant cathode flow. The impact of doubling methanol massflow is not important on the whole spectrum whereas doubling the methanol concentration determines a strong modification on it. The strong increase in the inductive behaviour at low frequencies confirms that, in a DMFC spectrum, the anode spectrum is superimposed respect to the cathode one but it is mainly evident at low frequencies.

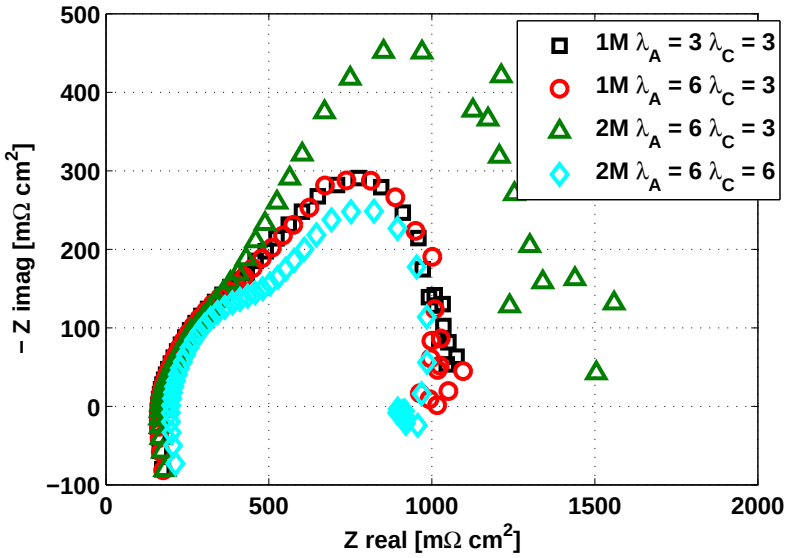

Figure 4.5: DMFC EIS at 0.25 $A \cdot cm^{-2}$ at $75^{o}C$.

Increasing the current density to the nominal one as showed in figure 4.5, the qualitative interpretation of the EIS leads to a deeper comprehension of the effect of methanol crossover on the cathode performance and spectra. Starting from the reference conditions spectrum (the red EIS), if the methanol massflow is reduced (the black EIS) anode mass transport limitation appears next to the real axis according to figure 3.4 of chapter 3.On the other hand, if the methanol concentration is doubled to 2M (the greenfinch EIS) important disturbances due to mass transport limitations occurs and they are probably due to the effect of the increased methanol crossover (according to 4.2) on the cathode oxygen concentration; this disturbances appears quite far from the real axis contrarily to the anode mass transport limitations previously explained. As a confirmation of the cathode mass transport limitation, if the cathode massflow is doubled (the cyan EIS), the disturbances completely disappear and a small inductive behaviour is evident at low frequencies due to the anode increased methanol concentration. This methanol crossover effect at the cathode of a DMFC determines the lowest performances of the 2M polarization curve reported in figure 4.1.

4.4 Steady state operation

4.4.1 Mass transport measurements on the preliminary MEA

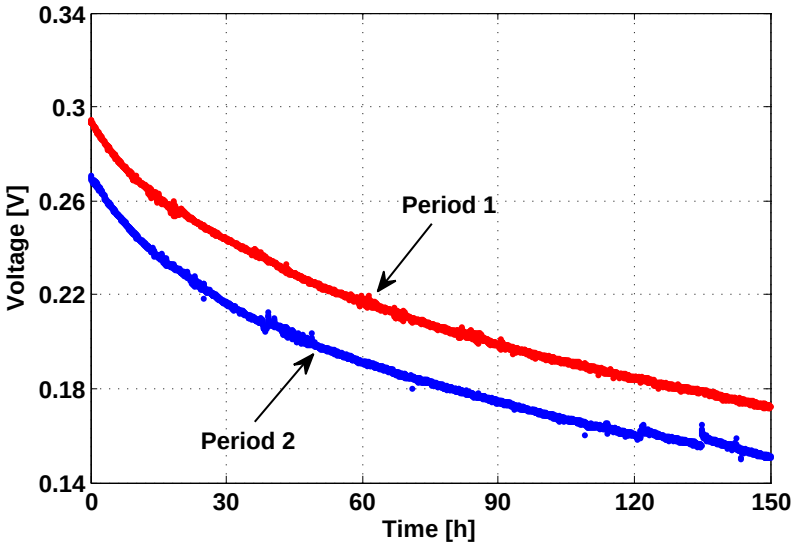

Figure 4.6: Voltage decay during two consecutive tests in continuous operation performed on the first MEA at 0.15 $A \cdot cm^{-2}$.

The test performed on the first MEA is composed of two continuous operation periods at constant current density interspersed with an interruption when diagnostic is performed, as reported in Fig. 4.6. The following procedure, previously described as long refresh, is performed before each test: OCV is hold for few seconds with air feeding, then the air supply is switched off, while the methanol solution circulation is kept for five hours. This procedure allows recovering most of the temporary degradation resulting in a considerable voltage recovery, but the reasons are still not fully understood [19, 20, 28]. In Fig. 4.6 the two components of the DMFC degradation can be clearly distinguished: the temporary one, that can be recovered, and the permanent one, that appears as a downward shift of the performances between the two tests.
Permanent degradation, calculated as in [71], is equal to 148 $\mu V \cdot h^{-1}$, a small part of the overall degradation, 770 $\mu V \cdot h^{-1}$, calculated as the difference between the initial and final voltages of the first test divided for the test duration; in fact the voltage drop associated with the first test is considerably higher than the downward shift between the two tests. Some researchers

attribute DMFC temporary degradation to mass transport issues in cathode GDL and platinum oxide formation on cathode electrode [37]. An anode contribution to temporary degradation has been recently described in Ref. [82] and attributed to the reduction of methanol and water concentrations in the anode GDL and electrode.

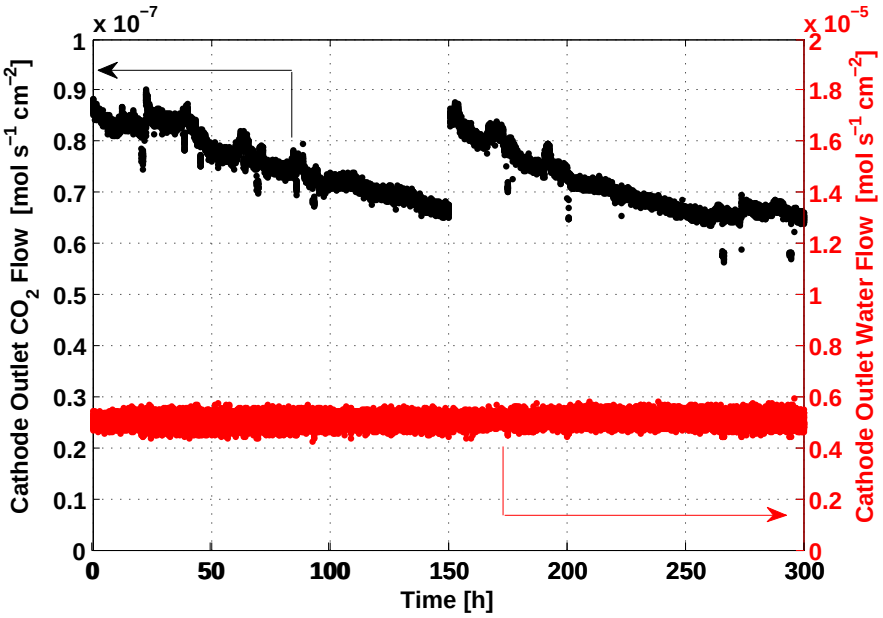

Figure 4.7: CO_2 and water content at cathode outlet during the continuous degradation tests performed on the first MEA.

Figure 4.7 shows the measurements of CO_2 and water content in cathode exhaust during the two consecutive degradation tests; they highlight a decrease of CO_2 content at cathode outlet during each test during each test and a considerable recovery after operation interruption. Such reduction could be due to two possible reasons:

- a reduction of cathode effectiveness to methanol oxidation; in this case the methanol crossover could be constant while the CO_2 content in cathode outlet could decrease;
- a reduction of methanol concentration at the anode electrode due to CO_2 bubbles accumulation that can determine mass transport limitations [28, 82]; since the methanol crossover is related to methanol concentration gradient across the membrane, the lower is the concentration at anode electrode, the lower is methanol crossover.

A considerable variation of membrane properties (i.e. electro-osmotic drag and diffusivities), able to determine the observed reduction of methanol crossover, is excluded, because it can occur in such intensity exclusively during long-term tests and can not be recovered so quickly and easily. Likewise cathode GDL degradation can be excluded since water content in cathode exhaust, mainly dependent on cathode GDL properties [9], remains approximately constant during the tests. Analogously a considerable anode GDL degradation is improbable: it usually determines a reduction of material hydrophobicity [85] and an increase of diffusivity[1] that would determine an increase of methanol crossover.
As a consequence two possible explanations for the recovery of CO_2 content after the diagnostics are plausible; they are coherent respectively with the two previously proposed interpretations:

- the refresh procedure performed during the interruption determines a strong increase in cathode performance for two different reasons: the first period with air supply at OCV allows removing water flooding, that hinders cathode electrode performance; the second period without air supply permits to decrease the cathode potential under 0.5 V, allowing the reduction of platinum oxides with a consequent recover of platinum active surface [37];

- the interruption determines a progressive removal of CO_2 bubbles that hinder the correct operation of the anode electrode, determining an increase of methanol concentration at the anode and the consequent increase of methanol crossover [82].

A more detailed analysis has been carried out on the second MEA, previously described, to elucidate further these phenomena.

4.4.2 Mass transport measurements on the reference MEA

Thanks to experimental setup improvements, the second MEA has been characterized more completely, including the analysis of cathode exhaust composition. Two consecutive continuous operation tests have been performed at two different methanol concentrations, keeping the mixture flow constant (1M during period 1 and 2M during period 2), in order to investigate the effect of anode methanol concentration on crossover evolution, as reported

[1] affected also by the capability to stay effectively hydrated, therefore related to membrane cristallinity and extension of the hydrophilic ionic zone [86].

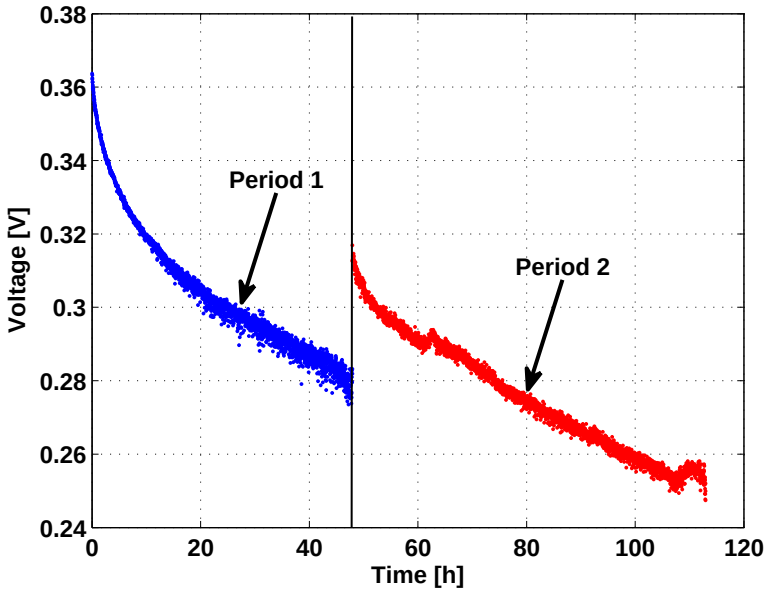

Figure 4.8: Voltage decay during two consecutive tests in continuous operation, performed on the second MEA at 0.25 $A \cdot cm^{-2}$: period 1 at 1M, period 2 at 2M.

in Fig. 4.8.

During the first period the cell has been operated for 50 hours with 1M concentration. As previously CO_2 and water content in cathode outlet are continuously measured; furthermore cathode exhaust is connected to the gas chromatograph where the dry composition is continuously analysed. From the exhaust composition acquired during period 1, Fig. 4.9, it is possible to highlight the following key points:

- the CO_2 content in cathode outlet decreases during operation, while water content remains approximately constant, coherently with the previous test;
- the amount of unconsumed methanol detected in the cathode exhaust is very limited and remains almost constant during the test[2];
- the oxygen content in cathode outlet progressively increases.

[2]It is necessary to underline that methanol concentration in the cathode exhaust is significantly lower than the saturation value at ambient temperature, confirming the measurement reliability.

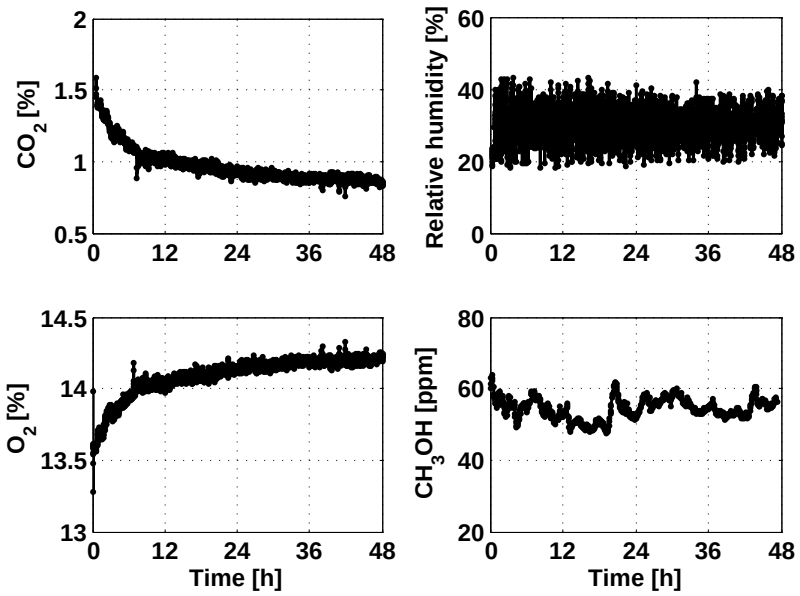

Figure 4.9: Cathode outlet composition analysis during continuous operation test during period 1 (1M).

These results permit to state that methanol crossover effectively decreases during the DMFC continuous operation, implying a reduction of CO_2 content in cathode exhaust, a constant methanol content and a reduction of oxygen consumption. Therefore CO_2 content in cathode outlet is confirmed to be a proper proxy for methanol crossover also during degradation tests. Moreover, a substantial recoverability of both voltage degradation and methanol crossover decrease has been verified, confirming the results obtained with the first MEA. Consequently the most probable origin of such methanol crossover reduction is the second possibility previously mentioned: the decrease of local methanol concentration in the electrode, caused by gas-phase CO_2 accumulation within electrode and GDL, as recently proposed in Ref. [82].
Doubling the methanol concentration, period 2, DMFC performance is hindered. Since methanol crossover is proportional to methanol concentration in the anode electrode and considering that the air stoichiometry is kept constant during all the tests, it is clear that oxygen transport limitations can occur at cathode due to a more intense methanol oxidation.

The exhaust composition results related to period 2, Fig. 4.10, are coherent with the proposed interpretation:

- the CO_2 content in cathode exhaust is significantly higher than in the

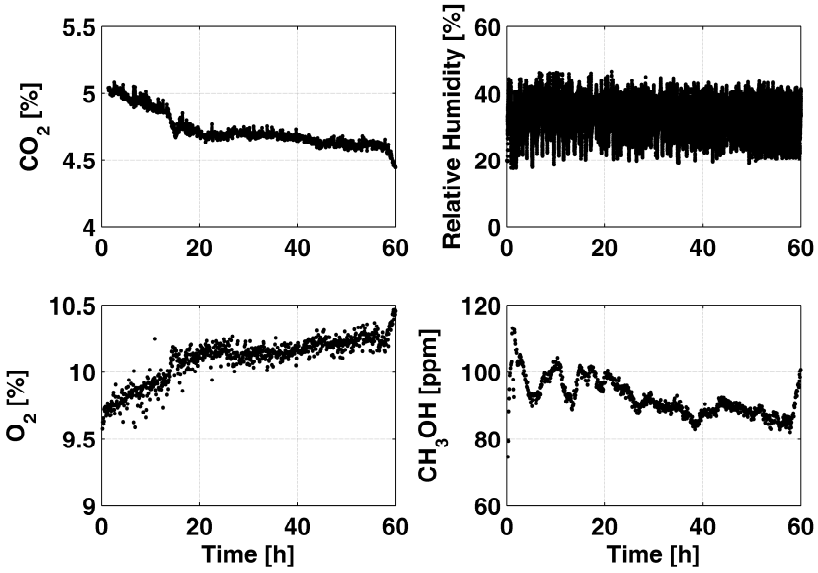

Figure 4.10: Cathode outlet composition analysis during continuous operation test during period 2 (2M).

previous test coherently with the doubled anode methanol concentration; it significantly decreases in absolute value, but the relative decrease is lower than in the previous case;

- the oxygen content is considerably lower than in the previous case coherently with a strong increase in methanol crossover; it increases during the test as the CO_2 content decreases;
- the unconsumed methanol content is higher than in the previous case but still not relevant; it remains almost constant during the operation.

4.4.3 Effects on DMFC efficiency

Despite the continuous operation is not the common way to operate a real DMFC system, it is interesting to compare the influence of performance and methanol crossover reductions on the DMFC efficiency as defined in Ref. [8], considering unconsumed fuel recirculation:

$$\eta = \frac{V \cdot I}{\left(N_{CH_3OH}^{a,reaction} + N_{CH_3OH}^{crossover}\right) \cdot LHV_{CH_3OH}} \tag{4.1}$$

where the converted fuel flow includes the fractions used in the anode electrochemical reaction $N_{CH_3OH}^{a,reaction}$ and wasted with methanol crossover at

the cathode $N_{CH_3OH}^{crossover}$. In this work the fuel recirculation is not really performed in order to avoid fuel contaminant accumulation that could have an unpredictable effect on degradation tests.

	After 2 hours	After 20 hours	After 50 hours
1 Molar (period 1)			
Power reduction [%]	100	87	80
Crossover reduction [%]	100	72	61
Efficiency reduction [%]	100	92	86
2 Molar (period 2)			
Power reduction [%]	100	93	85
Crossover reduction [%]	100	93	90
Efficiency reduction [%]	100	94	86

Table 4.2: Summary of power, methanol crossover and efficiency reduction during continuous operation at 1 M and 2 M.

Tab. 4.2 shows a comparison among the variations of power, methanol crossover and efficiency during tests. Period 1 is characterized by a crossover reduction that is more intense than the power one; this determines a less pronounced reduction of DMFC efficiency compared to power one. During period 2 power and crossover reductions are less severe than during period 1; in this case the positive effect of crossover reduction on efficiency appears less evident. This analysis permits to conclude that in some conditions methanol crossover evolution, determining a reduction of cathode parasitic loss and methanol wasting, can partially mitigate the effect of performance degradation on DMFC efficiency, in fact the voltage decrease, caused by membrane and electrodes degradation, still remains the dominant effect.

4.5 Cycling operation

4.5.1 Description of the operating strategy

The literature presents different operating strategies to minimize the temporary degradation that, adopting continuous operation, leads to a dramatic reduction of DMFC power, as previously discussed. For this reason, DMFCs are often coupled with batteries to cover load peaks and operation interruption, ensuring power continuity for the user. Among different possible

operating strategies, one suggested by IRD Fuel Cell A/S has been chosen: it consists in 20 minutes of operation interspersed by 1 minute refresh procedure. The latter is composed of a sequence of OCV and cathode air feeding interruption, similar to that reported in Ref. [20], that allows recovering the temporary degradation. During the OCV period, after the air feeding is switched off, the cathode potential drops to less than 0.3 V and, when the operation restarts, a significant positive effect on performances is obtained. The reason of such refresh effect on temporary degradation is still not fully understood. The following interpretation can be proposed. The OCV period reduces the cathode flooding, because of the temporary absence of electro-osmosis and water production, as also reported in Ref. [39]. Furthermore, when the air feeding is interrupted, oxygen is depleted by methanol crossover leading to a strong decrease of cathode potential, resulting in a reduction of cathode platinum oxides, that were previously formed during operation at high potential [37]. Moreover during operation interruption, the gas-phase CO_2 accumulated in anode GDL and electrode is removed [82].
However the aspect of refresh procedure will be deepen in the continuation of this PhD thesis.

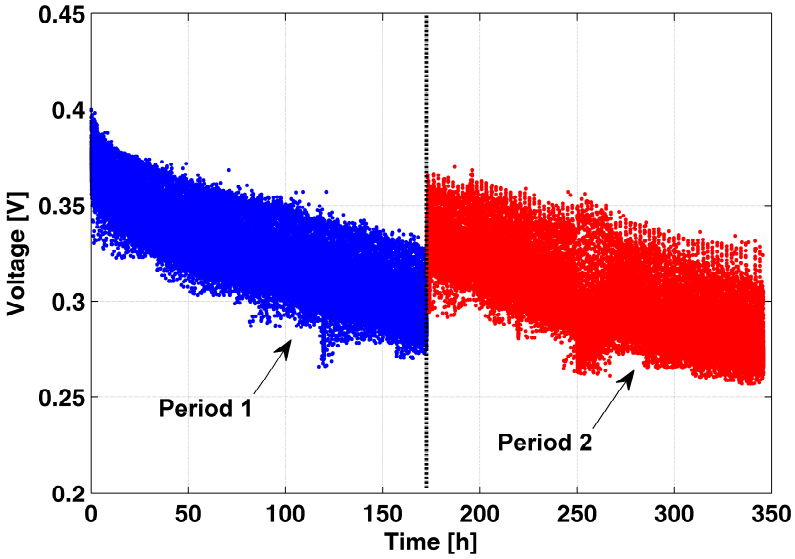

Figure 4.11: Voltage decay during two consecutive tests in cycling operation performed on the second MEA at 0.25 $A \cdot cm^{-2}$.

Fig. 4.11 shows the degradation test performed on the second MEA; it is composed of two test periods in similar conditions: period 1 and period 2, interspersed by a long refresh, as previously described. Such procedure

still permits a considerable performance recovery: the voltage value at the beginning of period 2 is considerably higher than that at the end of period 1, suggesting that the adopted operating strategy is not sufficient to fully recover temporary degradation. In both cases the appearing degradation rate is about 320 $\mu V \cdot h^{-1}$, calculated with the method reported in Ref. [71] and in chapter 2.

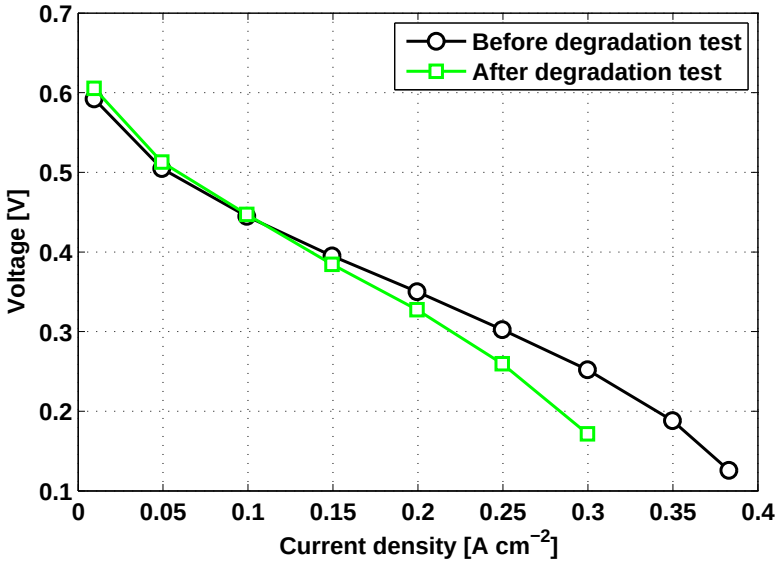

Figure 4.12: Polarization curves at start/end of the degradation test (3.86 $g \cdot min^{-1}$ of mixture at 1M, 0.336 $g \cdot min^{-1}$ of air).

Polarization curve tests, including mass transport measurements, have been performed before and after the whole degradation test, in order to evaluate the permanent degradation[3], Fig. 4.12. A difference of 40 mV between the two curves, at the nominal current density of 0.25 $A \cdot cm^{-2}$, is calculated; the resulting permanent degradation rate is equal to 123 $\mu V \cdot h^{-1}$, much lower than the appearing degradation.

4.5.2 Mass transport analysis

The measurements of methanol crossover, during the above-mentioned tests, are reported in Fig. 4.13: methanol crossover tends to decrease during period 1, then, during the interruption, it recovers and decreases again during

[3]The polarization curve test is performed after a long refresh procedure in order to nullify the effect of accumulated temporary degradation.

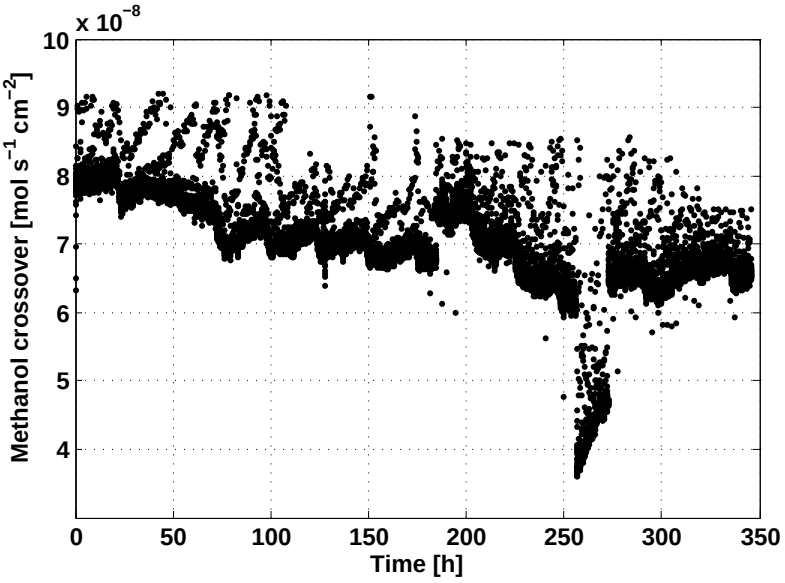

Figure 4.13: Methanol crossover evolution during the degradation test.

period 2[4]. This result is coherent with the continuous operation ones, but the decrease of methanol crossover now is less pronounced, confirming a correlation between temporary degradation and methanol crossover decrease. Fig. 4.14 shows the methanol crossover values measured during the two polarization curves reported in Fig. 6: a reduction of methanol crossover in reference conditions is evident.

As a consequence the reduction of methanol crossover during the DMFC operation appears determined by two contributions, similarly to voltage degradation: a temporary one, that can be recovered by refilling the anode with fresh mixture during the operation interruption, and a permanent one, that could be indicative of a membrane alteration. The latter, in accordance with the measurements reported in [47, 31], can be related to a loss of ionomeric groups and an increase in cristallinity, that implies a reduction of hydrophilic proton conductive zone, and can be already evident after 200 h of operation.
Methanol crossover evolution is related to two main factors: methanol concentration at the anode electrode and transport properties of the electrolytic membrane. Since polarization curves are comparable and acquired in reference conditions, a similar methanol concentration profiles at the electrode

[4]Unfortunately a testing setup failure determined a period of improper operating conditions about the 240^{th} hour, hindering the reliability of period 2 data.

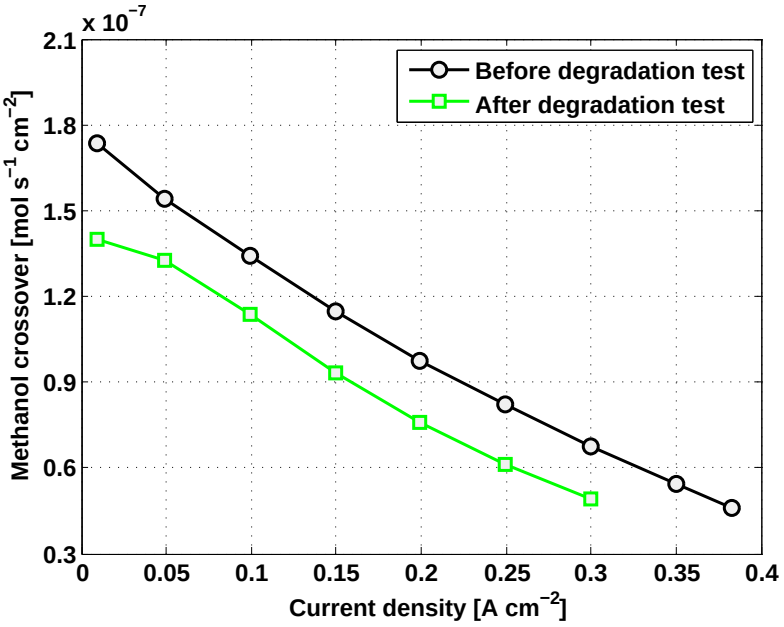

Figure 4.14: Methanol crossover measured during polarization curves.

can be reasonably assumed; therefore the permanent reduction of methanol crossover is probably related to a modification of membrane properties. This is confirmed by an increase of membrane ionic resistance, measured by the AC milliohmeter: respectively equal to 155 $mOhm \cdot cm^2$ and 191 $mOhm \cdot cm^2$ at beginning and end of test. Note that no significant membrane properties modification is observed in the previous tests, probably because the first MEA presented a thicker and more stable membrane, while the continuous tests on the second MEA have a too short duration. Hence, by applying the Ohm's law, it is possible to calculate the potential drop that can be associated to the membrane degradation: 9 mV less than 25% of permanent degradation calculated from polarization curves. Once the contribution of membrane degradation is quantified and the degradation of the GDLs is assumed negligible, more than 75 % of permanent degradation can be attributed to the electrodes. The DMFC efficiency reduction is comparable with power decrease, because the reduction of methanol crossover is appreciable but its effect is not very significant, similarly to the 2 M case of the first MEA. Further ex-situ investigations are needed to identify the mechanisms that lead to membrane modification during operation and to clarify the degradation mechanisms that occur at the anode and cathode electrodes.

4.6 Summary on Methanol crossover characterization in DMFC degradation tests

This part of the chapter presents an experimental investigation of methanol crossover during degradation tests, performed adopting different operating strategies on two different MEAs. The main conclusions that can be drawn are:

- the methanol crossover decreases considerably in continuous operation, while the reduction is less pronounced adopting a suitable operating strategy, coherently with the performance degradation;
- the water content at cathode outlet remains almost constant during degradation tests; therefore cathode GDL degradation seems to be negligible;
- the methanol crossover reduction could be associated to two different phenomena: a temporary one, probably due to a decrease of methanol concentration and CO_2 accumulation at anode electrode, and a permanent one that seems to be related to membrane alteration;
- the methanol crossover reduction during degradation tests has a significant positive impact on DMFC efficiency, especially during operation with 1 M methanol feeding.

4.7 Investigation on the other main temporary degradation mechanisms

In the first part of this chapter, the methanol crossover evolution during DMFC degradation tests has been investigated as a confirmation for the proposed anode temporary degradation mechanism. However, the literature tends to identify other temporary degradation mechanisms that should be investigated in order to look for a DMFC temporary degradation minimization procedure such as Platinum oxides formation, water management and anode hydrogen evolution.
In chapter 2, a comparison of DMFC operating strategies is presented and the refresh cycle is introduced as the most effective procedure for the temporary degradation reduction. However, coherently with what observed in 3.4, the refresh duration can be changed in order to understand the main temporary degradation mechanisms. Analogously to chapter 3, a sensitivity analysis on the effect of the operation interruption duration has been carried

out in galvanic operation and the voltage behaviour in time is reported in figure 4.15.

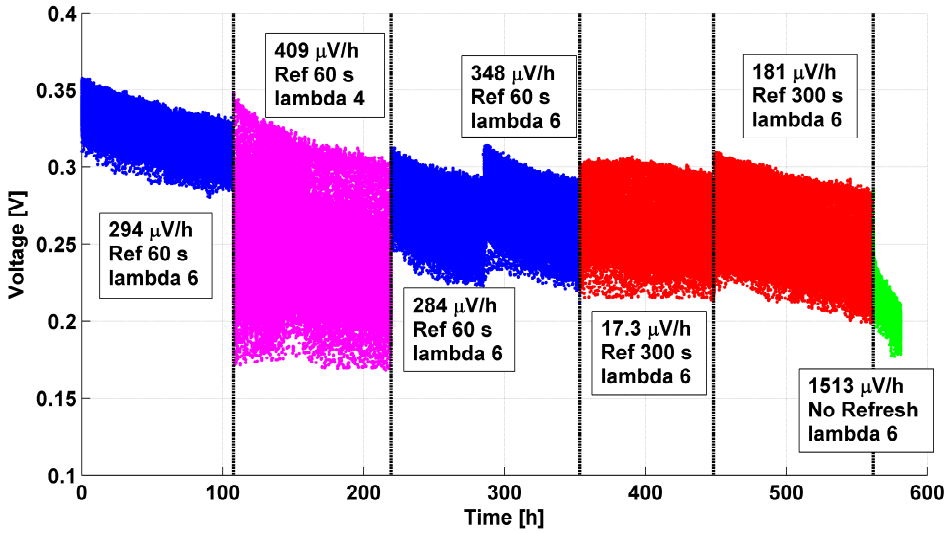

Figure 4.15: Sensitivity analysis on the effect of refresh duration and anodic λ on degradation at 0.25 $A \cdot cm^{-2}$.

In Fig. 4.15 a summary of the most interesting results is reported. In reference condition, acquisition from hour to 0 to 110 in Fig. 4.15, operating with a 1 *min* interruption with refresh cycle every 20 *min*, the DMFC degradation rate is higher than in the anode operation, 294 $\mu V \cdot h^{-1}$ in comparison with 147 $\mu V \cdot h^{-1}$ (obtained from figure 3.5) confirming that there are other temporary degradation mechanisms that should be taken into account. Nevertheless, an important performance recovery is obtained when the operation is interrupted for diagnostic confirming that the greatest part of the degradation is recoverable.
During the second period, from hour 110 to 210, cathode stoichiometry is reduced to 4 (3 does not permit a continuous and regular operation) and performance fluctuations resulting in the higher width of the acquisition points. In the third period the reference conditions have been again set and the degradation rate is comparable and no coupling effects are evident. Increasing the refresh duration from 1 *min* to 5 *min*, from hour 450 to 550 an important reduction of degradation rate is obtained to 181 $\mu V \cdot h^{-1}$; on the other hand a very interesting behaviour can be observed in the periods from hours 290 to 450. A reference test is performed during from hour 290 to 350 and a degradation rate of 340 $\mu V \cdot h^{-1}$ is observed; after hour 350 the refresh duration has been increased to 1 *min* to 5 *min* without any interrup-

tion for diagnostic and this test, from hour 350 to 450 presents a very low degradation rate and a unusual behaviour.
Indeed, when the refresh duration is increased, a immediate positive effect on the performances is observed (with a duration lower than 1 hour) together with a significant change of the time-voltage slope that becomes positive for about 40 hours; during this period, methanol crossover increases contrarily to all the other degradation tests. This two different phenomena that have significantly different recovery time further confirms that there are other temporary degradation mechanisms and, according to what explained in chapter 3, the CO_2 removal from the anode electrode, has the longest recovery time coherently with the methanol crossover increase from hours 340 to about 390. The probable origin of the fast performance recovery observed at hour 340 is a change in the dynamic of platinum oxides formation and reduction that is favoured from the no-air period increase of the refresh cycle and this argument is deepened in the next sub-paragraph (4.7.1) or a re-equilibrium in the hydration of the cathode electrode ionomer.
The degradation rate calculation described in paragraph 2.5.1 provides information on the slope of performance loss but it cannot provide information on the effectiveness on the refresh cycle to recovery the voltage[5]. A Refresh Recovery Index (RRI) is introduced as a tool to provide information on the effectiveness of each refresh cycle on the performance recovery. It consists in the evaluation of the performance recovery that corresponds to each operation interruption and it is calculated as the average of the differences between the values (described in 2.6) of the 1^{st} minute of the cycle i and of the 20^{th} minute of the cycle $i-1$ during all the test duration; Its uncertainty can be expressed by means of the 95% confidence interval. A typical value for Refresh Recovery Index in reference conditions (1 min refresh every 20 min operation) is 21.8 mV.

4.7.1 Platinum Oxides

Since the DMFC anode overpotential is usually significant, a high cathode potential is required in order to obtain a high DMFC efficiency and, for this reason, a DMFC cathode operates at potential that could often be higher than 0.8 V versus the hydrogen reference electrode (RHE). Indeed, literature does not propose reliable and feasible in-situ hydrogen reference electrodes for DMFC [87] and it results in an unknown cathode potential during the operation. Thus, according to the anode overpotential measurements obtained

[5]It is possible to imagine that two tests can have the same degradation rate but a very different performance loss / performance recovery after 20 min of operation / 1 min of interruption

in chapter 3 and to the DMFC galvanic performances, it is possible to estimate the cathode potential and, in reference conditions (i.e. 0.25 $A \cdot cm^{-2}$) it results equal to 0.8 V.
There are few oxygen reduction electro-catalysts that are enough active and stable under the operating conditions of a DMFC cathode. None of these catalysts remains unaffected by the cathode operating conditions, especially at long operating times. On platinum, which is by far the most important cathode catalyst for polymer electrolyte fuel cells (DMFC included), a layer of oxide slowly develops, influencing the electro-catalytic properties of the metal. Literature reveals that the Platinum Oxides Layer can affect several processes such as electro-oxidations [88] and electro-reductions [89], which take place at high positive potentials.
The Oxidation Reduction Reaction (ORR) on platinum catalyst is deeply studied both on ex-situ and in-situ PEFC operating conditions but the influence of the Pt oxide layer on the ORR is not yet understood. One difficulty associated with such studies is the narrow width of the potential window where the coverage of Platinum by the oxide layer and the rate of oxygen reduction (ORR) are both significant. The existing literature provides evidence of oxygen reduction being inhibited in the presence of the oxide layer. However, the nature and extent of the inhibition are yet unknown. In particular, it is not known whether Pt oxide formation induces a change in the ORR mechanism, modifies the rates of the ORR constituent steps, or simply diminishes the number of active catalyst sites. There is a continuing controversy regarding the mechanism of the oxidation process. According to Conway et al. [90], Pt oxide formation takes place in at least two phases: first, reversible formation of $Pt - OH$ and, second, irreversible $Pt - OH$ turnover process. Depending on the electrode potential, these two steps may or may not be followed by $Pt == O$ and PtO_2 formation. Harrington et al. [91] do not confirm the existence of reversible surface species at the early stage of Pt surface oxidation. Instead, they propose one-step formation of the oxide species, followed by fast surface migration of the species, a process responsible for the Pt surface reconstruction once the oxide is reduced.
In [37], the kinetics of Pt oxide formation on the fuel-cell-type electrode was examined at electrode potentials in the absence of gas-phase oxygen. The law appears to be fulfilled in the case of the nanoparticle Pt electrode in Nafion electrolyte up to a time of about 2 hours. At even longer oxidation times, the oxide formation process seems to reach saturation. In general, for the Pt oxide formation to break from the direct logarithmic growth law and reach sub-monolayer saturation coverage, either a relatively fast reverse oxide reduction process is required or some long-range "repulsive" interaction in the oxide layer should be present, but, according to the author, the first

theory seems to be more reliable. Furthermore Eickes et al. [37] reveals that the oxide reduction peak shifts to more negative potential as the oxidation time is increased. However, as showed in figure 4.6, cell performance keeps decreasing at times longer than 2 h, i.e., after saturation with surface oxide should already be reached. Clearly, blocking of metallic Pt sites by the oxide cannot be used as the sole reason of the recoverable drop in the cathode performance, certainly not at long operating times. From the comparison of the percentage decrease of the oxide-free Pt surface area and the percentage drop of the cell current, one may conclude that surface oxidation is more likely to result in the ultimate formation of $Pt == O$ rather than $Pt - OH$. This reasoning is based on relatively well-founded assumptions that firstly the rate of oxygen reduction remains kinetically controlled and secondly surface Pt oxide shows no activity in oxygen reduction.
It is possible to speculate [37] that some kind of oxide reconstruction process continues beyond the time required to reach saturation of the catalyst surface with the oxide. In principle, this reconstruction process can be responsible for the recoverable performance degradation beyond the first 2 h of cell operation. The oxide restructuring process appears even more important in limiting cathode performance in view of the fact that under true DMFC cathode operating conditions the rate of Pt oxide formation is probably faster than established in [37] in the absence of molecular oxygen.
Moreover it could be an unknown effect of Ruthenium crossover from the anode to the cathode that is one of the main DMFC permanent degradation mechanisms and, as described by ex-situ measurements performed at DLR in the frame of Premium ACT project, it starts also during the DMFC activation; indeed Ruthenium can be easily oxidized and it could promote both platinum oxidation and a reduction of ORR kinetic.

Coming back to the experimental data obtained in chapter 2 and taking into account the theoretical explanation founded in [37], it is possible to conclude that the refresh cycle reduces the surface oxides during the air-break phase (when cathode potential is lowered). When the cathode air feeding is interrupted, oxygen in the cathode channel is quickly consumed, predominantly in the oxidation of crossover methanol. This leads to the lowering of the cathode potential below the value required for complete reduction of the cathode surface and this results in a strong different behaviour between refresh and OCV cycles for a 120 hours test performed in reference conditions and whose biexponential interpolations are showed in figure 4.16.
The Refresh Recovery Index obtained during the OCV cycles is equal to 4.8 mV that is significantly lower than the reference value that is equal to 21.8 mV confirming that there is a strong difference in the physical phenomena

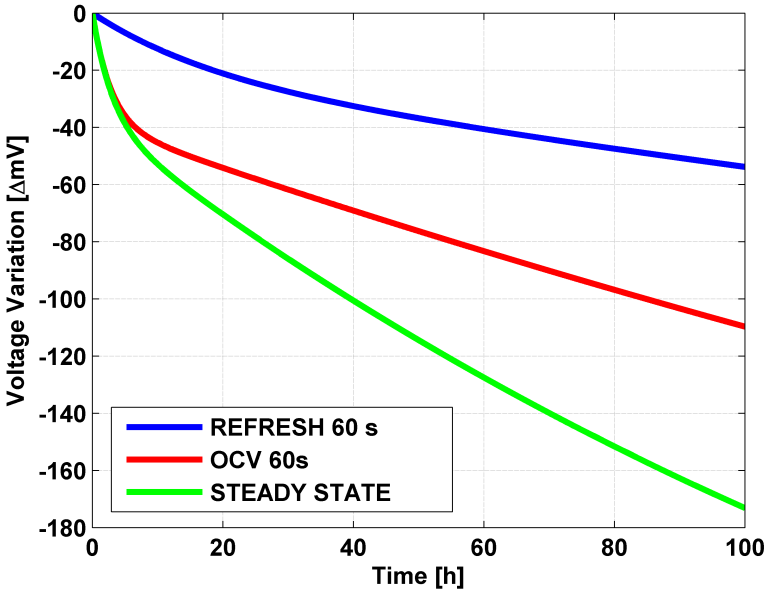

Figure 4.16: Biexponential interpolation of Steady State, OCV and Refresh tests.

that occurs during the Open Circuit Voltage period and the Refresh Cycle. According to what observed in [37], it is also possible to speculate that increasing the refresh duration, as reported in figure 4.15, can have a positive effect on surface platinum oxides reduction .

4.7.2 Electrolytic Hydrogen Evolution

Another interesting DMFC temporary degradation mechanism that has been previously also cited in chapter 3 is the so-called "Electrolytic Hydrogen Evolution" and it occurs during the refresh cycle; it has been independently and simultaneously reported from two research groups, one from Hong-Kong university [78, 92, 93] and one from Julich research Center [79, 94, 95, 96].
According to [78], the mechanism leading to the gas evolution in the anode flow field under the conditions after the external electrical load is removed and the oxygen supply is cut off or started up can be explained as follows. Because the methanol solution feed is kept open, the crossover of methanol and water from the anode to the cathode continues. Thus, on the cathode, the permeated methanol reacts with oxygen, if available. After the oxygen supply is cut off, the residual oxygen primarily in the flow field channels sustains the reaction between the permeated methanol and oxygen. As schematically

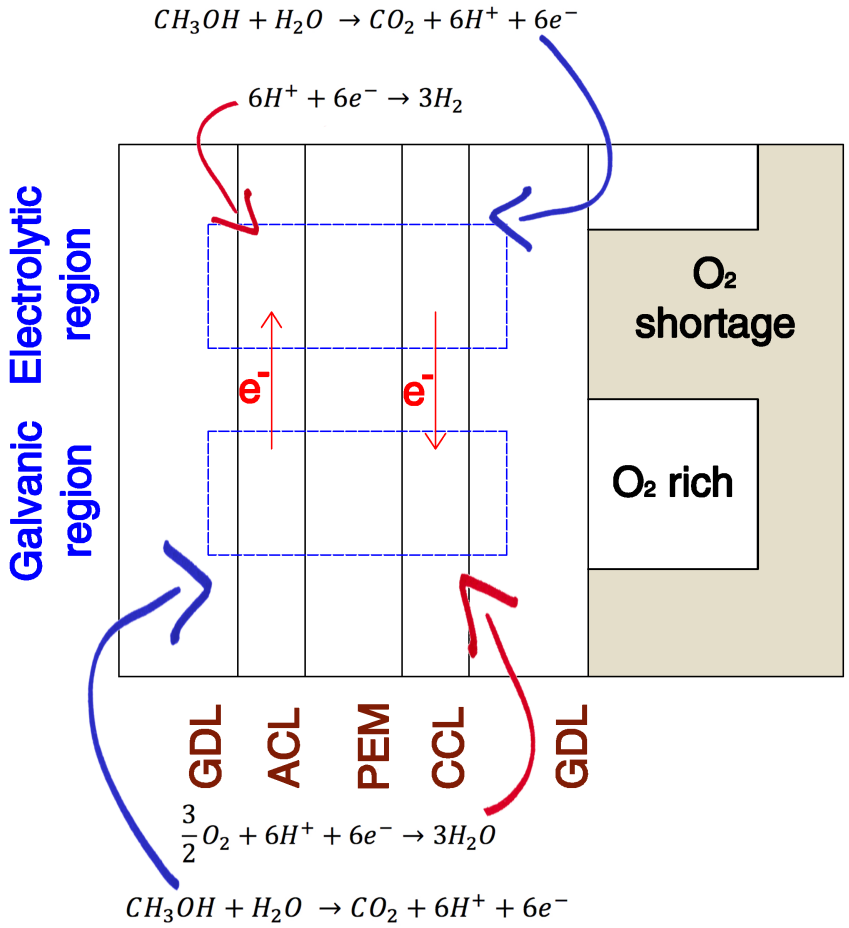

Figure 4.17: Schematical explanation of the electrolytic hydrogen evolution mechanism.

illustrated in Fig. 4.17, this reaction will cause oxygen in the region under the channel ribs to be exhausted first, forming an oxygen depletion region. On the other hand, in the region under the channel openings oxygen still remains relatively richer, forming a localized oxygen-rich region. Although the two regions are connected in parallel by both of the electrodes and the electrolyte membrane, the lateral proton conduction in the electrolyte is so low that the oxygen-lean and oxygen-rich sections of the cell act as if they were two independent cells that are connected electrically but not ionically. The oxygen depletion region acts as an electrolytic cell, whereas the oxygen rich region still acts as a galvanic cell (the usual DMFC operation) that provides a voltage between the two electrodes. In the oxygen depletion region, the following electrolytic reactions take place:

$$CH_3OH + H_2O \longrightarrow CO_2 + 6H^+ + 6e^- \qquad (on\,the\,DMFC\,cathode) \quad (4.2)$$

and

$$6H^+ + 6e^- \longrightarrow 3H_2 \qquad (on\,the\,DMFC\,anode) \quad (4.3)$$

The above reactions are powered by the following galvanic cell reactions:

$$CH_3OH + H_2O \longrightarrow CO_2 + 6H^+ + 6e^- \qquad (on\,the\,DMFC\,anode) \quad (4.4)$$

and

$$\frac{3}{2}O_2 + +6H^+ + 6e^- \longrightarrow 3H_2O \qquad (on\,the\,DMFC\,cathode) \quad (4.5)$$

which take place in the oxygen rich-region. Reactions 4.3 and 4.4 explain why the hydrogen evolution is observed in the anode flow field of the DMFC under open-circuit conditions after the oxygen feed was cut off. Reactions 4.2 and 4.5 originate from the non-uniform distribution of oxygen on the cathode caused by the oxygen supply cut-off. Therefore, hydrogen evolution, Reaction 4.3, lasting several minutes, will cease when the residual oxygen in the cell is consumed. In a fashion similar to the oxygen supply cut-off, the oxygen supply start-up can also cause a non-uniform distribution of oxygen on the cathode, that could lead to hydrogen evolution, which could last several seconds and cease when the oxygen distribution in the cathode flow field becomes more uniform under a steady state. Hence, the hydrogen evolution, induced by the oxygen supply interruption (either cut-off or star-tup) is a behaviour that is transient in nature.

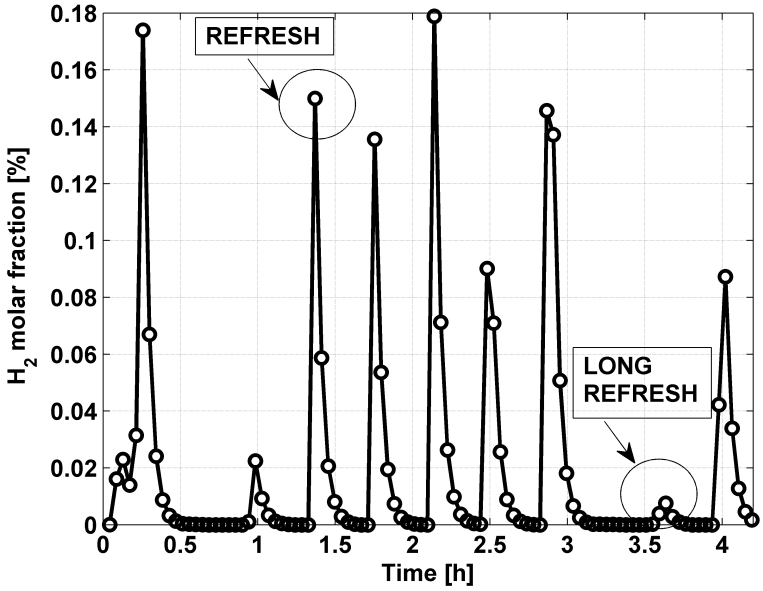

Figure 4.18: Hydrogen content in DMFC anode effluent during refresh cycles.

Despite in paragraph 3.5, the hydrogen crossover from the cathode to the anode has been founded as negligible in performance gain, this DMFC temporary degradation mechanism has been investigated by means of the μGas-Chromatograph during both steady state operation and operating strategies. The experimental tests have been carried out using different operating strategies and the measurements do not reveal hydrogen presence in anode exhaust during steady state operation (continuous operation) coherently with the continuous oxygen presence in the cathode channel. Instead, as reported in figure 4.18, during the cycling operation with refresh, hydrogen peaks are periodic with a 20 *min* frequency that is synchronous with the refresh cycle. Hence, it is confirmed that the refresh cycle determines a slight production of hydrogen at the DMFC anode, which is carried to the μGC by means of the CO_2 produced after the refresh when the current is drawn again. However, increasing the refresh time from 1 *min* to 20 *min*, the hydrogen peak is very low also after the end of the refresh cycle. However, this is due to the continuous methanol feeding and the lack of CO_2 production; in these conditions, the hydrogen is continuously removed by means of the methanol, but the small quantity does not permit a correct measurement by the μGC. As a summary, it should be pointed out that the lack of relevance of anode hydrogen presence (due to hydrogen crossover) in electrolytic operation does not automatically imply that the anode hydrogen evolution during the

refresh is negligible on the performance recovery associated to the refresh cycle.

4.7.3 Water management issues

In order to take into account all the possible temporary degradation mechanisms, water management, including flooding or dehydration of the cathode electrode, should be investigated; the water management issue has a fundamental importance for low temperature hydrogen fuel cells (PEFC) and it has been deeply investigated in the literature, while in DMFC it is usually underestimated. However, thanks to the strong similarity between the two technologies, the Gas Diffusion Layer optimization is a key-point to ensure a correct water management for DMFC.
The on-design water management of DMFC is typically flooding avoiding oriented because at high current densities and with an anode liquid feeding, cathode dehydration is very poorly probable. For this reason, a MicroPorous Layer is usually deposited on the DMFC cathode Gas Diffusion Layer to avoid flooding phenomenon. Furthermore, in the tested DMFC, the MicroPorous Layer is also present on the Anode GDL in order to avoid a to high methanol crossover from anode to cathode. This kind of layout could be problematic for DMFC off-design conditions.

In figure 4.19 a test performed at 0.1 $A \cdot cm^{-2}$ (the reference current is 0.25 $A \cdot cm^{-2}$) with two different cathode air massflows is presented. In the first part of the test, the cathode flow is kept equal to the one used in reference current leading to a stoichiometry equal to 7.5. In this part of the test, the degradation rate is very high. At hour 50, the cathode massflow is halved leading to an air stoichiometry equal to 3.75 and two effects are evident from the time-voltage curve:

- a sudden increase of DMFC performance just after the cathode air flow variation;
- a significant change in the slope of the voltage decay.

During the test the methanol solution feeding the anode has been kept constant and equal to the reference conditions leading to a very high stoichiometry equal to 15 and temperature equal to 75 ^oC.

The Electrochemical Impedance Spectra, related to the figure 4.19, are reported in figure 4.20. The progressive increase in the DMFC total resistance is coherent with the progressive performance loss but it is also clearly

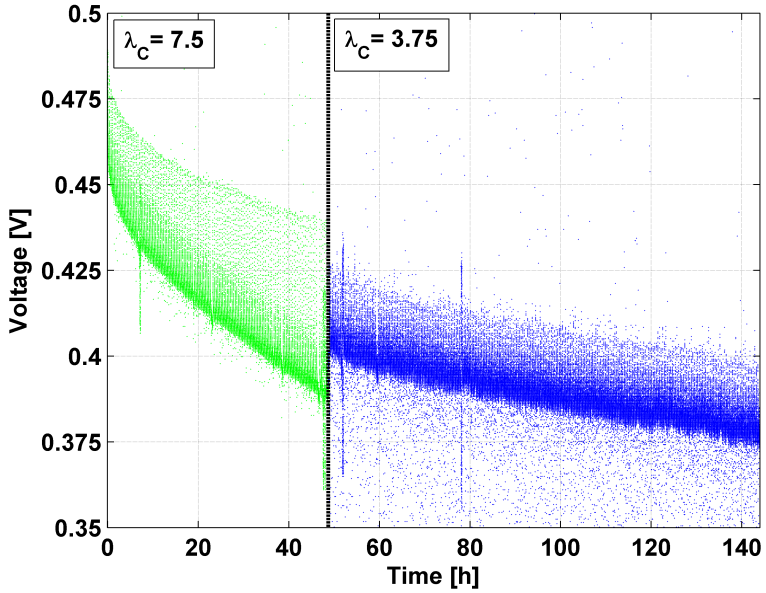

Figure 4.19: Degradation tests at 0.1 $A \cdot cm^{-2}$ with two different cathode air massflows.

related to the effect of the decrease of oxygen content in cathode outlet due to the halving of air; in these conditions, since the methanol feeding remains constant, the methanol crossover effect at low air feeding determines an increase of the cathode impedance coherently with the one reported in figure 4.5. However, despite a worst cathode operation, a increase of performance is evident after the halving of cathode air and from the zoom on the EIS reported in figure 4.20 a significant change in membrane ohmic resistance is highlighted. During the high cathode air feeding period, the membrane resistance significantly increase (from blue to green circles); the halving of the cathode air feeding determines a significant decrease in the membrane resistance that is due to the lower water removal from the cathode air (from green circles to red triangles). However the strong increase in performance is not only due to membrane re-hydration but it is probably more related to the cathode electrode ionomer re-hydration that, due to the very small weight, probably presents faster dynamics than the electrolytic membrane. During the second part of the test the membrane ohmic resistance progressively shows a slight increase that is coherent with what reported in paragraph 4.5.2 (from red to black triangles).
The experimental results presented in this paragraph shows that both the membrane and cathode electrode dehydration can also be responsible for the

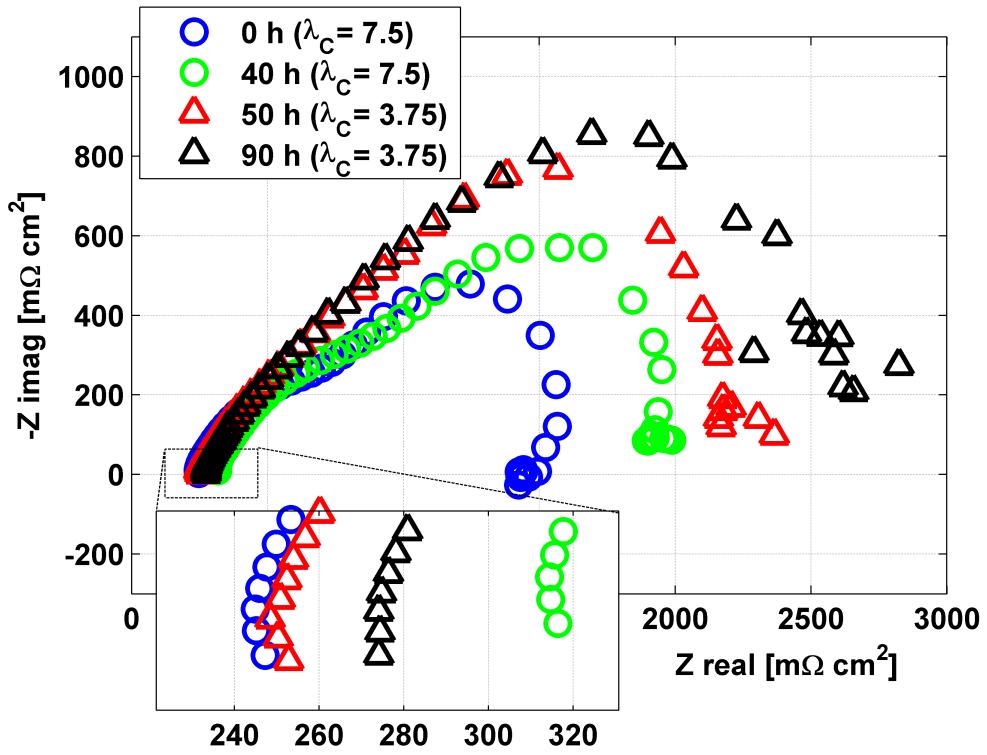

Figure 4.20: EIS performed during the degradation tests at 0.1 $A \cdot cm^{-2}$ with two different cathode air massflows.

DMFC temporary degradation; despite the membrane dehydration effect on DMFC voltage is quantifiable by means of the Ohm's law and it is not very important in comparison with the observed performance losses, the cathode electrode dehydration cannot be quantified nor easily identified. Furthermore its effect can be recovered during the refresh cycles in the low voltage period when, with the continuous anode feeding and the cathode air interruption, the cathode electrode ionomer hydration again increases and this results in a performance increase that cannot be easily distinguished from the Pt oxides formation and reduction effect.

Tests with humidified air

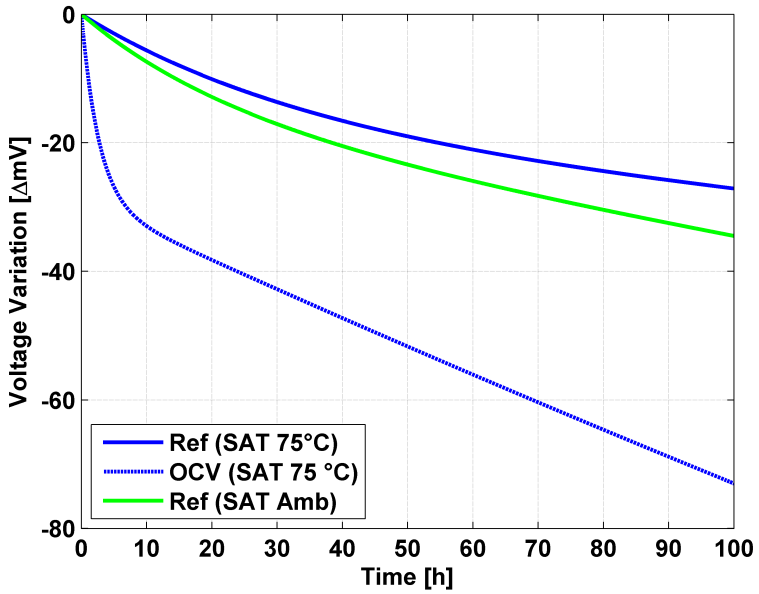

Figure 4.21: Biexponential Interpolations on the effect of air humidification on OCV and Refresh Operating Strategy.

The only way to try to separate the effects of electrode dehydration and Pt oxides formation/reduction is an important rise in the humidification of the cathode air feeding. Increasing the air saturation temperature from room temperature to DMFC temperature should result in modifications in the water balance through the membrane. The high water content in the cathode feeding avoids the cathode electrode dehydration but it can result in the flooding of the cathode electrode; for this reason the cathode air saturation temperature has been set equal to the DMFC temperature (75^oC). Figure

4.21 reports the biexponential interpolations of three tests, performed on the same MEA, for the temporary degradation evaluation: the room temperature humidified refresh cycles, the 75^oC humidified refresh cycles and the 75^oC humidified OCV cycles. The goal is to separate the effects of the cathode electrode dehydration and the cathode platinum oxides formation and reduction.
From the comparison it is possible to pointed out that:

- the high humidification of the cathode air slightly decrease the degradation rate in comparison with the room temperature humidification;
- the modification in the water management associated to the strong humidification could have an unknown effect on the anode temporary degradation mechanism;
- under the assumption of full hydration of the cathode electrode, the important difference between the humidified OCV and Refresh tests shows that the role of platinum oxides is very important;
- the other important difference between the OCV and Refresh corresponds to the anode electrode hydrogen production during the air-break. However, from the anode degradation test is seems negligible but those tests are not DMFC representative with a high certainty for this purpose.

The performances obtained with the rise in the cathode humidity corresponds to the highest performances ever acquired during all the work meaning that the modifications in the water balance, leading to a decrease in membrane and electrode resistivity can act as a tool for a better DMFC efficiency.

4.8 Preliminary Optimization of the Operating Strategy

The optimization of the DMFC operating strategy is a very complex argument because both performances and degradation depends on several external and internal parameters that are hardly controllable; among the internal parameters, activation procedure, test duration, cell history (previous tests, diagnostics) can hinder the results repeatability. Furthermore there are some external parameters that can introduce modifications in the standard procedures worsening the results reliability such as experimental setup failures, long operation interruption for holidays and operator changes for the DMFC

assembly. For these reasons it is very hard to compare different operating strategies on a same MEA for tests of an adequate duration; however, shorting the test duration, as in paragraph 2.4, permits to have qualitative but not quantitative information. Furthermore, the goal of the operating strategy has to be defined because the minimization of the degradation rate (i.e. the temporary degradation) does not guarantee the minimization of the permanent degradation that can be evaluated only by long-term tests.
Two directions have been chosen for the preliminary optimization of the operating strategies with the goal of the minimization of the temporary degradation rate:

- to increase the duration of each refresh as reported in figure 4.15 as a trade-off between operation and temporary degradation reduction;
- to introduce periodic long interruptions ("long refresh") to permits periodic strong temporary degradation recovery;

	Degradation $\mu V \cdot h^{-1}$	RRI mV
Anode 60 s refresh	148 ±10%	6.6 ±12%
DMFC 60 s refresh	295 ±9%	21.8 ±3%
Anode 300 s refresh	33 ±6%	7.5 ±7%
DMFC 300 s refresh	181 ±7%	37.1 ±2%
Anode Long Refresh	118 ±9%	6.4 ±18%
DMFC Long Refresh	311 ±8%	22.3 ±23%

Table 4.3: Summary of degradation rates and RRI for different operating strategies for the optimization.

The first strategy has been already analysed in paragraph 4.7 and it permits an important reduction of the degradation rate; the Refresh Recovery Index can provide further information on the refresh modifications also thanks to analysis of the anode degradation tests reported in chapter 3. From the RRI analysis on the experimental data reported in paragraph 3.4, it is possible to note that increasing the operation interruption (OCV in

Electrolytic Operation) duration the overpotential gain is switched from 6.6 mV to 7.5 mV confirming the improvement in the interruption effectiveness. Table 4.3 reports the anode and overall RRI and degradation rates calculated as in 2.5.1 for the reference and the samples of the explained operating strategies for the temporary degradation rate minimization. Coming back to the results reported in figure 4.15, increasing the refresh duration from 1 minute to 5 minutes the overpotential gain is switched from 21.8 mV to 37.1 mV confirming the improvement in the refresh effectiveness. Comparing the difference in the RRI respect to the anode RRI previously obtained, as reported in table 4.3, it is possible to assert that the growth in the refresh duration determines a improvement that is not only due to the better anode operation thanks to the to CO_2 removal but it is due to the temporary degradation mechanisms that occur at the cathode such as platinum oxides formation and reduction.
The other possible path lead to the definition of the long refresh strategy: it consists in the modification of one refresh cycle every 6 refresh cycles; it becomes longer than the usual one and equal to 20 minutes of operation interruption without load and air feeding. The results of both anode and DMFC operation are reported in table 4.3 but they are less interesting than the stretching of each refresh cycle duration[6]. Furthermore this kind of procedure presents an additional issue for the industrial approach. Indeed the DMFC cannot be operated alone as a continuous power supply because of the high temporary degradation and for this reason they are usually coupled with a battery. The battery dimension (and cost) depends on the energy storage and power density: the long refresh strategy corresponds to the highest energy storage at the same power density, but this analysis is out of the interest of this work.
The optimization of the DMFC operating strategies is still an open matter because the here presented analysis is neither exhaustive nor systematic but it represents a starting point for a work that has fundamental industrial importance. Further works should present a more exhaustive analysis, including wide experimental campaigns and ad-hoc developed characterization tools.

4.9 Conclusions

This chapter provides a complete experimental investigation on the DMFC temporary degradation mechanisms involving performances, electrochemical and mass transport measurements; each temporary degradation phenomenon is analysed with the goal of the separation of the different superimposed

[6]The high uncertainty on the RRI is due to the two different refresh durations.

mechanisms in order to understand the reasons for the effectiveness of the refresh cycle presented in chapter 2. Finally the temporary degradation investigation acts as a tool to develop a preliminary strategy for the minimization of the degradation rate. The main scientific conclusions on the temporary degradation mechanisms are described as follows:

- the DMFC anode suffers of a temporary degradation mechanism related to the CO_2 accumulation during the operation. This leads to a reduction of water and methanol concentration in the anode electrode resulting in a increase of the anode overpotential (see chapter 3) and in a decrease of methanol crossover from anode to cathode confirmed by GC analysis;

- the air interruption synchronous to the low voltage period of the refresh cycle determines the so-called "Electrolytic Hydrogen Evolution" at the anode due to the galvanic/electrolytic operation of the DMFC. This hydrogen production seems to have a weak effect on the anode performances but it has been investigated only in anode operation in paragraph 3.5;

- during the DMFC operation, due to the high cathode potentials, platinum oxides are formed at the cathode electrode causing a recoverable cathode performance loss. This phenomenon could also be related to the ruthenium crossover from anode to cathode that is a typical DMFC permanent degradation mechanism. The low voltage period in the refresh procedure, due to air-break, permits the reduction of platinum oxides leading to the cathode performance recovery;

- water management is a key issue for a good DMFC performance despite it is less important than in hydrogen PEFC; cathode electrode and membrane dehydration can result in low performances and high temporary degradation rates.

Chapter 5

Mass transport characterization in Gas Diffusion Layers

In the following chapter the influence of GDL type on mass transport properties is investigated. The experimental investigation of water transport through the GDL is performed by means of an ad-hoc designed experimental setup. MPL deposition determines a reduction in diffusive water transport and a strong increase in breakthrough threshold. Finally a preliminary Accelerated Stress Test for GDL degradation is developed and tested.

5.1 Introduction

The previous chapters of this PhD Thesis permits to clarify the strong relationship between mass transport phenomena and DMFC temporary degradation mechanisms. For this reason, the research has been addressed to the Gas Diffusion Layer characterization since it governs both the complex two-phase flow at the DMFC anode and the flooding/dehydration of the DMFC cathode. Gas diffusion layers (GDL) have strong hydrophobic properties in order to ensure a correct water management; furthermore a microporous layer (MPL) is usually present at cathode side in order to reduce the effects of flooding and to improve the contact between the catalyst layer and the GDL [97, 98]. There are two main mechanisms for water transport in PEFC and

DMFC GDL: diffusion and permeation. The first is due to a concentration gradient, occurs in vapour phase and is generally the dominant mechanism at low-medium current densities. Differently, the latter is due to an absolute pressure gradient, occurs mainly in liquid phase and, because of GDL hydrophobicity, takes place only if the pressure difference between the two sides of the porous medium overcomes the capillary pressure.
Many in-situ characterizations of the impact of GDL properties on fuel cell performance are present in the literature [99, 100, 8], but they do not clearly separate the complex and interconnected phenomena related to water transport that occur during fuel cell operation. Literature presents also a very high number of PEFC and DMFC models in which the water transport through the GDL, the saturation, the effect of MPL presence and the flooding phenomenon are deeply investigated [101, 102, 103, 104]. Hence, the improvement of numerical models requires accurate estimation of GDL mass transport properties; in fact the literature presents a continuously growing number of ex-situ characterizations especially of diffusive phenomena [105, 106, 107]. These works are usually not carried out in conditions representative of real PEFC operation such as temperature, flow rates or GDL assembly into the experimental setup structure.
Diffusion is also investigated in [108] where the authors propose a quantitative method to determine GDL transport coefficient and in [83] where the effect of flooding is investigated through a combined experimental and modelling approach under real representative PEFC or DMFC operating conditions; the GDL was placed between two serpentine flow fields, humid and dry airflows was fed at the two side of the GDL and equimolar diffusive flow was measured due to water concentration gradients. The effect of MPL presence on the GDL properties is investigated by optical methods both ex situ where the changes in tortuosity and diffusivity due to MPL are studied in [109] and in-situ in [110] where different operating conditions are investigated and the positive effect of MPL presence is demonstrated.
Experimental investigation of water content in cathode outlet of a DMFC is presented in [9] where the authors analyse the effect of the MPL presence in cathode GDL. They revealed that, when MPL is present, the effect of increasing current is negligible in water transport and it remains constant. When the water production is very high, it causes a strong increase in water content in cathode outlet due to the onset of the liquid water transport. These experimental results confirm that the water transport through the GDL, especially when MPL is present, mainly depends on the water pressure at cathode electrode that is related to current density.
The literature presents some experimental investigations of liquid water permeation through the GDL [111, 112, 113]; these works pointed out two im-

portant considerations:

- it is possible to define a breakthrough threshold for the GDL [112] as the pressure difference that causes the onset of liquid water transport through the porous medium;
- liquid water transport occurs mainly through preferential pathways [77].

Liquid water transport and hysteresis effects are also investigated in [114] where a lateral water flow through the GDL is demonstrated and the importance of a small number of large pores to ensure a liquid water flow is emphasized. However this work is performed with a not-compressed and not heated gas diffusion layer in contrast to a real PEFC or DMFC operation.
The water transport characterization reported in this chapter aims to further understand water transport phenomena in GDLs and the role of MPL by performing ex-situ experiments under real PEFC and DMFC representative operating conditions such as operating temperature and serpentine flow field:

- to characterize water permeation through the GDL;
- to estimate GDL water diffusivity and breakthrough threshold, evaluating also the effect of MPL presence;
- to provide accurate estimation of GDL properties for PEFC and DMFC modelling.

Furthermore, in order to understand the effect that a permanent degradation of this component could have on a DMFC, the second part of the chapter is focused on the preliminary development of a Accelerated Stress Test for Gas Diffusion Layers by means of a chemical degradation procedure. Thanks to the tools developed for the water transport characterization, this AST procedure aims to compare the mass transport properties of a pristine and degraded GDL.

5.2 Experimental methodology

5.2.1 Experimental Approach

The goal of the experimental setup is the investigation of water transport through the GDL both in vapour and liquid phases as a function of the pressure difference across the GDL. The experimental approach consists in

supplying one face of the GDL with dry air while the other face is in contact with liquid water in rest at a pressure determined by the height of a liquid water column as shown in Figure 5.1.

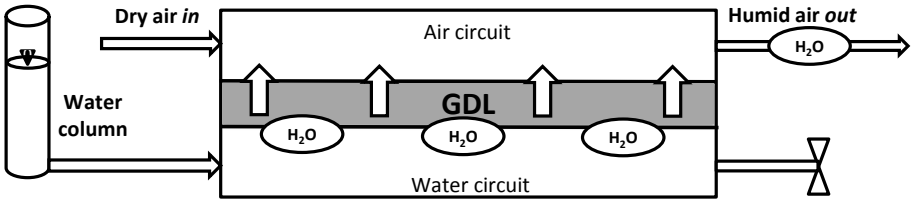

Figure 5.1: Simplified scheme of testing apparatus

Because of the hydrophobicity of the porous medium, diffusion is the only transport mechanism until a threshold pressure difference across the GDL is reached. Stefan-Maxwell equations describe multi-component diffusion and, for a generic multicomponent ideal mixture of ideal gases, it takes this form [115]:

$$\nabla \left(\frac{p}{RT} \cdot x_i \right) = \sum_j \frac{x_i N_j - x_j N_i}{D_{ij}} \tag{5.1}$$

Where x are the molar fractions, N the specific molar fluxes, p is the total pressure of the gases at temperature T and D_{ij} is the diffusion coefficient of the i specie into j specie, which is equal to Dji . Equation 5.1 is based on the hypothesis that each component of the gas mixture moves into a continuous medium where it is subject to friction forces due to other components. When one species of the two components mixture (water in this case) can diffuse from one side of the porous medium to the other side, but there is no opposite equimolar diffusive flux (air) that balances this flux, unimolar diffusion takes place. Assuming air as single pseudo-specie, Stefan-Maxwell equation describing unimolar diffusion takes this form:

$$\nabla \left(\frac{p}{RT} \cdot x_{H_2O} \right) = \frac{-x_{air} \cdot N_{H_2O}}{D_{H_2O,air}} \tag{5.2}$$

In a porous medium, Stefan-Maxwell diffusion is the main transport mechanism in gas phase when the mean free path of molecules is significantly smaller than the mean porous radius, otherwise Knudsen diffusion has to be considered. Knudsen diffusion occurs when the number of gas-solid collisions become larger than the number of gas-gas collisions; if the mean free path of molecules and the mean porous radius are comparable, then both the two mechanisms must be taken into account and relation 5.2 becomes:

$$\nabla\left(\frac{p}{RT}\cdot x_{H_2O}\right)=\frac{-x_{air}\cdot N_{H_2O}}{D_{H_2O,air}}-\frac{N_{H_2O}}{D_{k,H_2O}} \tag{5.3}$$

Since the liquid water circuit is closed, dry air conservation is a simple equality between inlet and outlet dry air flux:

$$N^{dry}_{air,in}=N^{dry}_{air,out} \tag{5.4}$$

Considering that dry air is supplied, water flux through the GDL can be quantified by the water molar fraction $x_{H_2O,out}$ at the outlet as:

$$N^{GDL}_{H_2O}=\frac{N^{dry}_{air,in}\cdot x_{H_2O,out}}{(1-x_{H_2O,out})} \tag{5.5}$$

where:

$$x_{H_2O,out}=\frac{p_{sat}(T)\cdot RH}{p_{total}} \tag{5.6}$$

Five measures are necessary to quantify water transport through the GDL in this experimental setup: dry flow and pressure at air inlet, temperature, pressure and relative humidity at air outlet. Furthermore other one pressure has to be measured and controlled: liquid water pressure at the GDL.

5.2.2 Experimental Setup

A scheme of the experimental setup is reported in Fig. 5.2. The gas diffusion layer (surface area exposed to water and air: $42mm$ x $42mm$), bounded by fiberglass + PTFE gaskets, is contained between two graphite distributors, where channels for liquid water in rest and dry air flowing have been grooved (both distributors have a triple serpentine channel with a square section: depth 0.8 mm, width 0.8 mm, length 700 mm). Graphite distributors are held together with two stainless steel plates using 8 retaining bolts closed with a controlled torque of 12 ($\pm$ 0.5) Nm applied with a certified instrument. A slot in one of the steel plates accommodates a calibrated thermocouple (uncertainty 0.1 K), connected with a data acquisition system. Two electrical heaters, connected to a PID controller, are placed within the steel plates, to control the temperature of the assembly. Since heat capacity of the plates is much greater in comparison with those of graphite distributors and GDL, high temperature stability is attained.

Furthermore, GDL thickness is sufficiently small to assume thermal equilibrium with plates and distributors. Dry airflow rate is controlled and measured by a calibrated flow controller (maximum flow rate: 2 $Nl\cdot min^{-1}$;

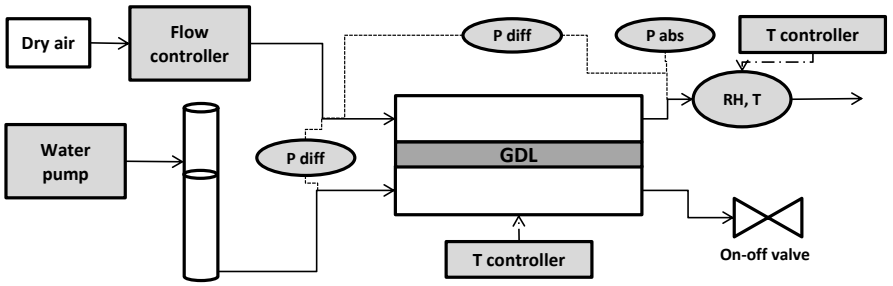

Figure 5.2: Experimental setup scheme; grey squares represent controlled parameters, while grey rounds represent measured parameters

uncertainty: 0.7% + 0.004 $Nl \cdot min^{-1}$). Water column consists in a PTFE tube (height 1 m, internal diameter 10 mm) filled by a peristaltic pump (water flow rate 3-100 $g \cdot h^{-1}$, uncertainty 1%). Absolute pressure is measured at air outlet by a pressure transducer (pressure range: 0-3 bar, uncertainty: 2 $mbar$). Two differential pressure transducers are used to measure pressure differences respectively between the airflows at GDL inlet and outlet (range: 0-350 $mbar$, uncertainty: 0.2 $mbar$) and between the airflow at GDL outlet and the liquid water in rest (range: 0-500 $mbar$, uncertainty: 0.5 $mbar$). The absolute pressures of liquid water and air flow at inlet are thus obtained as the sum of the measured absolute and differential pressures. The airflow rate is regulated considering two opposite needs: minimizing pressure drops along the air flow channel, and avoiding air saturation in the circuit. Pressure difference between air and liquid water is regulated by setting the level of liquid column. Relative humidity measurement is carried out at GDL outlet on the airflow with a certified temperature and humidity transmitter based on a capacitive sensor (temperature range: 0-120^oC, uncertainty: 0.3^oC; humidity range 0-100%, uncertainty (over 40^oC): 1.5% + 1.5% of RH measure). This transmitter is housed in a heated metal case set to prevent water condensation.

A rigorous procedure has been developed in order to guarantee measure reliability and repeatability. Liquid water circuit is initially filled by pumping water into the column until a hydrostatic pressure of 10 $mbar$ is reached and then water outlet valve is closed. Afterwards, a dry air flow of 0.2 $Nl \cdot min^{-1}$ is fed to air circuit, pressure difference between air and water is measured and, after a transitory, experimental test can start. After the conclusion of a measurement, water pressure is increased of 3 $mbar$ and another measurement can start. During the permeation regime, when the water flow through the GDL is high, the peristaltic pump adds continuously small water quantities

into the column in order to keep the average hydrostatic pressure constant (i.e. the height of the water column) during each test despite the pressure fluctuations due to very unstable flow regime. All the measured parameters (pressures, flow rate, temperatures and relative humidity) are recorded at 1 Hz frequency for 900 s in steady state conditions during each test. Data are processed with a robust method for outliers elimination implemented by mean of Matlab software. Representative values of each parameter are obtained as the average of the first 600 elements among the remaining ones and each experimental test is represented by a set of average parameters such as water flow through the GDL, pressure of the hydrostatic column and GDL temperature. Uncertainty is evaluated for water flow through the GDL, combining the uncertainties of the different controlled parameters as indicated in [116]. The estimated value depends on temperature and mass transport regime as reported in Table 5.1.

	$T_{GDL} = 40^oC$	$T_{GDL} = 60^oC$	$T_{GDL} = 80^oC$
Diffusion water flow uncertainty	3%	4%	8%
Permeation water flow uncertainty	10%	10%	15%

Table 5.1: Uncertainties on water flow through the GDL

The higher value of permeation flow uncertainty is due to the strongly dynamic behaviour of such phenomenon. Results reproducibility is verified by repeating every single experimental measure in three different days.

5.3 Characterization of diffusion

5.3.1 Experimental Results

Table 5.2. summarizes the physical properties of the two investigated commercial GDLs. The only morphological difference between these two porous media is the presence of a micro-porous layer that influences thickness, areal weight and air permeability. The experimental characterization of the GDL with MPL is carried out by posing the MPL on the liquid side to investigate also the superficial effects.

Figure 5.3 shows the water flux through the GDL without MPL as a function of the average pressure difference between liquid water in rest and

	GDL + MPL	GDL
Type	Carbon fiber paper	Carbon fiber paper
Thickness (uncompressed)	$415\,\mu m$	$400\,\mu m$
MPL thickness	$50\,\mu m$	
PTFE content	10%	10%
Surface	$18.14\,cm^2$	$18.14\,cm^2$
Areal weight	$145\,g \cdot m^{-2}$	$90\,g \cdot m^{-2}$
Air permeability	$1.45\,cm^3 \cdot cm^{-2} \cdot s^{-1}$	$85\,cm^3 \cdot cm^{-2} \cdot s^{-1}$

Table 5.2: GDL physical properties

airflow, varying GDL temperature until the onset of liquid water transport due to GDL breakthrough.

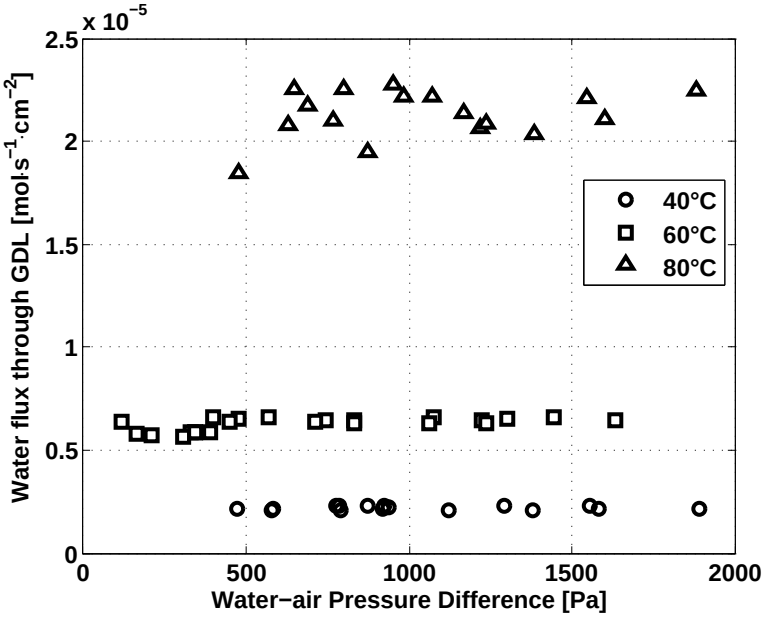

Figure 5.3: Diffusive water flux through the GDL without MPL as a function of temperature and water/air pressure difference

Coherently with the literature, the higher the temperature and the higher the diffusive flux; this trend depends on two main effects: firstly, water saturation concentration increases with temperature, therefore the mean concentration difference across the GDL is higher causing an increase of diffusive water transport; secondly diffusion coefficients increase with the temperature as reported for example in [117]. Diffusive water flux remains approximately constant over a wide range of pressure difference across the GDL.

Until breakthrough pressure is reached, capillary forces prevent liquid water passage through the porous medium.

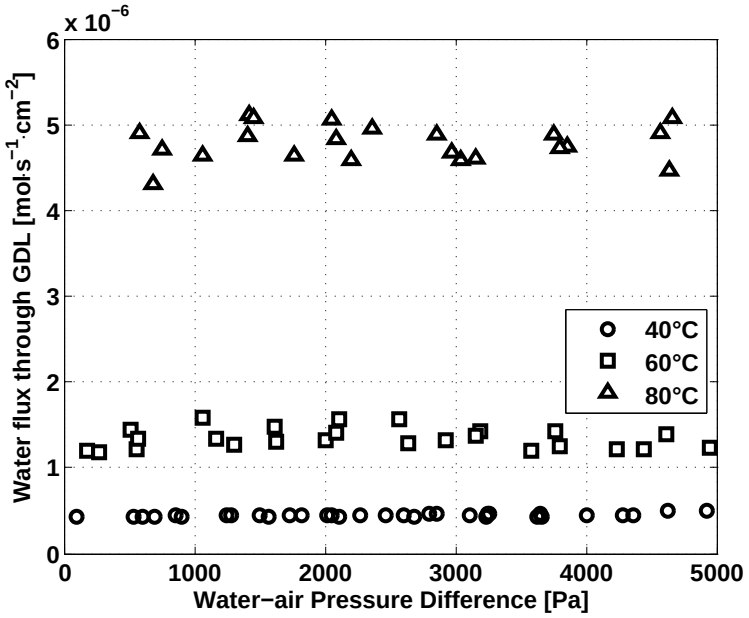

Figure 5.4: Diffusive water flux through the GDL with MPL as a function of temperature and water/air pressure difference

Figure 5.4 shows water flux through the GDL with MPL as a function of average pressure difference across the GDL until the onset of liquid water transport due to GDL breakthrough. The effect of a temperature increase is very similar to the previous case. However two differences in diffusive water transport are evident comparing GDL with and without MPL:

- the MPL presence heavily increases the breakthrough pressure difference. This effect is coherent with a superficial effect of the microporous structure. Indeed, the capillary pressure is inversely related to mean pore radius, thus a higher water pressure is necessary to force liquid water into the microporous layer;

- the MPL presence drastically reduces the diffusive water transport through the GDL, approximately by a factor 5. This is coherent with the literature [83]; there are two possible reasons for this increase in transport resistance: firstly the MPL presents strongly different values of porosity and tortuosity compared to the GDL, secondly Knudsen effect could be significant in MPL pores.

5.3.2 Interpretative modelling and discussion

A simplified model is developed in order to have a reliable tool to interpret the experimental data and to estimate the GDL water diffusion coefficient. The model is valid only for the diffusive regime, because it does not take into account water permeation through the GDL. The 1D + 1D developed model describes the steady state water diffusion through the GDL and permits to estimate water concentration profile and the effective Stefan-Maxwell diffusivity.

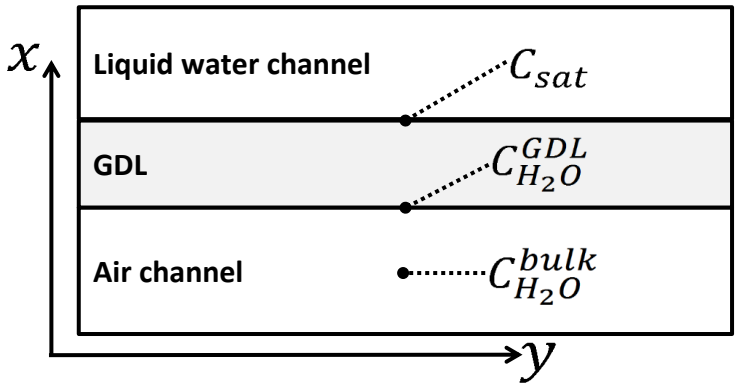

Figure 5.5: Scheme of local water concentration in 1D + 1D model for single layer domain

The model is based on the following assumptions, referring to Figure 5.5 where local water concentration in x direction are reported:

- the GDL properties are homogeneous;
- the domain is considered isothermal;
- air is considered as a single chemical pseudo-specie;
- the gases and the gas mixture are considered ideal;
- air channel has a square section;
- triple serpentine flow field is simplified to a straight channel;
- the pressure drop along the channel in y direction has a linear distribution;
- gas pressure variation within the GDL in x direction are negligible;

- GDL thickness is equal to the gasket thickness;
- water concentration in vapour phase at GDL/liquid water interface is equal to saturation concentration at GDL temperature;

Single Layer Domain

The first approach to have an estimation of diffusion coefficients for both the GDLs is to consider also the GDL with MPL as a single layer with average homogeneous properties neglecting Knudsen diffusion. A two-layer detailed analysis is carried out in the next section. The model is a differential-algebraic system (DAE), composed of 6 equations, and is solved with the Matlab software. The first and second equations (5.7 5.8 describe respectively dry air conservation and water flux through the GDL interface to the air channel:

$$\frac{\partial \left(v \cdot C_{air}^{bulk}\right)}{\partial y} = 0 \tag{5.7}$$

$$\frac{\partial \left(v \cdot C_{H_2O}^{bulk}\right)}{\partial y} = \frac{h}{a} \cdot \left(C_{H_2O}^{GDL} - C_{H_2O}^{bulk}\right) \tag{5.8}$$

where h is the convective mass transport coefficient and a is the air channel width. The third and fourth equations (5.9 5.10) describe the gas phase concentrations in the air channel and at the interface between GDL and channel, respectively:

$$C_{H_2O}^{bulk} + C_{air}^{bulk} = \frac{p}{RT} \tag{5.9}$$

$$C_{H_2O}^{GDL} + C_{air}^{GDL} = \frac{p}{RT} \tag{5.10}$$

where T is the domain temperature and R is the universal gas constant. The fifth equation 5.11 describes diffusive water flux through the GDL and it derives from the integration of Stefan-Maxwell equations for unimolar diffusion [117]:

$$\frac{Q \cdot D_{GDL}^{eff}}{t_{GDL}} \cdot \left(\frac{p}{RT}\right) \cdot \ln \frac{C_{air}^{GDL}}{\left(\frac{p}{RT} - C_{sat}\right)} = h \cdot \left(C_{H_2O}^{GDL} - C_{H_2O}^{bulk}\right) \tag{5.11}$$

where t_{GDL} is GDL thickness and D_{GDL}^{eff} is the effective GDL water diffusivity. Q is a factor that takes into account the 2D geometric effect on

diffusion through the GDL due to the investigated flow field as in [83]. The last equation 5.12 describes the linear pressure distribution along the channels:

$$\frac{\partial p}{\partial y} = -\frac{(p_{in} - p_{out})}{L} \tag{5.12}$$

where L is the total channel length, and pin and pout are the pressures of the air flow at GDL inlet and outlet. GDL effective diffusivity depends on water-air diffusivity $D_{air,H2O}$ and on GDL porosity ε and tortuosity τ as in the following relationship 5.13:

$$D_{GDL}^{eff} = \frac{D_{air,H2O} \cdot \varepsilon}{\tau} \tag{5.13}$$

The procedure to estimate convective mass transport coefficient is reported in detail in [19] and it consists in three main considerations:

- validity of Lewis analogy: mass transport boundary layer can be described by thermal boundary layer models;
- the airflow is completely mixed and every bend of the channel determines a subsequent developing region;
- the channel can be modelled as a square tube with only one exchanging face.

The estimated values for convective mass transport coefficient are respectively 7.1 $cm \cdot s^{-1}$ at 40 ^oC, 7.9 $cm \cdot s^{-1}$ at 60 ^oC and 8.7 $cm \cdot s^{-1}$ at 80 ^oC. The GDL effective diffusion coefficient is determined minimizing the squared residuals between experimental and modelling results for each experimental condition, then mean value and uncertainty are evaluated, 5.3 reports the effective diffusivity for GDL with MPL and without MPL as a function of the GDL temperature. The obtained values are in agreement with the literature for both GDL with MPL and GDL without MPL [83].

The uncertainty of GDL effective diffusivity is far higher than the uncertainty of water flux through the GDL, because of error propagation; indeed, high variations of diffusivity correspond to low variations of water flux through the GDL.

		Present work		Literature [83]
Effective diffusivity	40^oC	60 ^oC	80 ^oC	60 ^oC
GDL	0.144 $cm^2 \cdot s^{-1}$ $\pm$ 15%	0.161 $cm^2 \cdot s^{-1}$ $\pm$ 15%	0.316 $cm^2 \cdot s^{-1}$ $\pm$ 15%	0.159 $cm^2 \cdot s^{-1}$
GDL+MPL	0.029 $cm^2 \cdot s^{-1}$ $\pm$ 12%	0.033 $cm^2 \cdot s^{-1}$ $\pm$ 12%	0.053 $cm^2 \cdot s^{-1}$ $\pm$ 15%	0.055 $cm^2 \cdot s^{-1}$

Table 5.3: GDL effective diffusivity and its uncertainty

Two Layers Domain

The model is integrated to consider the MPL as an additional layer of known thickness and characterized by both Stefan-Maxwell and Knudsen diffusion coefficients. A further equation 5.14 is added to the model in order to describe diffusive water flux through the MPL as a combination of Stefan-Maxwell (SM) and Knudsen diffusion fluxes

$$\frac{Q \cdot D_{MPL}^{eff}}{t_{MPL}} \cdot \frac{p}{RT} \cdot \ln \frac{C_{air}^{MPL} D_k^{eff} + (p/RT)\, D_{MPL}^{eff}}{((p/RT) - C_{sat})\, D_k^{eff} + (p/RT)\, D_{MPL}^{eff}} = h \cdot \left(C_{H_2O}^{GDL} - C_{H_2O}^{bulk}\right) \tag{5.14}$$

where D_{MPL}^{eff} is the effective diffusivity of only MPL, t_{MPL} is its thickness and D_k^{eff} is the effective Knudsen diffusivity of the MPL. The MPL effective diffusivity depends on water-air diffusivity $D_{air,H2O}$ and on MPL porosity and tortuosity:

$$D_{MPL}^{eff} = \frac{D_{air,H2O} \cdot \varepsilon_{MPL}}{\tau_{MPL}} \tag{5.15}$$

The fifth equation 5.11 is modified to consider the microporous layer presence:

$$\frac{Q \cdot D_{GDL}^{eff}}{t_{GDL}} \cdot \left(\frac{p}{RT}\right) \cdot \ln \frac{C_{air}^{GDL}}{C_{air}^{MPL}} = h \cdot \left(C_{H_2O}^{GDL} - C_{H_2O}^{bulk}\right) \tag{5.16}$$

Since the effective diffusivity of GDL without MPL is previously estimated, D_{GDL}^{eff} is already known. A fitting procedure to determine both SM and Knudsen diffusion coefficients cannot be used reliably. A sensitivity analysis on pore radius is performed to evaluate the contribution of the two transport mechanisms. Knudsen diffusivity is estimated as function of mean

pore diameter by mean of the following relationship available for small pores and low gases pressures [117]:

$$D_k = 48.5 \cdot d_p \cdot \sqrt{\left(\frac{T}{M_{H_2O}}\right)} \tag{5.17}$$

under this assumption the effective Knudsen diffusivity of the MPL becomes:

$$D_k^{eff} = \frac{D_{air,H2O} \cdot \varepsilon_{MPL}}{\tau_{MPL}} \tag{5.18}$$

where tortuosity is estimated from Wakao and Smith with the following correlation [117]:

$$\tau_{MPL} = \frac{1}{\varepsilon_{MPL}} \tag{5.19}$$

Instead, Stefan-Maxwell diffusivity of the microporous layer is a function of MPL porosity and tortuosity, as in 5.18, and water-air molecular diffusivity, according to [118]:

$$D_{air,H2O} = \frac{0.00143 \cdot T^{1.75}}{p \cdot M_{air,H_2O} \cdot \left[(\Sigma_\nu)_{H_2O}^{\frac{1}{3}} + (\Sigma_\nu)_{air}^{\frac{1}{3}}\right]} \tag{5.20}$$

where Σ_ν are the molecular diffusion volumes and M_{air,H_2O} is estimated by:

$$M_{air,H_2O} = 2\left[\left(\frac{1}{M_{H_2O}}\right) + \left(\frac{1}{M_{air}}\right)\right]^{-1} \tag{5.21}$$

Both SM and Knudsen diffusivities depend on MPL porosity, while Knudsen one depends also on pore radius; therefore it is possible to perform a sensitivity analysis on the effect of MPL pore radius on the two transport mechanisms. Because effective diffusivity of GDL layer has been previously estimated and both D_K and $D_{air,H2O,MPL}$ are calculated by correlation, it is possible to determine MPL porosity through a fitting procedure on the experimental data. The typical distribution of pore radii in MPL is in the range between 0.05-1 μm, as reported in [119], thus the sensitivity analysis is carried out in this range.

Table 5.4 presents Knudsen and SM effective diffusivities as a function of MPL pore radius at 60^oC. For pore radius smaller than 0.5 μm the two coefficients have the same order of magnitude, while for larger pore radius

Pore radius	D_{GDL}^{eff}	ε_{MPL}	D_{MPL}^{eff}	D_k^{eff}	$\frac{D_k^{eff}}{D_{MPL}^{eff}}$
μm	$cm^2 \cdot s^{-1}$		$cm^2 \cdot s^{-1}$	$cm^2 \cdot s^{-1}$	
0.05	0.161	0.182	0.0102	0.0069	0.68
0.1	0.161	0.160	0.0070	0.0094	1.25
0.5	0.161	0.119	0.0043	0.029	6.77
1	0.161	0.114	0.0040	0.054	13.5

Table 5.4: Sensitivity analysis of pore radius variation on SM and Knudsen MPL diffusivities

Knudsen contribution can be neglected. The calculated values of porosity are coherent with the literature and they are very similar for tests at 40^oC and 60^oC (difference $< 4\%$) while for tests at 80^oC this difference is higher, but still acceptable ($< 10\%$).

5.4 Characterization of permeation and hysteresis

5.4.1 Experimental Results

Figure 5.6 shows the specific water flux through the GDL with MPL at 60^oC as a function of the pressure difference between water and air.
Three different regions are highlighted: a diffusion region, a permeation region and a hysteresis region. The diffusion region is already discussed in paragraphs 5.3.1 and 5.3.2. During water pressure step-by-step increase, explained in 5.2.2, the pressure difference between the two sides of the GDL can overcome the capillary pressure and the onset of liquid permeation can occur causing an important increase in total water flux. This threshold depends on the GDL hydrophobicity and mean porous radius as described, for cylindrical pores, by the Young-Laplace relation 5.22:

$$\Delta p_{cap} = \frac{2\sigma \cdot \cos\theta}{r_p} \tag{5.22}$$

where σ is the surface tension, θ is the contact angle and r_p the mean porous radius. Darcy law 5.23 usually describes permeation flux into porous media as a function of pressure gradient across the GDL:

$$N_{H_2O} = \frac{k}{\mu} \cdot \nabla p \tag{5.23}$$

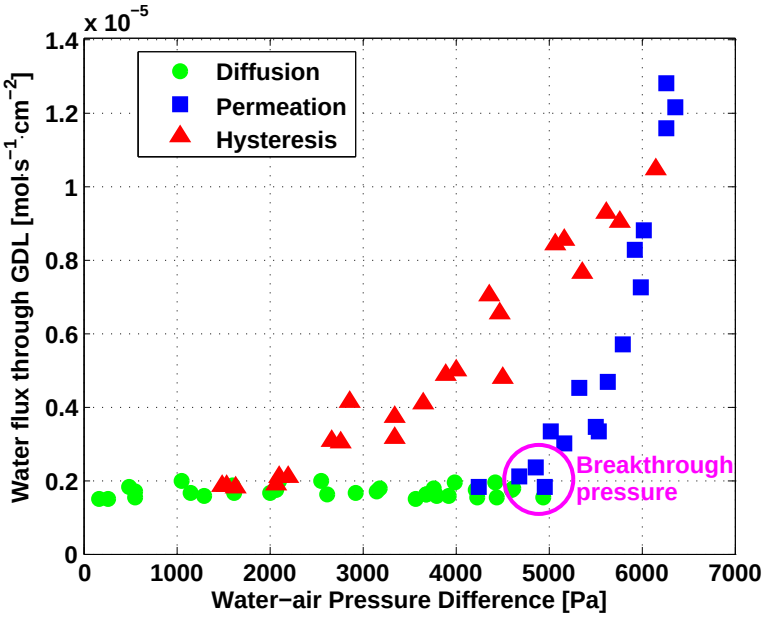

Figure 5.6: Specific water flux through GDL with MPL at 60^oC as a function of water/air pressure difference

where k is the permeability and μ the dynamic viscosity of the fluid. Coherently with the explanation of permeation mechanism, the higher the pressure and the higher the water flux.

	$T_{GDL} = 40^oC$	$T_{GDL} = 60^oC$	$T_{GDL} = 80^oC$
GDL	1395 Pa $\pm$ 24%	1347 Pa $\pm$ 22%	1492 Pa $\pm$ 27%
GDL+MPL	5112 Pa $\pm$ 13%	4950 Pa $\pm$ 12%	4801 Pa $\pm$ 14%

Table 5.5: Breakthrough pressure of GDL with and without MPL

Table 5.5 reports breakthrough pressure values for the two investigated GDLs as a function of operating temperature. Temperature does not affect significantly the breakthrough pressure, while the presence of the MPL, as already stated, results in a considerable increase of this threshold: more than 3 times. Two different samples of each GDL have been tested in order to evaluate results reproducibility: the average breakthrough thresholds values are comparable (differences less than 20%) with the above presented results, as well as the phenomenological behaviour. Great fluctuations of pressure and relative humidity mark these regions coherently with [77] where liquid water flow through the GDL is presented as a strongly dynamic phenomenon.

After reaching the maximum water pressure, it is gradually reduced with a $3mbar$ step and hysteresis is evaluated. A considerable hysteresis effect is evident between 30 and 60 $mbar$ for GDL with MPL, Figure 5.6, while diffusion mechanism returns to be dominant under 25 $mbar$. Similar results are obtained at 40^oC and 80^oC. Unfortunately the characterization of permeation and hysteresis for GDL without MPL is less accurate, because of limits caused by both the process and the experimental setup. In fact the permeation regime is characterized by high capillary pressure fluctuations: the higher the water flux the higher the fluctuation. Since with just the GDL the permeation regime starts at low pressure, 15-20 $mbar$, fluctuations reach 30% of pressure difference leading to important uncertainties. Furthermore small increases in water pressure are enough to determine a strong increase in water flux that can cause saturation at the humidity sensor. For this reason, tests on GDL without MPL are conducted only until the onset of liquid flux through the GDL.

Young-Laplace equation 5.22 allows evaluating the equivalent pore radius related to a certain breakthrough pressure as a function of porous medium hydrophobicity. Using a contact angle of $139^o \pm 4^o$ [120], the resulting pore radius for the GDL without MPL is 82 μm, a value coherent with the literature [77] and manufacturer analysis; on the contrary Young-Laplace equivalent radius for GDL with MPL results 23 μm, more than one order of magnitude higher than expected. This value is not coherent with MPL typical pore dimension, 0.08 μm and 1 μm [119] already reported in the previous section, whose corresponding breakthrough pressure should be 2 bar, according to the Young-Laplace equation. This breakthrough pressure reduction effect could be due to strong heterogeneities in the MPL pore hydrophobicity, however imaging technique [110] reveals a good uniformity of the microporous layer properties and, according to Kandlikar [77], this enormous difference can be attributed to defeats or cracks on the MPL surface, originated during GDL fabrication or assembling into the experimental setup. There is a need of a further investigation on the effect of different supports (such as carbon paper or cloth) in order to improve the understanding of the effects of GDL fabrication and MPL deposition on the breakthrough pressure. These cracks probably have dimensions comparable with GDL pores and cover a very limited fraction of the whole GDL area. Therefore while diffusion is a mechanism that involves the overall GDL surface and is marginally influenced by cracks presence, a considerable permeation flow can be located just where cracks or defects are present, a minor portion of the overall GDL area. When the GDL is assembled and tested for the first time, the breakthrough pressure is approximately 20% higher than those reported in Table 5.5. This is probably

due to permanent changes in pore structure and hydrophobicity during the first breakthrough test, as reported in [111, 112]. Successively breakthrough measures do not vary significantly. In a hydrophobic medium, the liquid water transport obtained increasing pressure difference between water and air is named drainage process. Instead, when pressure difference between water and air is decreasing it is named imbibition process [62]. Porous media saturation curves show that capillary pressure varies considerably comparing drainage and imbibition processes. A few experimental works presents this wetting effect on GDLs; the literature generally agrees in attributing this hysteresis to the difference between superficial and internal contact angle or the ink-bottle effect [62]. For the GDL with MPL the liquid water transport onset occurs at a pressure difference of 50 $mbar$, if the porous material is dry, at about 20 $mbar$ if the material is already wetted. According to Young-Laplace equation it is possible to estimate the internal contact angle of MPL cracks imposing the radius equal to 23 μm and the capillary pressure equal to 2000 Pa; the resulting internal contact angle estimation is 109^o, much lower than superficial one, equal to $142^o \pm 6^o$ [120]. Therefore the permeation can occur through a wet GDL at less than half the pressure necessary for a dry GDL.
The hysteresis, due to pores wetting, results in different values of saturation at the same capillary pressure during drainage and imbibition. For this reason experimental results show the same water flux through the GDL at different applied pressure difference. Repeatability and reproducibility of measurements have been evaluated also on more than one GDL sample; the described behaviours are confirmed.

5.4.2 Dynamic behaviour analysis

Figure 5.7 shows the qualitative behaviour of instantaneous water flow (IWF) through the GDL during the permeation regime and the corresponding water-air pressure difference fluctuations. The IWF is the water flow calculated as in equation 5.5 from the instantaneous values (acquired at 1 Hz frequency) of airflow, pressures and relative humidity. These fluctuations of instantaneous water flow are related to corresponding pressure fluctuations; this is probably due to the variation of local capillary pressure after the passage of water into the minimum section of the pore. These strong pressure oscillations hinder the observation of full permeation regime in GDL without MPL as previously explained.
Minimum, average and maximum instantaneous water flow (IWF) through the GDL can be determined by mean of a data analysis as above explained: minimum and maximum water flows are respectively obtained by the lower

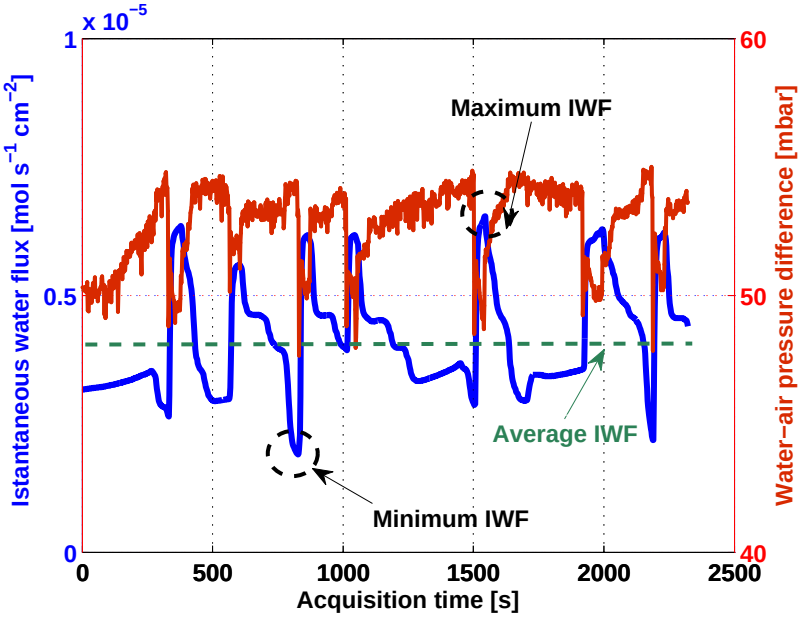

Figure 5.7: Dynamic behaviours of instantaneous water flow through the GDL with MPL (blue line) and instantaneous water/air pressure difference (red points) in permeation.

and higher measured IWF values.

Figure 5.8 shows the values of average, minimum and maximum IWF during permeation regime at 60^oC. Minimum IWF is comparable with diffusive water flux; this confirms that permeation occurs locally and temporary while the overall GDL surface continuously contributes to diffusive mass transport. From 4700 Pa to 5700 Pa, water flow fluctuations are characterized by a fast growth of maximum IWF while the average value is close to the minimum. This suggests that, in this region, liquid transport phenomena are sporadic and involves a small number of the above-cited cracks that increases rising the pressure difference across the GDL. Indeed, defects or cracks in the MPL can have various characteristic dimensions and, according to Young-Laplace equation, the higher is the pressure, the lower is the dimension of the activated crack. After 5700 Pa approximately, the maximum IWF remains about constant while the average IWF presents a fast growth. Accordingly with [77], cracks are preferential pathways for liquid water transport and, when the water drop erupts on GDL surface, it carries away water from adjacent pores determining the immediate interruption of that preferential pathway. Once the pathway has been refilled by water a new drop eruption can occur. When droplets eruption frequency is high, minimum IWF increases, because

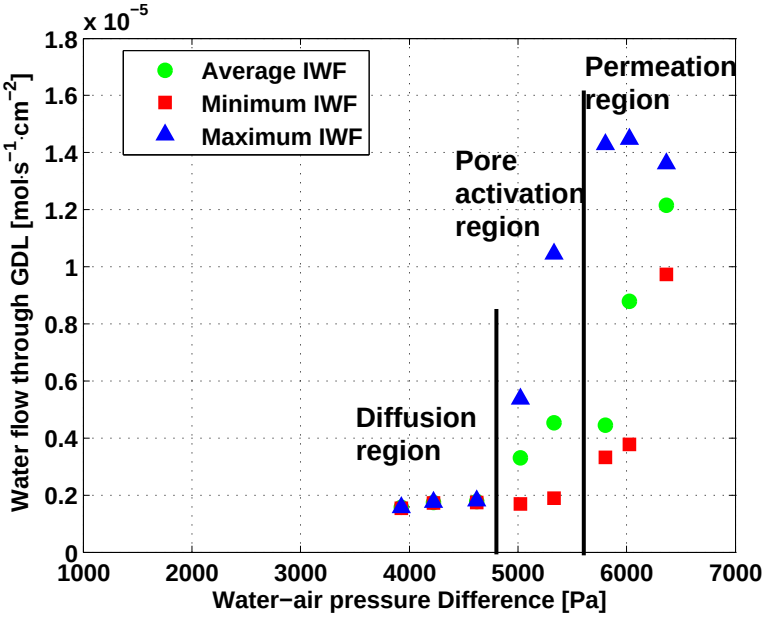

Figure 5.8: Instantaneous water flows increasing water pressure at 60^oC as a function of pressure difference between GDL sides for the GDL with MPL.

at least one permeation site is always active. Therefore in this region, the strong increase in average IWF is related to a strong increase in drop eruption frequency but it is not related to an increase of the number of activated pathways, in fact the maximum IWF remains constant. The liquid pathways number is limited, once all the cracks are activated, drop eruption frequency is responsible for the increase of average water transport.

Figure 5.9 shows the values of average, minimum and maximum IWF decreasing pressure difference. The results are coherent with the proposed interpretation. In particular a comparison between Figure 5.8 and Figure 5.9 highlights that hysteresis is evident for both maximum and average IWF: liquid pathways, once formed gradually in the pressure range 4700-5700 Pa, deactivate progressively in a more extended pressure range, till 2000 Pa. Moreover no considerable hysteresis is evident on minimum IWF: reducing the pressure difference, the drop eruption frequency decreases, thus minimum IWF rapidly reaches the diffusion value.

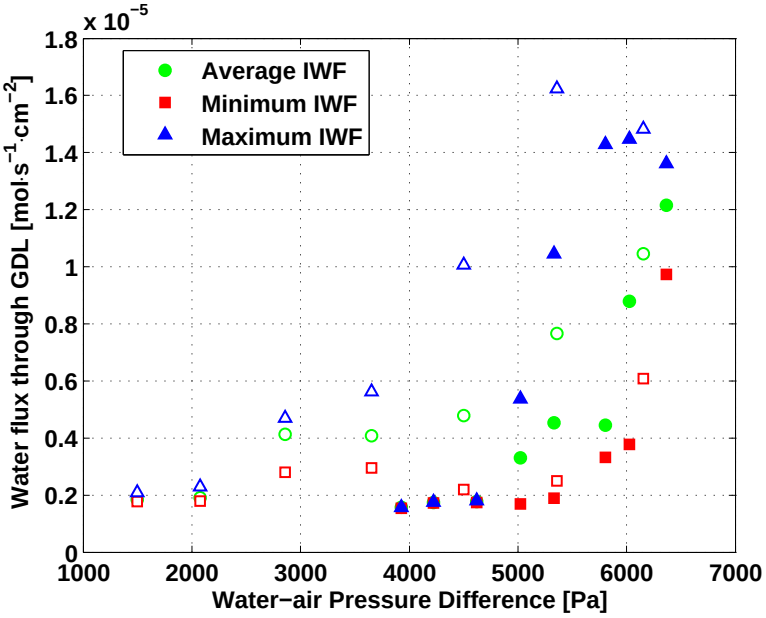

Figure 5.9: Instantaneous water flows at 60^oC as a function of pressure difference between GDL sides for the GDL with MPL. Full symbols are done by increasing pressure, empty symbols are done by decreasing pressure.

5.5 Summary on the water transport characterization

This part of the chapter presents an experimental investigation of water transport through commercial gas diffusion layers in representative conditions of DMFC operation providing a deeper understanding of transport phenomena in GDL's and accurate values of their properties for fuel cell modelling; the following conclusions can be drawn:

- the MPL increases mass transport resistance of the GDL; this effect is related both to lower MPL Stefan-Maxwell diffusivity and to Knudsen effects;
- the MPL presence increases GDL breakthrough pressure from about 1500 Pa to about 5000 Pa. Temperature does not have significant effects on breakthrough pressure;
- the obtained values of breakthrough pressure of GDL with MPL are coherent with the literature: they are probably due to cracks or defects in the MPL;

- a considerable hysteresis effect is evident; the permeation can occur through a wet GDL at less than half the pressure necessary for a dry GDL;
- liquid water pathways number is limited, once all the cracks are activated, the drop eruption frequency is responsible for the increase of liquid water transport.

5.6 Preliminary Accelerated Stress Tests for GDL

5.6.1 AST design and testing

Despite the fundamental importance of GDL for correct DMFC operation, a few experimental investigation of GDL degradation has been carried out in the literature both in-situ and ex-situ [121, 122, 123]; there are no standard procedures for GDL Accelerated Degradation although some research centers developed internal procedures. Generally GDL degradation mechanisms are distinguished in:

- physical degradation that is related to alteration in mechanical and termo-physical properties;
- chemical degradation that is related to chemical properties variation;

Literature focus on compression, freezing or gas flowing into GDL pores effect on performances [121, 124, 125] while GDL chemical degradation is investigated by means of acid solutions in order to simulate the real DMFC operation [126, 127, 122].

In this work a solution of water and water peroxide (at 30% w/w), kept at 80^oC constant temperature by means of a thermostatic bath (5.10, is used as degrading solution because water peroxide as in the following reaction can produce radical species that can attack GDL carbon fibers or PTFE (unless it is very stable).

$$2H_2O_2 \rightarrow 2H_2O + O_2$$

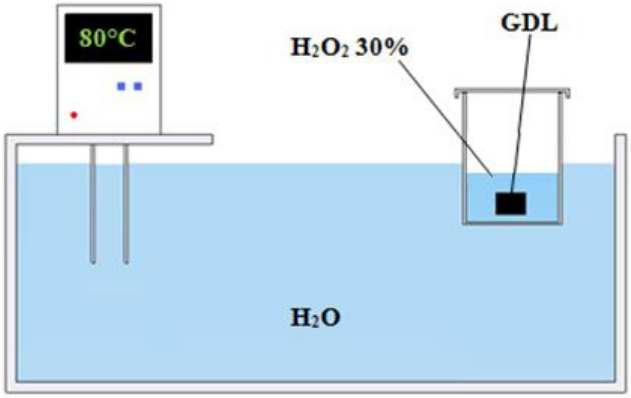

Figure 5.10: Schematical representation of the Accelerated Stress Test for GDL procedure.

GDLs have been immersed for an overall period of 5 days and 10 hours while the water peroxide container has been covered in order to minimize the evaporation.

Three different GDLs, used in DMFC degradation tests, have been tested for the preliminary AST development:

- a carbon felt GDL without MPL and without PTFE. 0% PTFE, 265 μm;
- a carbon felt GDL with PTFE and without MPL. 20% PTFE, 260 μm
- a carbon felt GDL with PTFE and with MPL. 20% PTFE + MPL, 320 μm

	Weight [g]		
	new	degraded	variation [%]
GDL	0.117	0.090	-23.1
GDL+PTFE	0.130	0.110	-15.4
GDL+PTFE+MPL	0.260	0.230	-11.5

Table 5.6: GDL weight loss after AST

Table 5.6 reports GDL weight variation after and before AST after a drying procedure in order to ensure measurement repeatability. The weight is measured ten times by means of a high precision balance (Mettler Toledo 2500, accuracy $\pm$ 0.001 g) and the average value is acquired.

The most pronounced weight variation regards the GDL without PTFE and MPL while both the GDLs with PTFE demonstrate a less important change confirming a PTFE protective effect on carbon fiber corrosion. Furthermore the effect of preliminary AST on MicroPorous Layer seems to be less relevant and it could be due to the high MPL hydrophobicity or to a different carbon structure in comparison with GDL structure. However the absolute weight losses are comparable for all the GDLs and, for this reason, some other measurements are needed in order to clarify the AST effects.

5.6.2 Effect on GDL mass transport properties

Pristine and degraded GDLs are tested in the experimental setup already described in paragraph 5.2 in order to investigate the effect of GDL Accelerated degradation on its mass transport properties.
Since the GDL acts as a barrier for the liquid water, the GDL without PTFE cannot be tested because it permits liquid water flow without a pressure difference hindering diffusion water measurement. The other two Gas Diffusion Layers have been tested and the main results are reported in table 5.7.

	New		Degraded	
	D_{eff} $[cm^2 \cdot s^{-1}]$	Δp_{BT} $[Pa]$	D_{eff} $[cm^2 \cdot s^{-1}]$	Δp_{BT} $[Pa]$
GDL+PTFE	0.085		0.106	
GDL+PTFE+MPL	0.047	>9000	0.068	6500

Table 5.7: AST effect on GDL mass transport properties

As already described in 5.4.1 the experimental characterization of permeative regime in GDL without MPL is complex and the high uncertainty on the breakthrough threshold hinders the quantification of the effect of AST on this property. Hence, for the GDL without MPL, only the diffusion regime is investigated. On the contrary, the GDL with MPL (that is slightly different if compared with the one tested in 5.4.1) demonstrates significant hydrophobicity hindering the quantification of breakthrough threshold of the pristine GDL since at the maximum pressure difference attainable in the experimental setup ($\sim 90\ mbar$), still diffusive water flux occurs.
The AST generally results in a increase of GDL diffusivity and in a reduction of breakthrough pressure confirming that, with the corrosion of carbon fibers, a probable PTFE detachment occurs lowering GDL hydrophobic properties.

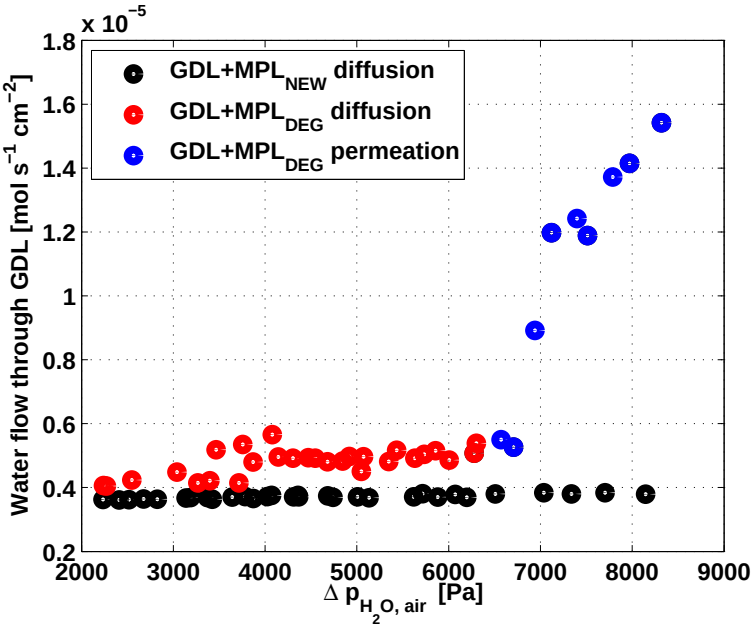

Figure 5.11: Comparison between Specific water flux through GDL with MPL at 60^oC as a function of water/air pressure difference for pristine and degraded samples.

Figure 5.11 shows the specific water flux through the pristine and degraded GDLs as a function of water-air pressure difference where it is confirmed the diffusive regime for the pristine GDL and the permeation onset for the degraded GDL at about 6500 Pa.

5.6.3 Effect on GDL contact angle

GDL contact angle measurement has been performed in ThermoFluidDyamic Laboratory of Department of Energy thanks to Dr. M. Guilizzoni contribution and the experimental results are reported in this paragraph.
The experimental setup consists in a anti vibration test bench with a aluminium alloy structure (Newport SA 1,2 $\times$ 0,8 mm), a 800 W lamp needed for a photographic correct acquisition through a Nikon D90 with AFS 60 mm; images are analysed through a ad-hoc Matlab software.

A technique similar to ADSA (Axisymmetric Drop Shape Analysis) is used; it exploits side drop profile view without a priori information on drop type but it is less accurate. As analysis input two images are used: a side profile of the drop and the background after drop has been dried as showed in figure 5.12. The two images are compared pixel by pixel through *Sobel Edge*

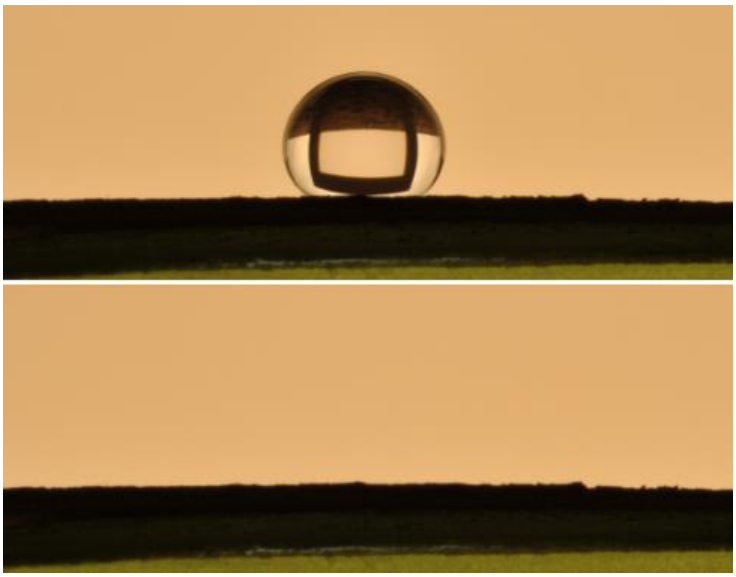

Figure 5.12: Example of Frame for contact angle data processing.

Detector software and both secant plane and drop outline are highlighted. During the acquisition, some water still remains on the surface loading it and it results in about 7 pixels shift. Afterwards it is possible to draw the contour curves as explained in the reference [128].

Figure 5.13 reports pristine and degraded contact angles; a significant degradation effect is evident for GDL without PTFE as confirmed by structure deterioration showed in figure 5.14 where contact angle measurements reveals that the GDL has become superficially hydrophilic.

Contact angle measurements confirm that the GDL with PTFE and without MPL maintains a strongly hydrophobic structure but the results reported in paragraphs 5.6.1 and 5.6.2 reveals a degradation that probably does not strongly involve the surface.

GDL with MPL presents a slight decrease of MPL contact angle confirming a MPL degradation that could be related to the increase in presence of defects on MPL surface as showed in figure 5.15 from a backlight image.

5.7 Conclusions

The most interesting results of the first part of the chapter have been previously summarized in paragraph 5.5 but they are mainly focused on the GDL characterization and they do not take into account the effect of the GDL on

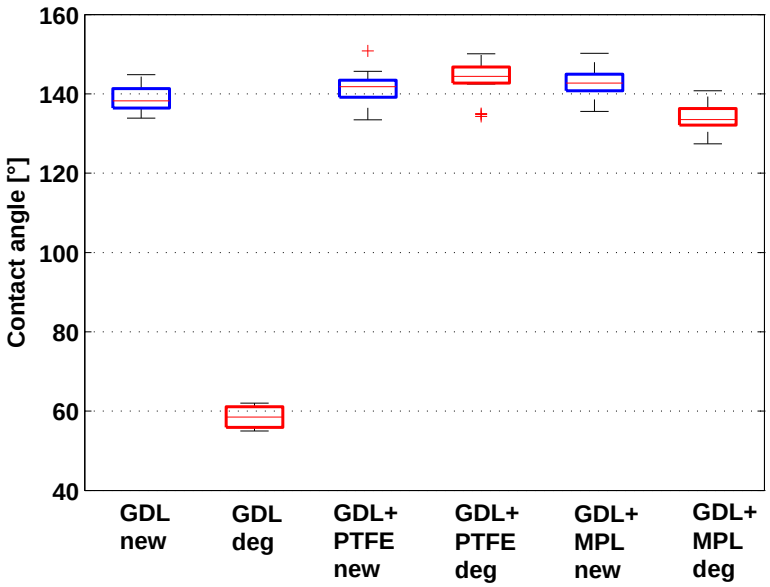

Figure 5.13: Contact angles for pristine and degraded GDL samples.

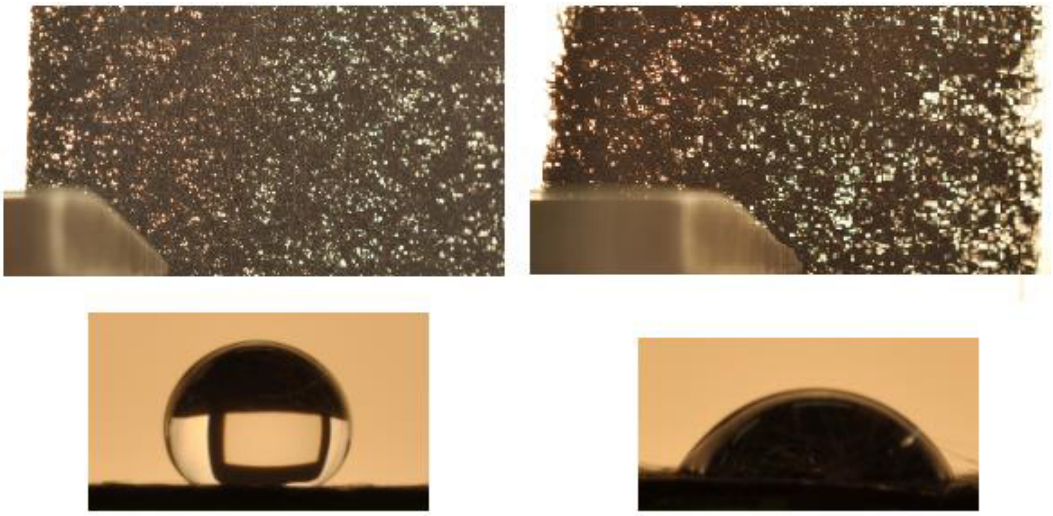

Figure 5.14: Frames comparison between carbon felt pristine and degraded GDL samples.

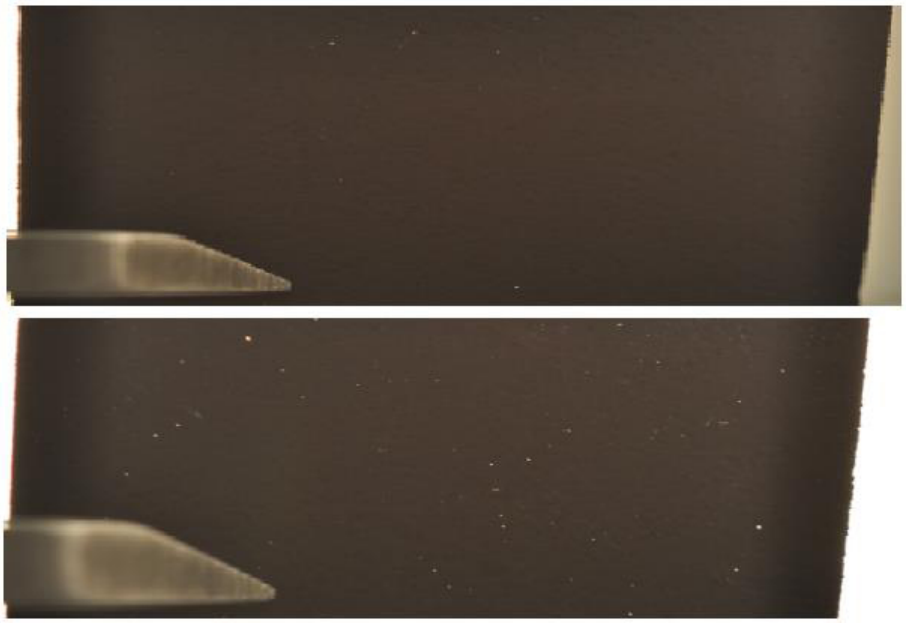

Figure 5.15: Frame of pristine (above) and degraded (below) MPL surface.

the DMFC.
Regarding the DMFC temporary degradation phenomena, a important relation between the mass transport phenomena and the described anode temporary degradation mechanism and refresh effectiveness is highlighted. In paragraph 5.4.1, hysteresis phenomena are showed meaning that a wetted GDL permits a higher mass transport in comparison with a dry GDL at the same water-air pressure difference. During the operation interruption at the anode, the CO_2 is progressively removed and the gas-phase pressure progressively decrease; in these conditions, according to the experimental results, the liquid-phase transport increases and the GDL pores tends to be flooded by liquid phase. When the operation is restarted and the CO_2 is again produced at the anode electrode, the GDL permits a high liquid transport of methanol and water to the anode electrode determining high anode performances (low anode overpotentials). After 20 *min* of operation, the GDL has been progressively dried and methanol and water concentration at the anode electrode decreases and, thus, the anode performances decrease. Coherently with this mechanism, the increase in the refresh time results in a amplified effect of the hysteresis phenomenon and in a reduction of the anode temporary degradation mechanism.
Secondly the MicroPorous Layer presence results in a decrease of diffusivity and in a increase of breakthrough threshold and the differences in the mass

transport properties of GDL with and without MPL have a effect on DMFC mass balances that is investigated in chapter 7.
Finally a permanent degradation of the GDL, obtained by means of a Accelerated Stress Test, determines a significant modification both in diffusivity and breakthrough threshold and these characteristics are fundamental for the DMFC mass balances. For this reason, a permanent degradation of the GDL during the DMFC operation could result in a permanent modification of the DMFC Mass Balances such as methanol crossover and water content in cathode outlet. However, the relationship between ex-situ properties modifications and in-situ effect is not yet completely explained; moreover, the presence of cracks is responsible for the liquid phase transport, which is very important for the methanol crossover, and the effect of the degradation on the cracks could hinder the comprehension of DMFC mass balances during the degradation tests.

Chapter 6

Investigation on DMFC Permanent Degradation

The previous chapters allow to clarify the main DMFC temporary degradation mechanisms and the relation between DMFC performances and mass transport phenomena. Once the temporary degradation has been investigated, the permanent degradation is characterized thanks to a systematic investigation on a long-term test of more than 1100 hours of DMFC operation. The cell has been continuously monitored during the test and finally it has been investigated in post-mortem analysis at the Premium ACT project partners' laboratories.

6.1 Introduction

The characterization of the DMFC permanent degradation is a key-point from the industrial point of view, because it leads to the lifetime requirements and, consequently, to the product desirability on the market. However, as explained in the previous chapters, the temporary and permanent degradation rates are not uniquely defined and standardized and the temporary degradation can alter the permanent degradation measurement.
The lack of systematicity and standardized procedures is one of the main issues of the experimental investigations on DMFC degradation available in

the literature because the in-operando analyses are usually limited; moreover the lack of identification of the main temporary degradation mechanisms does not permit a reliable quantification of the permanent degradation. A detailed literature analysis on the main DMFC permanent degradation mechanisms has been presented in paragraph 1.3.3 and, thanks to the powerful tools available for the partners of the Premium ACT European Research Project, they are directly investigated on the degraded MEA also by the comparison with a pristine one.
The aim of the first part of this chapter is to provide a compete and systematic experimental analysis on DMFC degradation, distinguishing and minimizing temporary degradation in order to quantify the real permanent degradation and its behaviour during the experimental test. Furthermore the systematic in-operando performance of diagnostic, including electrochemical and mass transport measurements, allows to identify the main MEA components responsible for DMFC permanent degradation.
The second part is focused on the summary of the post mortem characterization performed at DLR and CEA of the degraded DMFC and the comparison with pristine and activated samples.

6.2 Experimental

6.2.1 Experimental Setup

The experimental approach for single cell DMFC characterization is described in paragraph 2.2.2, where the set of equations governing mass transport and the components of the experimental setup are explained in details. The DMFC MEAs used in this work, both for the preliminary tests on full refresh procedure and for the long-term test, are commercial 25 cm^2 manufactured by IRD Fuel Cell A/S: membrane is Nafion115, anode catalyst loading is 1.8 $mg \cdot cm^{-2}$ (Pt/Ru), cathode catalyst loading is 1.2-1.4 $mg \cdot cm^{-2}$ (Pt). Both anode and cathode diffusion layer are Sigracet SGL35DC (thickness 325 μm, 20% PTFE content, with microporous layer). During testing, unless differently indicated, anode and cathode are fed respectively with 1.0 M methanol solution with stoichiometry equal to 6 and air, saturated by water at ambient temperature, with stoichiometry equal to 3. Nominal current density is 0.25 $A \cdot cm^{-2}$ and the fuel cell temperature is kept at 75^oC.

6.2.2 DMFC Operation and Diagnostic

According to the experimental results obtained during the DMFC operating strategies comparison reported in paragraph 2.4 the DMFC cannot be operated with continuous operation due to an excessive degradation rate and for this reason, they are usually operated by means of operating strategies. For this long-term test, the DMFC has been operated by cycles of 20 minutes followed by 1 minute of Refresh procedure. About every 120 hours operation, an interruption for diagnostic is performed to evaluate permanent degradation. The Refresh is an IRD Fuel Cell confidential procedure that consists of a sequence of OCV and cathode air feeding interruption already presented in chapter 2, which allows recovering the temporary degradation. During the OCV period, after the air feeding is switched off, the cathode potential drops to less than 0.3 V and, when the operation restarts, a significant positive effect on performances is obtained. A preliminary interpretation of the positive effect of refresh cycles on DMFC performance has been already presented in 4.7 where temporary degradation is mainly investigated. However, despite this operating strategy determines a lower temporary degradation than the steady state operation, it does not allow to fully remove temporary degradation as confirmed in 4.5.
A set of diagnostic tools has been used for the characterization of permanent degradation once the temporary degradation has been minimized during each long operation interruption for diagnostic by means of full refresh technique as will be explained in the next paragraph.
As well as the innovative diagnostic tools, tuned and adapted for permanent DMFC degradation characterization, polarization curves and EIS, already described in 2.2.4, have been used to investigate degradation. EIS are performed by means of the potentiostat at 0.1 and 0.25 $A \cdot cm^{-2}$ during the polarization curves. Furthermore it should be noted that the voltage values obtained from the polarization curves, especially at high current densities, are affected by temporary degradation resulting in lower values in comparison with the ones obtained during the degradation test.

Cyclic Voltammetry

Cyclic Voltammetry (CV) is a measurement technique, which is normally applied in the study of catalyst systems and electrochemical reactions. In the fuel cell field, CV is widely used to evaluate the catalyst active area of the electrodes [129]. In this experimental activity, it was used to measure the catalyst active area of the cathode electrode, because it results not reliable for platinum-ruthenium alloy used as DMFC anode catalyst.

During this measurement the fuel cell was fed with hydrogen on the anode side (3.5 $Nml \cdot min{-}1$) and 80 ^oC saturated nitrogen on the cathode side (0.6 $Nl \cdot min{-}1$). In this condition the cathode is covered by hydrogen coming from the anode side, which cannot be consumed, due to the absence of oxygen. The CV was performed by cyclically scanning the potential of the cathode between $0.04V$ and 0.6 V with a speed rate of 25 $mV \cdot s^{-1}$. As a consequence of this continuous voltage variation, a non stationary current was generated inside of the fuel cell because of the successive hydrogen desorption and adsorption on the cathode catalyst. By plotting the measured non-stationary current as a function of the imposed voltage a voltammogram is obtained. This plot represents the outcome of CV and shows a positive current peak, which is related to the hydrogen desorption from the cathode catalyst particles. By integrating this non-stationary current peak over time, an estimation of the charge adsorbed on the cathode catalyst can be obtained. The catalyst active area can therefore be calculated assuming that the catalyst is covered by a monolayer of hydrogen with a charge density of 210 $\mu C \cdot cm^{-2}$ [129]. During the measurement, the potential was intentionally limited below 0.6 V to observe only hydrogen adsorption-desorption without entering the oxygen adsorption-desorption region [130]. As explained above, the CV cannot be performed under real operative conditions. For this reason it was essential to reproduce measurement conditions which are as similar as possible to the real operative ones. The proper choice of flow rates and humidification was therefore critical and was done with particular care.

Linear Sweep Voltammetry

Linear Sweep Voltammetry is a common diagnostic tool for PEFC that, in this work, has been adapted to DMFC diagnostic; it permits to quantify the hydrogen crossover through the membrane and the short circuit current. During this measurement, hydrogen was supplied to the anode of the fuel cell (3.5 $Nml \cdot min^{-1}$) and 80 ^oC saturated nitrogen was supplied to the cathode (0.6 $Nl \cdot min^{-1}$), as done for Cyclic Voltammetry 6.2.2. In this condition hydrogen diffuses from the anode and deposits on the catalyst on the cathode electrode. The LSV consisted in linearly raising the potential of the cathode over the anode from 0.085 V up to 0.55 V so that the hydrogen adsorbed on the cathode catalyst [129] is progressively oxidized. During this measurement the potential was increased slowly, with a speed rate of 1 $mV \cdot cm^{-2}$, in order to avoid current peaks and achieve the equilibrium between hydrogen crossover and oxidation. The current related to the hydrogen oxidation was measured as indication of the hydrogen crossover rate. When the voltage is sufficiently high, equilibrium between the hydrogen crossover and its desorp-

tion can be achieved allowing for its quantification [131]. The linear increase in current density is due to internal short circuit across the electrolyte membrane that occurs as the potential is increased. Generally, during operation the membrane progressively could thin with the consequent formation of pinholes and micro-cracks [132]. Therefore the electrical separation of the fuel cell electrodes cannot be fully guaranteed, and current is generated when a voltage difference is imposed. In this situation the membrane behaves like a pure resistor obeying Ohm's law and this explains the linearity of current with voltage. This measurement will be hence used as a diagnostic tool for the membrane degradation in order to ensure information of its integrity and on its evolution in time and it will be performed during the operation interruption as the cyclic voltammetry (CV).

Methanol Stripping

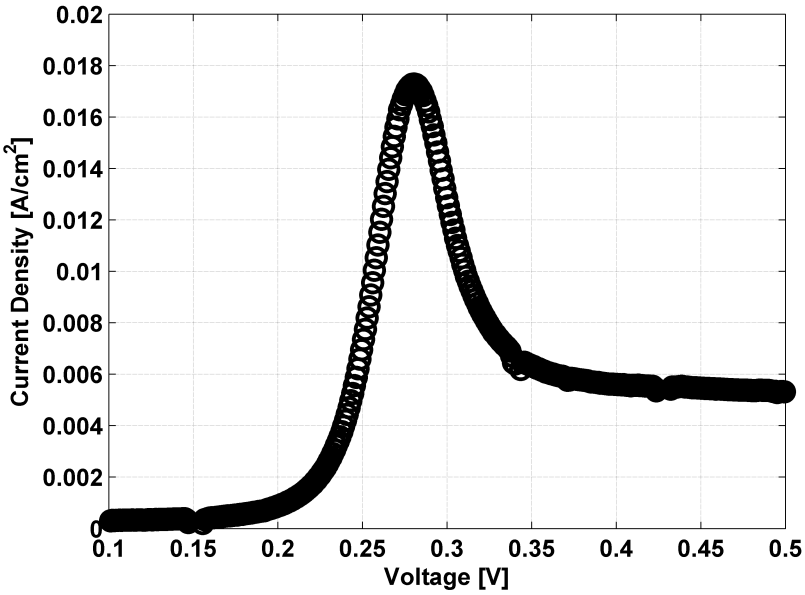

Figure 6.1: Example of Methanol Stripping measurement result

As previously explained 6.2.2, cyclic voltammetry seems not to be a reliable measurement for the anode electrode characterization; for this reason, during this PhD thesis, an additional measurement has been added and adjusted to provide a characterization of anode electrode degradation. Literature [133] often reports about *CO* stripping as a DMFC anode characterization tool but, a few works propose methanol stripping to individuate

the activity of the anode catalyst [68] by flowing water and methanol in the anode and keeping cathode as a hydrogen reference electrode.
Such technique has been adapted in this work in order to maintain the oxidation peak under the potentiostat current full-scale value and, through a continuous improvement of technique mastery, the final procedure consists of the following key-points:

- 5 minutes washing of the anode electrode with bidistilled water (mass flow 12 $g \cdot min^{-1}$);
- 5 minutes at 100 mV versus the DHE with 1M methanol solution flowing with a massflow of 3.9 $g \cdot min^{-1}$ in order to adsorb species on the anode catalyst;
- 5 minutes at 100 mV versus the DHE with bidistilled water flowing with a massflow of 3.9 $g \cdot min^{-1}$ in order to remove the unadsorbed species;
- a linear increase of potential from 100 mV to 500 mV with a slew rate of 1 $mV \cdot s^{-1}$ acquiring the current that presents a non-monotonic behaviour with a maximum;

A example of Methanol Strip technique results is reported in figure 6.1. The shift of the oxidation peak from lower to higher values of overpotential can be related to a loss of activity of the anode catalyst as explained in [68].

6.3 Minimization of Temporary Degradation

Despite the operating strategy used for DMFC operation is very effective in comparison with others as reported in [71], it does not permit to completely remove the temporary degradation. In figure 6.2 two consecutive tests with the refresh operating strategies, performed in reference conditions, are showed; they are interspersed by an operation interruption for diagnostic and this long operation interruption allows a higher performance recovery than a usual refresh procedure. This confirms that the operating strategy does not avoid temporary degradation accumulation and, for this reason, the minimization of temporary degradation can be obtained only during the operation interruption.
An innovative "full refresh" technique has been actually developed in order to get the highest recovery of performances; it has been applied during the degradation tests just before and after the performance of the diagnostic

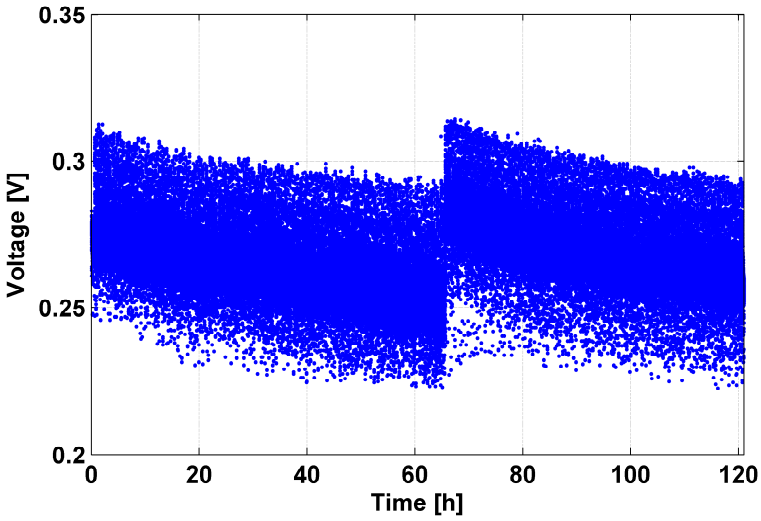

Figure 6.2: Voltage behaviour during two consecutive tests performed with refresh operating strategy

techniques in order to guarantee that the diagnostic tools reveal only the permanent component of DMFC degradation and to ensure the reliability of permanent degradation calculation method. It consists in 16 hours of methanol solution continuous circulation in the anode serpentine at very low mass flow ($0.33\ g \cdot min^{-1}$) while both the inlet and the outlet of the cathode distributor have been plugged to avoid oxygen infiltration in the cathode and the cell is kept at 75 ^oC. During this long interruption, the anode GDL and electrode saturation should increase due to progressive hydration resulting in optimal anode performances at the restarting coherently with [82] and chapter 3 and electrolytic membrane is fully hydrated resulting in low ohmic resistance. Furthermore the cathode potential progressively reduces to about 0 V and this has a strong positive effects on DMFC performances that is not fully explained but platinum oxides reduction could be probably responsible for this behaviour.

The full refresh positive effect on performances is reported in figure 6.3 where a DMFC MEA, already activated with the IRD Fuel Cell A/S standard activation described in 2.2.5, is subjected on this procedure after just 50 hours of test. The voltage value obtained after the full refresh interruption is higher than the beginning of life value confirming that it permits to minimize temporary degradation effects; for this reason, full refresh can be also helpful to reduce DMFC activation procedure duration.

The Nyquist plot of the impedance spectra, performed after and before

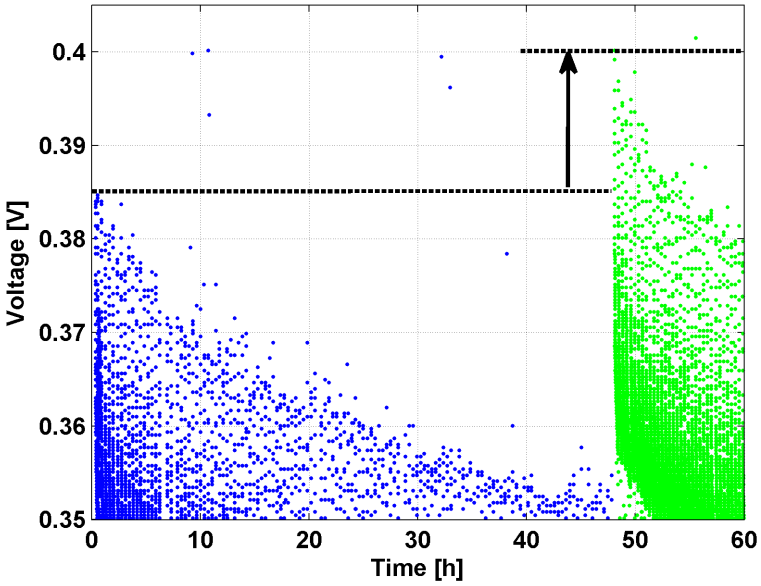

Figure 6.3: Performance recovery respect to Begin-of-Life for a DMFC activated with IRD activation procedures and subjected to full refresh technique

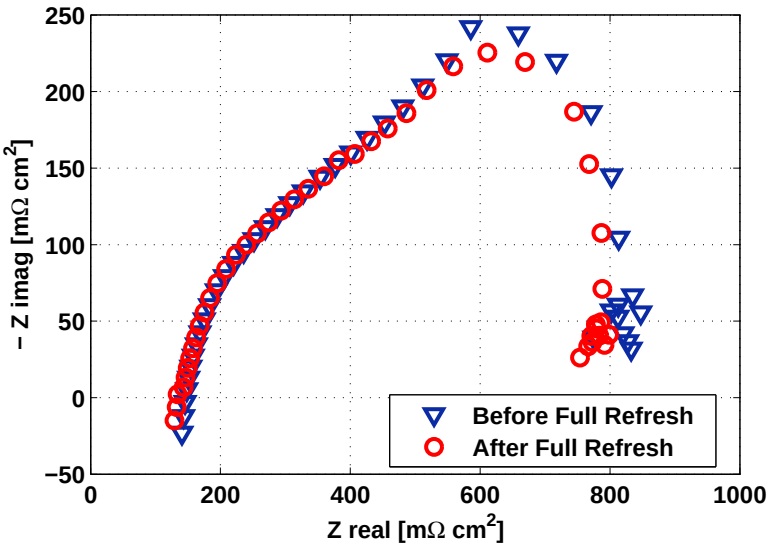

Figure 6.4: Nyquist plot of EIS performed after and before the Full Refresh procedure in reference conditions

the first Full Refresh, are reported in figure 6.4 where three main evidences can be pointed out: first a decrease of membrane ohmic resistance that should be related to the high membrane hydration that can be obtained during the Full Refresh; secondly the cell total resistance diminishes and this is coherent with the performance gain and thirdly a reduction of the capacity feature at intermediate frequencies related to the kinetics is achieved but the reasons are not completely explained.

6.3.1 A new procedure for the DMFC activation

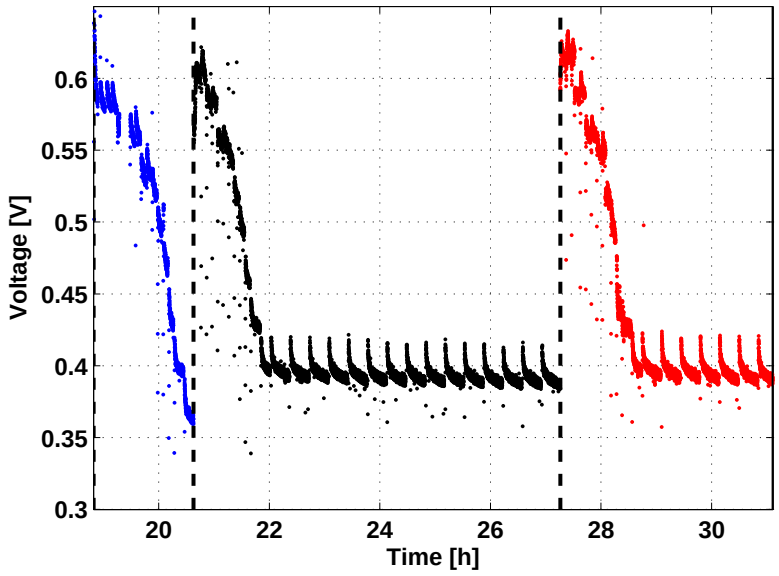

Figure 6.5: DMFC Voltage during the new activation procedure developed at PoliMi.

The IRD Activation procedure does not guarantee the highest cell performances as a reference for the begin-of-life (BoL) (see figure 6.3); a new activation procedure has been designed with two main goals: first, to reach the reduce the activation procedure duration, secondly to define a standard for the Begin of Life performances definition.
The new activation procedure is similar to the IRD procedure described in paragraph 2.2.5, but it includes a different shut down each day. After the hydration with water until nominal temperature, the DMFC operates on the same current ramp of IRD procedure. However, at the end of the first and of the second day, a full refresh procedure is applied and it permits to make the activation procedure faster.

Figure 6.5 reports the voltage history during the first three day of life of a DMFC activated with the new procedure. It highlights that at the end of the third day, the performances are very similar to the end of the second day and, for this reason, the third day is not mandatory. In order to define a standard, the BoL polarization of each cell is performed at the third day, after the ramp and a long refresh of 5 hours of the DMFC.

6.4 Voltage decay analysis in long-term test

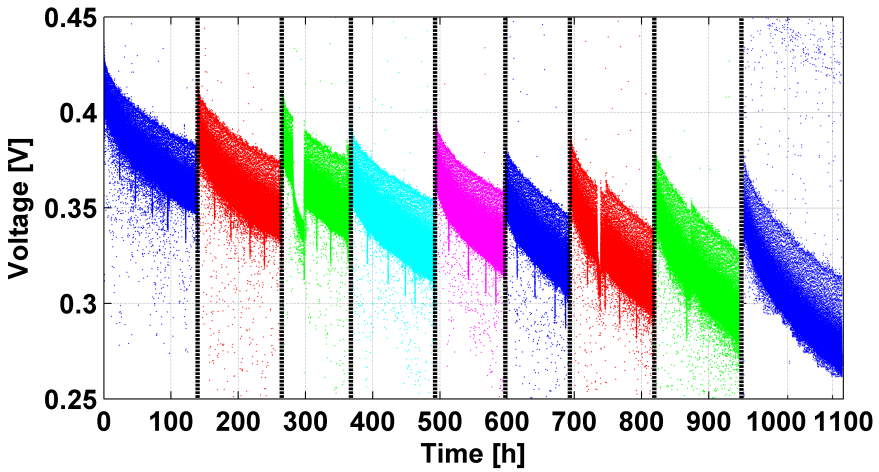

Figure 6.6: Voltage decay during the long-term test performed at 0.25 $A \cdot cm^{-2}$. Each performance recovery corresponds to the operation interruption for diagnostic with full refresh procedure.

Figure 6.6 reports the DMFC MEA voltage behaviour during the long-term test performed at constant current and stoichiometries. The long-term test has been performed by means of cycles of about 120 hours of operating strategy followed by diagnostic that is preceded and followed by a full refresh in order to minimize temporary degradation. During each interruption the previously described diagnostic techniques have been performed and a performance recovery has been observed.

The slope of each part of the test has been characterized with the method described in 2.5.1 and the results are reported in table 6.1; the coherency between the values of degradation of table 6.1 suggests that no significant alteration in temporary degradation mechanisms occurs during the operation.

Figure 6.7 shows the polarization curves performed during each interruption for diagnostic that allows to quantify the DMFC permanent degradation

Part of the test	Duration	Degradation rate $\mu V \cdot h^{-1}$	Permanent degradation $\mu V \cdot h^{-1}$
I	140 h	286 $\pm$ 2.5 %	180
II	125 h	273 $\pm$ 2.9 %	70
III	95 h	280 $\pm$ 11.6 %	21
IV	120 h	264 $\pm$ 1.8 %	58
V	105 h	293 $\pm$ 2.9 %	133
VI	100 h	313 $\pm$ 2.8 %	0
VII	125 h	281 $\pm$ 3.8 %	171
VIII	125 h	321 $\pm$ 13.1 %	43
IX	150 h	343 $\pm$ 4.4 %	66

Table 6.1: Summary of degradation rates during each part of the Long-term test.

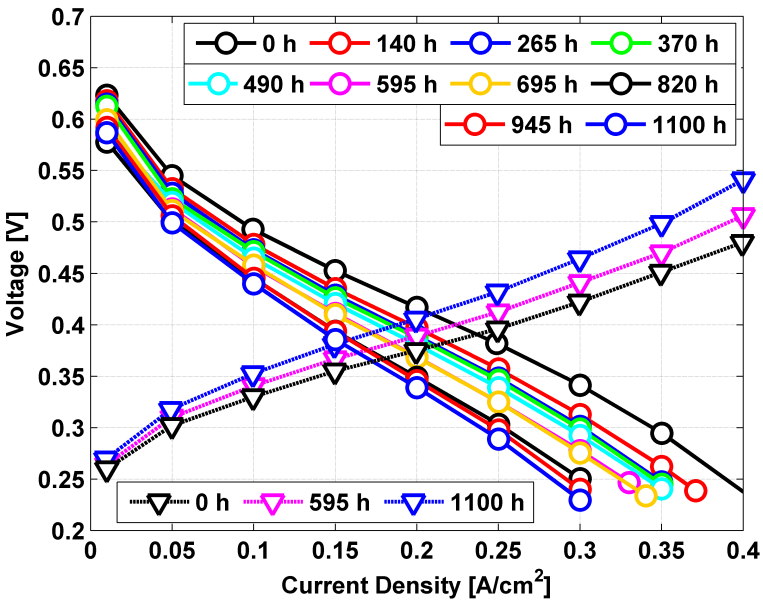

Figure 6.7: DMFC and Anode Polarization curves performed in diagnostic interruption during the long-term test.

during the long-term test; anode polarization curves are performed only at the beginning, middle and end of life in order to provide quantitative information on the anode electrode evolution. Assuming a complete removal of temporary degradation with the full refresh performed before the diagnostic and keeping constant the duration of the polarization curve (i.e. a constant temporary degradation during each polarization curve), the permanent degradation can be quantified as the ratio between the performance loss in the polarization curves at reference current (i.e. 0.25 $A \cdot cm^{-2}$) between the Begin of Life (BoL) and the End of Life (EoL) and the duration of the long-term test. A permanent degradation of 90 $\mu \cdot Vh^{-1}$ is calculated through this method and the anode component of the permanent degradation, obtained in the same way from the anode polarization curves, is equal to 31 $\mu V \cdot h^{-1}$ corresponding to about 34% of the total permanent degradation. This value is higher than what generally declared by the manufacturers (< 30 $\mu V \cdot h^{-1}$) but there are some possible reasons for this discrepancy:

- the methodology adopted by the manufacturers degradation testing and anaysis is different from the one presented in this work; furthermore temporary degradation evaluation is rarely conducted;
- the manufacturer flow-field is optimized for the performance and lifetime while the flow-field used in this laboratory test is a common triple serpentine for both anode and cathode and this can lead to local starvation or not correct operation;
- the orientation of DMFC manufacturer flow-field is generally optimized for the correct gas-phase CO_2 removal while typical laboratory flow-field are not designed for this purpose;
- from industry internal report (confidential), the methanol grade quality is found to be a critical aspect for both temporary and permanent degradation. The methanol used in PoliMi has a high grade of quality but it belongs to a different brand respect to the industrial one and this could lead to different results in degradation;
- the M.R.T. Fuel Cell Laboratory of Department of Energy (Politecnico di Milano) is placed into a trafficked city and the quality of the air could probably affect the DMFC operation. Indeed according to [134] the air pollutants such as NOx or can hinder the fuel cell operation;
- the definition of Begin of Life (BoL) performances has not ever been standardized in the literature.

6.5 In-Operando analysis on permanent degradation

6.5.1 Electrochemical investigation of electrodes degradation

Since about 66% of permanent degradation can be attributed to cathode electrode, membrane and GDLs, diagnostic allows to distinguish the components that are mainly responsible for the degradation.

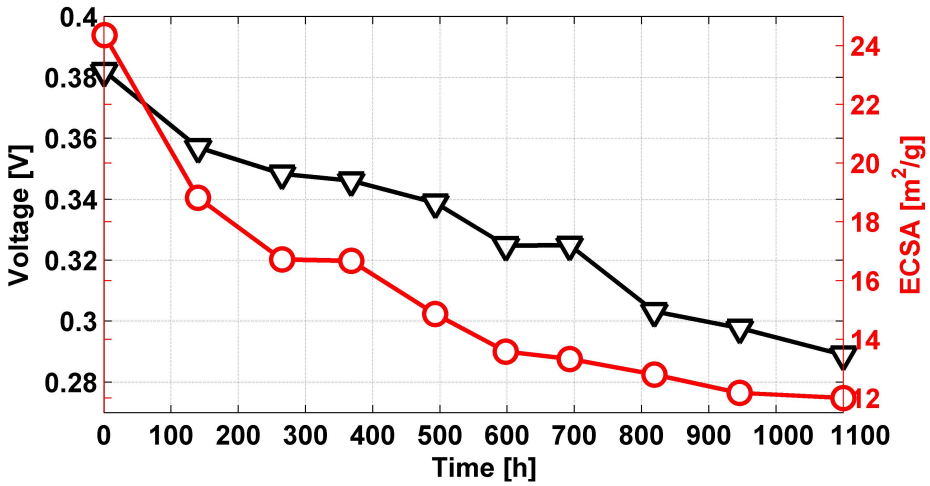

Figure 6.8: Comparison between cathode ECSA obtained through the CV and Voltage at nominal current density during the Polarization curves.

In figure 6.8 is reported a comparison between the voltage decay in the polarization curves at nominal current density and the ElectroChemical Surface Area calculated from the cyclic voltammetries. A non-linear decay, with a strong initial decrease, of ECSA is evident coherently with typical platinum degradation mechanisms reported in the literature [40], while the voltage decay does not have a similar behaviour; the long-term test determines a comprehensive reduction of about 50% of cathode ECSA in more than 1000 hours. Indeed, during the DMFC operation, the cathode catalyst works in strongly degrading conditions such as very high potentials ($\sim 0.8\ V$), high water content (that is the medium for the platinum ion transport) and high temperature (75^oC). In these conditions, a strong decrease of cathode surface area is expected and the cathode electrode will be deeply investigated in the second part of this paper by means of post mortem analysis.

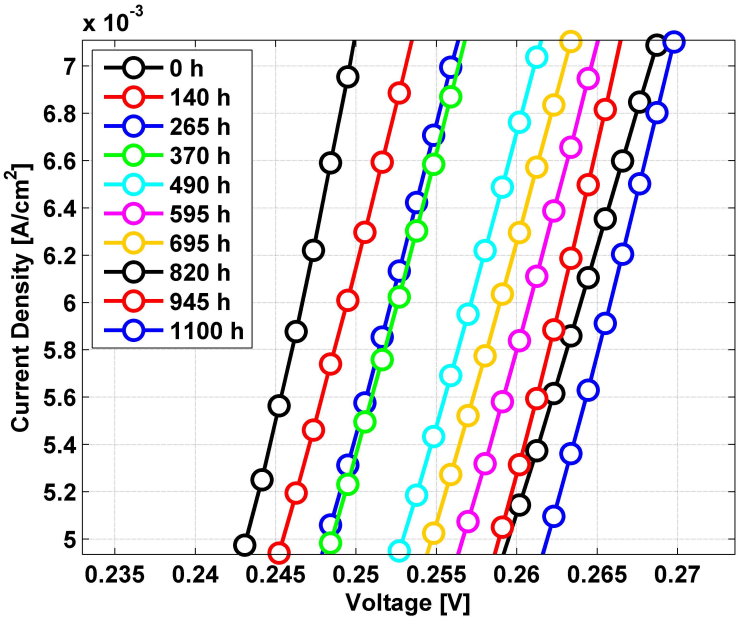

Figure 6.9: Zoom on oxidation peak sudden rise during Methanol Strip measurements performed in long-term test

Methanol stripping results, reported in figure 6.9, acts as a qualitative method to appraise anode effectiveness, evaluating the potential needed to begin adsorbed methanol oxidation as in [68]; in fact the progressive shift of the oxidation peak could be related with anode catalyst degradation mechanisms. The analysis of the methanol strip shows a regular increase of the activation potential suggesting that anode electrode has a regular and limited permanent degradation that is quantified by means of anode polarization curves. The progressive shift in the oxidation peak potential obtained through methanol stripping technique could be use as an indication of the Ruthenium loss at the anode electrode as in [68] that can also move into the membrane to the cathode electrode as discussed in the post mortem analysis summary reported in paragraph 6.7.

6.5.2 Investigation on membrane degradation

Figure 6.10 reports several diagnostic parameters to investigate polymer electrolytic membrane degradation including both electrochemical and mass transport measurements obtained during the polarization curves. Methanol crossover acquired at nominal current density do not highlight significant modifications with the degradation; this result is not completely coherent

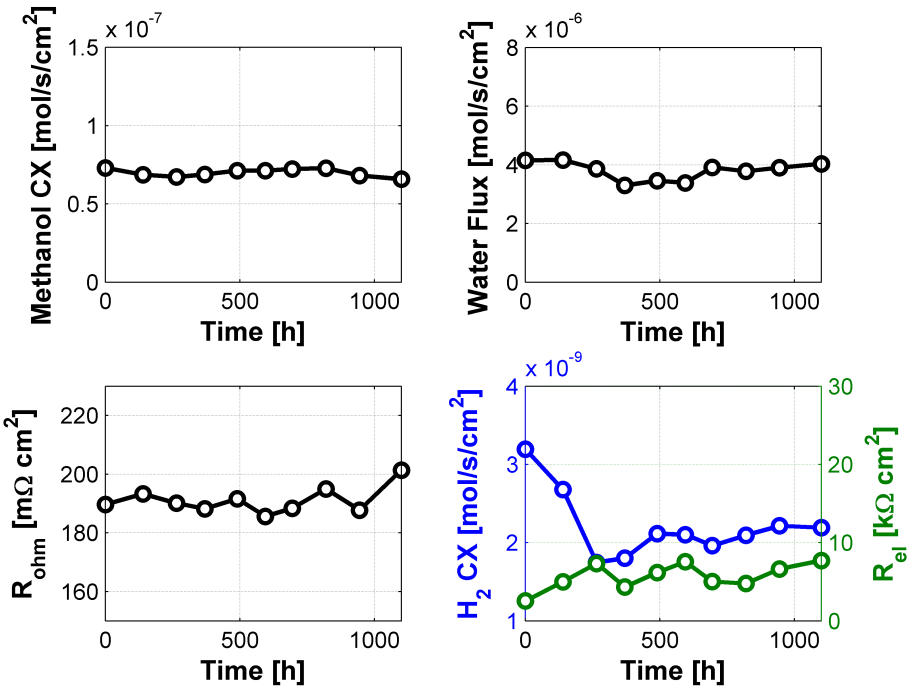

Figure 6.10: Diagnostic tools for membrane characterization: Methanol crossover and water content in cathode outlet at nominal current density (i.e. 0.25 $A \cdot cm^{-2}$) during the polarization curves; Membrane ohmic and electrical resistance and hydrogen crossover obtained through LSV and EIS.

with the one reported in paragraph 4.5.2 and it could probably due to two reasons: first, the MEA used in this work belongs to a different and more recent production batch. Secondly, some other preliminary tests not in nominal conditions were carried out on the MEA investigated in 4.5.2 and could affect the obtained experimental results. On the contrary, during each part of the long-term test, methanol crossover generally presents a slight downward trend coherent with the anode temporary degradation mechanism proposed in chapters 3 and 4. However, this methanol crossover decrement during the operation is fully recovered with the full refresh procedure confirming that the latter permits also to increase the methanol and water concentration at the anode electrode.
Water content at cathode outlet remains about constant, suggesting that membrane mass transport properties (and probably also cathode GDL mass transport properties) do not observe important changes. Indeed water content in cathode outlet is a function of mainly the cathode GDL and membrane diffusivity and permeability as discussed for example in [9].
However methanol crossover and water content in cathode outlet are regulated by a interconnection of very complex transport mechanisms and a GDL degradation could not inevitably results in significant alteration of DMFC mass balances; indeed the effect of degradation on MPL cracks, seen in chapter 5 is not known; also the effect of a slight diffusivity increase of anode GDL related to the degradation could not even determine significant variation on the methanol crossover because it is governed by means of a combination of liquid and gas phases transport mechanisms.
Membrane ohmic resistance can be measured through the Electrochemical Impedance Spectroscopy that is performed during the diagnostic polarization curves; the impedance value at first interception of the spectrum with the real axis (at very high frequencies) at nominal current density is reported in figure 6.10 and it does not highlight significant changes. These results are different from those reported in paragraph 4.5.2 where a slight increase of membrane ohmic resistance and a permanent reduction of methanol crossover were observed; on the contrary, during this long-term test both of them seems to be constant,suggesting that methanol crossover and membrane ohmic resistance could be related; further work is needed to investigate this phenomenon. From the Ohm law it is possible to quantify the permanent degradation that is attributable to the membrane: it is negligible in comparison with anode and cathode electrode degradation. Moreover, mass balances through the DMFC suggest that also the degradation of the Gas Diffusion Layers seems to be not significant on the performances, coherently with what reported in 5.7; as a consequence, the degradation of the cathode electrode turns out to be the most important component of DMFC permanent degra-

dation and it represents more than 65% of DMFC permanent degradation in this long-term test.

6.5.3 Impedance Spectroscopy analysis

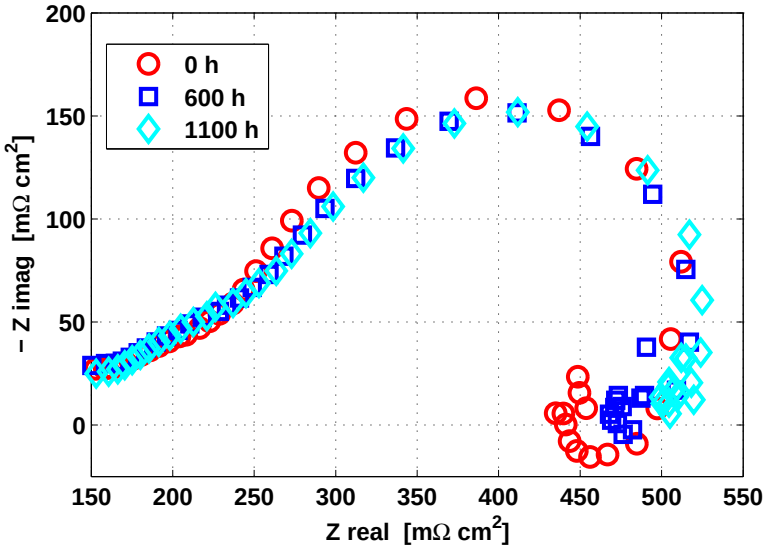

Figure 6.11: Nyquist plot of anode EIS performed at nominal current density during the anode polarization curves reported in figure 6.7.

Figure 6.11 shows the anode EIS[1] performed at the reference current density (i.e. 0.25 $A \cdot cm^{-2}$) during the anode polarizations reported in figure 5 at the beginning, the middle and the end of the long-term test; the anode spectra do not highlight any important modification during the test, in spite of the significant anode degradation rate. At low frequencies, the inductive behaviour typical of the DMFC anode and generally attributable to coverage of reaction intermediates as in [72] on Pt sites, progressively disappears and disturbances due to mass transport limitations occur.

The EIS performed during the DMFC polarization curves at reference current density are only partly reported for sake of comprehension in figure 6.12. The DMFC spectrum is the overlapping of anode and cathode contributions, therefore distinguishing each component is rather complex; anyway a qualitative analysis on the EIS points out a strong increase in the total resistance (i.e. the slope of the polarization curve in the reference current

[1]Data at frequencies higher than 1 kHz are not reported, because alterated by instrument limitation, as evidenced by Kramers-Kronig relations.

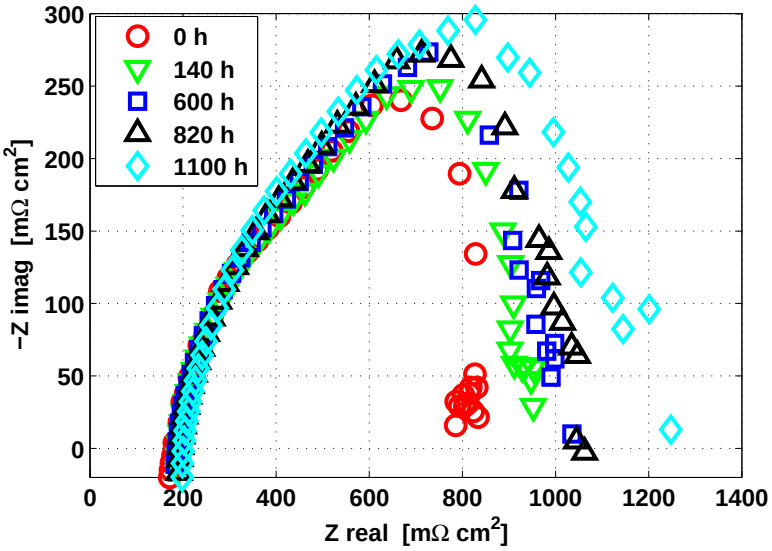

Figure 6.12: Nyquist plot of DMFC EIS performed at nominal current density during the polarization curves reported in figure 6.7.

density) and an increase of the capacitive feature at intermediate frequencies that is mainly the sum of the charge transfer resistance of the two electrodes. Since the anode impedance spectrum does not reveal significant modifications of the charge transfer resistance, the behaviour is probably due to the worsening of the cathode kinetic that could be related to the surface area loss observed by the CV. However mass transport limitations, probably related to cathode, hinder a more detailed interpretation of the EIS resulting in low frequencies disturbances; furthermore, the reduction of ECSA loss could determine a increase in cathode mass transport limitations because of the increase of reactants flux on each active site [135].

The Bode plot reported in figure 6.13 further confirms the previous interpretation showing that there are no changes in the relaxation frequencies of the different spectra; indeed the intermediate frequencies peak is generally attributed to the reactions kinetic while the low frequencies peak, when present, is attributed to the mass transport limitations. The complexity of the DMFC mass transport phenomena determines strong disturbances at low frequencies that are evident in the Bode plot, coherently with the previous interpretation on the effect of ECSA loss on the mass transport limitations.

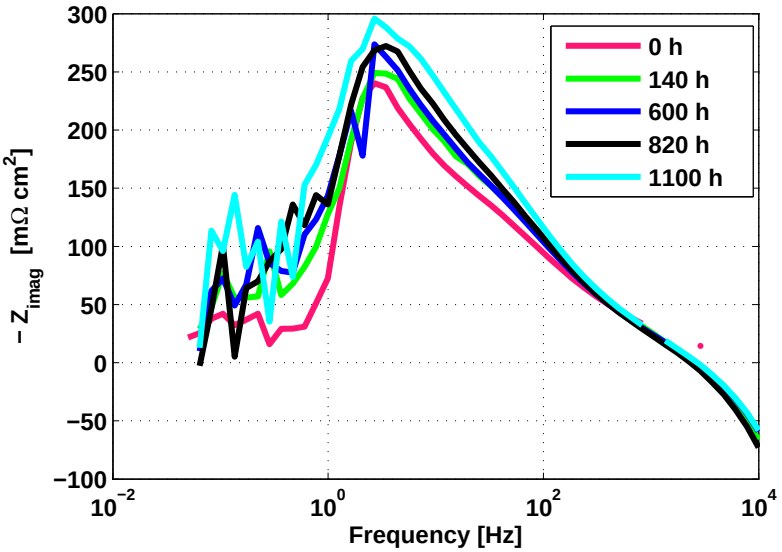

Figure 6.13: Bode plot of DMFC EIS performed at nominal current density during the polarization curves reported in figure 6.7.

6.6 Summary of in-operando analysis on DMFC Long-Term degradation test

This part of the chapter presents an experimental analysis on DMFC degradation carried out performing a long-term test of more than 1000 hours in nominal reference conditions quantifying the real permanent degradation; the systematic diagnostic permits to identify the main components affected by performance degradation and to draw the following conclusions:

- Full Refresh procedure permits to minimize temporary degradation allowing to quantify permanent degradation;
- a permanent degradation of 90 $\mu V \cdot h^{-1}$ has been quantified through the comparison of the polarization curves performed during the diagnostic in reference conditions;
- cathode ECSA decreases of 50% during 1000 hours of operation and cathode electrode degradation is responsible for more than 60% of DMFC permanent degradation while anode electrode is responsible for about 34% of permanent degradation;
- membrane and cathode GDL degradation seems to be negligible in comparison with the electrodes degradation and mass transport phenomena do not show significant changes during the long-term test;

- the EIS performed during the polarization curves confirms a worsening in the charge transfer that could be due to the cathode electrode degradation.

6.7 Summary of post mortem analysis results performed at DLR and CEA

The XPS measurements have been performed at the German Aerospace Center - Institute for Technical Thermodynamic (DLR) thanks to Dr. Pawel Gazdzicki and Dr. Mathias Schultze; the TEM and SEM measurements have been performed by the Commissariat à l'Energie Atomique (CEA) - Laboratoire d'Innovation pour les Technologies des Energies Nouvelles (LITEN) at the Grenoble Electron Microscopy at Minatec thanks to Dr. Laure Guetaz. The DMFC MEA has been disassembled at PoliMi and sent to CEA where it has been cut and again sent to DLR for the completion of the analysis. The results and the figures of the following paragraphs are provided by DLR and CEA and the PhD candidate only summarizes them as an insight into DMFC permanent degradation mechanisms.

6.7.1 XPS analysis performed at DLR

The X-ray PhotoElectron Spectroscopy measurements, by means of the peel-off technique (see Ref. [136]), provide the concentration of elements (given in atomic percent, at %) in the studied samples. The samples have been analysed as-received; as additional reference sample an activated DMFC MEA operated for 30 h was used.

XPS analysis of the degradation of catalyst material

In order to analyse the MPL/CL interfaces of the DMFC MEAs, peel-off depth profiles are measured with XPS. The profiles into the catalyst material in the pristine, the activated and the aged samples, plotted as atomic percentages versus peel-off steps, are depicted in Figure 6.14. The images comprise data measured at the anodic as well as cathodic MPL/CL interface. The main difference between the anode and the cathode CL of the pristine MEA is that on the anode side as Pt (0.6 at %) and Ru (0.4 at %) are observed as catalysts. The cathode catalyst layer, on the other hand, contains 1.6 at % Pt as the only catalytically active element; this is coherent with the technical data provided by the manufacturer.

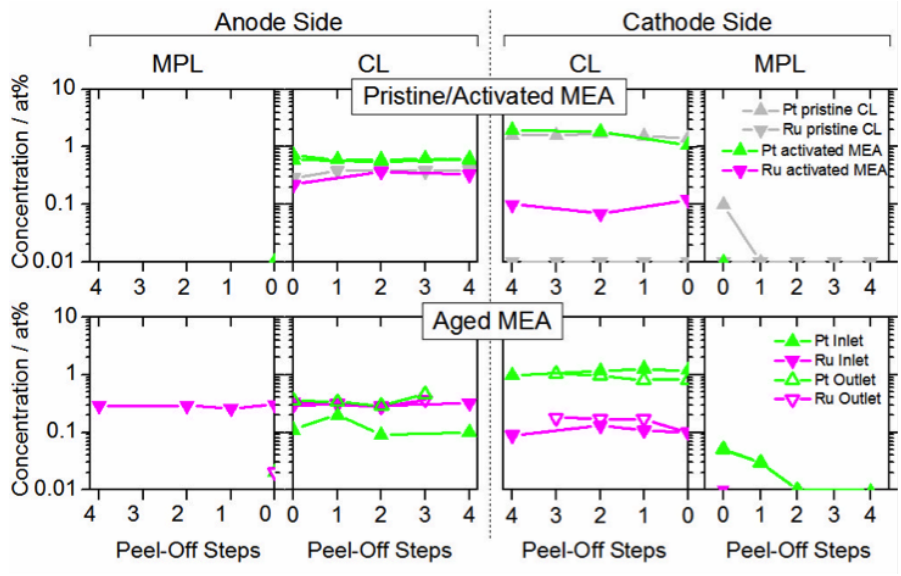

Figure 6.14: Peel-off depth profiles of the anode and cathode side MPL/CL interfaces of the pristine, activated (30 h operation) and aged MEA (1100 h operation). In the case of the aged MEA the solid and open symbols correspond to the inlet and outlet zone of the flow field, respectively.

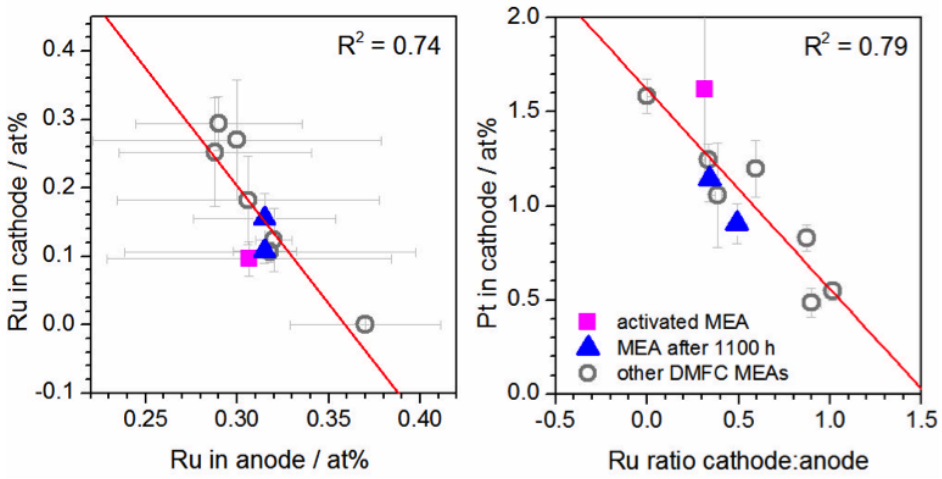

Figure 6.15: (A): Atomic percentages of Ru in cathode side CLs plotted versus the percentages of Ru in the anode side CLs. (B): Atomic percentages of Pt in cathode side CLs versus the ratio of atomic percentages of Ru in cathode CLs and anode CLs. (measure for amount of crossed-over Ru). The plots comprise data the activated MEA, the MEA after 1100 h operation and other differently aged DMFC MEAs. The strength of correlation expressed by means of the Pearson coefficient of correlation R is given in the figure.

Corresponding depth profiles of the MPL/CL interfaces of the activated and aged MEA exhibit significant amounts of Ru in the cathode CL likely due to crossover from the anode side; as the concentration of crossed-over Ru is only slightly higher in the aged MEA than in the activated MEA, it is concluded that this process occurs mainly at the beginning of the fuel cell operation and proceeds very slowly upon long time operation (see Figure 6.15). The initial strong degradation of the catalyst is in accordance with the initial strong performance loss observed in Figure 6.8. Hence, the Ru crossover effect is not expected to significantly contribute to the performance loss of the fuel cell after long time operation.

XPS analysis of the degradation of carbon and polymers in the CL and MPL

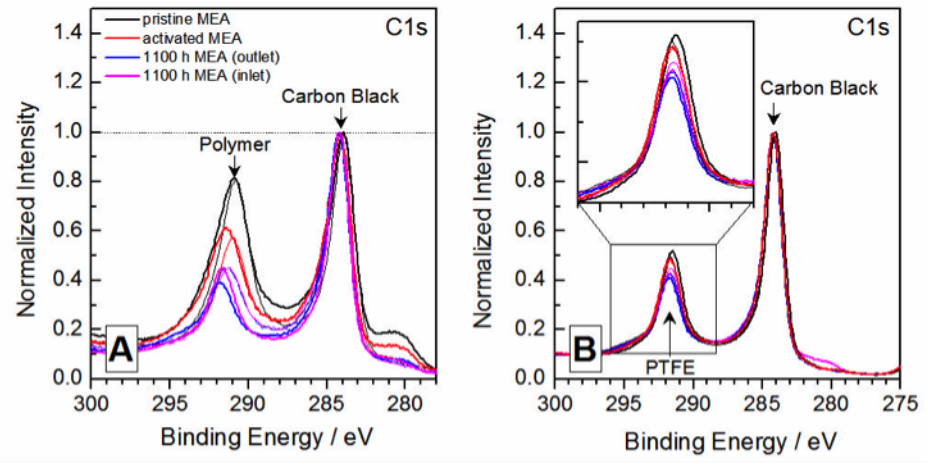

Figure 6.16: (XPS spectra of the C1s regions of the pristine, activated and 1100 h aged catalyst layers (A) and micro porous layers (B). The thick and thinn lines correspond to the anode and the cathode side, respectively. The spectra are normalized with respect to the intensity of the 284 eV peak.

A change observable in the CL due to the operation is the loss of the polymer concluded from the C1s details spectra of the catalyst layers shown in Figure 6.16. The plot shows normalized spectra of the carbon species in the pristine, the activated and the 1100 h aged sample. Thick and thin lines correspond to anode and cathode sides, respectively.
The ratio $C_{carbonblack}/C_{polymer}$, calculable from the peak areas is lowest for the pristine sample and equals to 1. After activation and 1100 h operation the value increases to 1.3 - 1.6 and to 1.7 - 2, respectively, i.e. as in the case of Ru crossover this effect occurs fast during the beginning of operation of the MEA

and proceeds slowly upon further (long time) operation. Generally, the loss of the polymer binder within the catalyst layer may lead to several different effects related to a performance loss of the cell, i.e. a poor ionic resistance within the CL, a decrease of the active surface area (poor attachment of catalyst to ionomer), or an increase of the electrical cell resistance due to poor connection of catalyst and carbon. A polymer loss is observed also in the MPL upon operation in figure 6.16. The $C_{carbonblack}/C_{polymer}$ ratios are 1.5 - 1.6, 1.6 - 1.7, and 1.8 - 2 for the pristine, the activated and the aged MPL, respectively. It is finally noted that the ratio of $C_{polymer}/F_{polymer}$ does not change upon operation for both the CLs and the MPLs suggesting that loss of PTFE in the MPL and ionomer in the CL is not associated with a chemical degradation (in contrast to GDLs, see next section).

XPS analysis of the degradation of the GDLs

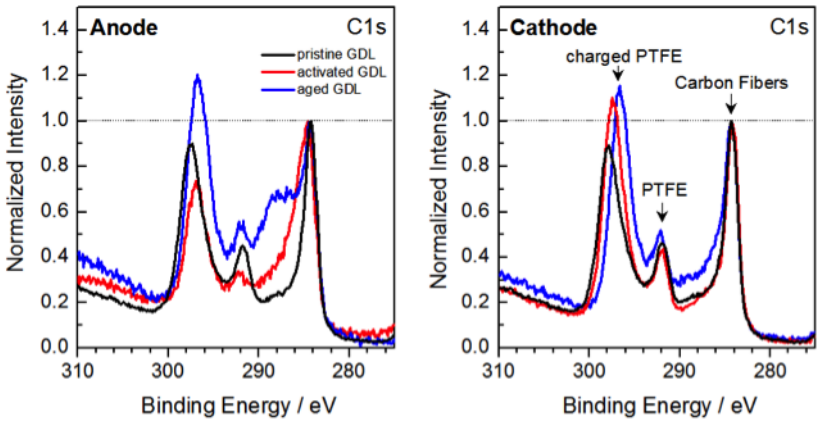

Figure 6.17: XPS spectra of the C1s regions of the pristine, activated and 1100 h aged GDLs. The spectra are normalized with respect to the intensity of the 284 eV peak.

In Figure 6.17, XPS spectra of the C1s region of GDL back sides of the pristine, the activatd and the aged MEAs are shown. The spectra exhibit three major peaks due to carbon fibers (284 eV), carbon bound in the PTFE (292 eV), and carbon within electrically charged PTFE (298 eV) due to x-rays ionization.
A drop of relative intensity after activation and a substantial increase after aging hat is observable for the PTFE peaks (292 and 298 eV) at the anode side. Probablyly, the initial drop may be due to structure changes such as covering of the carbon fibers by PTFE; the final increase of the relative

intensity of charged PTFE after 1100 h could be due to a rearrangement (or agglomeration) of PTFE leading to a de-wetting of the carbon fibers. Instead the cathode GDL degradation seems to be more limited. A further degradation effect is observed in the spectrum of the anodic GDL of the aged MEA where a new peak emerges in the range between 285 and 290 eV that is not observed in spectra of the other samples. This peak is typical for carbon in a CF-C compound and it is taken as an evidence for chemically decomposed PTFE (fluorine depletion).

6.7.2 Microscopy analysis performed at CEA

Dr. Laure Guetaz, at CEA - LITEN, performed Scanning Electron Microscopy (SEM) and Transmission Electron Microscopy (TEM) analysis on the degraded MEA focusing mainly on the electrodes and the electrolytic membrane. The microscopy analysis provides a first analysis, mostly qualitative, on the possible degradation mechanisms effects on the microstructures of the MEA. The preliminary results, which are reported in this paragraph, have to be further discussed and further work will be dedicated in the next future to investigate the relationship between the post mortem analysis and the in-operando diagnostic. The MEA has been investigated both in the reactants inlet and outlet regions and a summary of the most interesting observations is shortly discussed together with the images directly acquired at CEA - LITEN.

Figure 6.18 shows a SEM image of the aged MEA cross-section in the reactants inlet zone; the carbon fibers of the GDLs can be noted at the extremes of the section. The central region is the electrolytic membrane that seems whole in the microscale. The electrodes are in contact with the membrane and they have a thickness of about 10 - 31 μm for the cathode and 18 - 35 μm for the anode and the difference is evident in the cross-section. Between the GDL carbon fibers and the electrodes the MicroPorous Layer is evident.

A zoom in the cathode region of figure 6.18 can be founded in figure 6.19 where the complex microstructures of the cathode electrode can be appreciated. The cathode electrode is placed between the membrane (white since it charges with the electron beam) and the MPL (black); the structure is composed by carbon support and ionomer because the platinum nanoparticles are not recognizable on this scale. There are several structures of different dimensions probably due to the electrode production procedure, which it is very innovative and cannot be reported for consortium agreement. This innovative deposition technique usually results in the presence of big Pt/C paricles

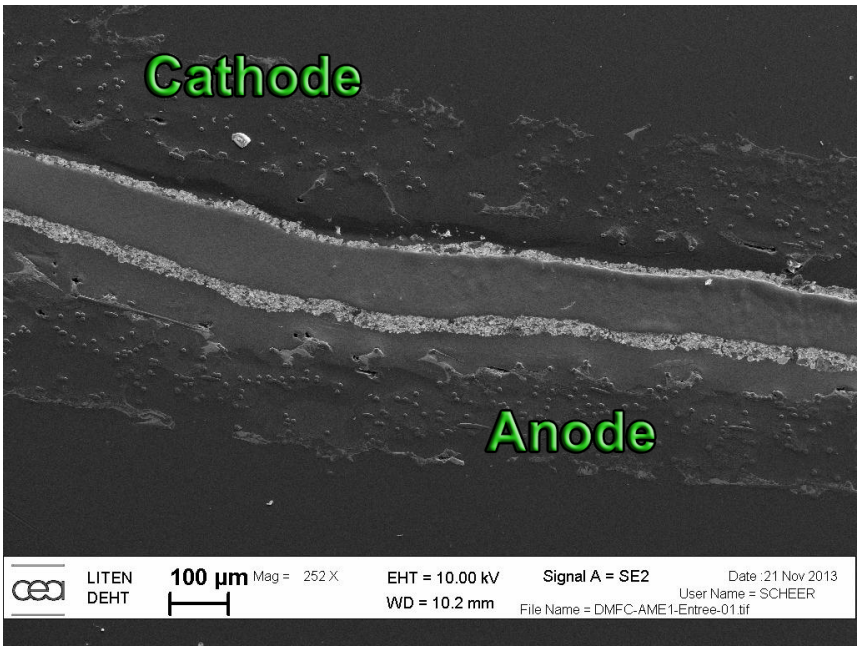

Figure 6.18: Cross section SEM observation of the aged MEA.

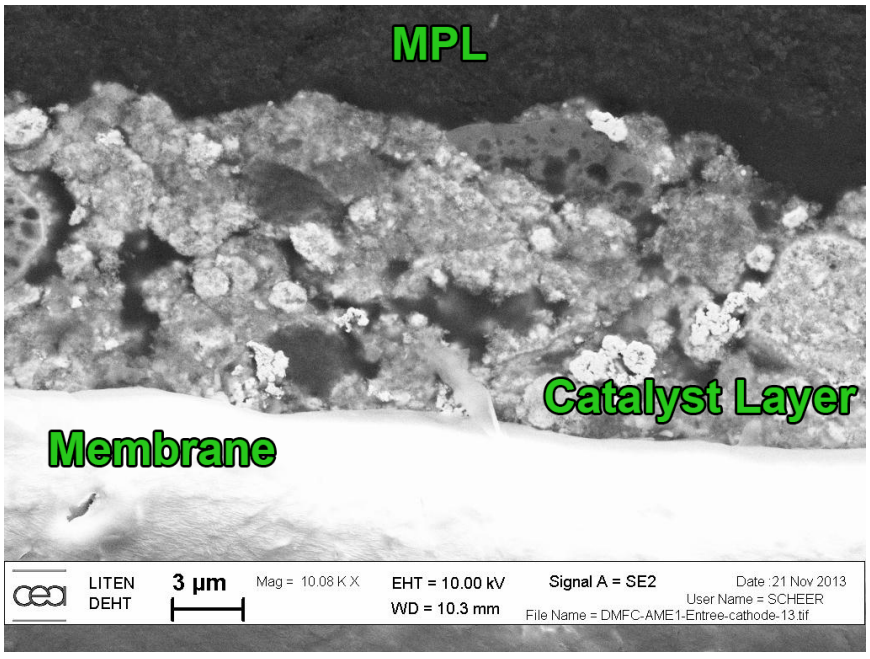

Figure 6.19: SEM observation of the aged MEA: zoom on the cathode region.

and, moreover the Pt particles are very heterogeneous form one big Pt/C particles to another and also inside the same agglomerate. Different levels of porosity can be attributed to the cathode electrode from the SEM and TEM images: there are macropores of micron-scale and, thanks to the complex agglomerates arrangement, pores tend to become smaller and smaller depending on the interconnection of the Pt/C particles. Furthermore, each agglomerate can present different levels of porosity because of the internal structure on which the catalyst nanoparticles are supported. Despite to the naked eye the deposited electrode could seem very regular as a coverage of the membrane, the microscope permits to appreciate the strong complexity that, during the operation, could determine mass transport limitations, lack of three phase contact and electrode typical degradation mechanisms.

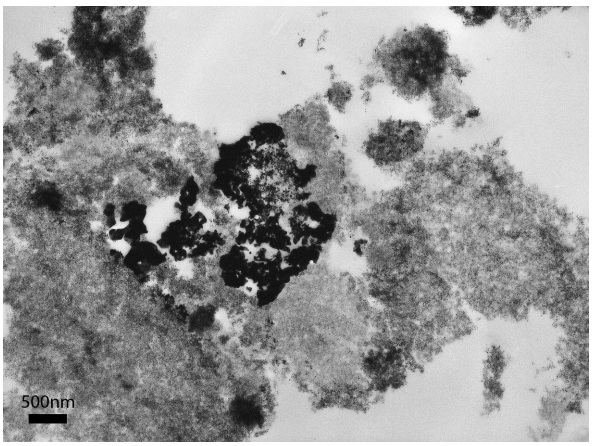

Figure 6.20: TEM observation of the aged MEA: cathode electrode.

The TEM images, figure 6.20 has been acquired on thin samples prepared by ultramicrotomy; on these TEM images, it is possible to clearly observe the sphere like Pt/C agglomerates for cathode. The different image grey levels between the different agglomerates that can also be observed on SEM images (see fig. 6.19) result from a difference of catalyst distribution inside the carbon. This configuration also depends on the cross cut of the sample where the three-dimensional agglomerates become two-dimensional plane carbon particles distribution. In the cathode, the size distribution of Pt catalysts is between 3 and 8 nm in the darker agglomerates whereas it is around 2 and 4 nm in the brighter agglomerates as highlighted from enlargement as, for example, reported in figure 6.21. The larger Pt nanoparticles generally are near the agglomerate surface.
The literature analysis usually attributes the surface area loss in carbon

supported platinum catalyst to degradation mechanisms such as platinum dissolution and redeposition or coalescence; this kind of mechanisms should result in a general increase in the average catalyst particle size.

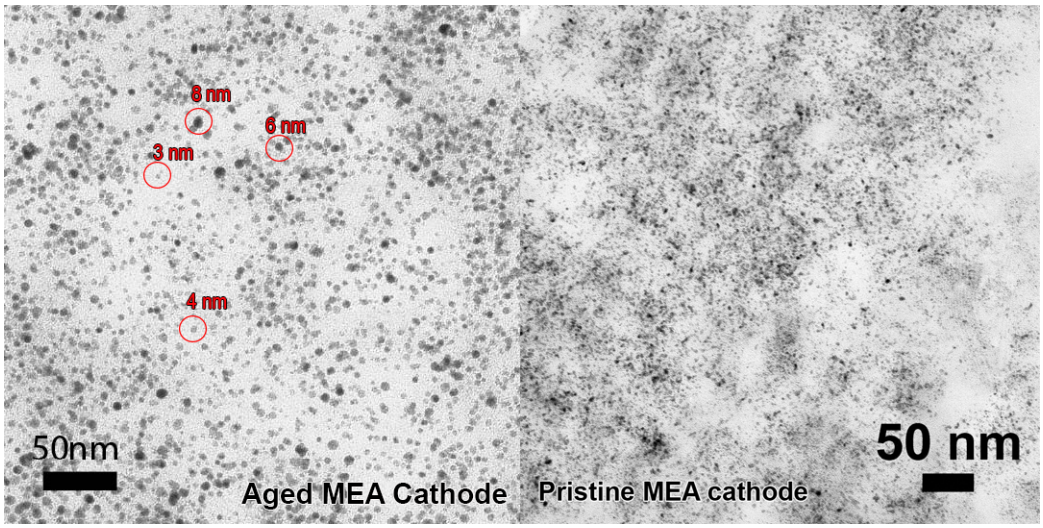

Figure 6.21: TEM observation of the cathode nanoparticles for both fresh and aged MEAs for cathode inlet region.

Figure 6.21 reports the images of the cathode inlet region platinum nanoparticles for both pristine and degraded MEAs; however the nanoparticles sizes are not homogeneous in the fresh MEA, so it is difficult to conclude doubtless any theory on their evolution during the degradation test. Indeed, from the analysis of the catalyst at the cathode inlet it is possible to observe nanoparticles of different size from 3 to 8 nanometers. On the other hand a significant cathode ECSA loss has been observed during the long-term test; one of the causes of the ECSA loss could be the dissolution mechanism without redeposition on the carbon support; in this case the platinum particles could be founded or in the ionomer or in the membrane or in the cathode MPL. For example, the XPS spectra reported in figure 6.14 shows the presence of Platinum on the cathode MPL after the long-term test. Generally the circular shape of the platinum particles is symptomatic of ripening mechanims while the presence of nano-agglomerated is more characteristic of coalescence; in the cathode inlet region, the aged MEA presents a average low radius distribution of nanoparticles, which have mainly circular shape.

Instead, in the cathode outlet region a significant increase in the catalyst average nanoparticles is evident as described in figure 6.22; the nanoparticles has a average radius of about 6 - 8 nm while in the anode inlet and in the fresh

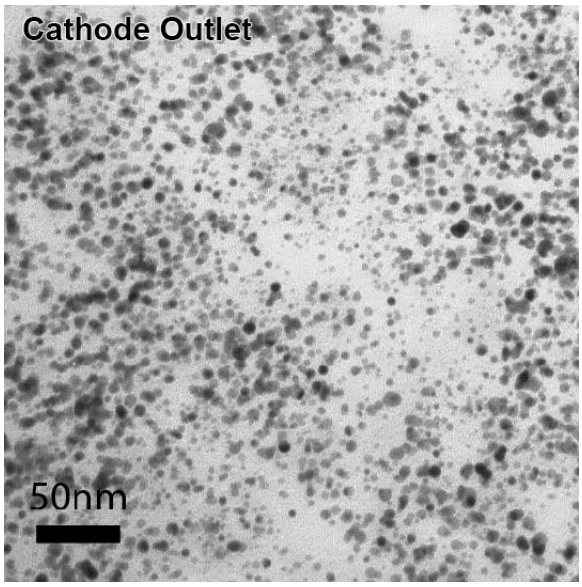

Figure 6.22: TEM observation of the cathode nanoparticles for aged MEA cathode outlet region.

MEA they have a average radius of about 3 - 5 nm. Hence, since the anode overpotential tends to increase along the channel length due to the lower and the cell potential is constant, the cathode potential is higher at the outlet of the reactants leading to a acceleration of degradation mechanisms related to the potential such as dissolution and redeposition. However, the shapes of the nanoparticles of cathode outlet, analysed in figure 6.22, are generally less circular respect to the cathode inlet reported in figure 6.21; the presence of agglomerates is more pronounced in the outlet TEM image according to a possible more significant weight of the coalescence mechanism.

The XPS measurements reported in figure 6.16 shows a reduction of polymer content in the catalyst layer respect to the pristine one; however, the measurements reported in figure 6.23 shows the fluorine distribution in the anode electrode, the ionomer seems to be well distributed but it is really hard to couple two measurements, which are such complex and different. The view of the ionomer distribution in the electrode permits to point out that the very dense agglomerates (the darker regions) seems to be inactive due to the lack of proton conductivity; instead the border regions well dispersed seems to have the three phase contact with simultaneous ionomer and carbon presence. The weak stability of catalysts nanoparticles in the DMFC environment is well known and a good relationship could be founded in the investigation of Ruthenium movement inside the operating MEA. Ruthenium

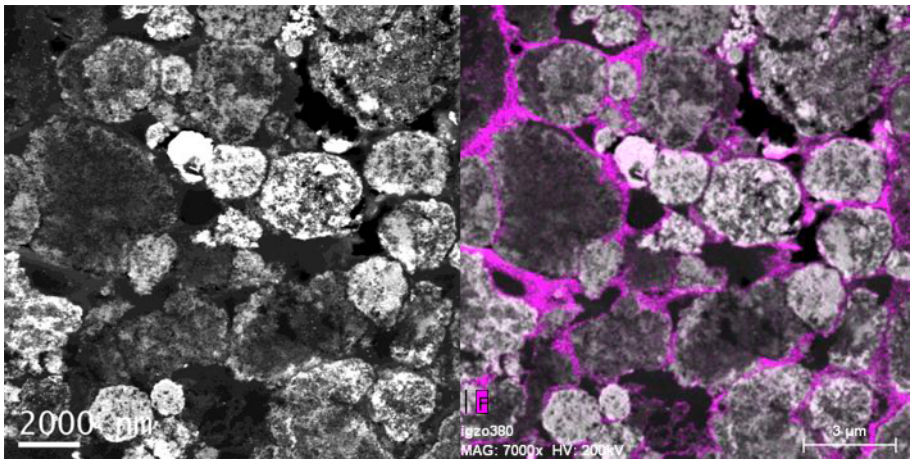

Figure 6.23: TEM observation of the anode electrode without and with fluorine distribution (proxy of ionomer presence).

can dissolve at the anode and it can be cross the membrane to the cathode or it can move in the anode ionomer to the anode microporous layer. XPS measurements reported in figure 6.14 shows the presence of Ruthenium at the cathode electrode and in the anode MPL, where it is confirmed to exist from TEM measurements of the anode MPL reported in figure 6.24

Moreover, the Ruthenium is founded also in the anode Gas Diffusion Layer where, through the EDX elemental mapping, it can be identified together with platinum inside the carbon matrix. Some small Ru nanoparticles are observed in the GDL near the electrode and the amount of Ru particles decreases while the distance from the anode electrode increases as described in figure 6.25.

Finally, the platinum and ruthenium nanoparticles wandering into the MEA carries them into the electrolytic membrane where they are investigated by TEM imaging; the precipitation of catalyst nanoparticles into the membrane is such a common degradation mechanism for PEFC and DMFC and it is also strictly related to Ruthenium crossover highlighted in paragraph 6.7.1; figure 6.26 shows the enlargement of two precipitates particles inside the electrolytic membrane next to the anode electrode.

It is possible to note that, in the nanoscale, the Ruthenium seems to cover the Platinum but it is not really known if this is real also during the DMFC operation particularly on the electrode changing the electrochemical potential. For example, it would be possible to speculate that the ruthenium founded at the cathode in figure 6.14 could cover the cathode catalyst reducing the ECSA; the signficant reduction of Ru crossover during the long-term test would be coherent with the cathode ECSA reduction. Indeed DLR

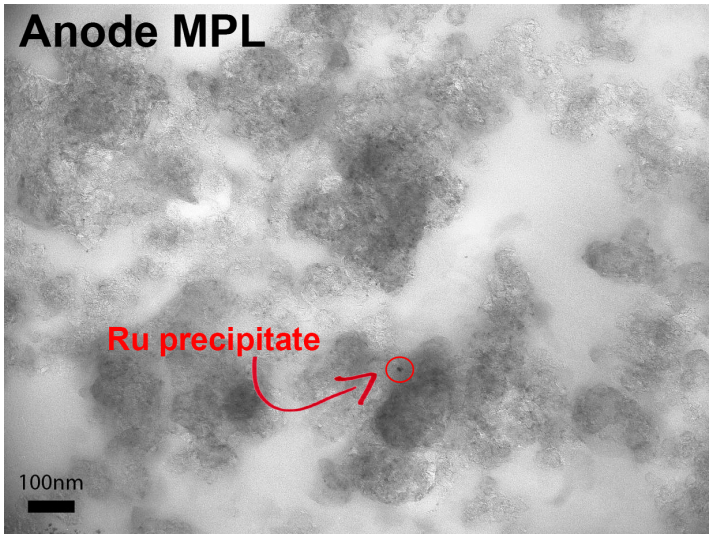

Figure 6.24: TEM observation of the anode MPL where small Ru particles are evidenced.

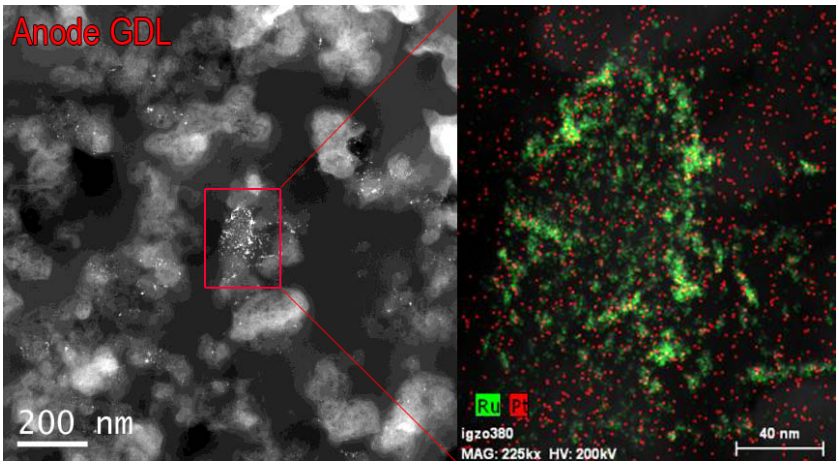

Figure 6.25: TEM observation of the anode GDL where small Ru particles are evidenced.

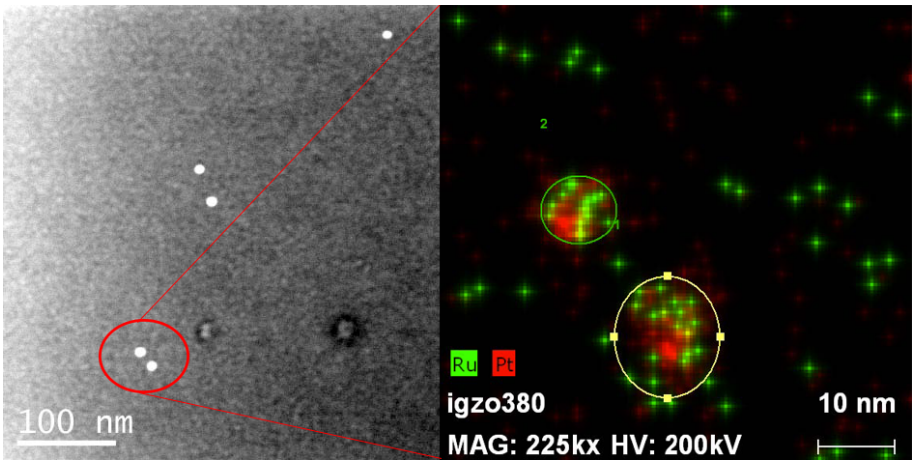

Figure 6.26: TEM observation of the membrane where small Pt/Ru particles are evidenced.

measurements confirm that ruthenium crossover occurs already during the activation procedure and it is mainly concentrated in the first hours of operation: the ECSA loss is also concentrated in the first hours and there could be a relationship between these two experimental evidences; however, the ECSA loss shape is coherent also with Pt dissolution with or without redeposition mechanism. Moreover, the Ruthenium loss at the anode would expose a higher fraction of platinum and the effect on the anode performance is not known. Maybe a long-term test in anode operation in the next future could be helpful for the understanding of this mechanism.

Finally, as shown in figure 6.27, the investigation on the electrolytic membrane in the region next to the cathode reveals the presence of Calcium based big nanoparticles, whose origin and effect on performances is actually unknown. They could be due or to a low quality of the bidistilled water or more probably, to the residual of the continuous water evaporation in the air humidifier. This unusual result, together with the confidential results on methanol quality obtained by IRD and the effect of air pollutants, which are difficult to quantify, shows the huge troubles in the comparison between DMFC degradation tests results between different research groups.

6.8 Conclusions

This chapter presents a rigorous and systematic experimental analysis on DMFC permanent degradation thanks to a long-term test of more than 1100 hours simulating the real DMFC operation. The cell has been analysed

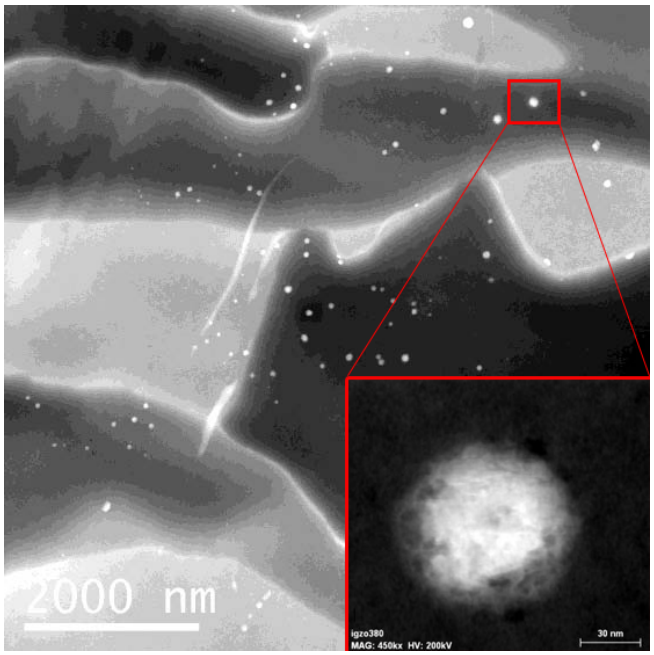

Figure 6.27: TEM observation of the membrane where big Ca-based nanoparticles are evidenced.

firstly during the operation thanks to continuous diagnostics during the operation interruption for the temporary degradation recovery and thanks to post-mortem analysis performed at the research centers partners of the European research project Premium ACT (DLR at Stuttgart-DE and CEA at Grenoble-FR). From the combined in-operando and post-mortem approach the following conclusions can be drawn:

- the correct performance of in-operando diagnostic is strictly related with the minimization of temporary degradation thanks to full refresh procedure. The diagnostic interruptions permits to evaluate DMFC permanent degradation that results equal to 90 $\mu V \cdot h^{-1}$, a value that is higher than the typical commercial degradation rates provided by industries;

- both in-operando and post-mortem analysis highlight a important degradation of the cathode electrode resulting in a strong decrease of Electro-Chemical Surface Area. This is compatible with different degradation mechanisms such as platinum dissolution but, from the post-mortem analysis is not feasible to doubtless attribute this behaviour to one specific degradation mechanism. Anyway the cathode outlet region suffers of a average increase of catalyst particle size not founded in the inlet

region;

- ruthenium crossover is investigated by peel-off XPS analysis and it has been highlighted also in an activated MEA; the increase in Ruthenium content in the cathode during the 1100 h test is limited. Hence the Ruthenium crossover seems to result in a anode electrode degradation mainly limited in the first period of operation. However, the effect of ruthenium nanoparticles at the cathode is not yet explained;

- the electrolytic membrane does not exhibit significant variation in its properties but microscopy analysis shows the precipitation of catalyst and inert particles into the membrane;

- the anode Gas Diffusion Layer suffers of a important degradation probably due to chemical PTFE decompostion while the cathode GDL does not reveal significant variation. The steady values of methanol crossover and water content in cathode outlet during the polarization curves reveals that the GDL degradation seems to have a limited effect on the DMFC overall mass balances.

Chapter 7

On the effect of GDLs on DMFC performances and degradation

In this chapter a Direct Methanol Fuel Cell with a different GDLs configuration is experimentally investigated; particularly the important difference between the reference MEA and this MEA regards the lack of the MicroPorous Layer (MPL) in the anode Gas Diffusion Layer. Performance, mass transport phenomena and EIS are evaluated during degradation tests.

7.1 Introduction

The relationship between the temporary degradation and the mass transport phenomena is deeply investigated in chapters 4 and 5; the former explains that both at the anode and at the cathode the mass transport phenomena through the diffusion layer and the electrode are responsible for temporary degradation mechanisms, while the latter presents ex-situ investigations on the influence of the MicroPorous Layer presence on the GDL on mass transport properties. For the temporary and permanent degradation experimental investigations, commercial MEAs have been used and they are based on a Gas Diffusion Layer configuration including the MPL presence both at the

anode and at the cathode.
A correct water management, resulting in a trade off between adequate membrane hydration and flooding of the cathode electrode, is a key parameter for a good operation of low temperature hydrogen PEFC [137, 138]; GDL configurations for PEFC have been deeply investigated due to the high scientific and industrial interest both for automotive and stationary applications [139, 140]. The MicroPorous Layer has been often added since few years ago to increase the cathode hydrophobicity resulting in low performance decay at high current densities related to flooding of the cathode electrode [141].
Water management issues in Direct Methanol Fuel Cells are less investigated due to the anode liquid feeding that should ensure adequate membrane hydration but the interest in the GDL configuration is also related to the methanol crossover limitation. In [8] a comparison of two DMFC MEAs with different cathode GDL configuration (with and without MPL) is presented to limit the methanol crossover from the anode to the cathode. Instead in [9], water content in cathode outlet is used as a tool to investigate the effect of the MPL on cathode flooding and DMFC performances also thanks to a combined experimental and modelling approach. The influence of the anode MPL presence is also investigated in [142] where a decrease of anode saturation due to the MPL is evaluated thanks to a model. However, the effect of the anode GDL configuration through the simultaneous characterization of the mass transport phenomena and Electrochemical Impedance Spectra yet has to be carried out and, moreover, the effect of the GDLs configuration on DMFCs should be take into account.
This chapter aims to propose the experimental investigation of performance, mass transport and EIS in a DMFC MEA with a different GDL configuration providing a comparison with the reference MEA. Furthermore the effect of the GDL configuration on the temporary and permanent degradation is carried out by performing a long-term test with the experimental methodology described in chapter 6.

7.2 Effect of anode GDL on Performances and Mass Transport Characterization

7.2.1 Experimental Methodology

The previously described experimental setups (chapter 2) have been used for the testing of the MEAs both for anode and overall operation and no modifications have been applied for these tests. The MEAs have been characterized in reference conditions where performances, mass transport measurements

and EIS have been acquired. The long-term test, reported in paragraph 7.4, has been performed according to the standard experimental methodology already described in paragraph 6.2.

MEAs description

The tested MEAs (named "$G-M$") are 25 cm^2 MEA manufactured by IRD Fuel Cell A/S: membrane is Nafion115, anode catalyst loading is 1.8 $mg{\cdot}cm^{-2}$ (Pt/Ru), cathode catalyst loading is 1.2-1.4 $mg \cdot cm^{-2}$ (Pt). Anode diffusion layer is Sigracet SGL24BA (thickness 190 μm, 5% PTFE content, without microporous layer) while cathode diffusion layer is Sigracet SGL25BC (thickness 235 μm, 5% PTFE content, with microporous layer). During testing, unless differently indicated, anode and cathode are fed respectively with 1.0 M methanol solution with stoichiometry equal to 6 and air, saturated by water at ambient temperature, with stoichiometry equal to 3. Reference current density is 0.25 $A \cdot cm^{-2}$ and the fuel cell temperature is kept at 75^oC. Moreover, during the anode polarization tests, dry hydrogen is fed to the cathode as a RHE.
Instead the reference MEAs (named "$M-M$") are commercial 25 cm^2 manufactured by IRD Fuel Cell A/S: membrane is Nafion115, anode catalyst loading is 1.8 $mg \cdot cm^{-2}$ (Pt/Ru), cathode catalyst loading is 1.2-1.4 $mg \cdot cm^{-2}$ (Pt). Both anode and cathode diffusion layer are Sigracet SGL35DC (thickness 325 μm, 20% PTFE content, with microporous layer). During testing, unless differently indicated, anode and cathode are fed respectively with 1.0 M methanol solution with stoichiometry equal to 6 and air, saturated by water at ambient temperature, with stoichiometry equal to 3. Nominal current density is 0.25 $A \cdot cm^{-2}$ and the fuel cell temperature is kept at 75^oC. Moreover, during the anode polarization tests, dry hydrogen is fed to the cathode as a RHE.

7.2.2 Comparison with the reference DMFC

Regarding the different design between the two MEAs, two main issues can be pointed out: both the anode and the cathode Gas Diffusion Layers are different. The cathode GDL of the $G-M$ MEA presents a lower PTFE content respect to the $M-M$ MEA but they both have the MPL; according to the results presented in chapter 5, the GDL analyzed in figure 5.11 has a PTFE content equal to 20% (it is the same of $M-M$ MEA) while the GDL analyzed in figure 5.7 has a lower PTFE content (10%) and this difference corresponds to a lower resistance to the permeation onset. The anode GDL of the $G-M$ MEA does not present the MPL and it has a lower PTFE

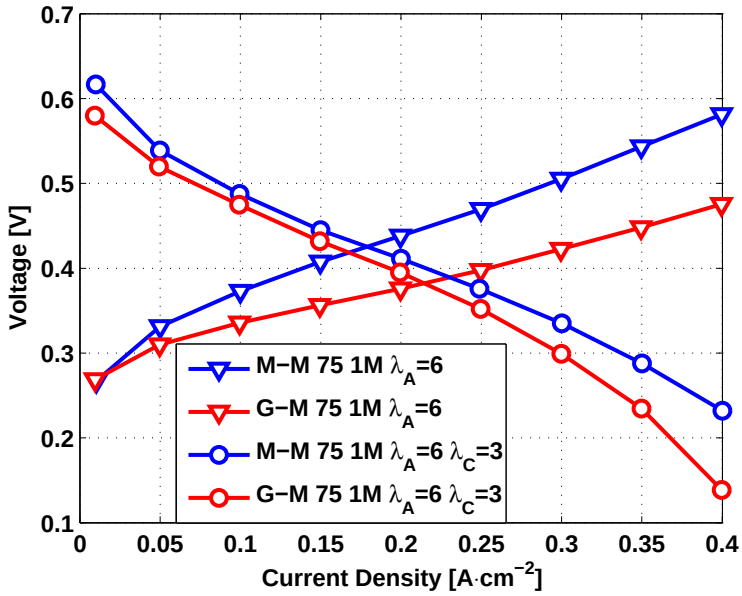

Figure 7.1: Comparison between the M-M and G-M overall and anode polarizations in reference conditions (75^oC, $\lambda_A = 6$, $\lambda_C = 3$) .

content respect to the $M - M$ anode one.
Figure 7.1 reports both the overall and anode polarization in the same reference conditions for the two investigated MEAs (red for the $G - M$, blue for the $M - M$); the anode polarizations reveal that the MPL removal permits a strong reduction of the anode overpotential. Indeed, according to chapter 5 a GDL without MPL has a higher diffusivity and a lower permeation threshold in comparison to a GDL with MPL; this results in an increase of water and methanol concentration at the anode electrode that determines an anode overpotential decrease. At very low current density ($0.01\ A \cdot cm^{-2}$), the overpotential of the two DMFCs is similar due to the same anode electrode configuration; indeed, in these conditions the mass transport phenomena are unsignificant and the regime is kinetically-dominated.
However, despite the improvement in the anode operation, the polarization curves in reference conditions reported in figure 7.1 shows that the reference DMFC ($M - M$) has better performances than the $G - M$ on the total range of current densities; indeed the $G - M$ MEA suffers of severe mass transport limitations at the cathode as evident from the change in the polarization curve slope at high current density.

Figure 7.2 shows methanol crossover and water content in cathode outlet measurements during the overall polarization curves reported in figure 7.1; the anode GDL without MPL results in a important increase of both

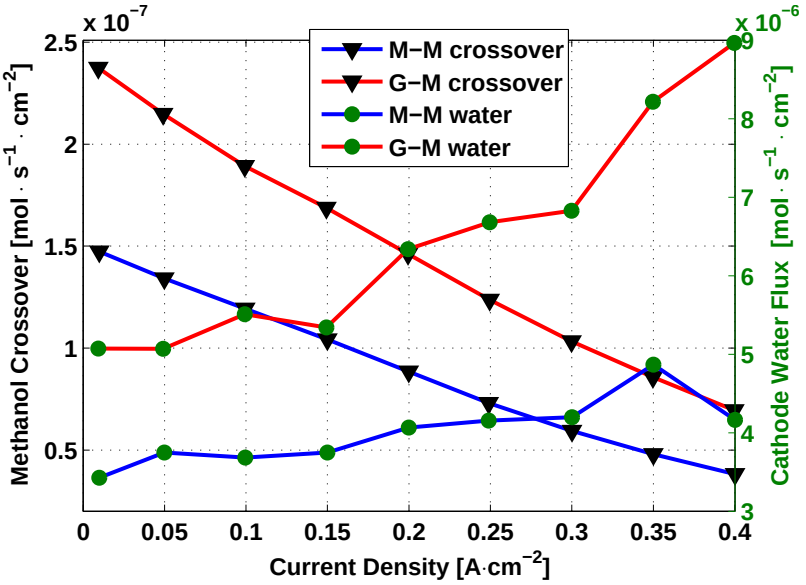

Figure 7.2: Comparison between the M-M and G-M methanol crossover and cathode water flow in DMFC polarizations in reference conditions (75^oC, $\lambda_A = 6$, $\lambda_C = 3$).

methanol crossover and water content in cathode outlet:

- the MPL absence determines a increase in methanol concentration at the anode electrode that results in a significant increase in methanol crossover;
- the anode MPL presence strongly reduces the water content in cathode outlet and the water remains constant on the total current densities range due to the diffusion from the cathode electrode to the distributor. However, also the slight modification in the cathode GDL can play a role on the DMFC water management;
- in the $G-M$ MEA, a sudden change in the water transport occurs while increasing the current density; probably the liquid water permeation is responsible of this breakthrough.

The water balance through a DMFC is a very complex argument that has been deeply investigated also in the M.R.T. Fuel Cell Laboratory ([9, 8]) and the breakthrough is attributed to the increase of liquid water pressure at the cathode electrode. Indeed, since the anode mass transport resistance without MPL is very low, the water and methanol concentration at the anode electrode increases (determining a low overpotential) as reported in figure 7.1

and the back diffusion mechanism does not permit a sufficient water removal from the cathode to the anode. In these conditions, the rise in current density determines the flooding of the cathode electrode that can be cause the breakthrough of the cathode GDL.

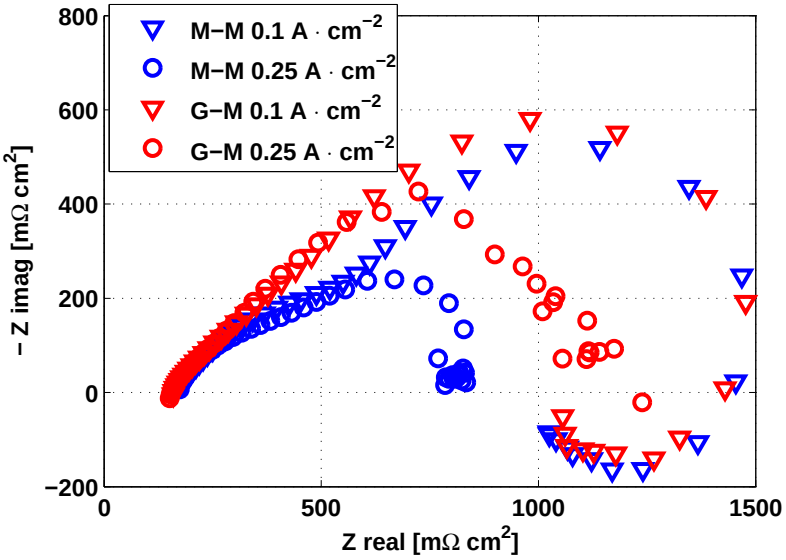

Figure 7.3: Comparison between the M-M and G-M EIS at 0.1 $A \cdot cm^{-2}$ and 0.25 $A \cdot cm^{-2}$ in DMFC polarizations in reference conditions (75^oC, $\lambda_A = 6$, $\lambda_C = 3$).

The comparison between the Impedance Spectra performed at 0.1 and 0.25 $A \cdot cm^{-2}$ and reported in figure 7.3 further confirms this interpretation:

- at the lower current density, the shape of the $G-M$ MEA and $M-M$ MEA is rather similar at low frequencies where a inductive behaviour due to the anode is evident; however, strong changes are shown in the medium frequencies region where the $M-M$ presents two circles, which are easily identifiable, while the $G-M$ spectrum is affected by the cathode limitations due to the increase in water concentration and methanol crossover already highlighted in figure 7.2;

- at the higher current density, the $M-M$ spectrum shows slight disturbances due to mass transport limitations but they are very limited in comparison with the disturbances occurring on the $G-M$ spectrum. Indeed, figure 7.2 shows the probable liquid permeation in the cathode GDL starting from 0.25 $A \cdot cm^{-2}$ meaning that the cathode electrode is probably flooded. The flooding of the cathode electrode, resulting

in a significant reduction of oxygen diffusion to the active sites [83], determines mass transport limitations responsible for the performance loss of $G-M$ at high current densities.

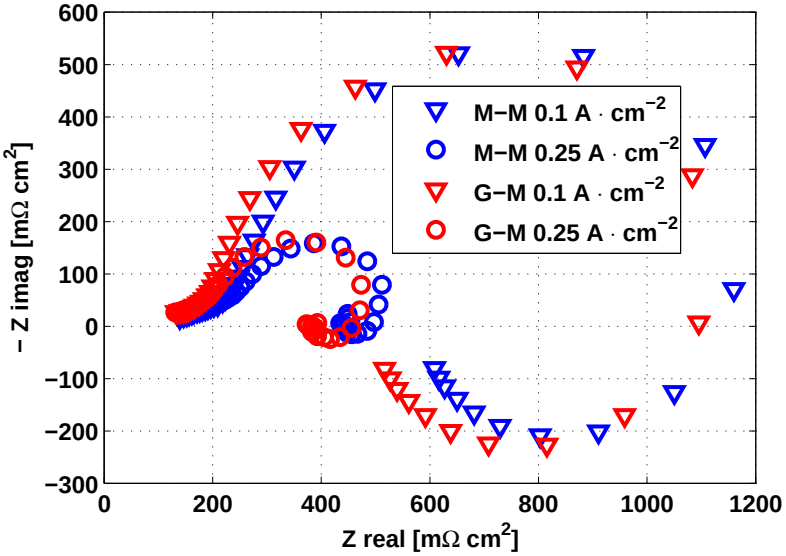

Figure 7.4: Comparison between the M-M and G-M anode EIS at 0.1 $A{\cdot}cm^{-2}$ and 0.25 $A \cdot cm^{-2}$ in DMFC polarizations in reference conditions (75^oC, $\lambda_A = 6$).

Figure 7.4 reports the anode Impedance Spectra at at 0.1 and 0.25 $A{\cdot}cm^{-2}$ of both the MEAs; the anode EIS presents a similar behaviour at both low and high current density and the $G-M$ EIS has a lower total resistance coherently with the better anode polarization performance reported in figure 7.1. However, a deeper explanation of anode EIS is performed in paragraph 7.3.

7.3 Effect of anode GDL on anode temporary degradation

In chapter 3 and 4, the DMFC temporary degradation mechanisms have been deeply experimentally investigated on the reference MEAs; the proposed anode temporary degradation mechanisms related to the CO_2 accumulation at the anode electrode is clearly related to the mass transport phenomena that occur through the anode GDL and electrode. Moreover, coherently with the results reported in paragraph 3.4, the absence of operation interruption

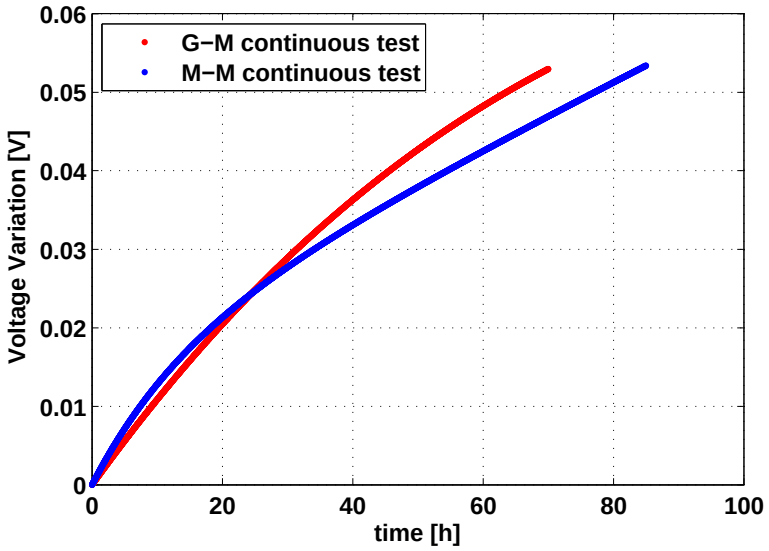

Figure 7.5: Comparison between the M-M and G-M biexpontential interpolations for anode continuous degradation tests (75^oC, $\lambda_A = 6$).

during the anode degradation test represents the worst case for the anode temporary degradation. This is due to the absence of periods for the CO_2 removal from the anode electrode corresponding to a change in the equilibrium between the liquid and gas phase pressures across the anode GDL and electrode.
For this reasons a continuous anode degradation test is performed on the $G-M$ MEA in reference operating conditions and its biexponential interpolation is reported in figure 7.5 together with the biexponential interpolation of the continuous test on the $M-M$ MEA already reported in figure 3.5.

The comparison between the anode EIS performed at the beginning and at the end of the continuous anode degradation test for both the MEAs are reported in figure 7.6 where a similar behaviour can be highlighted. For both the MEAs, a elongation of the linear branch due to a decrease of anode electrode proton transport conductivity can be observed; furthermore for both the MEAs, the inductive behaviour disappears during the test and it is replaced by disturbances due to mass transport limitations that are probably caused by the decrease of methanol concentration at the anode electrode as already described in paragraph 3.3. This confirms that the anode temporary degradation mechanism presented in chapter 3 occurs regardless the type of the anode Gas Diffusion Layer.
However the magnitude of the anode degradation remains the same despite the important differences between the two GDL types in mass transport

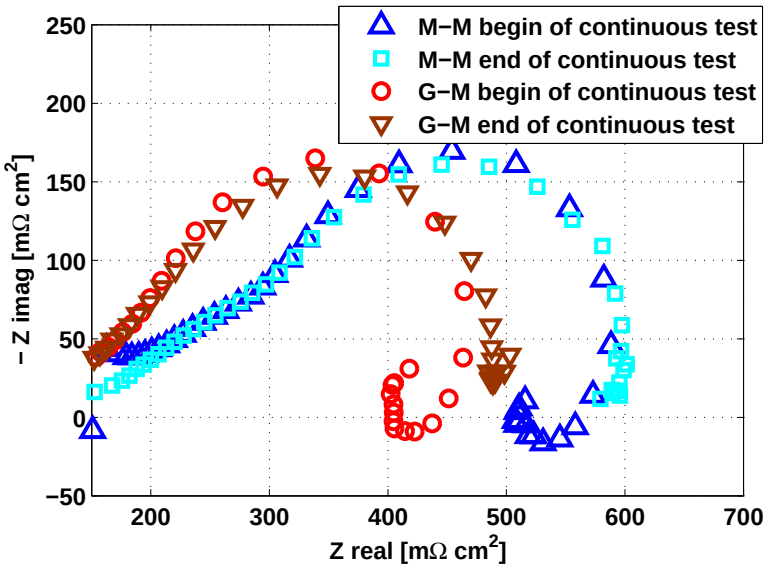

Figure 7.6: Comparison between the M-M and G-M anode EIS in anode continuous degradation tests (75^oC, $\lambda_A = 6$).

properties, such as diffusivity and permeation threshold, as investigated in chapter 5. It is possible to speculate that there are two conflicting mechanisms that could have opposite results in the comparison between $G-M$ and $M-M$ degradation rates: one that would make the $G-M$ degradation lower and one that would make $G-M$ degradation higher than $M-M$.

- the higher diffusivity of the GDL without MPL should permit an easier CO_2 removal leading to a lower degradation rate for $G-M$ MEA. Indeed, since the diffusive transport is proportional to the concentration gradient and to the diffusion coefficient, the higher the diffusivity and the higher the CO_2 removal rate. This would bring to a less pronounced decrease of methanol and water concentration at the anode electrode in absence of MicroPorous Layer on the anode GDL;

- the lower permeation threshold and, in general, the lower hydrophobicity of the GDL without MPL could result in such a "inverse flooding" effect. Indeed, cathode water flooding occurs easily when the cathode GDL is without MPL and it results in liquid water that obstructs the GDL pores and hinder both internally and superficially [83, 9] the gas phase transport leading to a apparent reduction of diffusivity. It is possible to speculate that, during the anode operation, the opposite phenomenon occurs: the continuous feeding of methanol and water keeps the liquid pressure high favouring the creation of pathways for

the liquid phase transport and, in general, a wetting of the GDL. Since a wetted GDL permits a higher mass transport in comparison of a dry GDL, at least part of the GDL is taken for the liquid transport or it is blocked by liquid phase. This inverse flooding could result in a reduction of the effective diffusivity for the CO_2 transport from the anode electrode to the distributor channels and it could lead to a continuous accumulation of the CO_2 at the anode electrode that hinder liquid phase transport. This would bring to a more pronounced decrease of methanol and water concentration at the anode electrode in absence of MPL on the anode GDL.

Obviously, this argument has to be further analysed because there is a need of tests reproducibility and repeatability, which should permit to statistically evaluate the difference between the anode degradation tests of $M - M$ and $G - M$ MEAs.

7.4 Preliminary results of a Long term test on a DMFC with different anode GDL

A long-term test is actually ongoing for the characterization of the permanent degradation of the $G - M$ MEA; it has never yet finished but the amount of hours of operation makes it reliable for a comparison with the same test performed on the $M - M$ MEA especially due to the use of the same methodology. Since the DMFC is still running the results could change with time due to different and not always predictable reasons; anyway the promising results reported in this paragraph will be deepened in the future.
In order to obtain a comparison with reference MEA, another long-term test on a $M - M$ MEA has been performed synchronously with the $G - M$ long-term test on a twin experimental equipment.

Figure 7.7 reports the voltage decay comparison between the $M - M$ and $G - M$ MEAs in two analoug long-term tests performed in reference conditions (see paragraph 7.2.1); each operation interruption corresponds to a full refresh used to minimize temporary degradation. The first period of life of about 100 h corresponds to a strong degradation rate for both the MEAs but, with the interruption and the full refresh, the $G - M$ MEA does not show any significant performance recovery. The shape of the voltage decay of $M - M$ MEA is more regular and each full refresh determines a strong performance recovery while the $G - M$ MEA shows a unusual shape of the voltage decay curve with a important inital decrease and a stabilization; after each stable region, the full refresh determines a little performance recovery.

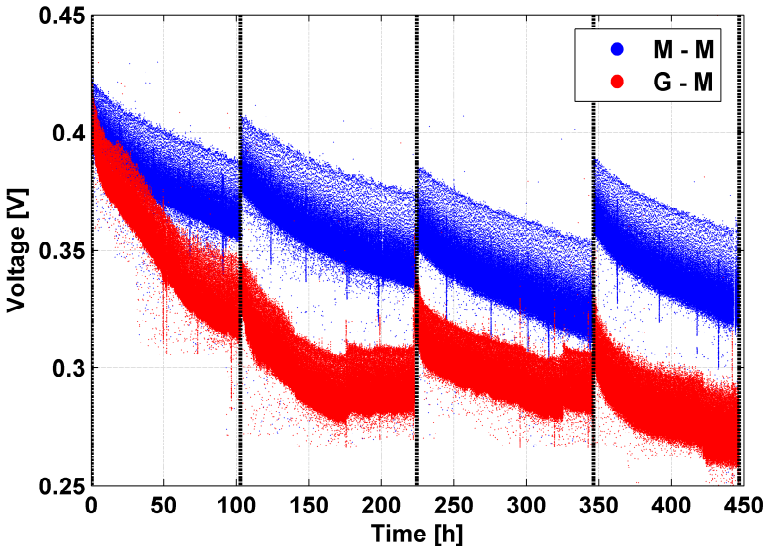

Figure 7.7: Comparison between the M-M and G-M voltage decay in preliminary long-term degradation tests ($I = 0.25\ A \cdot cm^{-2}$).

The reasons of such behaviour are not clear and this kind of test has never been performed in the literature; as highlighted in this chapter, the $G-M$ MEAs presents a more complex mass transport regime mainly at the cathode and it could be due one of the causes of such difference.

Figure 7.8 reports the methanol crossover comparison between the $M-M$ and $G-M$ MEAs in the two analoug long-term tests performed in reference conditions reported in figure 7.7; the reference MEA ($M-M$) presents a regular shape for the methanol crossover behaviour in time: the crossover slightly decreases during each part of the test and this decrease is recovered each operation interruption for full refresh coherently with what reported in paragraph 4.5.
Instead, the methanol crossover measured for the $G-M$ MEA reveals a very unstable behaviour with an average value slightly higher than the $M-M$ (coherently with figure 7.2 but with significant variations and high data dispersion); this confirms the strongly unsteady operation of the $G-M$ MEA probably both at anode and cathode.

The polarization curves performed during the interruption for diagnostic at the beginning and at the "end" of these long-term tests, which still are ongoing, are reported in figure 7.9; the BoL polarization curve for the $G-M$ MEA is better than the one obtained during the characterization and it is coherent with the high voltage value achieved at the beginning of figure

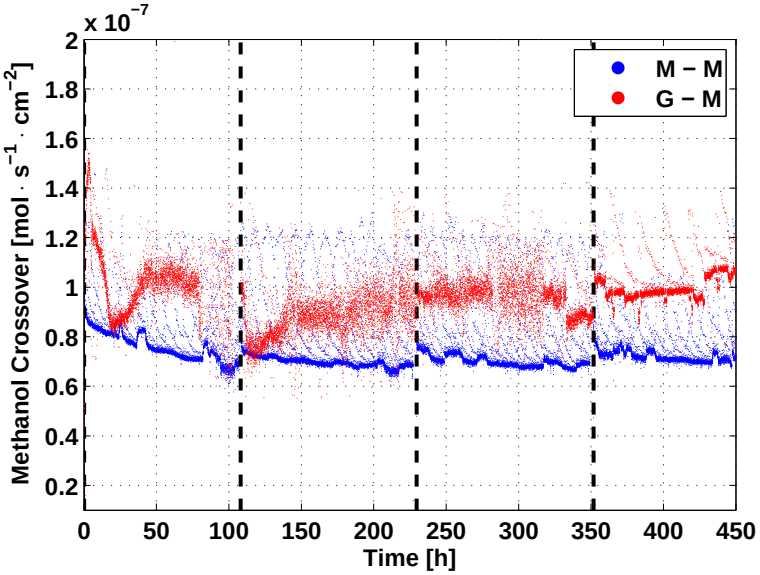

Figure 7.8: Comparison between the M-M and G-M methanol crossover in preliminary long-term degradation tests ($I = 0.25\,A \cdot cm^{-2}$).

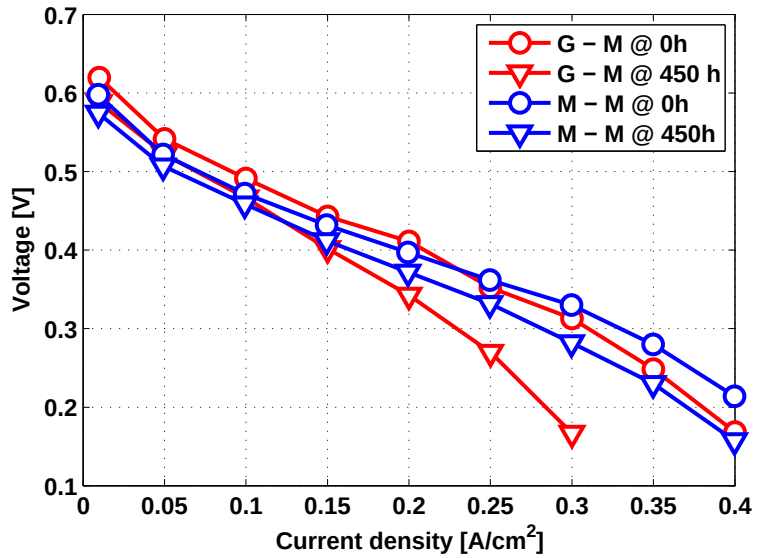

Figure 7.9: Comparison between the M-M and G-M polarization curves at beginning and end of the preliminary long-term degradation test ($I = 0.25 A \cdot cm^{-2}$).

7.7. Anyway, at high current densities, the $M - M$ MEA shows higher performances than the $G - M$ MEA as already discussed in paragraph 7.2.2. The $G - M$ MEA presents a higher permanent degradation due to a strong worsening of the performances after less than 500 hours while the permanet degradation of the $M - M$ MEA is coherent with what obtained in paragraph 6.4.

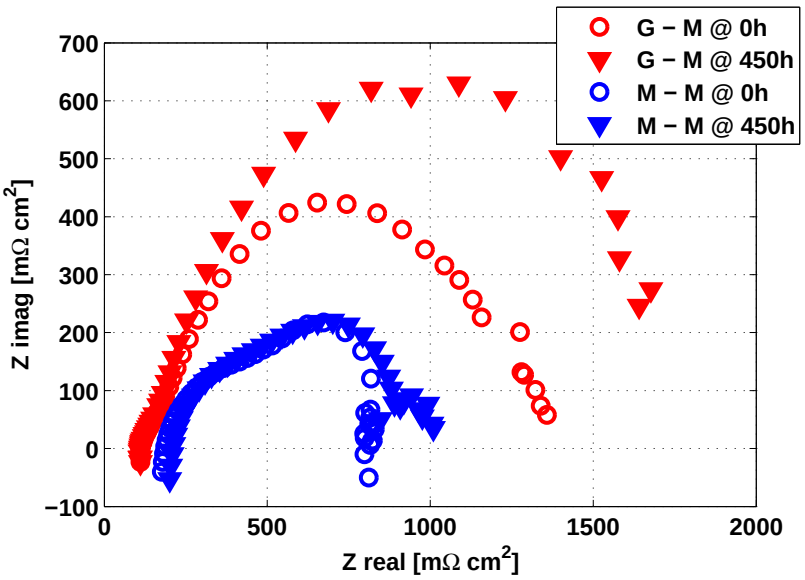

Figure 7.10: Comparison between the M-M and G-M EIS measured during polarization curves at beginning and end of the preliminary long-term degradation test @ I = 0.25 $A \cdot cm^{-2}$.

Figure 7.10 reports the Electrochemical Impedance Spectra acquired in reference conditions (0.25 $A \cdot cm^{-2}$) during the polarization curves reported in figure 7.9; coherently with what reported in figure 7.3, the $G-M$ EIS presents a different shape respect to $M - M$ EIS, which is probably due to mass transport limitations at the cathode attributed to the flooding in paragraph 7.2. Both the MEAs shows a worsening of mass transport phenomena, which for $M - M$ results in disturbances at low frequencies already highlighted in figure 6.12; however, the $G - M$ MEA presents a important increase in the total resistance that is typical for the mass transport limitations at the cathode.

The comparison between the $G - M$ and $M - M$ cathode ECSA loss is reported in figure 7.11 and it does not highlight significant differences; for this reason it is possible to assume that the mass transport limitations at the cathode of $G - M$ highlighted by the EIS of figure 7.10 are not due to a pure

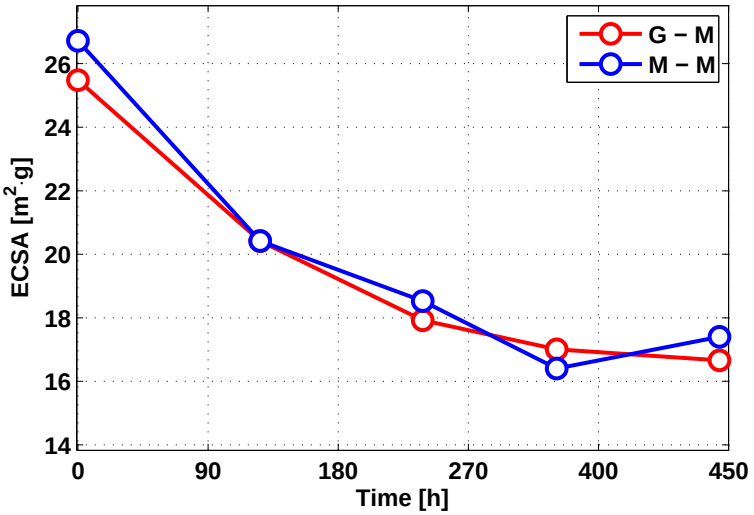

Figure 7.11: Comparison between the M-M and G-M ECSA measured during the degradation tests.

ECSA loss but to other mechanisms related to cathode GDL or electrode degradation that could emphasize the mass transport limitations without increasing ECSA loss. Particularly it is possible to propose the following interpretation:

- a significant decrease in ECSA, working at the same current density, determines a higher flux of reactants/products to/from each active site;
- the flooding of the cathode electrode results in mass transport limitations caused by a decrease of the effective diffusivity of the reactants species as in [9];
- in the reference conditions, the $M-M$ MEA does not show signficant mass transport limitations at the cathode while the $G-M$ is probably flooded;
- the same decrease in the ECSA coupled with the important decrease in the effective diffusivity related to flooding is the reason of the strong degradation of the $G-M$ MEA. Indeed, on each active site, the coupling of the diffusivity reduction and of the increased flux (due to ECSA loss) causes significant mass transport limitations [135]. Coherently with this interpretation, the mass transport limitations during the $M-M$ degradation are less pronounced.

7.5 Conclusions

This chapter presents a experimental analysis of the effect of the Gas Diffusion Layers on performances, mass transport phenomena and degradation through the comparison of two analoug MEAs if excluded for the GDL configuration. Particularly the $G-M$ MEA presents an anode GDL without MicroPorous Layer while the $M-M$ MEA presents an anode GDL with MPL; this chapter permits to draw the following conclusions:

- the presence of the anode MPL results in a lower anode performance (i.e. higher anode overpotential) that is probably due to a lower methanol and water concentration at the anode electrode;
- the presence of the anode MPL ensure an improvement of DMFC performances due to a better cathode operation; despite a quite higher methanol crossover without anode MPL, the real issue of $G-M$ MEAs seems to be the flooding of the cathode electrode;
- the anode temporary degradation mechanism proposed in chapter 3 occurs with a different anode GDL configuration and it results in the same evolution of the anode EIS;
- the $G-M$ MEA presents a higher degradation rate and a less stable operation than the $M-M$ MEA and both these aspects could be related to the difficult management of mass transport phenomena;
- the ECSA loss of both the MEAs are comparable but the permanent degradation rates are significantly different; this is probably due to the coupling of ECSA loss with significant cathode mass transport limitations.

Chapter 8

Design of preliminary Accelerated Stress Tests for DMFC

This chapter presents the design and testing of preliminary Accelerated Stress Test for Direct Methanol Fuel Cell degradation; this procedure aims to representatively increase the degradation of a DMFC permitting to obtain the same degradation rate of a long-term test in a very short time test. Two batches of AST are developed, analysed and discussed.

8.1 Introduction

The experimental investigation on permanent degradation reported in chapter 6 is of fundamental industrial importance because it highlights the main component responsible for the degradation and because it defines standard procedures to characterize and quantify the permanent degradation. However, despite this long-term test takes more than 1000 hours of operation of a scientific laboratory, it is not sufficient for a real simulation of a typical industrial purpose. The lifetime requirements depend on the application and, for mobile applications, it has been fixed at 5000 hours while for stationary applications it has been fixed at more than 10000 hours; it is obvious that

is not acceptable and realistic to take one year of scientific laboratories to perform lifetime tests. Furthermore, also the definition of lifetime depends on the purpose of the application because it could correspond to a ratio between the End-of-Life and the Begin-of-Life performances that has not ever uniquely defined.
The degradation test duration issue is actually typical for hydrogen fed PEFC, which reached a sufficient technological maturity to have significant lifetime requirements. Durability studies can actually be for automotive application oriented meaning hard conditions to be applied like dynamic load, start/stop, freezing conditions but taking into account a lifetime requirement of about 5000 hours: this kind of application could again permit real experiments. Stationary applications present different specifications but, generally, the required lifetime of 40.000 hours does not allow the real experimental analysis but it calls for an accelerated methodology.
As reported in [134, 143], among the experimental data, it is possible to list the main accelerating stressors for the phenomena observed during PEFC ageing and for the accepted degradation mechanisms. These stressors are in majority operating conditions like temperature, relative humidity, potential, load cycles, mechanical stress, contaminants and fuel starvation. Accelerated degradation studies often consist in applying extreme protocols in order to enhance one degradation mechanism. For the membranes, the impact of hydrogen peroxide and related free radicals is the most used ex-situ test [144, 145] to simulate the possible chemical attack occurring during oxygen reduction process (at different parts of the MEA). The same chemical mechanism is simulated in-situ with open circuit voltage hold tests [147, 148] and mechanical degradation is mainly studied through hydrothermal cycling tests. For the electrodes, ex-situ ageing protocols [149, 150] are electrochemical cycles allowing to reach very high potentials such as 1.2 or even 1.5 V. Cycling operation [150, 151] including transient steps, high power peaks, high voltage steps, at high temperature and low relative humidity are well known to increase all the degradation mechanisms concerning the MEA materials of a PEFC.
However, the literature presents very limited number of works about the Accelerated Stress Tests for Direct Methanol Fuel Cells and there are two main reasons for this: first, the durability requirements are actually limited allowing acceptable long-term test in the laboratories, secondly, the technology is neither so widespread nor ready for the commercialization. For example, Bae et al [64] proposes the continuous DMFC operation as an Accelerated Stress Test but they do not take into account the temporary degradation. Temperature [152], local starvations [153] and different types of operation [68] effects on degradation have been investigated experimentally with dif-

ferent techniques. Another important issue regarding the Accelerated Stress Test is the representativeness; indeed the AST does not have only the goal of the degradation acceleration but it should be designed with the goal of a representation of the degradation mechanisms typical of a long-term test. In principle, the post mortem measurements of a MEA subjected to a long-term test and of a MEA subjected to a representative AST should be analogous. The aim of this chapter is to develop preliminary Accelerated Stress Tests for Direct Methanol Fuel Cell with the goal of a reliable and representative acceleration of the degradation.

8.2 Experimental

The experimental approach for the permanent degradation quantification has been kept analogous to the one exploited for the long-term test described in chapter 6 using the same experimental setup, diagnostic tools and method for the data interpretation. The DMFC MEAs used for the Accelerated Stress Test development are commercial 25 cm^2 manufactured by IRD Fuel Cell A/S: membrane is Nafion115, anode catalyst loading is 1.8 $mg \cdot cm^{-2}$ (Pt/Ru), cathode catalyst loading is 1.2-1.4 $mg \cdot cm^{-2}$ (Pt). Both anode and cathode diffusion layer are Sigracet SGL35DC (thickness 325 μm, 20% PTFE content, with microporous layer). During testing, unless differently indicated, anode and cathode are fed respectively with 1.0 M methanol solution with stoichiometry equal to 6 and air, saturated by water at ambient temperature, with stoichiometry equal to 3. Nominal current density is 0.25 $A \cdot cm^{-2}$ and the fuel cell temperature is kept at 75^oC.

8.3 First Batch of Accelerated Stress Test: Load Cycles

The first approach for the AST development directly derives from the typical approach used for Low Temperature Hydrogen Polymer Electrolyte Fuel Cells and it is based on the cycling of the current, which the literature highlights as one of the most common techniques for the acceleration of the degradation. The cycling of the load has been found as a accelerating factor in several work performed on PEFC [150, 134] but, for hydrogen PEFC, the low current periods corresponds also to very high voltages that have a effect on typical electrodes degradation mechanisms. Regarding the DMFC, there are some works that investigates load cycling as an operating strategy both as a voltage controlled variation as in [34] or due to start/stop operations [154] but no

Accelerated Stress Tests have been proposed.

8.3.1 Design of the AST

The high number of degrees of freedom available for the AST development makes the design of a Load Cycle (LC) a complex issue; there is a great amount of operation parameters that can be changed, whose impact on the performances and degradation is not completely explained. It is possible to choose the LC frequency, the current number and values, the possible voltage limits, the stoichiometry or massflows of both the anode and the cathode. However, it was not acceptable to create a complex experimental grid to analyse the coupling effects of the different parameters and, for this reason, the effectiveness of a Load Cycle has been investigated founding on preliminary tests already performed in the frame of the characterization of the temporary degradation mechanisms reported in chapter 4.
During both the DMFC operation and diagnostic, two current densities have been deeply tested: the reference one equal to 0.25 $A \cdot cm^{-2}$ and the current density equal to 0.1 $A \cdot cm^{-2}$. For coherency with all the experimental campaigns already done, the load cycles are designed between these two current densities. The second operation parameter that has been evaluated is the frequency of the current variation and two periods have been identified: 30 *seconds* and 5 *minutes*. Regarding the massflows of anode and cathode, they have been maintained constant during all the tests because of a technical limitation; the peristaltic pump controlling the anode massflow is only manually controllable and, for coherency, the cathode airflow has been kept constant. The cathode stoichiometry variation at low current density determines dehydration issues that are described in the next paragraph 8.3.2. The last key-point for the AST design regards the operation interruptions: in order to limit the temporary degradation accumulation, the operation in LC mode is periodically interrupted every 20 *min* for a 1 *min* refresh cycle. The goal is the accelerated degradation of the electrodes according to the effect of an acceleration of the typical DMFC operation for a long-term test, as reported in chapter 6.

8.3.2 Results and discussion

Figure 8.1 reports the voltage decay in time during the Load Cycles AST previously described; the first part of the plot regards the test with constant current period equal to 30 s while the second one regards the test with constant current period equal to 5 *min*. The second part of the test shows a more pronounced decay of the voltage especially in the periods at higher

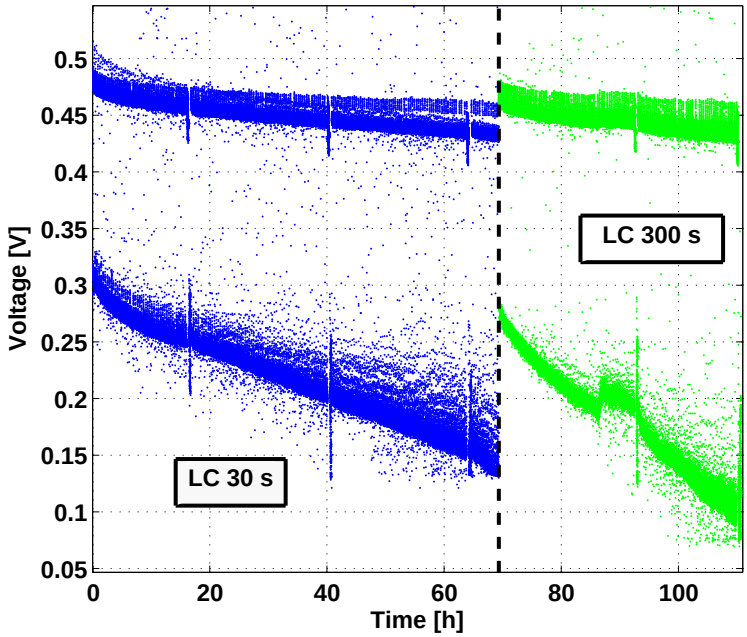

Figure 8.1: DMFC Voltage decay during preliminary AST based on load cycles.

current density (i.e. lower voltages) while at high voltages the performance decay is similar. A superficial interpretation could conclude that the higher the period duration and the higher the degradation rate but there are some key-points that can determine this result:

- the second test is consecutive to the first one; the 30 s load cycle could have a coupling effect on the second part of the test;
- both the tests have been performed with constant cathode massflow and, for this reason, the period at 0.1 $A \cdot cm^{-2}$ could lead to a dehydration of both membrane and cathode electrode and, due to the dynamic of water transport, during 5 min of low current operation dehydration can occur. However the strong performance drop is observable at the high current density but it is probably due a slow re-equilibrium of the membrane and electrode hydration. According to this interpretation, 30 s are not sufficient to observe important variation in the hydration while 5 min corresponds to a worsening of membrane and cathode performances during the low current period that determine the performance drop evident at high current density.

The EIS performed during the tests and reported in figure 8.2 further demonstrate that dehydration has an important role in determining the

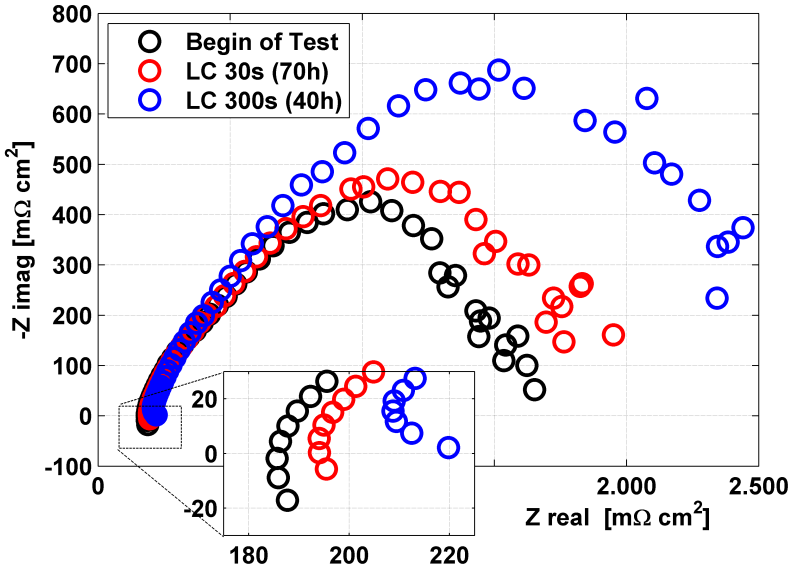

Figure 8.2: EIS performed during preliminary AST based on load cycles.

strong degradation observable in the second part of the LC test. The tests determine a progressive increase in the DMFC total resistance coherently with the continuous degradation but, from the analysis of the first EIS intercept with real axis corresponding to membrane ohmic resistance reported in the zoom of figure 8.2, a important increase in membrane resistivity is shown.

Figure 8.3 reports the polarization curves performed during the Load Cycle Accelerated Stress Test and they permit the permanent degradation quantification; the first test presents a permanent degradation of 202 $\mu V \cdot h^{-1}$ while the second test presents a permanent degradation significantly higher and equal to 1173 $\mu V \cdot h^{-1}$ but this high permanent degradation is probably overestimated because the cell has seriously suffered the period at 0.1 V highlighted after 100 hours in figure 8.1. It is possible that the greatest part of the permanent degradation has been accumulated in a very short time at low potentials at it could be a starting point for a future new kind of AST development.

8.3.3 Beyond the Load Cycles as an AST for DMFC

The preliminary tests conducted using Load Cycles as an AST are not satisfactory because Load Cycles for DMFC presents some issues that make

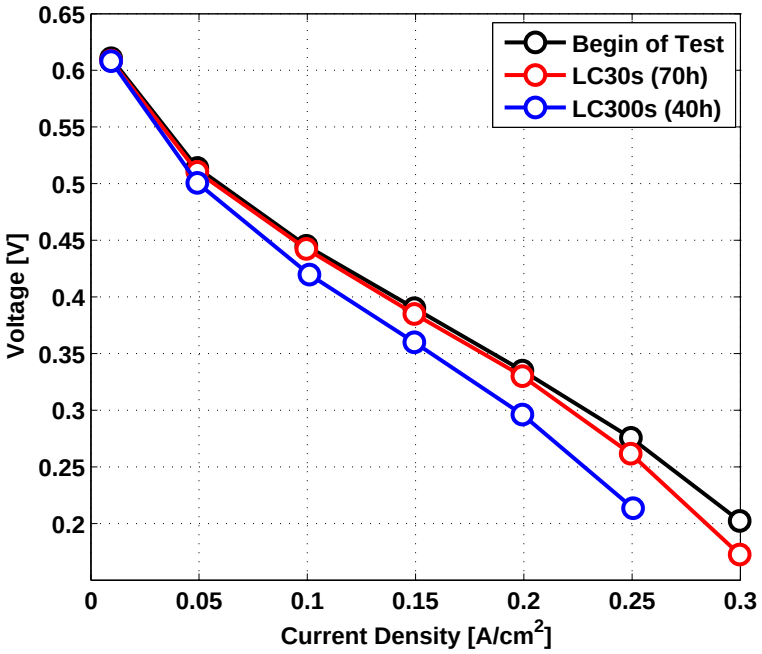

Figure 8.3: Polarization curves performed during preliminary AST based on load cycles.

them strongly different in comparison with PEFC. The following list shows the most important differences that make the load cycle not fully proper for Direct Methanol Fuel Cells AST design; a comparison of typical PEFC AST requirements that load cycles satisfy and effect of the same requirements on the DMFC is presented.

- PEFC generally presents a negligible anode overpotential and this determines a known cathode potential more or less equal to the cell potential; DMFC has a significant anode overpotential and this results in an unknown cathode potential;
- PEFC anode degradation is usually very low and the main investigations are focused on cathode where platinum degradation mechanisms such as dissolution are proposed, which depend on the cathode potential. DMFC anode degradation could be important due to the weak stability of the Pt/Ru alloy. This results in ruthenium loss, worsening anode performance, that can cross over the membrane and reach the cathode where could have a further degradation effect. Moreover the DMFC cathode potential is generally high and the relation between a

more complex scene of degradation mechanisms and a unknown potential makes the understanding very difficult;

- the methanol crossover is a phenomenon that is unique for DMFC and its effect on the degradation of the electrodes is unknown;
- PEFC Load Cycles generally present a period at low current (i.e. high voltages) where the permanent degradation mainly occurs; DMFC Load Cycles cannot present periods at high voltage because it is not possible to reach very high voltages in DMFC operation due to the low OCV caused by the mixed potential associated to methanol crossover;
- the mass balances of a PEFC are simpler than in a DMFC; load cycles in a PEFC should mainly involve the membrane water continuous re-equilibrium. In a DMFC the complex two phase anode mass transport can be critical during continuous change of current resulting in unknown contributions on temporary and permanent degradation;
- finally the PEFC temporary degradation is very limited while in DMFC the temporary degradation is the main cause of performance loss; however it determines strong degradation rate that could lead to very low voltages due to difficult in mass transport or maybe starvation; these phenomena introduce further troubles in the control of the degradation mechanisms.

The high number of uncertainties related to the DMFC Load Cycles as an AST does not directly imply the impossibility of a reliable AST design based on LC; however, a great experimental and theoretical effort should be put to go inside each critical aspect and to improve the understanding of the critical phenomena. Therefore, another path can be selected for the design of a AST for DMFC that aims to accelerate the degradation mechanisms highlighted by the long-term test, reported in chapter 6, and it is described in the next paragraph, 8.4.

8.4 Second Batch of Accelerated Stress Test: OCV cycles

The design of the second batch of AST takes origin from three main considerations addressing the procedure development:

- the DMFC degradation long-term test described in chapter 6 highlights that the main component responsible for DMFC degradation is

the cathode electrode; an important surface area loss is observed and it is at least partially due to cathode catalyst degradation mechanisms such as platinum dissolution or coalescence. Platinum dissolution rate is generally related to potential and water content [155] but, unfortunately, during the DMFC operation, the cathode potential is unknown if excluded the OCV periods where the anode overpotential is negligible;

- the Load Cycles has been evaluated as not fully satisfactory as AST for DMFC because of the reasons reported in paragraph 8.3.3;
- Platinum Oxides, which is probably one of the main causes for DMFC temporary degradation, can have a not completely explained relationship with platinum degradation mechanisms that is explained in the continuation of this paragraph.

Indeed a few works in the iterature propose that the formation of oxide layer coverage on platinum (that occurs at high potential at cathode during the operation) could act as a protection to the platinum dissolution and coalescence that are considered as the main cathode surface area loss mechanisms [156]. Furthermore it is unknown the permanent effect that the oxide layer could have on the platinum cathode catalyst.

8.4.1 Design of the AST

According to the considerations of paragraph 8.4, the promotion of the platinum cathode catalyst dissolution should be favoured by high potentials and low platinum oxide presence. The high potentials at the cathode can be obtained both during the Open Circuit Voltage and during the DMFC operation; however, during the operation, the cathode potential is unknown and not easily controllable due to the lack of reliable in-situ reference electrodes for DMFC. Moreover, the OCV progressively decreases in time due to methanol crossover as experimentally observed in [157] and, in presence of continuous air flow, the platinum oxides layer could reach saturation and the coverage effect on the Pt sites could occur.

For this reasons a new kind of AST is proposed. It aims to promote platinum dissolution limiting the coverage of platinum oxide by means of OCV and air interruption cycles as reported in figure 8.4; in fact, when the cathode air is interrupted during OCV, the cathode potential decrease at less than 0.2 V and platinum oxide reduction occurs [37]. When the air is fed again, the potential quickly increase to 0.8 V: in this condition limited platinum oxides coverage is present and platinum dissolution is enhanced, as

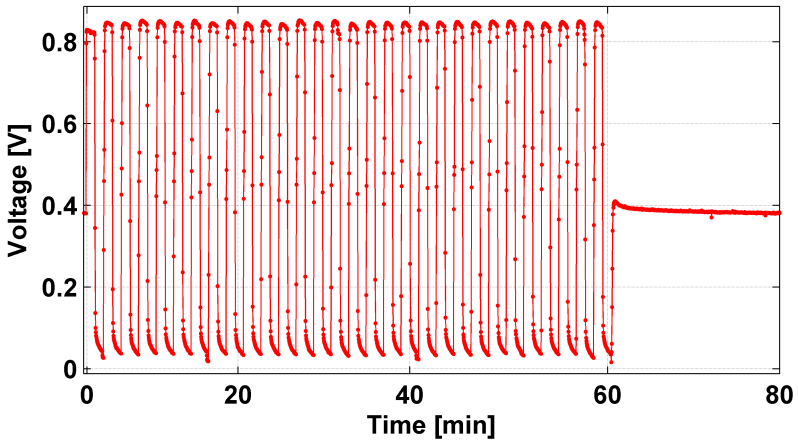

Figure 8.4: Sample of the OCV cycle used as DMFC Accelerated Stress Test.

well as platinum oxides formation. These cycles are divided in 1 *min* periods at OCV and 1 *min* periods at No-Air and they take 60 *min*. Furthermore an operation period at 0.25 $A \cdot cm^{-2}$ of 20 minutes has been added to the cycle, reported in figure 8.4, in order to monitor frequently the DMFC performance degradation. If excluded for the period of current production, the DMFC cathode is set at a high and known potential during the periods in OCV; the anode operation is very limited during the cycles but, the increase in methanol and water crossover caused by the absence of reactions could have an effect on ruthenium dissolution and crossover. The evaluation of the permanent degradation is performed thanks to the methodology reported in chapter 6 including the full refresh procedure.

8.4.2 Results and discussion

Figure 8.5 reports the voltage decay obtained during the AST above described during the operation period at 0.25 $A \cdot cm^{-2}$ while the traits in OCV/No Air are not reported; it highlights a regular voltage decay during the first 160 hours of operation while, after this period, a very irregular behaviour is shown marked by sudden voltage variation of unknown origin. Hence, despite the first period is characterized by very promising results, the second part makes them not reliable and, for this reason, the test has been repeated after the first test performance.

The polarization curves for the permanent degradation quantification are reported in figure 8.6 together with the anode polarization curves performed at the BoL and at the EoL. However, the polarization curves, performed after

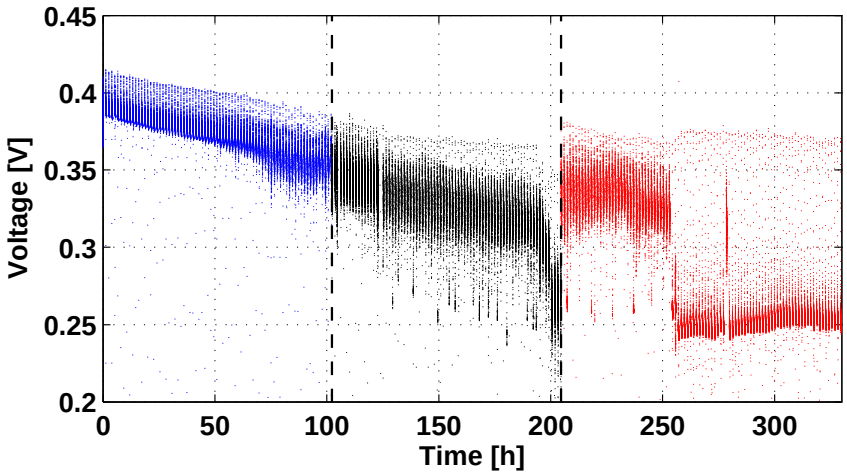

Figure 8.5: Voltage decay during the AST in the 0.25 $A \cdot cm^{-2}$ periods.

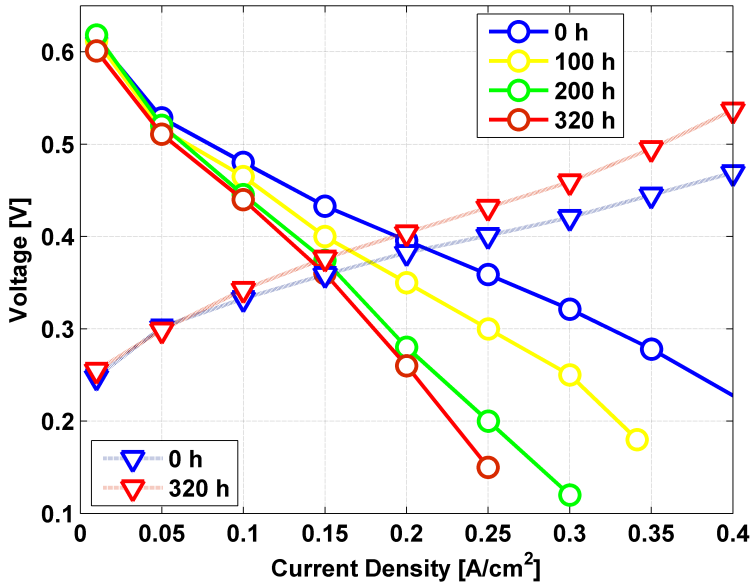

Figure 8.6: Polarization curves during the OCV AST in reference conditions.

the beginning of the performance fluctuations, still maintains a very unstable behaviour, which reason is actually not explained. It is possible to suspect three main causes determining this sudden effect of strong performance decay and recovery:

- experimental setup defects and troubles;
- DMFC strong degradation due to the AST;
- DMFC strong degradation due to the experimental setup wrong operation or troubles;

Anyway the permanent degradation can be estimated equal to 635 $\mu V \cdot h^{-1}$ among which 95 $\mu V \cdot h^{-1}$ are attributable to the anode degradation; however the strong degradation occurs between the polarization curves at 100 h and 200 h, the period of time that corresponds to the strong performance decay occurred after 160 hours. For this reason, the part of the test after the strong performance decay and marked by the performance fluctuations is considered as not reliable. There are probable similarities between this phenomenon and the performance decay observed in figure 8.1.
The increase in the anode permanent degradation in comparison with the long-term test reported in chapter 6 could be related to the Ruthenium crossover mechanism that could be linked to the methanol crossover, which in this test is high because of the lack of current production.

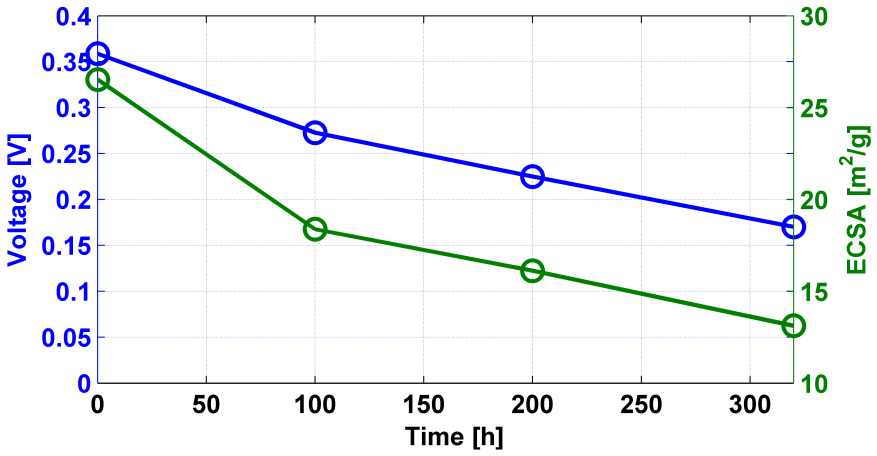

Figure 8.7: Comparison between cathode ECSA obtained through the CV and Voltage at nominal current density during the Polarization curves reported in figure 8.6.

In figure 8.7 is reported a comparison between the voltage decay in the polarization curves at nominal current density and the ElectroChemical Surface Area calculated from the cyclic voltammetries performed as described in paragraph 6.2.2. An important ECSA reduction is observed and, particularly, the ECSA is more than halved after 300 h of AST based on the OCV cycles. This supports the forecasts on the AST effectiveness on the cathode ECSA loss increase: a acceleration factor of about 3 is obtained for the halving of the ECSA in comparison with the Long-Term test reported in chapter 6.

8.4.3 Second test on the OCV cycles based AST

There are two slight differences in the second test on the OCV cycles based Accelerated Stress Test: indeed a third simplified experimental equipment (with a new electronic load) has been realized to perform the AST repeatability. The lack of an additional air humidifier does not allow the air humidification and, in order to avoid too long dry OCV duration, the procedure for the second AST performance consists in cycles, divided in 30 *sec* periods at OCV and 30 *sec* periods at No-Air and they take 60 *min*. Furthermore an operation period at 0.25 $A \cdot cm^{-2}$ of 20 minutes is present in the cycle, in order to monitor frequently the DMFC performance degradation. The second test is named AST2 in the following figures while the name AST1 is referred to the test reported in paragaph 8.4.2.

Figure 8.8 reports the voltage decay obtained during the second AST during the operation period at 0.25 $A \cdot cm^{-2}$ while the traits in OCV/No Air are not reported; it shows a very important performance decay in the first 50 hours of operation and a more regular decrease until the end of the test. The operation interruption for diagnostic determines a slight performance recovery coherently with a limited temporary degradation accumulation.

The polarization curves at the beginning and after 200 hours (for the second AST is the end of life) of both the tested AST are reported in figure 8.9; the good repeatability of the reference MEA is confirmed by the strong similarity in the BoL performances. Considering the differences between the voltage behaviours of figure 8.5 and figure 8.8, it is evident as the performance fluctuations associated with the voltage sudden collapse after 150 h of figure 8.8 determine a stronger permanent degradation.
The acceleration factor for the permanent degradation of the second AST respect to the long-term test of chapter 6 is more limited ($\times$ 4) but more reliable than the first AST, leading to a permanent degradation of 392 $\mu V \cdot h^{-1}$.

The comparison between the ECSA loss during the two ASTs acquired in

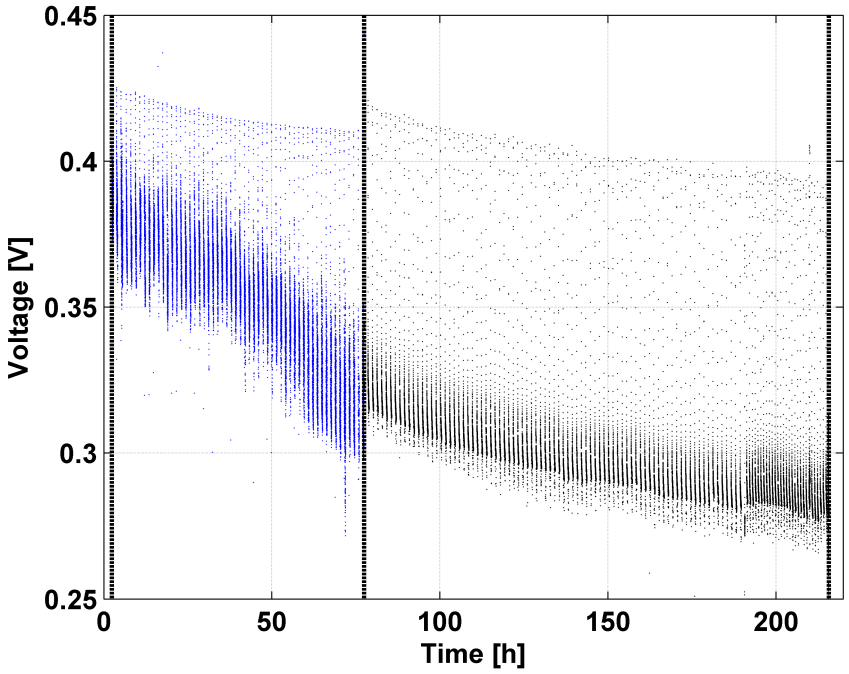

Figure 8.8: Voltage decay during the second AST in the 0.25 $A{\cdot}cm^{-2}$ periods.

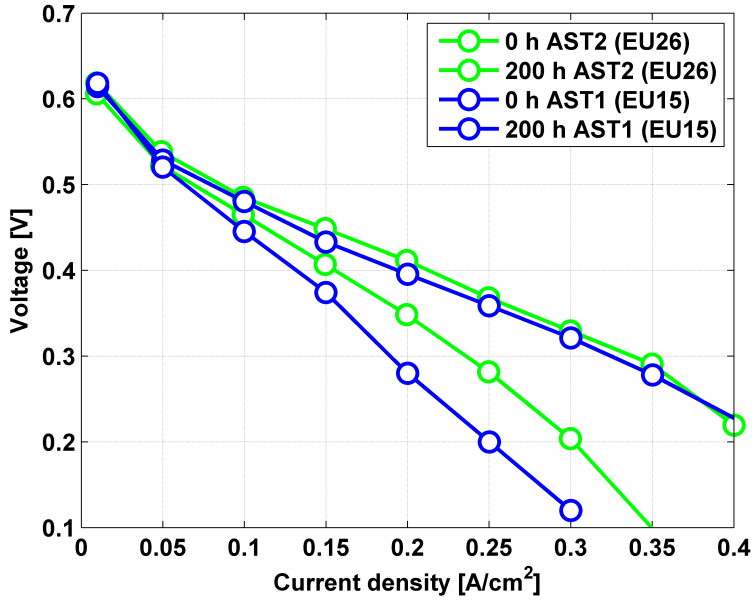

Figure 8.9: Polarization curves at BoL and 200 h during the OCV ASTs in reference conditions.

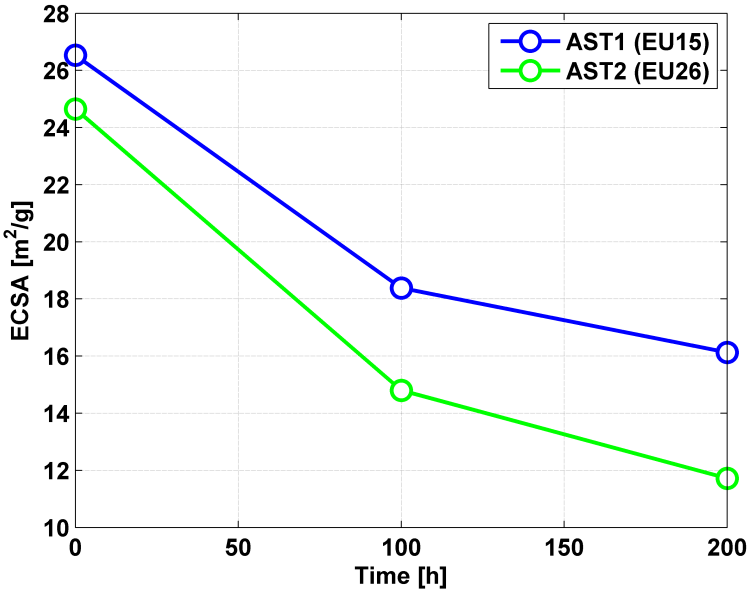

Figure 8.10: ECSA measured through CV during the OCV ASTs .

the diagnostic interruptions is reported in figure 8.10; the ECSA decreases coherently in both the ASTs confirming an acceleration factor of $\times$ 3 for the ECSA loss in comparison with the long-term test described in chapter 6. Hence, the unusual strong instability in the performance of the first OCV cycles based AST is not due to a excessive ECSA loss.
As a summary, the second test on the OCV based AST permits to conclude that the proposed AST permits the acceleration of the cathode ECSA loss in comparison with the long-term test.

8.5 Conclusions and future improvements

Two kinds of preliminary Accelerated Stress Tests for Direct Methanol Fuel Cell degradation are designed and tested, one based on Load Cycle and one based on Open Circuit Voltage Cycles. Both of them show a significant increase of degradation and both of them manifest unusual behaviour in the performance decay, which motivation are still not explained. Particularly, the Load Cycles are considered not really suitable as an AST for several reasons discussed in paragraph 8.3.3. Instead, the OCV cycles seems to be a promising way to develop reliable AST for the acceleration of cathode ECSA loss due to degradation mechanisms such as Platinum Dissolution, which are related to cathode potential. However, still there are technical problems hin-

dering the results reliability particularly due to the operation period at less than 0.1 V that seems to determine a very significant permanent degradation is a very short time.
For this reason the OCV cycles based AST has been repeated in a second test where no performance fluctuations attributable or to experimental setup troubles or to internal issues of the MEA have been observed; the proposed AST permits the acceleration of the cathode ECSA loss in comparison with the long-term test. This chapter could act as a foundation for further works on the Accelerated Stress Test development for a representative acceleration of the DMFC degradation. However the high complexity of DMFC degradation mechanisms makes the AST design very difficult because not all the mechanisms are completely described and explained and, moreover, a preliminary modelling approach could be helpful for the AST design. Further improvements will consider repeatabilty test on the already developed AST and the development of new batches of AST based on a combined approach of different accelerating stressors both already tested and not already adopted. The maintenance of a standard methodology for the results quantification and detailed post-mortem analyses should guarantee the effectiveness of new procedures.

Conclusions

This PhD thesis, performed in the frame of the European Research project Premium ACT, proposes a systematic experimental investigation on Direct Methanol Fuel Cell degradation, based on combined DMFC electrolytic and galvanic operation, which takes into account recoverable and not recoverable performance losses and the relationship between the mass transport phenomena and degradation mechanisms.
An already existent experimental setup has been tuned for the degradation tests performance, improving the reliability of the controls and reducing the measurement uncertainties. A comparison between different DMFC operating strategies has permitted to define the methodology to perform the degradation tests thanks to the introduction of the refresh procedure, based on OCV and cathode air interruption and provided by IRD Fuel Cell A/S, which allows a important performance recovery. Statistical methods, based on linear regression and bi-exponential interpolation, are used to obtain degradation rates and to compare different degradation tests. The high degradation, obtained in continuous steady state operation respect to operating strategies based on refresh cycles, clearly highlights the need for an improvement of temporary degradation mechanisms comprehension.
For the first time in the literature, the anode overpotential behaviour in time has been characterized in electrolytic operation with cathode set as a hydrogen reference electrode, highlighting the existance of a anode temporary degradation. Through a sensitivity analysis on the operating strategies effect on the overpotential and by means of a qualtative interpretation of the anode Electrochemical Impedance Spectra (EIS), a mechanism for the anode temporary degradation has been proposed and the origin could be related to

a reduction of water and methanol concentrations in both the Gas Diffusion Layer and the electrode, promoted by the accumulation of gas-phase CO_2 during the operation. The anode temporary degradation mechanism results in a reversible decrease of methanol crossover during the operation as confirmed by Gas-Chromatographic measurements.
However, the anode degradation rate is lower than the degradation rate obtained in galvanic (DMFC) operation suggesting the presence of other temporary degradation mechanisms including the probable formation of platinum oxides at the cathode that occurs at high potentials typical of DMFC cathode operation. Hence, the anode temporary degradation mechanism is not sufficient to explain the refresh cycle effectiveness on the performance recovery; water management can result in cathode electrode dehydration and, above all, the cathode air feeding interruption, including a strong lowering of the cathode potential, causes a small hydrogen production at the anode and the probable reduction of platinum oxides, which increases cathode performances.
The ex-situ characterizaton of the Gas Diffusion Layer has allowed the investigation of the influence of MicroPorous Layer presence on both water diffusion and permeation: the MPL presence reduces GDL effective diffusivity and increases permeation threshold. Furthermore, hysteresis phenomena have been observed meaning that a wet GDL permits a higher mass transport than a dry GDL and this could influence the refresh effectiveness. Changing the GDL configuration (removing the anode MPL) has important effects on DMFC performances and degradation resulting in a better anode operation and in a worst cathode operation and degradation. Preliminary Accelerated Stress Tests for GDLs have been developed and a significant GDL degradation determine a variation of GDL mass transport properties.
DMFC permanent degradation has been investigated through the performance of a long-term test of more than 1100 hours with continuous in-operando consolidated diagnostic such as polarization curves, EIS and innovative tools as Cyclic Voltammetry and Linear Sweep Voltammetry. The experimental methodology, including the minimization of the temporary degradation obtained by means of the "full refresh" procedure, permits the permanent degradation estimation through the polarization curves comparison. A important cathode electrochemical surface area (ECSA) decrease is observed; the DMFC used in this test has been characterized through advanced post-mortem analysis in order to provide a deep insight into DMFC permanent degradation mechanisms. XPS measurements, performed at DLR, highlight ruthenium crossover from the anode to the cathode and a chemical decomposition of the anode GDL while the SEM and TEM measurements, performed at CEA, show catalyst particle size increase in the cathode outlet region,

ruthenium presence in the anode GDL and MPL and, finally, catalysts and inert particles precipitation into the electrolytic membrane.
Finally a preliminary Accelerated Stress Test for DMFC degradation has been designed and tested with the goal to accelerate the degradation of the cathode electrode by means of promoting the platinum dissolution, which is favoured at high potentials. This test is based on Open Circuit Voltage cycles in order to avoid that platinum oxides formation could hinder the effectiveness of high potentials on platinum dissolution.

Bibliography

[1] T. Schultz, S. Zhou, K. Sundmacher. *Current status of and recent developments in the direct methanol fuel cell.* Chemical Engineering and Technology 24 (2001) 1223-1233.

[2] S. Wasmus, A. Küver. *Methanol oxidation and direct methanol fuel cells: a selective review.* Journal of Electroanalytical Chemistry 461 (1999) 14-31.

[3] F. Liu, C. Wang. *Mixed potential in a Direct Methanol Fuel Cell.* Journal of the Electrochemical Society 154 (2007) B514-B522.

[4] X.Ren, W.Henderson, S.Gottesfeld. *Electro-osmotic drag of water in ionomeric membranes.* Journal of the Electrochemical Society 144 (1997) L267-L270.

[5] T.A. Zawodzinski, C. Derouin, S. Radzinski, R.J. Sherman, et al. *Water uptake by and transport through Nafion 117 membranes.* Journal of the Electrochemical Society 140 (1993) 1041-1047.

[6] S. Litster, G. McLean. *PEM fuel cell electrodes.* Journal of Power Sources 130 (2004) 61-76.

[7] S. Park, J.W. Lee, B.N. Popov. *A review of gas diffusion layer in PEM fuel cells: materials and designs.* International Journal of Hydrogen Energy 37 (2012) 5850-5865.

[8] A. Casalegno, C. Santoro, F. Rinaldi, R. Marchesi. *Low methanol crossover and high efficiency direct methanol fuel cell: the influence of diffusion layers.* Journal of Power Sources 196 (2011) 2669-2675.

[9] M. Zago, A. Casalegno, C. Santoro, R. Marchesi. *Water transport and flooding in DMFC: experimental and modeling analyses.* Journal of Power Sources 217 (2012) 381-391.

[10] C.E. Shaffer, C.Y. Wang. *Role of hydrophobic anode MPL in controlling water crossover in DMFC*. Electrochimica Acta 54 (2009) 5761-5769.

[11] D. Gerteisen. *Transient and steady-state analysis of catalyst poisoning and mixed potential formation in direct methanol fuel cells*. Journal of Power Sources 195 (2010) 6719-6731.

[12] M.R. Shivhare, C.L. Jackson, K. Scott, E.B. Martin. *Simplified model for the direct methanol fuel cell anode*. Journal of Power Sources 173 (2007) 240-248.

[13] J.P. Meyers, J. Newman. *Simulation of the direct methanol fuel cell. II. Modeling and data analysis of transport and kinetic phenomena*. Journal of The Electrochemical Society 149 (2002) A718-A728.

[14] K. Scott, P. Argyropoulos. *A one dimensional model of a methanol fuel cell anode*. Journal of Power Sources 137 (2004) 228-238.

[15] A.S. Arico, P. Creti, E. Modica, G. Monforte, et al. *Investigation of direct methanol fuel cells based on unsupported Pt-Ru anode catalysts with different chemical properties*. Electrochimica Acta 45 (2000) 4319-4328.

[16] X. Ren, P. Zelenay, S. Thomas, J. Davey, S. Gottesfeld. *Recent advances in direct methanol fuel cells at Los Alamos National Laboratory*. Journal of Power Sources 86 (2000) 111-116.

[17] M. Ahmed, I. Dincer. *A review on methanol crossover in direct methanol fuel cells: challenges and achievements*. International Journal of Energy Research 35 (2011) 1213-1228.

[18] X. Ren, T.E. Springer, T.A. Zawodzinski, S. Gottesfeld. *Methanol transport through Nafion membranes. Electro-osmotic drag effects on potential step measurements*. Journal of The Electrochemical Society 147 (2000) 466-474.

[19] A. Heinzel, V.M. Barragon. *A review of the state of the art of the methanol crossover in direct methanol fuel cells*. Journal of Power Sources 84 (1999) 70-74.

[20] Y.J. Chiu. *An algebraic semi empirical model for evaluating fuel crossover fluxes of a DMFC under various operating conditions*. International Journal of Hydrogen Energy 35 (2010) 6418-6430.

[21] S.S. Sandhu, R.O. Crowther, J.P. Fellner. *Prediction of methanol and water fluxes through a direct methanol fuel cell polymer electrolyte membrane*. Electrochimica Acta 50 (2005) 3985-3991.

[22] V. Gogel, T. Frey, Z. Yongsheng, K.A. Friedrich, et al. *Performance and methanol permeation of direct methanol fuel cells: dependence on operating conditions and on electrode structure*. Journal of Power Sources 127 (2004) 172-180.

[23] S.R. Yoon, G.H. Hwang, W.I. Cho, I.H. Oh, et al. *Modification of polymer electrolyte membranes for DMFCs using Pd films formed by sputtering*. Journal of Power Sources 106 (2002) 215-223.

[24] A. Casalegno, F. Bresciani, V. Di Noto, C.S. Casari, A. Li Bassi, E. Negro, R. Marchesi, F. Di Fonzo. *Nanostructured Pd barrier for low methanol crossover DMFC*. International Journal of Hydrogen Energy; http://dx.doi.org/10.1016/j.ijhydene.2013.09.028.

[25] V. Neburchilov, J. Martin, H. Wang, J. Zhang. *A review of polymer electrolyte membranes for direct methanol fuel cells*. Journal of Power Sources 169 (2007) 221-238.

[26] A. Casalegno, R. Marchesi, D. Parenti. *Two-phase 1D+1D model of a DMFC: development and validation on extensive operating conditions range*. Fuel Cells 8 (2008) 37-44.

[27] A. Casalegno, R. Marchesi. *DMFC performance and methanol crossover: experimental analysis and model validation*. Journal of Power Sources 185 (2008) 318-330.

[28] Q. Liao, X. Zhu, X. Zheng, Y. Ding. *Visualization study on the dynamics of CO_2 bubbles in anode channels and performance of a DMFC*. Journal of Power Sources 171 (2007) 644-651.

[29] W. Chen, G. Sun, J. Guo, X. Zhao, S. Yan, S. Tang, Z. Zhou, Q. Xin. *Test on the degradation of direct methanol fuel cell*. Electrochimica Acta 51 (2006) 2391-2399.

[30] P. Liu, G. Yin, K. Cai. *Investigation on cathode degradation of direct methanol fuel cell*. Electrochimica Acta 54 (2009) 6178-6183.

[31] L.S. Sarma, C.H. Chen, G.R. Wang, K.L. Hsueh, et al. *Investigations of direct methanol fuel cell (DMFC) fading mechanisms*. Journal of Power Sources 167 (2007) 358-365.

[32] H. Kim, S. Shin, Y. Park, J. Song, H. Kim *Determination of DMFC deterioration during long-term operation.* Journal of Power Sources 160 (2006) 440-445.

[33] J. Park, M. Scibioh, S. Kim, H. Kim, I. Oh, T. Lee, H. Ha. *Investigations of performance degradation and mitigation strategies in direct methanol fuel cells.* International Journal of Hydrogen Energy 34 (2009) 2043-2051.

[34] J. Park, J. Lee, J. Sauk, I. Son. *The operating mode dependence on electrochemical performance degradation of direct methanol fuel cells.* International Journal of Hydrogen Energy 33 (2008) 4833-4843.

[35] H. Cha, C. Chen, Y. Shiu. *Investigation on the durability of direct methanol fuel cells.* Journal of Power Sources 192 (2009) 451-456

[36] H. Yang, T. Zhao, Q. Ye. *In situ visualization study of CO_2 gas bubble behavior in DMFC anode flow fields.* Journal of Power Sources 139 (2005) 79-90.

[37] C. Eickes, P. Piela, J. Davey, P. Zelanay. *Recoverable Cathode Performance Loss in Direct Methanol Fuel Cells.* Journal of The Electrochemical Society 153 (2006) A171-A178.

[38] D. Rolison, P. Hagans, K. Swider, J. Long. *Role of Hydrous Ruthenium Oxide in Pt-Ru Direct Methanol Fuel Cell Anode Electrocatalysts: The Importance of Mixed Electron/Proton Conductivity.* Langmuir 15 (1999) 774-779.

[39] C. Chen, H. Cha *Strategy to optimize cathode operating conditions to improve the durability of a Direct Methanol Fuel Cell* Journal of Power Sources 200 (2012) 21-28.

[40] Y. Shao-Horn, W. Sheng, S. Chen, P. Ferreira, E. Holby, D. Morgan *Instability of Supported Platinum Nanoparticles in Low-Temperature Fuel Cells.* Topics in catalysis 46 (2007) 285-305.

[41] A. Virkar, Y. Zhou. *Mechanism of Catalyst Degradation in Proton Exchange Membrane Fuel Cells.* Journal of the Electrochemical Society 154 (2007) B540-B547.

[42] H. Chizawa, Y. Ogami, H. Naka, A. Matsunaga, N. Aoki, T. Aoki, K. Tanaka. *Impacts of Carbon Corrosion on Cell Performance Decay* ECS transactions 11 (2007) 981-992.

[43] L. Roen, C. Paik, T. Jarvi *Electrocatalytic corrosion of carbon support in PEMFC cathodes*. Electrochemical Solid-State Letters 7 (2004) A19-A24.

[44] A. Franco, M. Gerard. *Multiscale Model of Carbon Corrosion in a PEFC: Coupling with Electrocatalysis and Impact on Performance Degradation*. Journal of the Electrochemical Society 155 (2008) B367-B384.

[45] H. Tang, S. Peikang, S. Jang, F. Wang, M. Pan. *A degradation study of Nafion proton exchange membrane of PEM fuel cells*. Journal of Power Sources 170 (2007) 85-92.

[46] S. Knights, K. Colbow, J. St-Pierre, D. Wilkinson. *Aging mechanisms and lifetime of PEFC and DMFC*. Journal of Power Sources 127 (2004) 127-134.

[47] X. Cheng, C. Peng, M. You, L. Liu, Y. Zhang, Q. Fan. *Characterization of catalysts and membrane in DMFC lifetime testing*. Electrochimica Acta 51 (2006) 46204625.

[48] European Project *DECODE: degradation mechanisms to improve components and design*.

[49] European Project *Premium Act: predictive modelling for innovative unit management and accelerated testing procedures of PEFC*.

[50] M. Zago *DMFC modeling: Mass Transport Phenomena and Electrochemical Impedance Spectroscopy*. PhD Thesis 2013.

[51] H. Dohle, J. Divisek, J. Mergel, H.F. Oetjen, et al. *Recent developments of the measurement of the methanol permeation in a direct methanol fuel cell*. Journal of Power Sources 105 (2002) 274-282.

[52] Z.H. Jiang, D.R. Chu. *Comparative studies of methanol crossover and cell performance for a DMFC*. Journal of the Electrochemical Society 151 (2004) A69-A76.

[53] T.S. Zhao, C. Xu, R. Chen, W.W. Yang. *Mass transport phenomena in direct methanol fuel cells*. Progress in Energy and Combustion Science 35 (2009) 275-292.

[54] A. Casalegno *Direct Methanol Fuel Cells: experimental analysis and model development*. PhD Thesis 2007.

[55] Y. Kim, W. Hong, S. Woo, H. Lee. *Analysis of the polarization of a direct methanol fuel cell using a pseudo-reversible hydrogen reference electrode*. Journal of Power Sources 159 (2006) 491-500.

[56] E. Barsoukov, J.R. Macdonald. *Impedance spectroscopy. Theory, experiment, and applications*. Wiley 2005.

[57] M.E. Orazem, B. Tribollet. *Electrochemical impedance spectroscopy*. Wiley 2008.

[58] S.K. Roy, M.E. Orazem, B. Tribollet. *Interpretation of low-frequency inductive loops in PEM fuel cells*. Journal of The Electrochemical Society 154 (2007) B1378-B1388.

[59] C. Ming Lai, J.C. Lin, K.L. Hsueh, C.P. Hwang, et al. *On the electrochemical impedance spectroscopy of direct methanol fuel cell*. International Journal of Hydrogen Energy 32 (2007) 4381-4388.

[60] J.T. Müller, P.M. Urban. *Characterization of direct methanol fuel cells by ac impedance spectroscopy*. Journal of Power Sources 75 (1998) 139-143.

[61] J.T. Müller, P.M. Urban, W.F. Hölderich. *Impedance studies on direct methanol fuel cell anodes*. Journal of Power Sources 84 (1999) 157-160.

[62] M. Mench. *Fuel Cell Engines*. J. Wiley and Sons 2008.

[63] C. Xie, J. Bostaph, J. Pavio. *Development of a 2 W direct methanol fuel cell power source*. Journal of Power Sources 136 (2004) 55.

[64] S. Bae, S. Kim, J. Park, J. Lee, H. Cho, J. Park. *Lifetime prediction through accelerated degradation testing of membrane electrode assemblies in direct methanol fuel cells*. International Journal of Hydrogen Energy 35 (2010) 9166-9176.

[65] S. Bae, S. Kim, S. Um, J. Park, J. Lee, H. Cho.*Aprediction model of degradation rate for membrane electrode assemblies in direct methanol fuel cells*. International Journal of Hydrogen Energy 34 (2009) 5749-5758.

[66] M. Neergat, T. Seiler, E.R. Savinova, U. Stimming. *Improvement of the Performance of a Direct Methanol Fuel Cell Using a Pulse Technique*. Journal of the Electrochemical Society 153 (2006) A997-A1003.

[67] A. Casalegno, R. Marchesi, F. Rinaldi *Systematic Experimental Analysis of a Direct Methanol Fuel Cell*. Journal of Fuel Cell Science and Technology 4 (2007) 418-424.

[68] N. Wongyao, A. Therdthianwong, S. Therdthianwong, S.M. Kumar, K. Scott. *A comparison of Direct Methanol Fuel Cell Degradation under different Modes of Operation*. International Journal of Hydrogen Energy 38 (2013) 9464-9473.

[69] A. Casalegno, R. Marchesi. *DMFC anode polarization: Experimental analysis and model validation*. Journal of Power Sources 175 (2008) 372-382.

[70] D. Montgomery, G. Runger, N. F. Hubele. *Engineering Statistics*. 3rd edition, J. Wiley and Sons 2004.

[71] F. Bresciani, A. Casalegno, J.L. Bonde, M. Odgaard, R. Marchesi. *A comparison of operating strategies to reduce DMFC degradation*. International Journal of Energy Research 38 (2014) 117-124.

[72] M. Zago, A. Casalegno. *A Physical Model for DMFC anode Impedance*. Journal of Power Sources 248 (2014) 1181-1190.

[73] S.K. Roy, M.E. Orazem. *Error analysis of the impedance response of PEM fuel cells*. Journal of The Electrochemical Society 154 (2007) B883-B891.

[74] Y.J. Kim, W.H Hong, S.I. Woo, H.K. Lee. *Analysis of the polarization of a direct methanol fuel cell using a pseudo-reversible hydrogen reference electrode*. Journal of Power Sources 159 (2006) 491-500.

[75] S.H. Yang, C.Y. Chen, W.J. Wang. *An impedance study of an operating direct methanol fuel cell*. Journal of Power Sources 195 (2010) 2319-2330.

[76] F. Bresciani, A. Casalegno, G. Varisco, R. Marchesi. *Water Transport into PEFC diffusion layer: experimental characterization of diffusion and permeation*. International Journal of Energy Research 2013 DOI: 10.1002/er.3065.

[77] Z. Liu, M. Daino, C. Rath, S. Kandlikar. *Water management studies in PEM fuel cells, part III: Dynamic breakthrough and intermittent drainage characteristics from GDLs with and without MPLs*. International Journal of Hydrogen Energy 35 (2010) 4222-4233.

[78] Q. Ye, T.S. Zhao. *Electrolytic Hydrogen Evolution in DMFCs Induced by Oxygen Interruptions and Its Effect on Cell Performance*. Electrochemical and Solid-State Letters 8 (2005) A211-A214.

[79] D.U. Sauer, T. Sanders, B. Fricke, T. Baumhofer, K. Wippermann, A.A. Kulikovsky, H. Schmitz, J. Mergel. *Measurement of the current distribution in a direct methanol fuel cell-Confirmation of parallel galvanic and electrolytic operation within one cell*. Journal of Power Sources 176 (2008) 477-483.

[80] T. Tsujiguchi, T. Furukawa, N. Nakagawa. *Effect of the impurities in crude bio-methanol on the performance of the direct methanol fuel cell*. Journal of Power Sources 196 (2011) 9339-9345.

[81] J. Park, K. Park, K. Kim, Y. Na, H. Cho, J. Kim. *Influence and mitigation methods of reaction intermediates on cell performance in direct methanol fuel cell system*. Journal of Power Sources 196 (2011) 5446-5452.

[82] F. Bresciani, A. Casalegno, M. Zago. *A parametric analysis on DMFC Anode Degradation*. Fuel Cells 2013. DOI: 10.1002/fuce.201300132

[83] A. Casalegno, F. Bresciani, G. Groppi, R. Marchesi. *Flooding of the diffusion layer in a polymer electrolyte fuel cell: Experimental and modelling analysis*. Journal of Power Sources 196 (2011) 10632-10639.

[84] Y. Tian, G. Sun, Q. Mao, S. Wang, H. Liu, Q. Xin. *In situ analysis on water transport in a direct methanol fuel cell durability test*. Journal of Power Sources 185 (2008) 1015-1021.

[85] S.G. Kandlikar, M. Garofalo, Z. Lu. *Water Management in A PEMFC: Water Transport Mechanism and Material Degradation in Gas Diffusion Layers*. Fuel Cells 11 (2011) 814-823.

[86] P. J. James, J. A. Elliott, T. J. McMaster, J. M. Newton, A. M. S. Elliott, S. Hanna, M. J. Miles. *Hydration of Nafion studied by AFM and X-ray scattering*. Journal of Material Science 35 (2000) 5111-5119.

[87] S. Eccarius, T. Manurung, C. Ziegler. *On the Reliability of Measurements Including a Reference Electrode in DMFCs*. Journal of the Electrochemical Society 154 (2007) B852-B864.

[88] B. Piela, P. Piela, P. Wrona. *Oxidation of Nitrite on the Solid Electrodes. Part II. Determination of the Reaction Mechanism on the Surface Covered by the Oxide Layer*. Journal of the Electrochemical Society 149 (2002) E357-E366.

[89] F. A. Uribe, T. A. Zawodzinski. *A study of polymer electrolyte fuel cell performance at high voltages. Dependence on cathode catalyst layer composition and on voltage conditioning*. Electrochimica Acta 47 (2002) 3799-3806.

[90] B. E. Conway, B. Barnett, H. Angerstein-Kozlowska, B. V. Tilak. *A surface-electrochemical basis for the direct logarithmic growth law for initial stages of extension of anodic oxide films formed at noble metals*. Journal of Chemical Physics 93 (1990) 8361.

[91] M.E. van der Geest, N.J. Dangerfield, D.A. Harrington. *An A.C. Voltammetry Study of Pt Oxide Growth*. Journal of Electroanalytical Chemistry 420 (1997) 89-100.

[92] Q. Ye, T. S. Zhao, H. Yang, J. Prabhuram. *Electrochemical Reactions in a DMFC under Open-Circuit Conditions*. Electrochemical and Solid-State Letters 8 (2005) A52-A54.

[93] Q. Ye, T. S. Zhao, J. G. Liu. *Effect of Transient Hydrogen Evolution/Oxidation Reactions on the OCV of Direct Methanol Fuel Cells*. Electrochemical and Solid-State Letters 8 (2005) A549-A553.

[94] A.A. Kulikovsky. *Direct methanol-hydrogen fuel cell: The mechanism of functioning*. Electrochemistry Communications 10 (2008) 1415-1418.

[95] A.A. Kulikovsky, H. Schmitz, K. Wippermann, J. Mergel, B. Fricke, T. Sanders, D.U. Sauer. *DMFC: Galvanic or electrolytic cell ?*. Electrochemistry Communications 8 (2006) 754-760.

[96] H. Dohle, J. Mergel, P.C. Ghosh. *DMFC at low air flow operation: Study of parasitic hydrogen generation*. Electrochimica Acta 52 (2007) 6060-6067.

[97] L. Cindrella, A.M. Kannan, J.F. Lin, K. Saminathan, Y. Ho, C.W. Lin, J. Wertz. *Gas diffusion layer for proton exchange membrane fuel cells - A review*. Journal of Power Sources 194 (2009) 146-160.

[98] S. Park, J. Lee, B. N. Popov. *A review of gas diffusion layer in PEM fuel cells: Materials and designs*. International Journal of Hydrogen Energy 37 (2012) 5850-5865

[99] S. Park, N. Popov. *Effect of a GDL based on carbon paper or carbon cloth on PEM fuel cell performance*. Fuel 90 (2011) 436-440.

[100] C. Lim, C.Y. Wang. *Effects of hydrophobic polymer content in GDL on power performance of a PEM fuel cell*. Electrochimica Acta 49 (2004) 4149-4156.

[101] U. Pasaogullari, C. Wang. *Two-phase transport and the role of micro-porous layer in polymer electrolyte fuel cells*. Electrochimica Acta 49 (2004) 4359-4369.

[102] G. Karimi, A. Jamekhorshid, Z. Azimifar, X. Li. *Along-channel flooding prediction of polymer electrolyte membrane fuel cells*. International Journal of Energy Research 35(2011) 883-896.

[103] P. Mukherjee, C. Wang, Q. Kang. *Mesoscopic modeling of two-phase behavior and flooding phenomena in polymer electrolyte fuel cells*. Electrochimica Acta 54(2009) 6861-6875.

[104] N. Zamel, X. Li. *A parametric study of multi-phase and multi-species transport in the cathode of PEM fuel cells*. International Journal of Energy Research 32 (2008) 698-721.

[105] A. Arvay, E. Yli-Rantala, C.H. Liu, X.H. Peng, P. Koski, L. Cindrella, P. Kauranen, P.M. Wilde, A.M. Kannan. *Characterization techniques for gas diffusion layers for proton exchange membrane fuel cells - A review*. Journal of Power Sources 213(2012) 317-337.

[106] L. Pant, S. K. Mitra, M. Secanell. *Absolute permeability and Knudsen diffusivity measurements in PEMFC gas diffusion layers and micro porous layers*. Journal of Power Sources 206 (2012) 153-160.

[107] R. Fluckiger, S. Freunberger, D. Kramer, A. Wokaun, G. G. Scherer, F. N. Buchi. *Absolute permeability and Knudsen diffusivity measurements in PEMFC gas diffusion layers and micro porous layers*. Electrochimica Acta 54 (2008) 551-559.

[108] A. Casalegno, L. Colombo, S. Galbiati, R. Marchesi. *Quantitative characterization of water transport and flooding in the diffusion layers of polymer electrolyte fuel cells*. Journal of Power Sources 195 (2010) 4143-4148.

[109] E.A. Wargo, V.P. Schulz, A. Cecen, S.R. Kalidindi, E.C. Kumbur, *Resolving macro- and micro-porous layer interaction in polymer electrolyte*

fuel cells using focused ion beam and X-ray computed tomography. Electrochimica Acta 87 (2013) 201-212.

[110] J. Lee, J. Hinebaugh, A. Bazylak. *Synchrotron X-ray radiographic investigations of liquid water transport behaviour in a PEMFC with MPL-coated GDLs*. Journal of Power Sources 217 (2012) 381-391.

[111] J. Benziger, J. Nehlsen, D. Blackwell, T. Brennan, J. Itescu. *Water flow in the Gas Diffusion Layer of PEM Fuel Cells*. Journal of Membrane Science 261 (2005) 98-106.

[112] A. Tamayol, M. Bahrami. *Water permeation through gas diffusion layers of proton exchange membrane fuel cells*. Journal of Power Sources 196 (2011) 6356-6361.

[113] Y. Chou, Z. Siao, Y. Chen, L. Sung, W. Yang, C. Wang. *Water permeation analysis on gas diffusion layers of proton exchange membrane fuel cells for Teflon-coating annotation*. Journal of Power Sources 195 (2010) 536-540.

[114] E. Gauthier, Q. Duan, T. Hellstern, J. Benziger. *Water Flow in, Through, and Around the Gas Diffusion Layer*. Fuel Cells 12 (2012) 835-847.

[115] L. Pisani *Multi-component gas mixture diffusion through porous media: A 1D analytical solution*. International Journal of Heat and Mass Transfer 51 (2008) 650-660.

[116] ISO, 1993, *Guide to Expression of Uncertainty in Measurement, BIPM, IEC, IFCC, ISO, IUPAC, IUPAP, OIML International Organization for Standardization*, Env.13005: 1999. led., Corrected and Reprinted 1995.

[117] R.H. Perry, D.W. Green. textslPerry's Chemical Engineer's Handbook. McGraw-Hill, 1999.

[118] B. Pooling, J. Prausnitz, J. O'Connell. *The properties of Gases and Liquids*. McGraw-Hill, 2001.

[119] J. Chun, K. Park, D. Jo, J. Lee, S. Kim, E. Lee, J. Jyoung, S. Kim. *Determination of the pore size distribution of Micro Porous Layer in PEMFC using pore forming agents under various drying conditions*. International Journal of Hydrogen Energy 35 (2010) 11148-11153.

[120] P. Gallo Stampino, C. Cristiani, G. Dotelli, L. Omati, L. Zampori, R. Pelosato, M. Guilizzoni. *Effect of different substrates, inks composition and rheology on coating deposition on Microporous Layer (MPL) for PEM-FCs*. Catalysis Today 147 (2009) S30-S35.

[121] J. Wu, J.J. Martin, F.P. Orfino, H. Wang, C. Legzdins, X. Yuan, C. Sun *In situ accelerated degradation of gas diffusion layer in proton exchange membrane fuel cell. Part1: Effect of elevated temperature and flow rate*. Journal of Power Sources 195 (2010) 1888-1894.

[122] T. Ha, J. Cho, J. Park, K. Min, H. Kim, E. Lee, J. Jyoung. *Experimental study of the effect of dissolution on the gas diffusion layer in polymer electrolyte membrane fuel cells*. International Journal of Hydrogen Energy 36 (2011) 12427-12435.

[123] J. W. Frisk, M. T. Hicks, R. T. Atanasoski, W. M. Boand, A. K. Schmoeckel, M. J. Kurkowski. *MEA component Durability*. Fuel Cell Seminar 2004, San Antonio, Texas.

[124] C. Lee, W. Merida. *Gas diffusion layer durability under steady-state and freezing conditions*. Journal of Power Sources 164 (2007) 141-153.

[125] Y. Lee, B. Kim, Y. Kim, X. Li. *Degradation of Gas Diffusion Layer through repetitive freezing*. Applied Energy 88 (2011) 5111-5119.

[126] G. Chen, H. Zhang, H. Ma, H. Zhong. *Electrochemical durability of gas diffusion layer under simulated proton exchange membrane fuel cell conditions*. International Journal of Hydrogen Energy 34 (2009) 8185-8192.

[127] R. John, F. Kumar, V. Radhakrishnan, P. Haridoss. *Effect of electrochemical aging on the interaction between gas diffusion lavers and the flow field in a proton exchange membrane fuel cell*. International Journal of Hydrogen Energy 36 (2011) 7207-7211.

[128] M. Guilizzoni. *Drop shape visualization and contact angle measurement on curved surfaces*. Journal of Colloid and Interface Science 364 (2011) 230-236.

[129] X.Yuan, H.Wang, J.C. Sun, J. Zhang. *PEM fuel cell diagnostic tools*. Number 13:978-1-4398-3920-1. CRC Press.

[130] D.Zhan, J.Velmurugan, M.V.Mirkin. *Adsorption/desorption of hydrogen on Pt nanoelectrodes: evidence of surface diffusion and spillover*. Journal of the American CHemical Society 131 (2009) 14756-14760.

[131] S. Vengatesan, M.W. Fowler, X. Yuan, H. Wang. *Diagnosis of MEA degradation under accelerated relative humidity cycling*. Journal of Power Sources 196 (2011) 5045-5052.

[132] F. DeBrujin, V.A.T.Dam, G.J.M.Janssen. *Durability and degrada- tion issues of PEM fuel cell components*. Fuel Cells 8 (2008) 3-22.

[133] J.W. Guo, T.S. Zhao, J. Prabhuram, R. Chen, C.W. Wong. *Preparation and characterization of a PtRu/C nanocatalyst for direct methanol fuel cell*. Electrochimica Acta 51 (2005) 754-763.

[134] S. Zhang, X. Yuan, H. Wang, W. Merida, H. Zhu, J Shen, S. Wu, J. Zhang. *A review of accelerated stress tests of MEA durability in PEM fuel cells*. International Journal of Hydrogen Energy 34 (2009) 388-404.

[135] S. Jomori, N. Nonoyama, T. Yoshida. *Analysis and modeling of PEMFC degradation: Effect on oxygen transport*. Journal of Power Sources 215 (2012) 18-27.

[136] P. Gazdzicki, I. Biswas, M. Schultze. *submitted to Surf. Interf. Anal. 2013*.

[137] N. Yousfi-Steiner, P. Mocoteguy, D. Candusso, D. Hissel, A. Hernandez, A. Aslanides. *A review on PEM voltage degradation associated with water management: Impacts, influent factors and characterization*. Journal of Power Sources 183 (2008) 260-274.

[138] H. Li, Y. Tang, Z. Wang, Z. Shi, S. Wu, D. Song, J. Zhang, K. Fatih, J. Zhang, H. Wang, Z. Liu, R. Abouatallah, A. Mazza. *A review of water flooding issues in the proton exchange membrane fuel cell*. Journal of Power Sources 178 (2008) 103-117.

[139] H. Atiyeh, K. Karan, B. Peppley, A. Phoenix, E. Halliop, J. Pharaoah. *Experimental Investigation of the role of a microporous layer on the water transport and performance of a PEM fuel cell*. Journal of Power Sources 170 (2007) 111-121.

[140] J. Owejan, J. Gagliardo, J. Sergi, S. Kandlikar, T. Trabold. *Water management studies in PEM fuel cells, part I: Fuel cell design and in situ water distribution*. International Journal of Hydrogen Energy 34 (2009) 3436-3444.

[141] K. Jiao, B. Zhou. *Innovative gas diffusion layers and their water removal characteristics in PEM fuel cell cathode*. Journal of Power Sources 169 (2007) 296-314.

[142] Q. Liu, C. Wang. *Water and Methanol crossover in direct methanol fuel cells - Effect of anode diffusion media*. Electrochimica Acta 53 (2008) 5517-5522.

[143] W. Schmittinger, A. Vahidi. *A review of the main parameters influencing long-term performance and durability of PEM Fuel Cells*. Journal of Power Sources 180 (2008) 1-14.

[144] S. Kundu et al. *Comparison of two accelerated Nafion^{TM} degradation experiments*. Polymer Degradation and Stability 93 (2008) 214-224.

[145] V. Sethuraman. *Durability of Perfluorosulfonic Acid and Hydrocarbon Membranes: Effect of Humidity and Temperature*. Journal of the Electrochemical Society 155 (2008) B119-B124.

[146] A. Ohma et al. *Membrane degradation mechanism during open circuit voltage test*. Journal of Power Sources 182 (2008) 39-47.

[147] S. Kundu et al. *Degradation analysis and modeling of reinforced catalyst coated membranes operated under OCV conditions*. Journal of Power Sources 182 (2008) 619-628.

[148] A, Kusoglu et al. *Mechanical response of fuel cell membranes subjected to a hygro-thermal cycle* Journal of Power Sources 161 (2006) 987-996.

[149] V.A.T. Dam, F.A. de Bruijn. *The stability of PEMFC electrodes: Platinum dissolution vs potential and temperature investigated by Quartz Crystal Microbalance*. Journal of the Electrochemical Society 154 (2007) B495-B499.

[150] R. Borup. *PEM fuel cell electrocatalyst durability measurements*. Journal of Power Sources 163 (2006) 76-81.

[151] D. Liu, S. Case. *Durability study of proton exchange membrane fuel cells under dynamic testing conditions with cyclic current profile*. Journal of Power Sources 162 (2006) 521-531.

[152] J. Park, J. Kim, Y. Seo, D. Yu, H. Cho, S. Bae. *Operating Temperature Dependency on Performance Degradation of Direct Methanol Fuel Cells*. Fuel Cells 12 (2012) 426-438.

[153] J. Park, S. Song, J. Lee, J. Kim, H. Cho. *The possible failure mode and effect analysis of membrane electrode assemblies and their potential solutions in direct methanol fuel cell systems for portable applications*. International Journal of Hydrogen Energy 35 (2010) 7982-7990.

[154] N. Wongyao, A. Therdthianwong, S. Therdthianwong. *The fading behavior of direct methanol fuel cells under a start-run-stop operation*. Fuel 89 (2010) 971-977.

[155] X. Wang, R. Kumar, D. Myers. *Effect of Voltage on Platinum Dissolution: Relevance to Polymer Electrolyte Fuel Cells*. Electrochemical and Solid State Letters 9 (2006) A225-A227.

[156] E. Redmond, P. Trogadas, F. Alamgir, T. Fuller. *The effect of Platinum Oxide growth on platinum stability in PEMFCs*. ECS Transactions 50 (2012) 1369-1376.

[157] Z. Qi, A. Kaufman. *Open circuit voltage and methanol crossover in DMFCs*. Journal of Power Sources 110 (2002) 177-185.

List of Figures

List of Tables

List of Symbols

a	channel height and width (m)
C	Local concentration in channel $(mol \cdot m^{-3})$
d	pore diameter (m)
D	diffusivity $(cm^2 \cdot s^{-1})$
h	convective mass transport coefficient $(m \cdot s^{-1})$
E_0	ideal potential difference (V)
F	Faraday constant $(C \cdot mol^{-1})$
I	DMFC current density $(A \cdot cm^{-2})$
k	permeability
L	channel length (m)
M	molecular weight $(g \cdot mol^{-1})$
N	flux $(mol \cdot cm^{-2} \cdot s^{-1})$
x	molar fraction (%)
p	pressure (Pa)
p_{cap}	capillary pressure (Pa)
p_{sat}	saturation pressure (Pa)
p_{total}	total pressure (Pa)
Q	2D factor
R	universal gas constant $(J \cdot mol^{-1} \cdot K^{-1})$
r	pore radius (m)
RH	relative humidity
T	fuel cell temperature (K)
t	GDL thickness (cm)
v	local velocity in channel $(cm \cdot s^{-1})$
V	DMFC voltage (V)
y	channel lenght axis

Greek symbol

τ	tortuosity
η	efficiency
μ	compound viscosity ($Pa \cdot s$)
ε	porosity
θ_c	contact angle (^{o})
Σ_ν	molecular diffusion volume
σ	surface tension ($N \cdot m^{-1}$)

Superscript

a	relative to anode
$bulk$	relative to channel bulk
c	relative to cathode
$crossover$	relative to methanol crossover
dry	relative to dry composition
eff	effective diffusivity
GDL	relative to gas diffusion layer
in	relative to inlet
mem	relative to membrane
MPL	relative to microporous layer
out	relative to outlet
$reaction$	relative to electrochemical reaction

Subscript

GDL	relative to gas diffusion layer
MPL	relative to micro porous layer
CO_2	relative to carbon dioxide
H_2O	relative to water
CH_3OH	relative to methanol
O_2	relative to oxygen
air	relative to air
i	relative to specie i
in	relative to inlet
j	relative to specie j
out	relative to outlet
k	relative to Knudsen diffusion
p	relative to pores
tot	relative to total
sat	relative to saturation

List of Acronyms

DMFC	Direct Methanol Fuel Cell
GDL	Gas Diffusion Layer
MPL	MicroPorous Layer
OCV	Open Circuit Voltage
PEMFC	Polymer Electrolyte Membrane Fuel Cell
PEFC	Polymer Electrolyte Fuel Cell
AST	Accelerated Stress Test
EIS	Electrochemical Impedance Spectroscopy
MEA	Membrane Electrode Assembly
CL	Catalyst Layer
PEM	Polymer Electrolyte Membrane
PFSA	PerFluorinated Sulfonic Acid
PTFE	PolyTetraFluoroEthylene
DHE	Dynamic Hydrogen Reference Electrode
μGC	Micro Gas-Chromatograph
LHV	Lower Heating Value
RRI	Refresh Recovery Index
ORR	Oxygen Reduction Reaction
SM	Stefan-Maxwell
IWF	Istantaneous Water Flow
CV	Cyclic Voltammetry
LSV	Linear Sweep Voltammetry
BoL	Begin of Life
EoL	End of Life
ECSA	Electro-Chemical Surface Area
XPS	X-ray PhotoElectron Spectroscopy
SEM	Scanning Electron Microscopy
TEM	Transmission Electron Microscopy
$M-M$	Reference MEA
$G-M$	Benchmark MEA

Appendix

DMFC experimental setup components specifications

This paragraph provides technical details on the components of the two experimental setups for the DMFC characterization, one that usually works in galvanic operation and one that usually works in electrolytic operation.

Peristaltic Pumps

Pump for station 1: Galvanic Operation
Model: *Watson-Marlow 323S*
Maximum Speed: 400 *rpm*
Uncertainty: 0.5 % of measurement
Head Model: Watson-Marlow 304MC
Maximum Head Speed: 110 *rpm*
Massflow range: 0.33 to 43 $g \cdot min^{-1}$
Calibration curve: $\dot{m}_{mix} = 0.1075 \cdot rpm - 0.0084$

Pump for station 2: Electrolytic Operation
Model: *Watson-Marlow 323Du*
Maximum Speed: 220 *rpm*
Uncertainty: 0.5 % of measurement
Head Model: Watson-Marlow 501RL
Maximum Head Speed: 2200 *rpm*

Massflow range: 0.33 to 27 $g \cdot min^{-1}$
Calibration curve: $\dot{m}_{mix} = 0.1293 \cdot rpm - 0.0167$

Flowmeters

Flow Controller for station 1: Galvanic Operation
Model: *Brooks 5850s*
Flow Range: 0 to 2 $Nl \cdot min^{-1}$
Uncertainty: 0.2 % F.S. + 0.7 % R.
Working gas: Air
Voltage Input: 15 to 28 V D.C.
Voltage Output: 0 to 5 V D.C.

Flow Controller for station 2: Electrolytic Operation
Model: *Brooks 5850s*
Flow Range: 0 to 50 $Nml \cdot min^{-1}$
Uncertainty: 0.2 % F.S. + 0.7 % R.
Working gas: Hydrogen
Voltage Input: 15 to 28 V D.C.
Voltage Output: 0 to 5 V D.C.

Electronic Load and Power Supply

Electronic Load for station 1: Galvanic Operation
Model: *TDI RBL 488 50-150-800*
Operation Mode: Voltage Reading
Range: 0 to 10 V (lowscale)
Resolution: 0.001 V
Uncertainty: 0.5 % $\pm$ 0.0005 A

Power Supply for station 2:Electrolytic Operation
Model: *Chroma DC Power Supply 62012P-80-60*
Operation Mode: Voltage Reading
Range: 0 to 80 V
Uncertainty: 0.05 %+ 0.1 % F.S.

MilliOhmeter

MilliOhmeter for station 1 and 2
Model: Tsuruga 3566
Uncertainty: 1 $m\Omega \cdot cm^2$

Pressure transducers

Pressure Transducer for cathode humidity measurement for station 1: Galvanic Operation
Model: *GE Druck PMP 4070*
FullScale: 3 *bar*
Voltage Input: 9 to 32 V D.C.
Voltage Output: 0 to 5 V D.C.
Non Linearity and Hysteresis: $\pm$ 0.004 % F.S.

Thermocouples

Model: Type K
Materials: Chromel, Alumel
Temperature Limits: -270^oC to 1370^oC
Calibration Range: 40 to 90^oC

CO_2 probe

Model: *Vaisala M170 with GMP222 probe*
Fullscale: 0 to 30000 *ppm* Probe Uncertainty: $\pm$ 20 *ppm* $\pm$ 2 % R. Detector Uncertainty: $\pm$ 0.2 % F.S.

Humidity Probe

The humidity and temperature probe is placed into a thermo-stated housing controlled by means of a Temperature Controller that acts on a Resistance placed inside the housing.

Humidity Probe for DMFC cathode
Model: *Vaisala HMT333*
Probe: *Humicap HMT333*
Voltage Input: 10 to 35 V D.C.
Voltage Output: 2 to 10 V D.C.
Temperature Range: 0 to 120 ^oC
Humidity Range: 0 to 100 %
Temperature Uncertainty: $\pm$ 0.1 ^oC at 22.13 ^oC
Humidity Uncertainty: $\pm$ 1 % RH

Temperature Controller for thermostated housing

Model: *ASCON Linea M3 Serie δ2*
Voltage Input: 220 V A.C.
Regulator: Internal PID
Resolution: 1 ^oC
Relay Model: *Carlo Gavazzi RS1A23D40*
Voltage Range: 230 V A.C or 3/32 V D.C.

Electrical Resistance
Model: *HAWCO HS37-3*
Power: 400 W
Shape: Cylinder
Lenght: 78 mm
Diameter: 9.4 mm
Voltage Input: 240 V

Tubes, fittings and humidifier

Tubes are both Stainless Steel SS316 and Teflon PFA tubes provided by Swagelok. Fittings are provided by Swagelok and they are made by Stainless Steel SS316 or Brass. Humidifier is provided by Fuel Cell Tech.

Potentiostat/Galvanostat

The modular potentiostat/galvanostat *MetroOhm AUTOLAB PGSTAT30*, combined with the *FRA2 (Frequency Response Analyzer) module* can measure impedance in the range from 1 $mOhm$ to 100 $GOhm$ in both galvanostatic and potentiostatic modes.

Mode of Operation: Voltage Reading
Range: $\pm$ 10 V
Resolution: 300 μV
Uncertainty: $\pm$ 0.2 % $\pm$ 2 mV

Mode of Operation: Voltage Setting
Range: $\pm$ 10 V
Resolution: 150 μV
Uncertainty: $\pm$ 0.2 % $\pm$ 2 mV

Mode of Operation: Current Reading

Range: $\pm$ 1.2 A
Resolution: 0.00003 %
Uncertainty: $\pm$ 0.2 %

Mode of Operation: Current Setting
Range: $\pm$ 1.2 A
Resolution: 0.03 %
Uncertainty: $\pm$ 0.2 %

Frequency Response Analyzer

Range: 10 μHz to 1 MHz
Uncertainty: $\pm$ 0.003 %.

Gas-Chromatograph

The Gas Chromatograph *μGC R3000 SRA Instruments* is fed by helium and nitrogen provided by cabinets with a pressure regulator at 5.6 *bar* and minimum purity equal to 99.9995% as carrier gases.
It is equipped with three capillar columns (2 $MolSieve$ and 1 $PlotU$) with Thermal Conductivity Dectectors (TCD). These detectors permits the identification of the species of the sample after the separation in the column thank to the comparison of thermal conductivity with the carrier.

GDL experimental setup components specifications

This paragraph provides technical details on the components of the experimental setup ad-hoc designed for the GDL ex-situ characterization.

Peristaltic Pump

Model: *Watson-Marlow 323S*
Maximum Speed: 400 *rpm*
Uncertainty: 0.5 % of measurement
Head Model: Watson-Marlow 304MC
Maximum Head Speed: 110 *rpm*
Massflow range: 0.33 to 43 $g \cdot min^{-1}$

Flowmeter

Model: *Brooks 5850s*
Flow Range: 0 to 2 $Nl \cdot min^{-1}$
Uncertainty: 0.2 % F.S. + 0.7 % R.
Working gas: Air
Voltage Input: 15 to 28 V D.C.
Voltage Output: 0 to 5 V D.C.

Pressure Transducers

Absolute Pressure Transducers
Model: *GE Druck PMP 4070*
FullScale: 3 *bar*
Voltage Input: 9 to 32 V D.C.
Voltage Output: 0 to 5 V D.C.
Non Linearity and Hysteresis: ± 0.004 % F.S.

Differential Pressure Transducers
Model: *GE Druck LPM 9481*
FullScale: 500 $mbar\ differential$
Voltage Input: 16 to 30 V D.C.
Voltage Output: 0 to 10 V D.C.
Non Linearity and Hysteresis: ± 0.1 % F.S.

Humidity Probe

The humidity and temperature probe is placed into a thermo-stated housing controlled by means of a Temperature Controller that acts on a Resistance placed inside the housing.

Humidity Probe for DMFC cathode
Model: *Vaisala HMT333*
Probe: *Humicap HMT333*
Voltage Input: 10 to 35 V D.C.
Voltage Output: 2 to 10 V D.C.
Temperature Range: 0 to 120 ^oC
Humidity Range: 0 to 100 %
Temperature Uncertainty: ± 0.1 ^oC at 22.13 ^oC
Humidity Uncertainty: ± 1 % RH

Temperature Controller for thermostated housing
Model: *ASCON Linea M3 Serie δ2*
Voltage Input: 220 V A.C.
Regulator: Internal PID
Resolution: 1 ^oC
Relay Model: *Carlo Gavazzi RS1A23D40*
Voltage Range: 230 V A.C or 3/32 V D.C.

Electrical Resistance
Model: *HAWCO HS37-3*
Power: 400 W
Shape: Cylinder
Lenght: 78 mm
Diameter: 9.4 mm
Voltage Input: 240 V

Tubes, fittings, valves

Tubes are both Stainless Steel SS316 and Teflon PFA tubes provided by Swagelok. Fittings are provided by Swagelok and they are made by Stainless Steel 316. Valves are On-Off valves in stainless steel SS316 provided by Swagelok.